UNIVERSITY OF SOUTHAMPTON

FACULTY OF ENGINEERING, SCIENCE AND MATHEMATICS

School of Electronics and Computer Science

Surface tracking in the inter-phase region of large transformers

by

Peter Mark Mitchinson

Thesis for the degree of Doctor of Philosophy

July 2008

UNIVERSITY OF SOUTHAMPTON

ABSTRACT

FACULTY OF ENGINEERING, SCIENCE AND MATHEMATICS
SCHOOL OF ELECTRONICS & COMPUTER SCIENCE

Doctor of Philosophy

SURFACE TRACKING IN THE INTER-PHASE REGION OF LARGE TRANSFORMERS

by Peter Mark Mitchinson

Transmission and distribution operators throughout the world manage significant populations of ageing large transformers which use mineral oil and paper as the dielectric insulation. Many of these transformers are reaching the end of their projected service lives and subject to various end-of-life failures. One failure mode occurs in the inter-phase region which leaves evidence of surface tracking along the barrier boards. The failure mode is thought to occur in three stages but the propagation mechanism is unclear. This project focuses on this failure mode in particular and considers surface tracking on the oil-pressboard interface in general. Interaction between mechanisms forms the overall theme.

The thesis reviews the current research into condition monitoring, ageing and internal electrical discharge in large liquid filled transformers and places the research in context with the industrial requirement for asset life extension. The project is experimentally based and resulted in the development of a unique test facility which formed a significant part of the work. The test facility permits high voltage from two independent sources to be applied to a model of the inter-phase barrier under controlled conditions of moisture and temperature.

The development of the test facility and a new approach to the study of surface tracking on the oil-pressboard interface are described along with results from experiments conducted on new and service aged pressboard. The experiments have revealed the role of the interfacial layer in the transport of charge across the surface of the oil-pressboard interface. It is found that the interaction between the electric fields from adjacent voltage coils enhances the polarisation of the interfacial layer at the oil-pressboard interface and plays a role in the mechanism for creeping discharge. Finally, the interfacial layer is also the mechanism which decreases the bulk voltage withstand of the liquid dielectric medium across barrier surfaces.

List of Contents

List of Figures

List of Tables

Author's Declaration

DECLARATION OF AUTHORSHIP

I, ...

declare that the thesis entitled

SURFACE TRACKING IN THE INTER-PHASE REGION OF LARGE TRANSFORMERS

and the work presented in the thesis are both my own, and have been generated by me as the result of my own original research. I confirm that: -

- this work was done wholly or mainly while in candidature for a research degree at this University;
- where any part of this thesis has previously been submitted for a degree or any other qualification at this University or any other institution, this has been clearly stated;
- where I have consulted the published work of others, this is always clearly attributed;
- where I have quoted from the work of others, the source is always given. With the exception of such quotations, this thesis is entirely my own work;
- I have acknowledged all main sources of help;
- where the thesis is based on work done by myself jointly with others, I have made clear exactly what was done by others and what I have contributed myself;
- parts of this work have been published as conference papers [See Appendix E].

Signed:……..

Date:.....

Acknowledgements

Firstly, I would like to acknowledge the support of National Grid plc for the provision of the test cell framework and the overall funding without which the project would have been impossible, and also to Paul Jarman of National Grid for steering the project.

I would like to thank all the technicians who work in the Tony Davies High Voltage Laboratory, namely Neil Palmer, Mike Smith, Brian Rogers and Steve Harrison, for their practical assistance during the refurbishment stages of the test cell and also other University of Southampton technicians, Richard Howell for repair work and, Barry Bailey for the loan of test equipment. My gratitude is expressed to my supervisor, Dr Paul Lewin, for vectoring me in the right direction at some times and keeping me solidly earthed at others. Thanks also go to Tobias Kleeman, a fellow student, who enhanced the existing Matlab program so that I could batch process the partial discharge results to produce the ϕ-q-n plots and so ended many hours of tedious mouse clicking.

I would also like to express gratitude to the following non-University of Southampton personnel who have freely given help and advice:

> Alan Darwin, from Areva T&D, Stafford, who donated pressboard samples and gave technical advice relating to aspects of HV transformer design.
> Richard Heywood, from Doble PowerTest, Guildford, who loaned the Tettex 5461 RVM equipment used in early RVM experiments to prove the operational integrity of the apparatus.

Finally, I dedicate this work to my wife, Cathryn, who never wavered with her support and encouraged me through both the sunny days and the dark days towards attaining this life goal of writing a big book.

Acronyms and Abbreviations

BS EN	British Standard Norme Européenne
CEGB	Central Electricity Generating Board
CIS	Commonwealth of Independent States
CIGRE	International Council on Large Electrical Systems
CO	Carbon monoxide
CO_2	Carbon dioxide
CTI	Comparative tracking index
DGA	Dissolved gas analysis
DP	Degree of polymerisation
EDL	Electric double layer
ERIP	Epoxy resin impregnated paper
ESKOM	Electricity Supply Commission (South Africa)
FEM	Finite element model
FRA	Frequency response analysis
GCS	Guoy-Chapman Stern (model)
GSU	Generator step-up (transformer)
HPLC	High performance liquid chromatography
HVDC	High voltage direct current (converter transformer)
IEC	International Electrotechnical Commission
OIP	Oil impregnated paper
PD	Partial discharge
PDC	Polarisation depolarisation current
PJM	Pennsylvania-New Jersey-Maryland (regional transmission organisation in USA)
PLC	Programmable logic controller
ppm	parts per million
RVM	Recovery voltage measurement
SQL	Structured query language
UHF	Ultra high frequency
UV/Vis	Ultra violet/visual (spectrum)
WG SC	Working group study committee

Chapter One

Introduction

When commercial electricity generation was first established in the UK at the turn of the 20th century to supply the emerging industrial and domestic markets, it was produced and distributed on the basis of local supply and demand. The result was a host of local electricity supply companies with diverse standards and overcapacity of generating resource. It was realised that a national network of generation and supply could achieve economic advantages as well as technical standardisation of supply and of end user equipment. A network or "grid-iron" was proposed and the National Grid came into being following the Electricity Act of 1926 which established the Central Electricity Board. The aim was to provide a country-wide service in order to standardise supply and provide a quality level of service free from interruption. Originally there was debate as to whether to continue with local generation and transport the fuel to the site of generation or to site the generation plant next to the fuel supply and transport the electricity to the centres of demand. The latter option was chosen as the transport costs outweighed the transmission costs at the time. The grid was developed over the next decade and, by 1935, the infrastructure for transmission at 132kV had more or less been put in place. This enabled a reduction in the amount of power plant to permit more economic operation as indicated by a fall in required generation reserve capacity from 70% to 26% at the time [1].

The post war years necessitated re-investment with the realisation for further growth in power demand and, following nationalisation in 1948, an upgrade to the system to work at 275kV was accomplished by the late 1950's. Further need for even greater capacity of power transmission to future proof expected demand led to another upgrade in the 1960's. The drive was to increase the voltage level to take advantage of a reduction in transmission loss at the higher voltage with a choice of developing either a 400kV or 500kV system. The 400kV system was chosen because this required less development of the higher rated infrastructure at the time. The 400kV transmission grid (known as the Supergrid) was rolled out with the installation of 400kV plant and equipment rated at 500MVA and above. The next significant change occurred in 1990 when the CEGB was denationalised and ownership and operation of the transmission system in England and Wales became the responsibility of the National Grid Company plc which is now National Grid plc [1].

1.1 The UK transmission grid today

As of 2008/2009, the overall UK transmission and distribution grid comprises three networks of 132kV, 275kV and 400kV transmission lines interconnected through 681 substations and supplied by a mix of 167 large power stations. The 132kV lines (approximately 5200km) are mainly associated with the transmission of hydroelectric power in the Scottish highlands. The 275kV transmission lines (approximately 6000km total length) are situated around the large conurbations of London, Birmingham, South Wales, East Midlands, the North East and the Glasgow-Edinburgh corridor. The 400kV system (approximately 11500km) provides the main power interconnect across country between these areas [2,3]. Electrical power is generated at 28kV and transformers are required throughout the network in order to step-up and step-down as appropriate the voltage between the generating stations, the networks and centres of demand giving rise to three broad classes of transformer.

Generator step-up (GSU) transformers convert voltage from the generator level of 28kV to the 132kV/275/400kV grid levels form one class of HV power transformers [1]. The end users are supplied through 346 grid supply points via distribution transformers which form a second class of transformers to feed local distribution networks at 132kV, 66kV and 33kV [3]. 1145 high voltage (HV) transformers, at various ratings (i.e.

400kV/275kV, 400kV/132kV and 275kV/132kV), comprise the third class which are located in substations and form the main interconnections between the three grids. The HV transformers are the focus of this thesis.

The UK therefore has a mature transmission and distribution network in which there are embedded over 1000 HV transformers rated at 132kV and above and thousands of other distribution and generator transformers. The problem facing National Grid is that the majority of the HV transformer base was installed before 1970 resulting in an aged population of equipment [4].

The demographic profile is not atypical. For example, in the United States, a parallel situation exists with one study highlighting the PJM utility, which covers the eastern area of the US, where 55% of its 500kV rated power transformers are aged 30 years or more. The study adds that the average life of the transformers is 36 years [5]. Jaegers [6] reports a similar demographic profile for the South African ESKOM network where 38% out of a population of 4015 units with primary voltage greater than 132kV are 30 years or older. Countries or utilities with more recently installed or developing infrastructure will not yet be facing the same demographic problem, but these utilities will face the same problem of end of life failure at some point in the future.

All network operators have to address three broad issues in relation to high voltage equipment which are controlled through the activity of asset management:

- prevention of early life failure
- extension of asset life
- technical management with planned replacement for elderly assets [7].

1.2 Asset management

Asset management has functions of plant maintenance, life extension and replacement of the major pieces of capital equipment. Asset management requires an interactive holistic approach and involves all business functions from finance to procurement to condition monitoring to maintenance. Asset management requires a strategy which balances cost of operation in terms of capital investment and maintenance with operational efficiency and performance. This involves juggling between the aspects of

the product life cycle, different equipment specifications and designs, asset redundancy, maintenance and end of life management. An overview of the asset management function relating to the transmission industry taking into account all the commercial and financial aspects is given by Brown and Humphrey [8]. A soft technical overview showing how weighted equipment attributes and equipment de-rating can be used as part of plant management is given by Vrey [9].

Transformers are expensive items of capital equipment and have long manufacturing lead-times which leads to the motivation of keeping aged equipment operational for as long as possible. To achieve this, the network operator must implement a program of condition monitoring and diagnostics in order to understand how the asset is performing in usage and degrading in performance over time. Because transformers are static pieces of equipment, their overall performance and degradation of performance relates to the insulation and component integrity, the understanding of which is the objective of condition monitoring. Manufacturers also wish to understand failure modes and lifetime characteristics of their equipment as they can take advantage of forensic evidence resulting from backward looking failure analysis to incorporate improvements into future designs. This is especially important for the new generation of designs which are now being rated at voltages up to 800kV [10] to take advantage of further decreasing the transmission loss by operating at even higher voltage. However, many large transformers over 275kV were installed in the 1940's and 1950's and continue to be in service. Their operation has furnished network operators with a picture of failure modes through the asset management activity by the accumulation of test data on equipment and systems. Failure analysis is often commercially sensitive and there are a limited number of published documents on this topic.

1.2.1 Failure surveys

A failure analysis, based on the CIGRE Working Group Study Committee (WG SC) 12 survey, is given by Allan and White [11]. This survey covers 47000 transformer-years in 13 countries over a 10 year period. It reported an average failure rate of 2% per annum at the time for 500kV transformers. It attributed 77% of the failures to design, manufacturing or material defects with 5% due to poor maintenance and only 6% due to operation difficulties such as lightning and power surges. In terms of individual

components, 69% of the failures were found due to the windings, terminals and magnetic circuit with only 13% attributed to the tank or dielectric fluid. This document also considered two individual surveys, one from the US and the other from the former CIS countries which reported respectively 10% and 27 % as the failure rate attributed to insulating oil and oil-barrier insulation. This highlights the problem of surveys in that difference emphasis is placed on classification which makes comparisons difficult. The current approach proposed by CIGRE SC A2 is to adopt a simplified and more directed form of survey by targeting three distinct stages in the transformer life cycle [12].

Probably the most comprehensive technical analysis of transformer failure is given by Sokolov who has published many papers and effectively adopted this topic as his own. An early paper [13] reports on a survey of a population of 5000 high voltage transformers in the1990's and compares it against a contemporary Doble clients' survey. In both surveys, over 50% of the failures were found due to the bushings and load tap changers (LTC) with only around 30% due to major or minor insulation involving the cellulose insulation. Within this group, Sokolov identifies 7 possible failure mechanisms of which 5 mechanisms involve water and/or surface contamination with the other two involving mechanical deformation due to over-currents. The contamination leads to partial discharge (PD) and/or surface discharge with either flashover or breakdown resulting from creeping discharge which may be precipitated by a surge or over-voltage. The report suggests that insulation failure is a result of a set of sequential and/or interacting events which overcome the weakened safety margin of a system due to the ageing effects of moisture or contamination or another fault such as a defect or over-voltage. This loss of system strength as a function of time, ageing and stress events is illustrated in Figure 1.1 [9].

Creeping discharge is classified by Sokolov as one of the most dangerous failure modes for the liquid paper insulation as it "results in catastrophic failures at normal operating conditions". Sokolov describes four stages in the development of creeping discharge but later combines two of the stages to give a three stage model [14]. In this model, creeping discharge is a result of a partial breakdown of an oil gap leading to surface discharges which, over time, results in tracking due to the drying out of the pressboard and the carbonisation of the oil/cellulose. No explanation is offered for the mechanism

of oil gap breakdown, the generation of the discharge or the propagation of the creeping discharge.

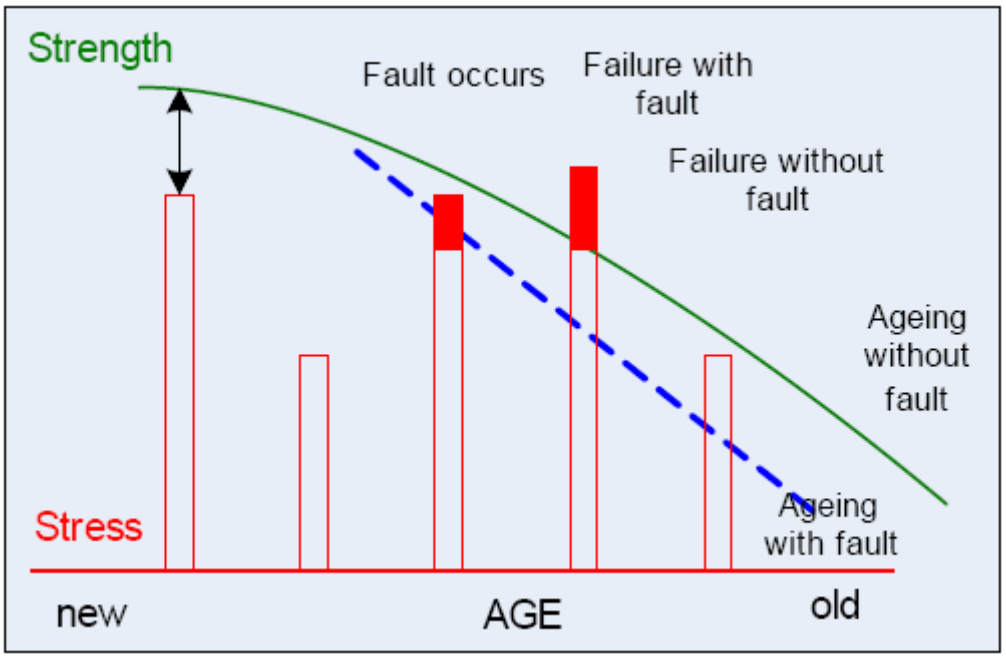

Figure 1.1 Diagrammatic representation of failure as a function of stress [9]

Another survey on transformer failures supports previous studies by concluding for power transformers [15]:

- the overall failure rate is low (typically 1%),
- equipment which fails, does so after 20 -25 years, and
- bushings and internal insulation are the biggest problem areas.

Transformers fail not only as a result of ageing but may also fail as a result of interaction with the transmission system, the failure of external ancillary equipment and poor asset management. Lapworth [16] describes several cases in the UK where failures of a variety of aged equipment have been attributed to overvoltage caused by remote energisation thus illustrating the effect of an external fault exceeding the inherent strength. Cancino et al. [17] document a case where a class of GSU transformers failed due to the use of aged silicone-carbide lightning arrestors which proved inadequate in a region of high lightning activity. McDermid et al. highlight a series of failures on a class of HVDC converter transformers illustrating the range of maintenance problems faced by a network operator [18].

A survey by Bartley [19], relating to insurance payouts in the USA on a set of transformer failures, identifies 24 out of 94 failures as being due to insulation failure with another 22 being due to design/material or workmanship defects. This report doesn't qualify the transformers in terms of voltage rating or the overall population and doesn't breakdown the failures according to component type. However, it confirms that transformers fail due to a variety of causes categorised broadly as electrical, mechanical and thermal. The real point of this survey is that failure can result in a consequential financial loss amounting to millions of dollars when taking into account business interruption as well as property loss. The task of asset management is more than just the technical understanding of failure mode or maintenance; it must prolong the life of the transformer whilst minimising the overall financial risk.

1.3 The role of the manufacturing process in failure mechanisms

Large transformers are manufactured using complex industrialised processes. Their assembly involves many manual operations. The fact is that, no matter how well a manufacturing process is controlled, the end product, be it the basic refined material or the final assembly of components or base materials can never be considered 100% defect free [11]. The more manual processes involved in the production process, the greater the risk of defects. It should be remembered that a defect may not be a material defect but may be something more intangible such as a design error or inadvertent contamination. Bartley [19] cites the second largest category of failures as due to design, materials and workmanship with foreign objects being a significant factor and this is acknowledged by a well known transformer manufacturer [20].

The real evidence is that product recalls are regularly initiated on a global basis to remedy some defect or other in all industries. History is actually littered with examples of product failure due to poor design, defect material or poor construction; the classic example is the 1940 collapse of the Tacoma Narrows bridge in Washington State caused by crosswinds leading to torsional mechanical resonance and structural failure the mechanism of which was not understood at the time [21]. In the electrical industry, the early porcelain or glass insulators often failed due to poor porosity or inclusions i.e. manufacturing and material defects [22]. An overview of the electrical industry perspective on the economic implications of product recall is given by Jacobs [23],

which illustrates the consequential interaction between poor manufacture and economics. A benign defect may exist within a product and the product will operate successfully throughout its entire life without failure. Equally, a defect may lead to a particular failure mechanism which develops only after a long period of time. The root cause can be traced by forensics to a seemingly innocuous item where there is enough evidence remaining after failure and many examples can be cited [14,15,16,17,18].

The surveys indicate that large transformers are inherently reliable as evidenced by the low overall failure rate and general average age before the appearance of a failure. In addition, the papers show that there is a wide knowledge base relating to failure modes and asset management in general. Bushing failure is considered the most significant often accounting for around 40% of transformer failure with major/minor insulation problems a close second for failure. Sokolov outlined 7 possible scenarios for insulation failure with creeping discharge and surface discharge identified only as sequential elements in these scenarios. Different mechanisms are proposed for both creeping discharge [13] and surface discharge [14] with surface discharge forming an element of creeping discharge. However, neither the root cause for their initiation nor the conditions for the progression of the phenomena are identified.

1.4 Project aim

National Grid manage a large population of transformers, many of which were installed in the 1960's and 1970's. There is a general concern, which is not limited to the UK, about the large population of ageing transformers. HV transformers are expensive items of equipment (approximately £1.5m) and subjected to long lead time for manufacture (up to 18 months) depending upon size and contract complexity [24]. There is no panacea to a multitude of possible failure mechanisms and the strategy must be one of understanding and eliminating individual failure mechanisms one at a time. The aim of the project is to identify the factors promoting the mechanisms for creeping discharge and surface discharge and to improve the overall lifetime of HV transformers by this understanding. The following milestones were identified for the project:

- An understanding of the current techniques used to evaluate the condition of aged transformers by means of a literature survey.

- An understanding of the role and operating conditions of the inter-phase barrier in the transformer.
- The construction of a suitable test facility capable of replicating the conditions in the inter-phase barrier region in term of electrical stress and temperature.
- The design and implementation of a model to simulate the inter-phase barrier region subject to a discharge source.
- A test program to gather data in order to identify the mechanism for creeping discharge.

1.5 Thesis contents

This chapter has outlined the role of transformers within the transmission and distribution network as well as the general failure mechanisms to which aged transformers are prone. Creeping discharge and surface discharge are two phenomena for which the mechanisms are as yet not fully understood. Mineral oil and paper form the key elements of transformer insulation and Chapter 2 gives a comprehensive review of the technical aspects of oil and paper and the methods used to assess insulation quality as well as diagnostic techniques.

Chapter 3 considers the role of electrical discharge, and static electrification on the insulation degradation process. The specific details of the construction and design of high voltage transformers are not covered with the exception of the inter-phase barrier region which is outlined in this chapter as well as the results of a finite element model (FEM) of a large autotransformer. The model illustrates the interaction of the electric fields from adjacent voltage coils on the surface of the barrier boards in the inter-phase barrier region.

The test facility constructed to contain the inter-phase barrier model is described in Chapter 4. This includes technical descriptions of the system and process controls, the high voltage upgrade and the independent bi-phase supply. The following chapter outlines the barrier model, the interaction of two electric fields and presents the results of a novel experiment conducted in an oil bath which gave an insight into surface tracking. Chapter 6 presents the results of experiments conducted on the barrier model using a discharge source and Chapter 7 considers the results of experiments conducted

on the barrier model using a floating discharge source. The final chapter summarises the findings, considers the implications and makes recommendations for further work.

1.6 Summary

The development of the transmission and distribution grid in the UK has been outlined with the HV transformer identified as the significant link in the conversion and transmission of energy around the system. In the UK, the majority of the network and associated equipment was installed over 40 years ago resulting in a large population of ageing transformers. This represents a huge capital investment and there is a drive to maintain the infrastructure as long as possible through the discipline of asset management which monitors and maintains the equipment. Many countries are facing the same concern and a wide international knowledge base of transformer problems and age related failure mechanisms has been established with many published case studies. The studies have indicated that transformers are generally reliable but do incur a wide variety of failures with internal insulation being a significant but not the dominant failure cause. Creeping discharge and surface discharge have been identified as part of the failure processes but their exact mechanisms remain unclear. The identification of the mechanism for surface tracking in the inter-phase barrier region is the primary aim of the project. Surface tracking occurs at the interface between the oil and pressboard components of the insulation. These materials are at the core of the insulation structure and their properties and ageing mechanisms are described in the next chapter.

Chapter Two

Cellulose and mineral oil degradation

Large power transformers using liquid /cellulose dielectric have been developed over the years to meet the varied needs for power transformation in the transmission industry. The industrial drive is the optimisation of the design and construction to achieve the maximum performance and reliability at minimal capital and operational costs. Optimisation involves the minimisation of material use against the maximisation of performance with energy efficiency and environmental issues new concerns.

The basic principle of all transformer operation is simple, but the design, manufacture and operational features of large liquid filled transformers are complex. These topics are documented by many standard texts [e.g. 25,26,27] and are not covered with the exception of two issues which will be considered in detail. The first is the technical features of paper and mineral oil and the industrial tools relating to insulation diagnostics. These issues form the focus of this chapter. The second exception is the inter-phase barrier region which will be considered in Chapter 3.

The materials traditionally used for insulation in HV transformers are paper, pressboard and oil. Paper and oil are natural materials which are refined by industrial processes to bring out the best electrical and mechanical properties of each. The aim is to meet the two fundamental goals of an insulating material which are to separate regions of

different electrical charge and at the same time provide mechanical support for the electrical system. Each material contributes to these goals by possessing complementary electrical and mechanical properties which must work in harmony.

2.1 Paper and pressboard

Paper is made from pulped wood which have been industrially processed to remove impurities. The pulp suspension of wood fibres is formed into thin layers of material known as paper sheet by the process of felting. This process removes the water by a combination of drainage, mechanical pressing and steam heated driers [28]. Pressboard is a thick insulation product formed from the pulping and processing of cotton rag and wood pulp. Pressboard is processed into sheets by pressing together several wet layers to produce board up to 8mm thick [29]. Even thicker pressboard is made by a lamination process where pressboard sheets are bonded together with glue. The intrinsic mechanical and electrical strength of paper and pressboard is due to the polymer chain structure of the cellulose molecules.

The basic building block (or monomer) of cellulose is the glucose unit ($C_6H_{10}O_5$) termed α-cellulose shown in Figure 2.1 [30]. The monomer units connect together in long chains to form cellulose polymer molecules with an atom of oxygen forming the link between the glucose units.

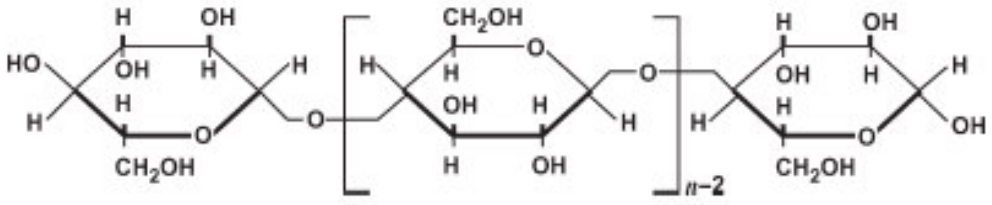

Figure 2.1 Cellulose polymer structure [30]

The number of glucose units (n) which form individual cellulose polymer chains for new electrical paper and pressboard is typically 1200. The length of the polymer chain is characterised by the number of links (i.e. n-2) and this is the degree of polymerisation (DP). The polymer chains are straight (i.e. not coiled) which allows parallel chains to cross link through hydrogen bonding between the hydroxyl groups. This process creates string like fibres which may be up to 6mm long depending on base wood type [30]. The

degradation of paper or pressboard breaks the links in the polymer chains effectively reducing the DP. The DP is measured using the viscometric method [31] and has become a diagnostic tool to estimate the remaining lifetime of paper.

The cellulose molecule is hygroscopic and this means that paper and pressboard absorb moisture very easily. The absorption and adsorption of moisture plays a key role in the water equilibrium mechanism which describes the transport of moisture around the system. Paper and pressboard are mature industrial products and their properties and characteristics are well documented [e.g.28,32]. The main mechanical properties of paper and pressboard are thickness, apparent density, porosity, tensile strength and tearing resistance. The main electrical properties are dielectric strength, dielectric loss and permittivity. The industrial manufacture and quality control of electrical paper, pressboard and laminated pressboard are covered by international standards [33,34,35,36].

2.2 Mineral oil

Mineral insulating oil is produced by refining natural crude petroleum (as distinct from synthetic oil which is a manufactured chemical product). Mineral oil is a mix of hydrocarbons in the form of chain and ring molecules with small amounts of sulphur, nitrogen and oxygen and trace metallic elements. Mineral oil is classified by the percentage content of the following three hydrocarbon groups (Figure 2.2):

- Paraffinic - straight and branched saturated hydrocarbons
- Naphthenic (cycloparaffins) – hexagonal ring of carbon-carbon single covalent bonds
- Aromatic – hexagonal ring modelled as alternating single and double carbon-carbon covalent bonds indicating delocalisation of the carbon-carbon bonding electrons.

Oils are classed as either naphthenic or paraffinic which indicates the majority constituent. Aromatics and other chemicals make up the balance. Mineral oils processed for use as transformer insulating oils are naphthenic in character as this type flows better under cold conditions. Mineral oils are mature industrial products and their properties and characteristics are well characterised with diverse mechanical and

electrical properties such as density, viscosity, flash point, pour point, dissipation factor and breakdown voltage [37].

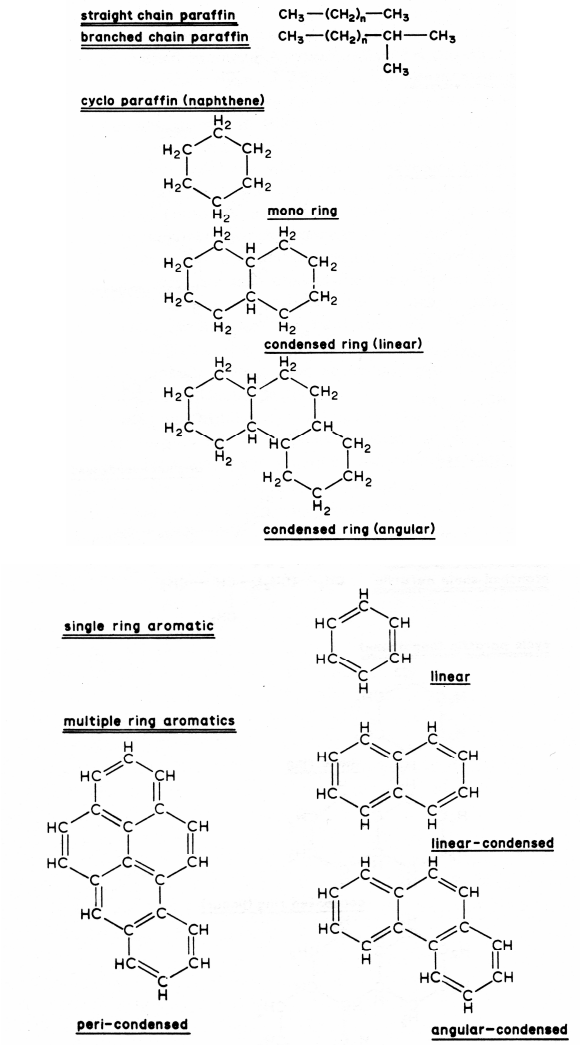

Figure 2.2 Paraffinic, naphthenic and aromatic hydrocarbons [37]

The properties need to be taken into account during the specification of a grade of mineral oil for use as a liquid dielectric as the property may be related to a seemingly unconnected operational reason. For example, pour point defines the temperature at which a liquid just begins to flow and hence is important for transformers which may be designed to operate in cold environments such as in the Arctic or at high altitude. A free flowing liquid is desired at low temperatures to ensure thermal transfer and to prevent mechanical damage to pumps during start up under freezing conditions. Dissipation factor defines the electrical loss of the oil when used as a dielectric. The dissipation factor increases with absorbed polar molecules and hence is a good indicator of oil

contamination. Dissipation factor is usually measured at 90°C using a capacitive measurement technique [38].

In general, the important points relating to mineral oils and high voltage equipment are:

- The oil should have high dielectric strength and stable properties under conditions of low temperature and good long term resistance to oxidation [39].
- The oil serves as a coolant and the thermal and viscometric properties of oil are important.
- Voltage breakdown is not to be taken as a measure of oil ageing as it is only a measure of contamination by moisture and particles [40].

An overview of mineral oils, their requirements, specifications and production is given by Eklund [41]. The industrial manufacture and quality control of transformer oils are covered by international standards [42,43].

2.3 The use of paper and oil in HV equipment insulation

Large transformers using a mineral oil /paper dielectric medium have evolved over the years to take into account the developing knowledge, experimentation and operational experience gained by individual manufacturers and network operators. Many designs exist with the subtleties of mechanical and electrical details often being highly confidential information associated with a particular manufacturer. However, oil and paper continue to be the materials of choice for the following reasons:

- Electrical grade paper possesses excellent dielectric strength and low loss and its flexibility facilitates application as insulating layers over complicated shapes.
- Insulating oil provides cooling through convection and also has high dielectric strength.
- The oil impregnates the paper/pressboard. This fills the spaces between the fibres and the spaces in the transformer and prevents the formation of gas voids which are possible sources for partial discharge (PD) activity.

An overview of the history and development of paper for use in transformers is given by Prevost and Oommen [30]. Currently, there is no real choice for an alternative combination of materials though there is much research on-going into the use of

vegetable and synthetic oils in an effort to replace the mineral oil as the liquid dielectric [44,45,46,]. The motivation for this research is cost reduction and environmental improvement in terms of biodegradability and fire resistance. (However, this thesis will only consider the industry standard mineral oil and electrical paper insulation as these materials still form the majority of insulation usage.)

One of the important stages during the construction cycle of HV equipment is the vacuum drying process. This process removes moisture from the paper and air from the whole system which permits all voids to be filled with oil. The standard industrial process [25,27] is considered in detail to distinguish from the modified process adopted for the experimental phase (see §4.8.2).

2.3.1 The industrial drying process for oil/paper insulation

Cellulose insulation for oil filled transformers is dried in two stages. The first stage is the drying of the winding coils by placing them in a heated vacuum tank at 100°C and under a vacuum of 100Pa absolute. The heat/vacuum combination drives off the moisture. The coils are clamped in order to consolidate the windings by taking up any slack from the shrunken insulation. The dried coils are assembled to the cores and yokes and the major insulation added. The assembly is then moved to a second drying process stage. Here, the assembly is dried in a large autoclave or (in the case of very large equipment) the transformer housing itself is used as the treatment vessel. The second stage drying process is achieved using one of two methods according to manufacturing choice. The first method is where alternating cycles of heat and vacuum are applied to the assembly. Heat is applied by forced circulation of air at 105°C. Care is taken to limit the air temperature to avoid heat damage to the cellulose molecules as this method is undertaken under atmosphere and thus in the presence of oxygen. The alternative process in called the vapour phase process. This process is undertaken under vacuum conditions (less than 500Pa). The vacuum permits the use of higher temperatures and so the problem of cellulose ageing is avoided. The heat energy is provided by introducing hot kerosene (at 130°C) into the evacuated chamber. The kerosene condenses onto the surfaces of the assembly and gradually heats up the insulation. Kerosene and water vapours are evolved which are drawn off and the moisture extracted by means of a condensation and separation process.

The advantage of the vapour phase process is that the process time is usually half that of the conventional process. The disadvantage is that a more complicated process plant is required. With either method, the drying time is not predictable and the process end is determined by continuous monitoring of the insulation resistance and winding power factor. The insulation is considered dry when these measurements have stabilised at satisfactory low values determined by experience.

After the second stage process is completed, the assembly is further tightened whilst still hot to take up slack from the shrunken insulation to further consolidate the windings and the assembly. The transformer is then ready for the "tank" process where it is filled with clean and dried oil under a vacuum to exclude both air and moisture from re-entering the insulation. The manufacturing process ensures that the insulation has the lowest possible moisture content at the start of the working life of the transformer. The accepted target value is 0.5% moisture content [47].

2.4 The mechanism of insulation degradation

When a transformer is energised, its natural operation creates an internal environment subjected to time varying electromagnetic fields and heat resulting from the joule effect of the associated circulating currents in the copper windings and magnetic core. The internal structure is subjected to thermal, chemical, electrical and mechanical stresses. The equipment is also subjected to the influence of external climatic conditions which contribute primarily to the internal thermal and mechanical stresses. These stresses act on the oil/paper insulation system and gradually alter the material structure(s) which in turn gradually change the electrical and mechanical properties of the insulation materials. Each stress mechanism acts on the both the oil and the paper/pressboard insulation in different ways.

2.4.1 Thermal stress

Heat affects long chain organic molecules by rupturing the molecular bonds leading to chemical changes of the structure. Within the transformer, the hydro-carbon molecules of paper, pressboard and oil components suffer gradual degradation due to heat generated in the energy conversion process. With the paper and pressboard, the cellulose polymer chains are ruptured to form smaller chains with the evolution of

water, CO, CO_2 and furanic compounds [47]. In the case of mineral oil, the heat breaks the hydrocarbons with the evolution of hydrocarbon gases. The degradation processes for paper and oil will be discussed further in §2.7.

2.4.2 Chemical stress

Chemical stress is where a substance is affected by direct chemical activity acting on an element or molecule to from a new compound. An example is the oxidation of copper to form copper oxide. Some metals accelerate the chemical reactions through catalytic action. Water is the by-product of the thermal stress on paper and acts further on both the paper and oil to further alter the physical and electrical properties of each. The copper windings act as a catalyst in oil ageing. Oxidation can occur from oxygen present in oil or from free oxygen or ozone in air breathing transformers [41].

2.4.3 Electrical stress

Electrical stress occurs where the field gradient is high enough to cause electronic ionisation of material and/or electrical partial discharges within a material. The ionisation may lead to further chemical action. The partial electrical discharges will act on the surrounding insulation media which may degrade it further through heat and further chemical activity. In a uniform electric field, sharp changes in geometry and discontinuities in the insulation media cause localised areas of high field gradients which results in partial discharges. The effects of electrical stress are more fully discussed in Chapter 3.

2.4.4 Mechanical stress

Mechanical stress occurs due to repeated mechanical action which leads to breakage of the molecular bonds (known as fatigue). An example is the repeated flexing of soft metal such as copper which eventually leads to material fatigue and failure. The metallic parts such as the windings and core within a HV transformer are subjected to electromagnetic forces which result in constant vibration. This may lead to displacement of mechanical parts resulting in further localised electrical and thermal stresses [19].

2.5 Ageing and age assessment

A change in the measured chemical or physical properties of an insulation material is termed ageing. This is a slow process taking many years and is distinct from the processes of insulation degradation, which occurs over the medium term (i.e. months), and of insulation breakdown which may occur over a very short time frame (i.e. seconds). The continued safe operation of the transformer depends upon how the insulation materials retain their properties (i.e. resist ageing) in the face of the four processes detailed above. These ageing processes change different properties of the two insulation materials. The detectable changes in these properties then offer a means of age measurement and characterisation. Condition monitoring is about the measurement and characterisation of these changing properties which is the assessment part of equipment maintenance. Asset management is about the subsequent interpretation of these measurements and the resulting activity to maintain the equipment which is the lifetime extension part.

The measurement of properties to determine the age leads to the question of the closeness of equipment to the end of life. The approach originally taken was through thermal stress and was addressed by Dakin in the 1940's who linked the thermal ageing of materials to the Arrhenius equation which describes the rate at which chemical reactions take place [48]. For electrical insulation, the time to thermal breakdown (i.e. the life of the insulation) is modelled by:

$$L = A\, e^{-B/T} \qquad (2.1)$$

where L is time to failure usually expressed in hours, T is temperature in Kelvin and A and B are positive constants determined by experiment. Thermal endurance characteristics are usually plotted as log - linear charts, with the horizontal axis adjusted to show the Celsius scale, Figure 2.3.

For example, various values have been determined for the Class A (signifying a continuous thermal rating of 105°C [49]) insulation paper as used for transformer conductor insulation. The standard transformer texts such as Blume et al. [26] find that the half-life ageing rate is 5°C to 10°C and settle on an average of 8°C; Wilson [37]

quotes the value of 7°C whilst Franklin [25] chooses 6°C all of which are in close agreement. The Arrhenius equation has effectively become the de facto method for the determination of the thermal endurance for electrical insulation materials [50].

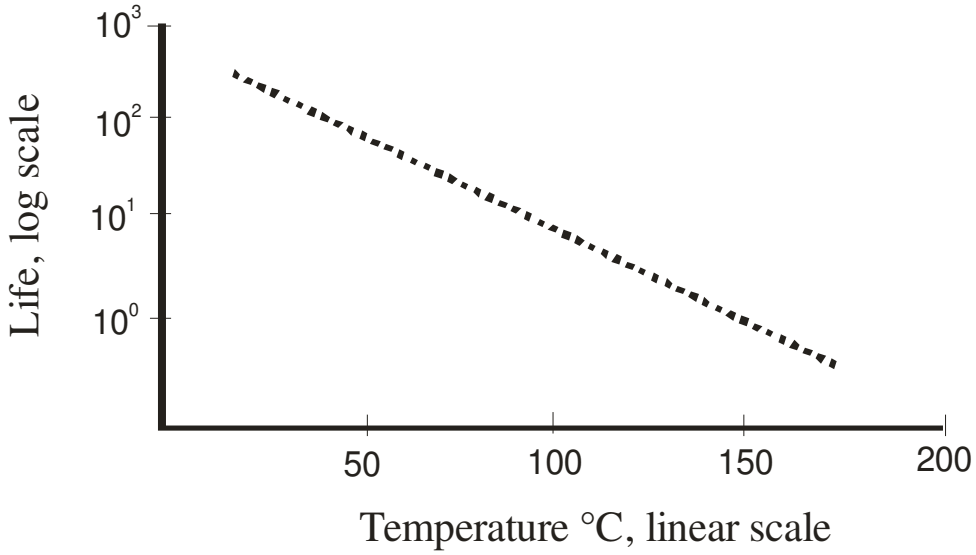

Figure 2.3 Typical life plot

2.5.1 End of life prediction

The end of life for paper insulation occurs when the mechanical strength has deteriorated sufficiently so that it is no longer able to withstand the applied electrical stress and electrical breakdown occurred as evidenced by flashover at rated voltage. This was traditionally taken to be when the tensile strength had fallen to 50% of the initial value. The degree of polymerisation (DP) method is more commonly used to determine the strength of paper with a DP value of 200 corresponding to 50% loss in tensile strength which is the generally accepted limit for end of life for paper [47]. This approach, however, considers insulation ageing due only to thermal effects. In reality, the stresses do not act in isolation but in combination where the combined effect of stresses is known as a synergistic effect.

2.5.2 Synergistic effects of stresses on ageing

The single stress thermal Arrhenius model has proved useful for predicting the life performance of solid insulation materials when subject to heat alone. However, it can not be expected to adequately describe the ageing process of HV equipment subject to electrical, mechanical and chemical stresses in addition to the thermal stress. This

demands the evolution of a multi-stress model and an overview of the available multi-stress models is given by Cygan [51]. Five different models combining electrical and thermal stress have been developed. The electrical stress component is modelled using either an exponential law (similar to the Arrhenius thermal model):

$$L = a\, e^{-bE} \qquad (2.2)$$

and/or an inverse power law:

$$L = kE^{-n} \qquad (2.3)$$

where L is the time to failure usually expressed in hours, E is the electrical stress in $kVmm^{-1}$ and a, b and n are positive constants determined by experiment.

The differences are that the Simoni and Ramu models (which are very similar in their approach) use equations which are based on the product of the inverse power law for the electric stress and the exponential law for the thermal stress. These models also consider a threshold for electrical stress thus linking ageing to operation above the rated voltage. The Fallou model considers an exponential law for both factors of temperature and electric stress. However, this model doesn't account for a threshold voltage. This leads to inaccuracies when extrapolating results at low stress levels and also makes results when taken at room temperature, difficult to fit to the model. The Montanari probabilistic model uses the inverse power law along with Weibull statistics to give a probability for time to failure under combined electric and thermal stress. The fifth model, known as the Crine model, uses a physical approach in that the lifetime is linked to the time for charge to cross the energy barrier. The model includes the Boltzman/Planck relationship and aims to link the ageing process to the physics of charge transport.

Cygan concludes that a multi-factorial approach is necessary to truly model interacting stresses whilst acknowledging the difficulty in achieving this. However, the multi-stress models are still based only on electro-thermal experiments with solid insulation and hence don't take into account either the mechanical or environmental (i.e. chemical factors). Thus, moisture, interacting chemical reactions and mechanical stresses, which

are significant interacting stress factors in the ageing process for the transformer liquid paper insulation, remain to be included in models.

2.6 Moisture in the oil/paper insulation system

Within the transformer there is a large mass of hydrophilic paper and pressboard and a large volume of hydrophobic oil. It has long been accepted that moisture has a detrimental influence on the performance of high voltage equipment because it presence depresses the voltage withstand of the both the paper and the oil insulation and the mechanical strength of the paper [47]. This explains why great care is taken to reduce the initial water content during the construction of a transformer. The measurement of moisture content in the insulation, its implications, the removal of moisture from the system over the life of the equipment and the techniques developed for preventing the ingress of moisture into apparatus are current themes in moisture research. The movement of water around the insulation system is described by the water-oil equilibrium mechanism. This is the key to understanding the role of moisture in the ageing processes.

2.6.1 Water-oil equilibrium mechanism

The cellulose and oil in an insulation system do not work in isolation but interact as a system. A significant interaction is caused by the exchange of moisture between the oil and the cellulose which is the water-oil equilibrium mechanism. As the oil-paper insulation system ages, the stress mechanisms release moisture due to the breakdown of the paper. There may also be moisture ingress due to bad maintenance leading to poor sealing or faulty air breathers [14]. The result is a build up of moisture in the cellulose which then diffuses into the oil. The study of the variation of moisture in paper with temperature has its roots in the 1940's with the so-called Piper charts [47]. These have been developed by various investigators to include the equilibrium interaction with moisture in oil. Perhaps the best historical review is given by Du et al. [52] which identifies Fabre-Pichon as the investigators to first publish water-oil equilibrium curves (Figure 2.4) in 1960. This has been followed by other researchers with their own sets of curves such as the Oommen and Griffin curves.

2.6.2 The use of equilibrium mechanism to describe the movement of moisture in the transformer

The moisture equilibrium diagrams are used as an aid to explain two issues. The first is the division of moisture between the two insulating media. Consider a large transformer which contains approximately 7,000kg of paper and pressboard and 80,000 litres of oil holding moisture. If the oil moisture is measured at 20ppm, this equates approximately to 2kg of moisture. At an operating temperature of 70°C, the moisture content of the paper is 3% which relates to 210kg of moisture in the cellulose [52].

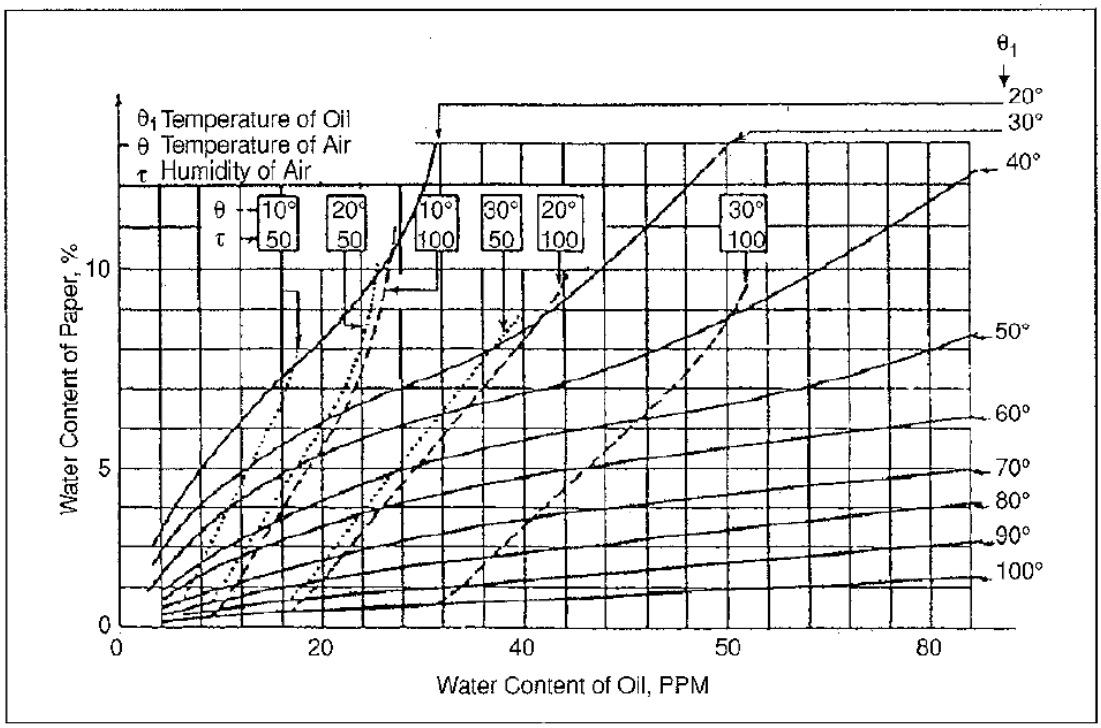

Figure 2.4 Fabré-Pichon curves [52]

The second issue relates to the change in moisture equilibrium following a temperature transition as would occur when bringing a large transformer on line from cold or taking a transformer out of service. One practical study by Buerschaper [53], using a scale model, finds that the moisture in the oil lags the temperature transition by about 10 to 20 hours with the moisture transition due to cooling occurring more rapidly. (The implication of this study is that, as the temperature rises, there is a movement of moisture from the pressboard to the oil and vice versa.) The results indicate that the moisture in the oil doubles over a temperature change from 40°C to 60°C. For the typical transformer already discussed, this would represent a movement of 2kg of water

from the paper to the oil thus leaving the overall paper/pressboard moisture content relatively unchanged.

The curves should be used with caution as they define moisture balance only under equilibrium conditions and they rely on the fact that the moisture in the paper is based on a measurement of moisture in the oil. Garcia et al. [54] suggest that, as the moisture diffusion process is slower for thick pressboard supporting structures, then the moisture movement is primarily from the than for the thinner insulation comprising pressboard barriers and conductor insulation paper. The curves do not account for the fact that there will be hotspots within the transformer thus creating regions of differential temperature with moisture gradients due to the solubility relationship with temperature for the moisture in oil. Finally, there is a choice of curves leading to the question as to which set one should use.

The curves were compared by Du et al. [52] and Pahlavanpour [55]. Both studies find that the Oommen curves place the emphasis of moisture in the oil whilst the Fabré-Pichon and Griffen curves (which are in close agreement) place the moisture emphasis towards the paper. However, the Du study also includes an experiment which shows that the Oommen curves fit experimental data better.

In summary, the moisture equilibrium mechanism shows that the paper/pressboard acts as the reservoir for the water which is absorbed and expelled according to the temperature, but, the majority of the moisture is always held in the paper/pressboard. The use of the curves should be treated with caution as the different curves place emphasis on either moisture in the oil or in the cellulose. Finally, the moisture can not be assumed to be uniformly distributed due to hot spots in the insulation media and the unequal distribution of the paper and pressboard volumes. However, the equilibrium mechanism does provide a practical means of moisture extraction which will be discussed in §2.8.1.

2.6.3 The effect of moisture on paper and pressboard

Paper naturally holds between 5-10 % moisture according to the ambient conditions and will rapidly absorb moisture until it reaches equilibrium according to the ambient

relative humidity. A simple experiment, involving the measurement of the change in mass over time of a single sheet of electrical paper under conditions of controlled relative humidity, shows that paper quickly absorbs moisture with moisture content stability achieved within 20 to 30 minutes (Figure 2.5 [28]).

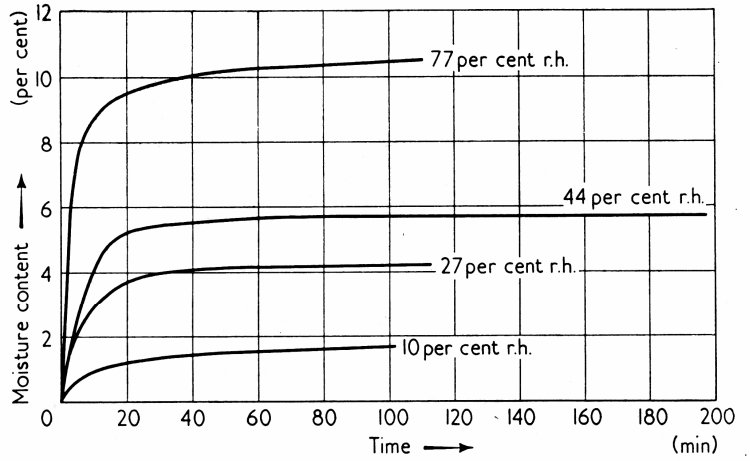

Figure 2.5 Rate of absorption of moisture by paper [28]

Figure 2.6 shows how the moisture content varies according to the relative humidity of the atmosphere. It is this hysteresis mechanism which explains how the paper absorbs and retains moisture. Paper dimensions vary with moisture content with the paper expanding as the moisture increases and vice versa. In addition, both the tensile strength and the dielectric strength vary with moisture content. The maximum tensile strength occurs when the moisture content is 5% but the dielectric strength falls off after about 3% [28]. So, there is a compromise between maximising dielectric strength and tensile strength. 3% is considered to be the maximum allowable water content for practical use as, beyond this, the dielectric strength falls and the dielectric losses of the paper rise. This explains why 3% moisture content is taken as the moisture limit for insulation in transformers.

Pressboard presents a slightly different picture and does not absorb moisture as rapidly as paper. The rate of moisture absorption depends upon the thickness and density of the pressboard as well as the ambient conditions of temperature and relative humidity [56]. Moisture absorption for pressboard is thus in terms of hours and days rather than in minutes as for paper although pressboard dries as quickly as paper at 105°C.

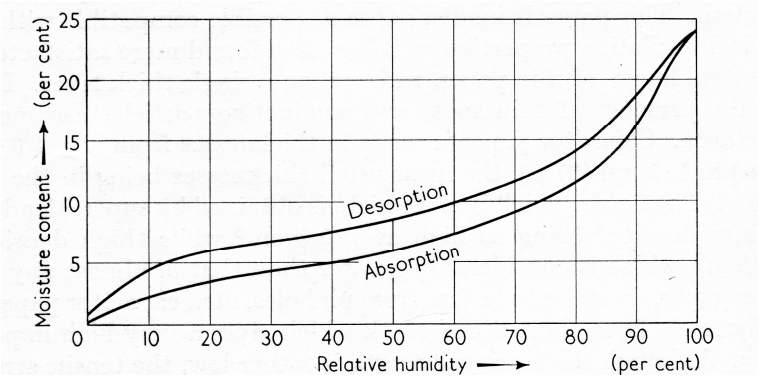

Figure 2.6 Variation of paper moisture with RH [28]

Research into how moisture in the paper and pressboard affects the insulation is usually achieved by subjecting conditioned paper and pressboard samples in a mineral oil using thermal means as the accelerating mechanism for ageing. The conditioning parameter is taken as initial moisture content and the studies examine the ageing profile using ageing markers such as DP or furfural analysis. The initial moisture content proves to be significant as one study shows that higher initial moisture content increases the rate of ageing. [57]. Temperature is crucial as an ambient temperature higher than 70°C increases the ageing rate as measured by DP and temperatures greater than 90°C affect the tensile strength [58]. Other research using dielectric strength and dissipation factor as the study parameter confirms initial moisture content and temperature as the significant degradation mechanisms on paper [59]. This research supports the original work that low operating temperatures and minimum cellulose moisture content will give greatest chance for a slow ageing profile.

2.6.4 The effect of moisture on oil

Oil is hydrophobic and oil and water do not readily mix but the real problem with moisture in oil is that, even in small amounts, it has a marked effect on the dielectric strength of the oil as shown in Figure 2.7 [60]. The breakdown characteristic is well characterised and current studies are more concerned with the effect of electrode shape and small gaps/spacing on voltage breakdown [61] or large gaps on streamers [62].

Moisture in oil has no effect on the ageing of the oil and is really only an indicator of contamination which is clearly stated in the standard for the measurement of oil breakdown [39]. Guidelines are given for acceptable levels of moisture according to transformer category in the standard for insulating oils in electrical equipment which

defines a minimum breakdown of 55kV/mm and a maximum water content of 10ppm for transformers rated at a minimum system voltage of 170kV [39].

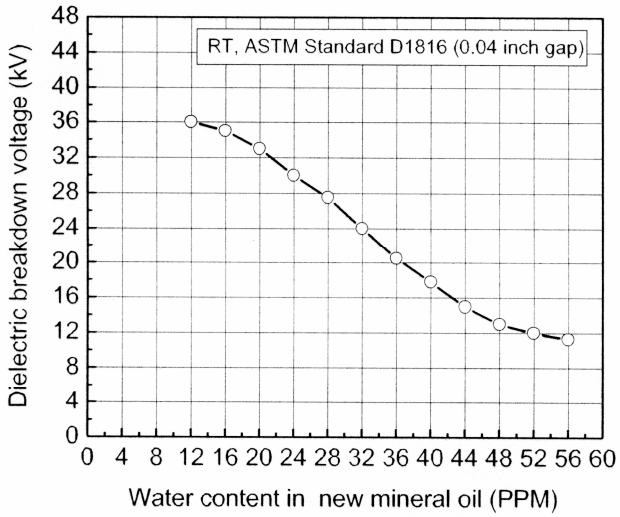

Figure 2.7 Voltage breakdown of oil due to moisture content [60]

2.7 The degradation process of paper/pressboard

Moisture affects paper and pressboard by depressing the voltage withstand and also the mechanical performance. However, the cellulose is also affected chemically by thermal and electrical stresses. A concise overview of the cellulose degradation process is given by Oommen [47] which describes three mechanisms for paper degradation. The principle mechanism is where the cellulose polymer chains are broken into smaller chains (termed chain scission) by thermal and high energy electrical activity to release CO, CO_2, water and furanic compounds. The water itself can break the cellulose polymer chains into smaller chains thus providing a second hydrolytic mechanism. Finally, oxidation of the cellulose chains results in a third mechanism to release CO, CO_2, water and acids. Lundgaard et al. [58,63] suggest that the oxidative mechanism may be the first process to cause paper degradation in new insulation when both the moisture and acid content are low. Thereafter the oxidation process is suppressed by the increasing acidity and the acids result in acid catalysed hydrolysis promoting the hydrolytic mechanism. Water is thus more significant than oxygen because of the hydrolytic catalytic reaction. Paper ageing is the combined result of three processes which slowly evolve water, acids and gases with thermal and electrical activity driving the main degradation process.

The presence of furanic compounds has enabled the use of a secondary method for determining the ageing of paper along side that of the DP method as outlined in §2.1. Furanic compounds are a range of heterocyclic organic compounds generated by either the low temperature oxidative process or the pyrolytic process at temperatures above 130°C [57]. The range is illustrated in Figure 2.8 with 2 furfuraldehyde or furfural being the most stable. Furfural is soluble in oil and can be detected in very low concentrations at less than 0.1ppm, using High Performance Liquid Chromatography (HPLC) [64] For concentrations of the order of 1ppm, a simple colour change test (using glacial acetic acid and aniline)can be used. A HV transformer, subject to high temperature paper degradation would show 1ppm of furfuraldehyde after about 10 years rising to 4ppm after about 40 years.

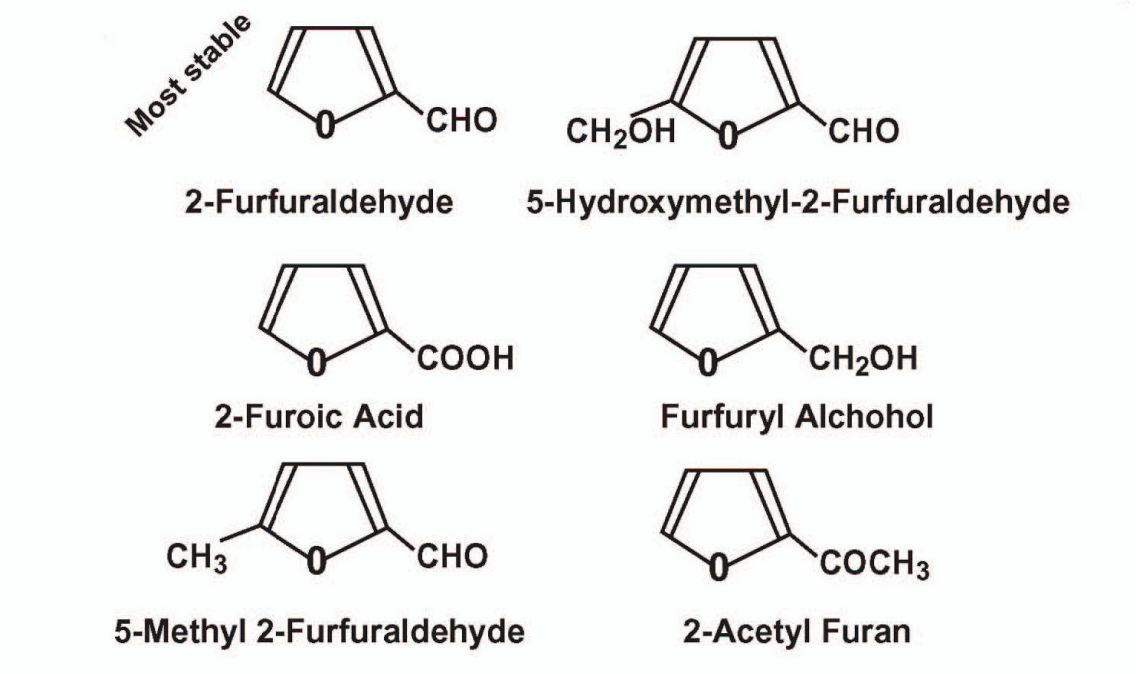

Figure 2.8 Furanic compounds resulting from paper degradation [47]

2.7.1 The degradation process of oil

Moisture and other physical particles affect oil such that the contamination only depresses the voltage withstand characteristic but it does not otherwise age the oil. However, the oil is aged by thermal stresses, electrical stresses (discharges), chemical actions caused by oxidation and the by-products of other processes and the presence of metallic catalysts [41]. The change in the oil is most marked by a visual change from transparent light yellow colour to a dark (usually) reddish/brown as well as changes to

electrical properties such as tan δ and resistivity. Palmer et al. [65] explain that the change in the colour spectrum is due to degradation of the paraffinic compounds into naphthenic and aromatic compounds with the creation of the UV absorbing double bonds. A significant feature of oil degradation is in the evolution of gasses such as hydrogen, acetylene and methane and ethylene. All these properties have been developed into distinct ageing and monitoring techniques with dissolved gas analysis (DGA) the preferred oil based method for insulation conditioning monitoring. A summary of the available oil assessment techniques is contained in BS5730 [39] along with the applicable standards for each test.

2.7.2 The degradation process on the combined paper/oil insulation

Transformer insulation is a three dimensional composite system of mineral oil and cellulose in the form of paper and pressboard which is acted upon by a range of stresses. The stresses do not act in isolation but in a synergistic way which chemically degrade both the mineral oil and cellulose. The cellulose degradation results in the generation of water, oxidising by-products and heterocyclic organic compounds knows as furans which dissolve in the oil. The mineral oil degradation results in the formation of acids and sludge and the evolution of hydrocarbon gasses. The chemical degradation process is self-sustaining with the evolution of water and acids which act further on the cellulose and compromising the electrical properties of both the insulation and the transformer as a whole. The changes in the properties are used as means of measuring the ageing process itself. This has lead to the development of a wide number of diagnostic tests. These tests have evolved to such an extent that a mature industry exists which works to a set of internationally accepted standards. The industry is known as condition monitoring and diagnostics with the goals of asset management and life extension.

2.8 Asset management through condition monitoring

A range of techniques have been developed which can be broadly divided into those measuring the by-products of internal paper/oil ageing or black box electrical tests on the transformer. Paper degradation is a key indicator of transformer life. However, the problem with age assessment of paper insulation is that it is virtually impossible to access the paper in an enclosed transformer. In addition, the location from which the paper sample is taken is critical as it may not be obtained from a “hot spot” which is

where an ageing failure is most likely to occur. Hence, the by-products of paper ageing dissolved in the oil are used as the ageing indicator.

Contemporary reviews of the available range of diagnostics tests as used in asset management are given by Ward [66] and Wang [67]. These review the range of available diagnostic tests such as water content, (acid) neutralisation number, dielectric breakdown and DGA and the black box tests such as frequency response analysis (FRA), recovery voltage measurement (RVM), power factor analysis and partial discharge measurements. The papers highlight some of difficulties of condition monitoring such as the cost, measurement problems and data interpretation. For example, the RVM technique, devised in the 1970's as a method of determining the moisture content of the cellulose insulation, became a favoured industrial technique in the 1990s. However, the technique requires a transformer to be taken out of service for a long time in order to establish equilibrium and make the tests [68,69]. Also, the determination of the true cellulose moisture content is difficult due to the complexity of the insulation structure [67, 70]. RVM is now viewed as a comparative measurement tool rather than an absolute measurement for moisture determination.

Another review from a UK network operator's perspective is given by Checksfield and Westlake [71] which suggests that a combination of automated on-line diagnostics coupled with off-line DGA is a successful strategy for condition assessment. The focus of current research in the science and application of transformer diagnostics is about improving the accuracy and reliability of the measurements and measurement systems or considering unusual phenomena observed in equipment operation.

Hohlein [72] examines the phenomenon of oil gassing which is the evolution of hydrogen and hydrocarbons at low temperatures which may interfere with DGA measurements. A study on working transformers indicates that the stray gassing is strongly temperature dependant and may be due to the use of hydro-treated oils and catalytic action grain orientated steels. Duval and Dukarm [73] address the inherent inaccuracies of DGA by proposing statistical calculations to improve the confidence factor at low gas concentrations. The effect of catalytic action by copper on oil ageing (both mineral and synthetic oils) has been demonstrated by laboratory aged experiments

with correlated changes recorded in oil acidity, the UV/Vis spectrum and dielectric spectroscopy all of which may offer new techniques for oil ageing diagnostics [74].

In the case of research on paper and pressboard, the aim is to improve methods of equipment age estimation to avoid the destructive process of taking paper samples. The recent innovation is the development of a reflective infra-red technique of determining the DP of paper without having to take samples of the paper insulation [75,76].

In the case of black-box techniques, current focus of research concentrates on PD measurements. General overviews of the PD technique applicable to all electrical machinery together with its applications and problems relating to data acquisition and interpretation are given by Bartnikas [77] and Stone[78]. Due to the size of transformers, localisation and interpretation of PD and not the actual detection of the PD is the prime concern. Current research is about the development of acoustic, UHF and optical fibre techniques to more precisely pinpoint the PD sources [79,80,81,82]. These techniques also offer electrical isolation over the standard directly coupled electrically based PD measurement technique.

2.8.1 Options for asset management and equipment life extension

The asset management activity is the continuous balance of cost and system performance against the risk of failure [9]. The role of the condition monitoring is to enable the network operator to make decisions in order to meet these goals. In terms of the liquid cellulose insulation the minimisation of moisture is still seen as the key to life extension [83]. It is now an established commercial activity with the following options open to a network operator:

- Oil drying by various process methods. These include on-site vacuum drying (termed oil reconditioning or purification) using either hot oil circulation or low frequency heating or return to factory for a hot vapour phase oven process [84].
- Oil reclamation where the oil is put through an additional chemical filter [85].
- Replacement of the oil.
- Refurbishment where the transformer is returned to the manufacturer for the winding assembly/insulation parts to be replaced.
- Transformer replacement.

Oil drying or reconditioning takes advantage of the moisture equilibrium mechanism where water moves into the oil at high temperatures. Reclamation requires the use of fuller's earth or zeolites which is an added cost and leaves the problem of disposal of the contaminated filter material. Reconditioning only removes moisture which improves the dielectric withstand whereas reclamation removes both the moisture and changes some of the ageing indicators such as acidity and UV/Vis characteristic [86]. Moisture extraction through the hot oil techniques also carries a risk of post processing failure as reported by Wasserberg [87] which is thought to be due to the change in the paper structure surrounding the conductors. In the case of oil retro-filling processes, the aged oil cannot be totally removed and the new oil is partially contaminated by a percentage of the old oil [88]. The refurbishment option is more expensive than oil processing techniques but gives a cost advantage over total equipment replacement. It is considered where the equipment type is in current production and use can be made of the existing mechanical containment vessel. Transformer replacement is the last resort as this is the costliest option. Refurbishment and replacement offer two more advantages in that a design with the latest technical innovations is put into service and the life clock for that particular asset is effectively re-set to zero.

2.9 Summary

A state of the art review has been completed covering recent research into cellulose and oil degradation, the moisture equilibrium mechanism and conditioning monitoring. The ageing of the oil/cellulose insulation is the result of the interaction of four stresses with heat and moisture being the dominant factors. The action of the stresses leads to a chemical change in both the oil and the cellulose structure which results in corresponding changes to the chemical and electrical profile of the transformer. The chemical changes are self sustaining with the evolution of water, acids and gasses which are the by-products of the ageing. An important part of the ageing process is the moisture equilibrium mechanism which explains how water migrates between the oil and paper according to temperature.

The by-products of the chemical changes due to the changes in the insulation have been developed into a set of conditioning monitoring tools. There is also available a set of black box measurement techniques which use electrical based parameters as indicators

of degradation and insulation breakdown. These are used by a mature and established industry to monitor and maintain HV transformers as part of the asset management strategy for network operators. Current research is focussed on developing certain techniques with the aim of improving interpretation of condition monitoring for asset management. The research addresses the chemical changes and the electronic techniques to measure them. However, all the techniques merely measure symptoms of degradation and hence are of little use in the determination of failure mechanisms such as tracking. Tracking occurs as a result of electronic action which is influenced by the electromagnetic environment and these topics are explored in the next chapter.

Chapter Three

Electrical processes within the transformer

Electrical resistivity is the measure of the resistance of a material to the flow of current. It is a function of the mobility of the charge carriers within the material and leads to three broad classes of materials under normal conditions; insulators, semi-conductors and conductors categorised by their resistivity in Ωm (the inverse of which is termed conductivity in Sm^{-1}). A typical conductor such as copper has resistivity of the order of 10^{-8}Ωm whilst an insulator such as polyethylene exhibits resistivity of the order of 10^{15}Ωm. This huge dynamic range is a result of the way in which the individual atoms join together to form a material structure and is generally explained by band gap theory covered by many standard texts [e.g. 89,90]. The resistive property of insulators gives these materials two characteristics which are individual to a particular material. The first characteristic is polarisation which is the accumulation of charge when the material is subject to an electric field as the material does not intrinsically conduct electricity. The second characteristic is dielectric breakdown which is the process of material degradation due to the ionisation of the material structure when the electrical stress exceeds the intrinsic bulk dielectric strength.

3.1 Dielectric polarisation

The way in which charge carriers move or are prevented from moving within an insulation structure is determined by two factors. The first is how the atoms within a

molecule are bound together to form the banding structure. The second is due to the molecules themselves and how they interact to form crystal elements or interact with different molecules. Polarisation is described using macro and micro models.

3.1.1 Macro model of polarisation

Consider the dielectric arrangement of an ideal capacitor plate where the homogenous insulation material is sandwiched between two conducting plates, Figure 3.1. When an electric field, E is applied between the plates, charge accumulating on the right hand plate at the inter-facial boundary gives rise to a mirror charge +Q which repels the bound charges inside the dielectric. This ripples through the dielectric until the electrons accumulating on the left hand interfacial boundary gives a charge – Q′ on the boundary resulting in a mirror charge of +Q′ at the left hand plate.

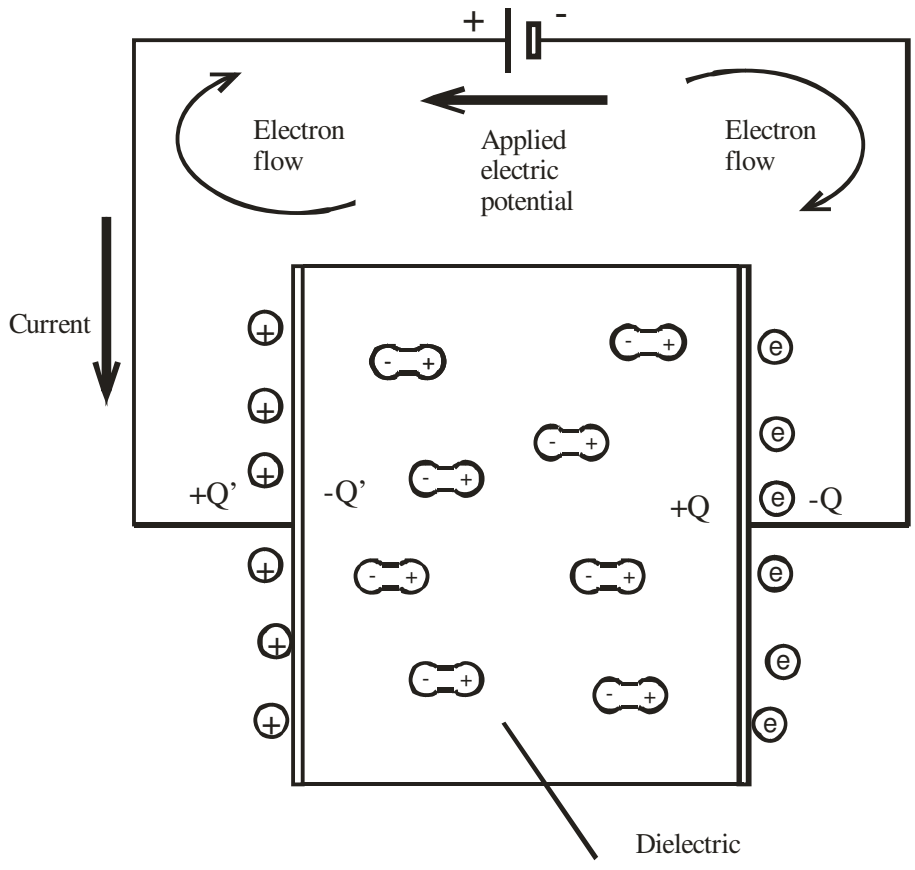

Figure 3.1 Capacitor plate with dielectric

The resultant field inside the dielectric is termed the Displacement field, D, and is (using vector notation):

$$\vec{D} = \vec{E} + \vec{P} \qquad (3.1)$$

where $\vec{P}$ is the polarisation vector associated with the introduction of the dielectric material implying that $\vec{D} = \vec{E}$ when in the dielectric is a vacuum. If D and E are now the electric forces per unit charge (i.e. electric field densities), P is the polarisation charge density associated with the introduced dielectric, then

$$\varepsilon E = \varepsilon_0 E + P \tag{3.2}$$

$$P = \varepsilon E - \varepsilon_0 E \tag{3.3}$$

$$P = \varepsilon_0 E\left(\frac{\varepsilon}{\varepsilon_o} - 1\right) \tag{3.4}$$

$$\frac{\varepsilon}{\varepsilon_0} = 1 + \frac{P}{\varepsilon_0 E} \tag{3.5}$$

$$\varepsilon_r = 1 + \chi_e \tag{3.6}$$

where ε_r is the relative permittivity and χ_e is the electric susceptibility. The material property of relative permittivity therefore defines the level of polarisation.

3.1.2 Micro model of polarisation

At the molecular level, the polarisation field is due to the following components [91]:

- Electronic polarisation, α_e, caused by the displacement of electrons within the atom due to the applied field.
- Ionic polarisation, α_i, which is due to the displacement of ions within the structure.
- Dipolar polarisation due to the displacement of permanent dipole moments, α_d, of complex molecules within the structure.
- Interfacial polarisation, α_f, which is polarisation localised at the interfacial boundary between composite materials such as the liquid-paper interface or at the boundaries of adjacent crystals in solid dielectrics and most notably at a metallic –insulator interface.

(Note: Alternative terms for these polarisation mechanisms are used. Electronic polarisation can be termed optical polarisation because the mechanism is caused by the elastic displacement of electrons. Dipolar polarisation and ionic polarisation are the result of the molecular structure and are sometimes considered together and termed molecular polarisation. The dipolar polarisation itself can be termed orientational polarisation because the mechanism is due to rotation of the molecule with the applied field. Finally, electronic and ionic polarisation can be lumped together and called distortional polarisation to distinguish it from the orientational polarisation.)

If the number of atoms or molecules per unit volume is N, then, using the Theorem of Superposition:

$$P = N(\alpha_e + \alpha_i + \alpha_d + \alpha_f)E \qquad (3.7)$$

This is the Clausius equation which relates the overall polarisation due to an electric field to the sum of its polarising components [91] and hence links the micro model to the macro model via equation (3.4).

3.1.3 Frequency response of polarising mechanisms

Electronic and ionic polarisations are associated with the electronic distribution around the atom and molecule respectively. The electrons respond very quickly to the application of electric field and thus, the electronic and atomic polarisation responses occur in the MHz to GHz region of the electromagnetic spectrum. This is a feature of mono-atomic gases and ionic solids. They can be classified as inherently non-polar materials. Dipolar polarisation is due to the movement of complex molecules and this is a feature of polarising liquids. This response is dominant in the MHz region. Interfacial polarisation is as a result of the movement of charge carriers through an insulation structure which gather at dielectric discontinuities. This response is dominant in the low frequency region (less than 100Hz) and hence primarily responsible for the charging and discharging effects seen in RVM and PDC measurements.

These charging responses of a material can be seen when the real permittivity ε' is plotted against frequency resulting in the dielectric spectrograph of the material. The change in permittivity with frequency is given in Figure 3.2 which shows the

contribution due to the specific polarising mechanisms. The frequency bands at which changes in permittivity occur are termed dispersion regions. Ionic and electronic polarisation mechanisms lead to sharp resonance regions whereas the dispersion region associated with interfacial polarisation changes more slowly and is termed a relaxation region [92].

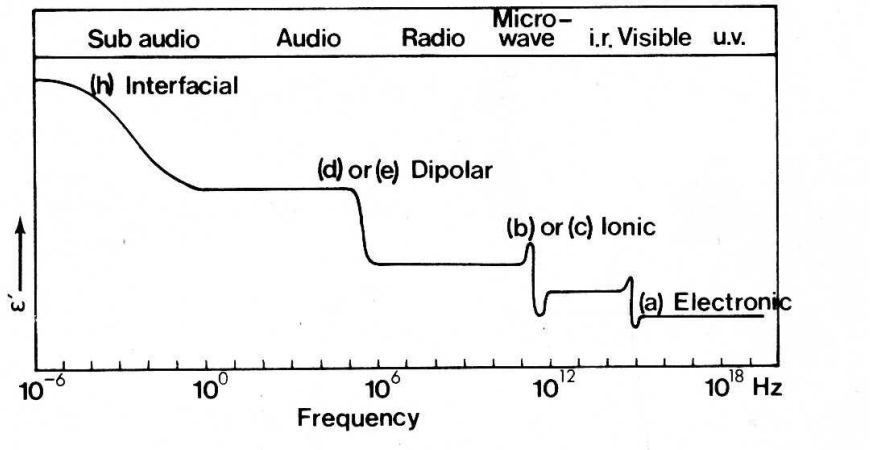

Figure 3.2 Real permittivity frequency spectrum [92]

The permittivity is clearly frequency dependent. Considering the parallel capacitive ac model from Figure 3.1, the current has real and imaginary components associated with the in-phase (or resistive element) and the out of phase (or capacitive element). From Ohm's Law, under a time varying electric field, the current i_C is related to the applied potential v by the capacitive reactance, i.e.:

$$X_C = j\omega C \tag{3.8}$$

$$i_C = j\omega C v \tag{3.9}$$

$$i_C = j\omega \varepsilon_r C_0 v \tag{3.10}$$

The permittivity ε_r is defined as a complex variable with real and imaginary components as follows:

$$\varepsilon_r = \varepsilon' - j\varepsilon'' \tag{3.11}$$

Thus:

$$i_C = j\omega(\varepsilon' - j\varepsilon'')C_0 v \tag{3.12}$$

$$i_C = j\omega(\varepsilon' - j\varepsilon'')C_0 v \tag{3.13}$$

$$i_C = \omega\varepsilon'' C_0 v + j\omega\varepsilon' C_0 v \tag{3.14}$$

The current in the capacitor thus comprises two out of phase elements. If the capacitor is almost ideal (i.e. with very low loss or $R_P \cong \infty$), then $i \cong i_C$. Thus, the (real) resistive current, i_R, is associated with the imaginary component of the permittivity and the (leading) or imaginary component of capacitive current, i_C is associated with the real component of the permittivity.

Also, since $$|i| \models \sqrt{(|i_R|^2 + |i_C|^2)} \tag{3.15}$$

$$\tan\delta = \frac{|i_R|}{|i_C|} \tag{3.16}$$

$$\tan\delta = \frac{|\omega\varepsilon'' C_0 v|}{|\omega\varepsilon' C_0 v|} \tag{3.17}$$

$$\tan\delta = \frac{\varepsilon''}{\varepsilon'} \tag{3.18}$$

Thus, for low loss i.e. $\tan\delta \to 0$, ε'' the imaginary component of permittivity (i.e. associated with the resistive element) needs to be zero. This is the background for the frequency response analysis method to assess the insulation condition over a wide frequency range. However, the dominant polarisation mechanism in large transformers, which operate at power frequencies, is the interfacial response. This is associated with dielectric discontinuities indicting that the design and physical structure of a transformer interact to form a key role in its dielectric response.

3.2 The transformer insulation structure

The typical three phase transformer is constructed with the three voltage coils physically positioned in line leaving two volumes known as the inter-phase barrier regions in

between. The design concept is a compromise between positioning the voltage coils as close as possible in order to minimise volume (i.e. material usage) whilst ensuring maximum clearance between the coils to avoid direct flash-over (i.e. to meet the voltage withstand test). The solution usually adopted is to place vertical pressboard barriers in a multilayered sandwich of oil and pressboard analogous to a mechanical labyrinth gland to increase the clearance distance through the addition of extra creepage distance.

3.2.1 The insulation structure as a holistic design concept

The design of insulation for equipment, as complicated as a large transformer, requires a co-ordinated approach. The mature manufacturing industry is able to take advantage of international standards governing general construction [93,94], a loading guide [95] and ancillary equipment such as tap changers [96] and bushings [97]. The two standards applicable to insulation are thermal classification [98] and insulation co-ordination [99,100].

These standards define external distances but, curiously none define internal spacing and distances. The principle adopted is that the level of internal insulation is determined by the manufacturer to meet the dielectric withstand tests as defined in BS171 [93] and BS EN 60071 [99]. Design curves for spacing and insulation are used by manufacturers which are usually commercially sensitive but a curve for creep length according to electric field strength is revealed by Nelson [101].

The insulation structure thus consists of a complex arrangement of paper, pressboard and oil surrounding the copper conductors and other metallic parts. The void volumes of the transformer are then filled with oil under an impregnation process to eliminate air and to fill the voids with oil. Within the structure there are many conductor/cellulose and cellulose/oil interfacial regions. In addition, there are other regions in which there are bulk volumes of insulation material such as thick sheets of pressboard or composite insulations around the bushings such as oil impregnated paper (OIP) or epoxy resin impregnated paper (ERIP).

When designing and building a large transformer, care must be taken over the small details as well as the larger construction. For example, small oil “wedges” will

inevitably occur throughout the insulation. An oil wedge is a triple point junction formed as two solid interfaces merge together within the oil volume. If the conjunction also happens to be in a region of high electric stress, PD activity may result due to the mismatch between the permittivity of the oil (typically 2.2) and that of the pressboard (typically 4.4). This concentrates the electric stress into the dielectrically weaker oil part. If the dielectric stress exceeds the oil breakdown voltage, PD activity may occur in the reduced dimension. It is a new driver for research into matching the permittivity of the oil and pressboard [102] to eliminate this type of PD activity.

Another factor to consider is the solid insulation material. The solid pressboard insulation is in fact not a "solid" but comprises a dense structure of cellulose fibres in which there are discontinuities and voids. The absorption of moisture and its extraction during the drying process confirms the existence of these voids. An overview of the fibrous pressboard structure, a model of breakdown mechanism and the effect of impurities on breakdown and partial discharge is given by Giese [103] which explains the decrease in intrinsic voltage breakdown with thickness [29]. The effect of cavities in pressboard on partial discharge and the implication of a poor impregnation is discussed by Wasserberg et al. [104] and confirms the importance of a good impregnation processes. The quality standards [33,34,35,36] do not include any tests for voids though apparent density and compressibility can be taken as such. However, the specifications include chemical tests for the detection of either embedded or surface inclusions of isolated metal fragments as these localised particles may be subject to field emission and generate space charge.

3.2.2 The model for the inter-phase barrier board

The inter-phase barrier board system is the sandwich of alternating pressboard and oil gaps (ducts). The design is based on the capacitive model with the principle that in a system with two dielectrics of different permittivity, the ratio of electric field strength in each material is in inverse proportion to the relative permittivity i.e.:

$$E_1/E_2 = \varepsilon_2/\varepsilon_1 \qquad (3.19)$$

The ratio of permittivity of the pressboard to oil is approximately 2:1 whilst the typical voltage breakdown/mm (30kV/mm) of the oil is less than the voltage breakdown/mm for the pressboard (80kV/mm). The design is based on the ratio of permittivity and dielectric strength and adjusting the thicknesses of the oil and the pressboard to distribute the electric field strength such that the pressboard takes the larger proportion of the electric stress to take into account the enhanced stress as a result of the development of space charge at the interfacial layer. The method for calculation is given by Moser et al. [105] which establishes an ideal board thickness to oil gap ratio of approximately 1: 4. This ratio was adopted for the barrier board model used in the experimental phase. Moser's model is for a single barrier board but it can be extended to have more pressboard sheets at the expense of increased manufacturing complexity whilst remembering to keep a large enough oil gap between the pressboard. A design may have up to 5 pressboard sheets with 4 appropriately dimensioned oil gaps.

3.2.3 The interfacial layer in the inter-phase region

The interfacial layers existing in the barrier region are one of the major locations subject to the electrical polarisation phenomena. It is the change in the capacitance and conductance properties of the insulation with ageing or moisture which form the basis of the dielectric response methods of condition monitoring. However, although polarisation is not cited as playing a role in any of Sokolov's 7 failure scenarios, its very existence is a sign that space charge exists at the interfacial regions throughout the transformer especially in regions of small insulation thickness and subject to strong electric fields [89]. How electrical polarisation is enhanced through the interaction of electrical fields is illustrated in §5.4. The interfacial layer is also known to be susceptible to static electrification due to the oil flow across the pressboard surface.

3.2.3.1 Static electrification

The transformer industry first became really aware of static electrification problem in the 1970's [106] following failures which were initially unexplained. The phenomenon of static electrification due to oil flow is termed (ironically) as static electrification but is also variously known as flow or streaming electrification by other investigators. Static electrification is caused by the presence of the electric double layer (EDL) [107,108,109]. The EDL, first proposed by Helmholtz, describes the variation in

potential across a surface interface between two different materials usually a conductor and a liquid. It is analogous to the depletion zone in the transition region at the junction between p-n semi-conductors. In the case of the solid liquid interface, the model has been developed into the diffuse Guoy-Chapman Stern model (GCS) which comprises two layers; a Stern layer which carries the charge and a diffuse layer where the liquid molecules are more mobile [110].

The static electrification mechanism is the result of the interaction of the oil movement across the pressboard on the EDL where the oil can develop a charge depending upon the surface over which it travels. If the oil travels over a region where there is an availability of free electrons (i.e. a conducting surface), then the oil acquires negative charge. Alternatively, if the oil travels across pressboard, the cellulose hydroxyl groups tend to acquire a negative charge from the moving oil leaving the oil positively charged [111]. The oil then relaxes the charge as it approaches earthed surfaces. This causes a static field to build up which may result in a discharge [112,113]. Numerous transformer failures have been ascribed to static electrification by Crofts [106], Sierota [114] and others [108, 115]. Research has determined that static electrification is a function of many parameters including temperature and moisture but primarily pressboard surface condition and oil condition (electrical charging tendency, ECT), [106,107, 116]. Dry oil and dry pressboard and surface roughness increase the likelihood of static electrification [106]. Paillat [113] has suggested that the presence of carboxylic groups also increases static electrification which has led to the proposal of the use of additives to combat the tendency [109, 117]. Static electrification is modelled using the macro-model parameters of permittivity and conductivity [111].

It is clear that interfacial polarisation and static electrification have the same roots through the charging tendency of different materials when in close proximity. This suggests that the two phenomena are different aspects of the EDL. Although static electrification has been attributed to transformer failure, the current view of National Grid is that static electrification is not thought to be the mechanism responsible for the electrical breakdown of inter-phase pressboard in the UK [118]. However, it raises the issue as to the possibility of a link between the electric field which leads to polarisation and static electrification caused by oil flow.

3.3 The different types of electrical breakdown

Chapter 2 has illustrated that insulation ageing is a multi-factorial process under which insulation slowly degrades over time with electrical and thermal activity being the dominant stress mechanisms. This explains why equipment will last many years and/or will continue to operate with a multitude of minor faults with an eroded margin of safety until some significant stress event overcomes the inherent resistance to failure as depicted in Figure 1.1. Failure thus depends not only upon the stress intensity but also the type of stress and the insulation structure.

Like ageing, electrical breakdown is also multi-factorial process. It depends not only on the electric stress but also upon the material, the temperature, the electromechanical environment and the condition of the material in terms of age profile and defect content [89]. Electrical breakdown is a space time event which leads to a continuum of possible scenarios. It can happen rapidly and extensively as in the case of flash-over or lightning and these are classified as streamer processes. Alternatively, it can occur as a localised process such as partial discharge and/or tracking. The rapid events are highly destructive and spell the end of insulation life whilst the localised processes occur over long periods of time [14]. In the case of solid insulation (such as polymers), electrical stress is the most significant element for rapid insulation breakdown which can occur within nanoseconds with thermal and electromechanical stresses as slower secondary factors. The solid insulation breakdown model considers 1000 seconds as the threshold for classification between breakdown and degradation with partial discharge considered as a symptom of the breakdown process [89]. Liquid and gaseous insulators have an advantage over solid insulation. These materials are effectively self healing as the insulation properties are restored (though slightly degraded) if the excessive electrical stress is removed [119]. Contamination with particles or bubbles plays a significant role in the breakdown process for liquid and gaseous insulation through PD activity. [120].

Research into electrical breakdown can be divided into the rapid destructive processes associated with streamer breakdown and pre-breakdown phenomena or the slower processes of tracking or partial discharge. Streamer breakdown in oil has been studied by a number of investigators such as Forster, Chadband, Lundgaard and Lesaint where the emphasis is on the bulk properties affecting the rapid breakdown process

[121,122,123,124]. However, the aim of this project is to investigate the slower low energy tracking process rather than the fast high energy streamer and breakdown processes as the presence of tracking or partial discharge (i.e. the evidence from Sokolov's 7 breakdown scenarios) indicates that the slower electrical degradation process is occurring rather than fast breakdown. However, electronic charge is clearly always associated with both fast electrical breakdown and the slower process of electrical degradation.

3.3.1 Charge emission

Charge emission will occur from bare conducting surfaces according to the modified Schottky process when a conductor is in a region of high electrical stress [119, 125]. This explains why great care is taken when designing and building oil filled transformers. The aim is to ensure that all conducting surfaces have blended geometries and are covered by paper (i.e. cellulose) insulation material. The solid insulation prevents the free emission of the charge into the oil. However, space charge can form at the pressboard/oil interface [126] due to the polarisation response. If the insulation is damaged through a mechanical or manufacturing fault, ageing of the insulation or the presence of a defect in the insulation, then, space charge may develop at the conductor/oil interface [127] in the EDL. Alternatively, charge emission may also occur from an exposed conductor due to photo-ionisation as a result of UV light arising from internal discharges [128]. Significant charge is also generated through partial discharges due to the interaction of high electric stress on insulation defects. The electric charge can lead to degradation of the solid insulation which is termed treeing or surface tracking depending upon the degradation characteristic. (Note: The charge emission mechanism, through the Schottky process, provides the method by which charge will be introduced under controlled conditions into the oil/paper dielectric system for the test cell as described in Chapter 5).

3.3.2 The difference between treeing and surface tracking

Charge emission on a solid insulation results in mechanical and chemical damage to the insulation as outlined in Chapter 2 through the action of excessive heat. For solid insulators the damage on the surface is termed tracking whereas the damage through the bulk of the (solid) material is termed treeing. In both cases, the permanent conductive

path reduces the voltage withstand of the material. It is the surface tracking behaviour which is of particular interest in this study. Tracking has long been associated with solid-air interfaces and polymeric insulators [129] and an historical overview is given by Yoshimura [130]. However, surface tracking is now acknowledged as a feature in the oil cellulose insulation interfaces as identified by Sokolov [14]. The term "creeping" discharge is used to describe the characteristic irreversible tree like patterns occurring on the interface as a result of the surface discharges. Surface tracking may deteriorate the surface resistance to such an extent that a sudden discharge flash-over may occur if the electrical stress is high enough. The sudden electrical breakdown over the surface is referred to as surface flashover thus implying that the breakdown occurs in the medium above the surface [131]. Substrate material, surface finish, surface contamination, condition of fluid material, temperature, pressure of fluid, level of applied electric stress and duration of application have been identified as the significant factors [130] (which are the same factors as involved in static electrification identified in §3.2.3.1). The degree of tracking or damage is a function of the duration and frequency of the surface discharges. In the case of a surface flashover, the degree of damage is a function of the energy of the discharge.

The measure of the resistance of solid insulation materials to tracking in air is given by the Comparative Tracking Index (CTI) standard [132]. Two such tests are described using either a horizontal surface or an inclined slope. The tests employ a liquid contaminant sprayed in droplet form onto the solid surface to promote the tracking. The standard does not consider a fluid medium above the surface other than air. This raises the issue as to how to quantify surface tracking at a liquid-solid interface. However, surface discharges result from partial discharges. Fortunately, PD forms repeatable and characteristic discharge patterns. These patterns offer a means for fault diagnosis and analysis to give an indication of insulation condition but not the age of the insulation.

3.4 Partial discharge

A partial discharge is defined as "an electrical discharge which only partially bridges the insulation between conductors and which may or may not occur adjacent to the conductor [120]." Partial discharge occurs in solid, liquid and gaseous insulations wherever there are sharp changes or discontinuities within the insulation medium *and*

where the electric field is sufficiently high to exceed the local breakdown value [89]. Surface contamination is a potential site for partial discharge due to the presence of inclusions and changes in bulk material.

The classic case for partial discharge within ac systems occurs when a small gas filled cavity, within a solid insulation, is located in an electric field at high electric strength. The cavity, modelled by the parallel capacitive network, is shown in Figure 3.3.

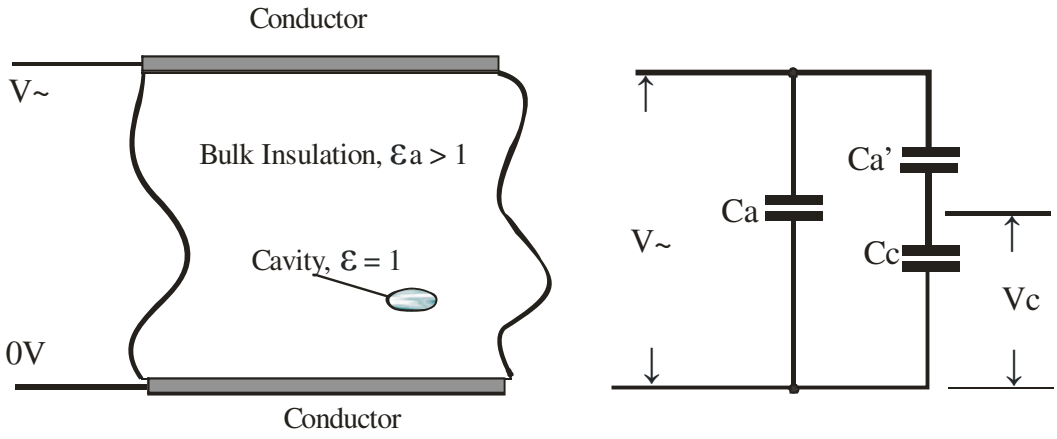

Figure 3.3 Cavity in insulation modelled as a capacitor

The small capacitance C_c has a lower permittivity (i.e. higher impedance value) than the bulk of the insulation (i.e. Ca and Ca') and is subjected to a proportionately higher electric field. If the local electric field exceeds the intrinsic breakdown voltage, V+, of the gas in the cavity, then, ionisation of the gas occurs. The positively and negatively charged ions impact on the cavity surfaces leading to erosion of the bulk material. This leads to the formation of the trees within solid insulation material. Similar processes occur in bubbles within liquids or at surface interfaces such as between solid and liquid insulation. In the latter case, the material erosion on the surface is known as tracking.

With each partial discharge there is a collapse of the electric field across the cavity shown diagrammatically as a fall in the cavity voltage Vc, Figure 3.4. If the system voltage is still rising, other partial discharges may occur resulting in a sequence of small discharges. The voltage source endeavours to supply charge during each discharge process and this is manifested as small current pulses which are nanoseconds in duration. They may be negative and/or positive depending upon the supply voltage. The existence of the current pulses provides the basis for the electric method for PD

detection and standard patterns have been established which are characteristic of the partial discharge mechanism.

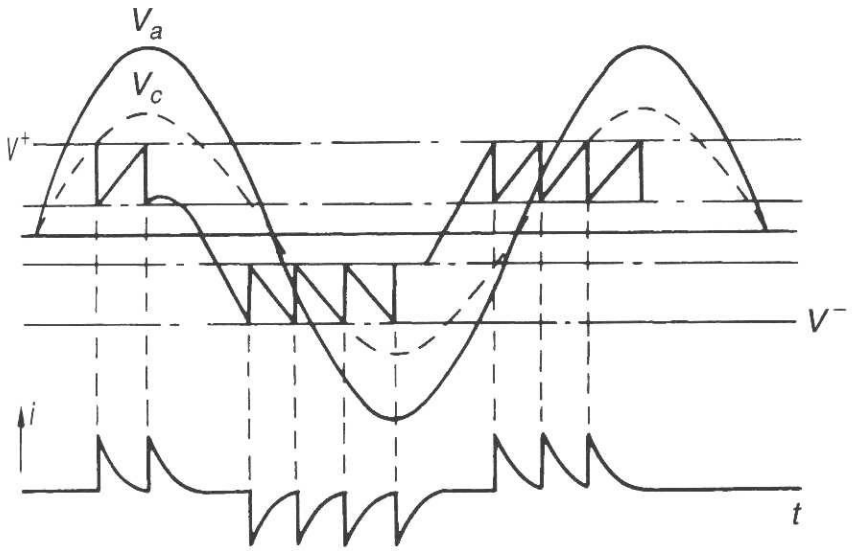

Figure 3.4 Partial discharges under ac voltage with associated current pulses [120]

3.5 PD patterns and their interpretation

PD detection is one of the diagnostic tools available to network operators to help assess the condition of transformers. PD detection relies on the measurement of either the acoustic, electrical, UHF or mechanical (i.e. pressure) energy which is released during an electrical partial discharge. The advantages of PD measurement are that they are non-destructive and non-invasive. However, all the techniques require sophisticated equipment, procedures and trained experts to interpret the results. PD detection using the electrical method is one of the easiest and most widely used techniques and it was chosen as the preferred investigative tool for this project.

3.5.1 The measurement and display of PD patterns

PD measurement using the electrical method requires a calibrated detection system, a means of visual display for real-time interpretation and a mechanism for data collection to enable post measurement analysis. The electrical method for PD measurement has evolved into a well developed investigative tool which is covered by the BS EN 60270 [133]. This standard gives guidance on the principles, definitions, acceptable detector circuits and procedures. The technique has been realised by industrial manufacturers

(e.g. Haefely Test, Robinson) who offer proprietary equipment to take care of the filtration and bandwidth constraints as defined in the standard.

The electrical method uses a capacitive coupling network in conjunction with a high impedance input, wide bandwidth amplifier to detect the peak current pulses and convert them into peak voltage representing the discharge. The peak voltages are displayed as vertical traces using a Lissajous figure on an oscilloscope to give real time data. The on-screen ellipse represents the continuous cycle of the mains supply with the ellipse implicitly taken as one cycle. The detector equipment is synchronised to the supply frequency so that the position of a pulse is related to its position in time (i.e. electrical phase) relative to the supply frequency. An individual pulse is thus defined in terms of its peak magnitude of charge, q (usually in picocoulomb) and its phase relationship, ϕ (in degrees electrical) with the supply. The sequence of PD pulses varies slightly over time for a fixed voltage. Some pulses may occur exactly at the same instant in the supply cycle as a previous pulse. The number of pulses which occur at a particular phase point in the cycle over a fixed number of cycles is termed n. Equally, other pulses may occur at slightly different times in the cycle. This accumulation and temporal shift of pulses over successive supply cycles results in a PD pattern which is characteristic of a discharge mechanism and/or insulation configuration. A PD pattern is then defined in terms of a 3D ϕ-q-n plot. These plots are used as a tool for insulation assessment and fault diagnosis. The polarity of the voltage cycle in which the PD pulse occurs is significant and the ϕ-q-n plot must indicate this to enable valid interpretation. As individual pulses last the order of nanoseconds, the real-time impression of a PD pattern depends upon the display screen persistence. This is satisfactory for "live" analysis but rather limited for later PD pattern interpretation. Hence, a means of data collection and storage is necessary to enable re-generation of the ϕ-q-n plots for later analysis. This is achieved by commercially available digital storage and display techniques.

For this project, a standard range of equipment was used for the collection of the PD data. The electrical detection of the current pulses was undertaken using a modular Haefely Trench measurement system [134]. The application and measurement of the high voltage is achieved using the regulating transformer unit, a HV transformer, a

computer operated control unit and a secondary measurement unit. The detection of PD is done using a 300kV rated 1nF HV coupling capacitor and coupling quadripole network to feed the low voltage PD response to the Robinson Model 700 PD detector used as the real-time display element. A block diagram of the system is shown in Figure 3.5 and photographs of the equipment are shown in Figure 3.6 Data capture and storage was achieved by means of a programmable Tektronix digital storage oscilloscope to store a "frame" of data comprising the PD pulses from 500 cycles. Each "frame" consumes 30Mbytes of data storage and a large amount of data storage capacity (more than 50Gbytes) was required to store the PD patterns collected during the data collection phase. The ϕ-q-n plots were visualised by means of a bespoke Matlab program which had been developed for a previous project. The data collection equipment was synchronised to the input side of the high voltage circuit and, due to the voltage inversion at the output of the Haefely HV transformer, the first half of the phase element in the ϕ-q-n plot represents data from the negative cycle of the supply voltage. Thus the ϕ-q-n plots have the phase axis labelled -180° to 0° and 0°to 180° elec. to denote the negative and positive cycles respectively.

3.5.2 Apparent charge and system calibration

The measurement of the PD pulse relies on its detection by means of the quadripole decoupling network which is remote from the actual site of the PD activity. The magnitude of the recorded pulse can only be proportional to the magnitude of the real partial discharge within the insulation. In fact, the actual magnitude can never be accurately calculated [120] and this is acknowledged by the standard [133]. To overcome the problem, the detection circuit must be calibrated to rationalise the scale of the detected pulse. The measured charge is then termed an "apparent" charge. Calibration is achieved by injecting into the measuring point a charge pulse with a defined magnitude (e.g. 5pC or 50pC). The magnitudes of the measured PD pulses are then referenced to the calibration pulse. Because any significant alteration of the circuit changes the overall circuit capacitance, the circuit must be re-calibrated each time a major change is made to the circuit.

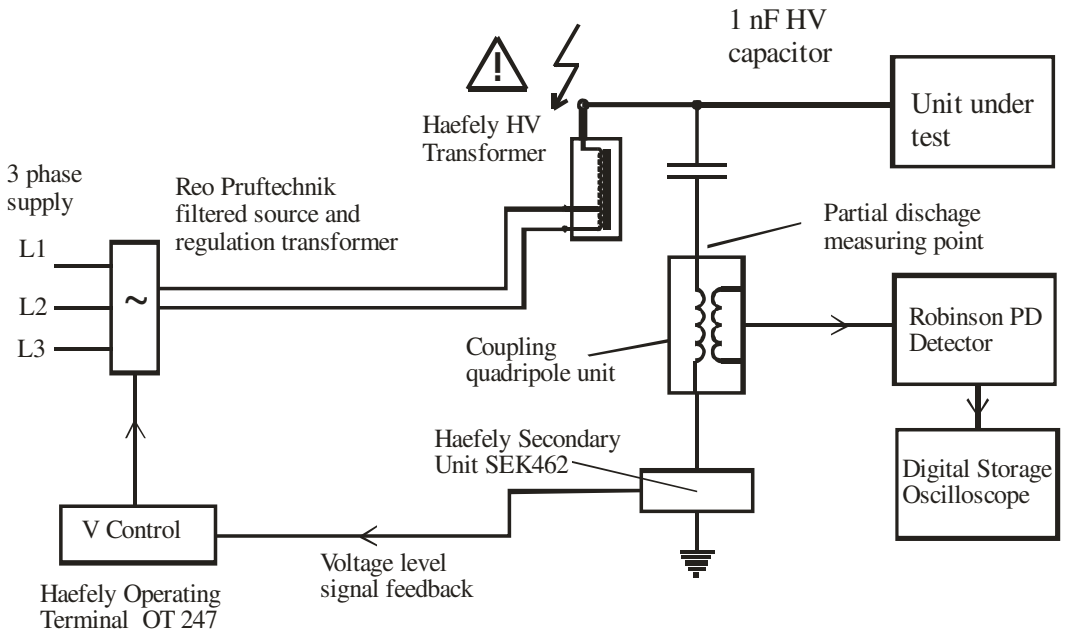

Figure 3.5 Block diagram of PD detection and measurement

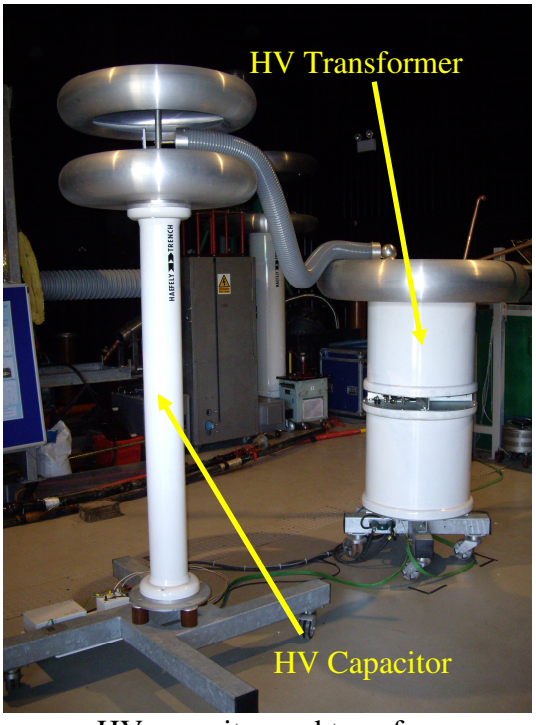

a - HV capacitor and transformer

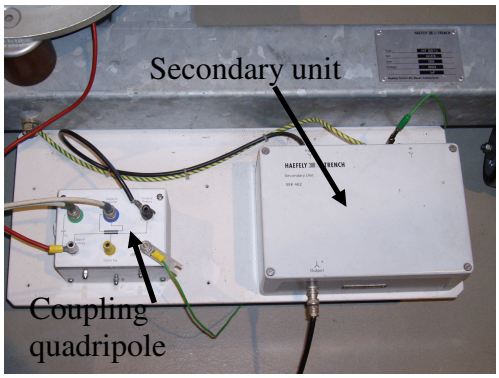

b - Coupling quadripole and secondary unit

c - Robinson Model 700

Figure 3.6 Equipment used in PD measurement

3.5.3 Representation of typical PD patterns

PD patterns are characteristic of both the insulation media and the configuration. Accepted discharge patterns have been documented by the CIGRE Working Group Committee No 21 for a range of typical insulation configurations and media [135]. For example, the PD pattern for surface discharge is characterised by discharges in the first and third quadrants. The PD pattern for corona discharge in an insulating fluid is characterised by discharges occurring around both peaks of the cycle with more discharges occurring in the negative cycle but with the discharge amplitudes greater at the positive peak. The typical PD patterns for these cases as would be seen in real-time on the Robinson and as a cumulative 2D ϕ-q plot on the Tektronix are illustrated in Figure 3.7.

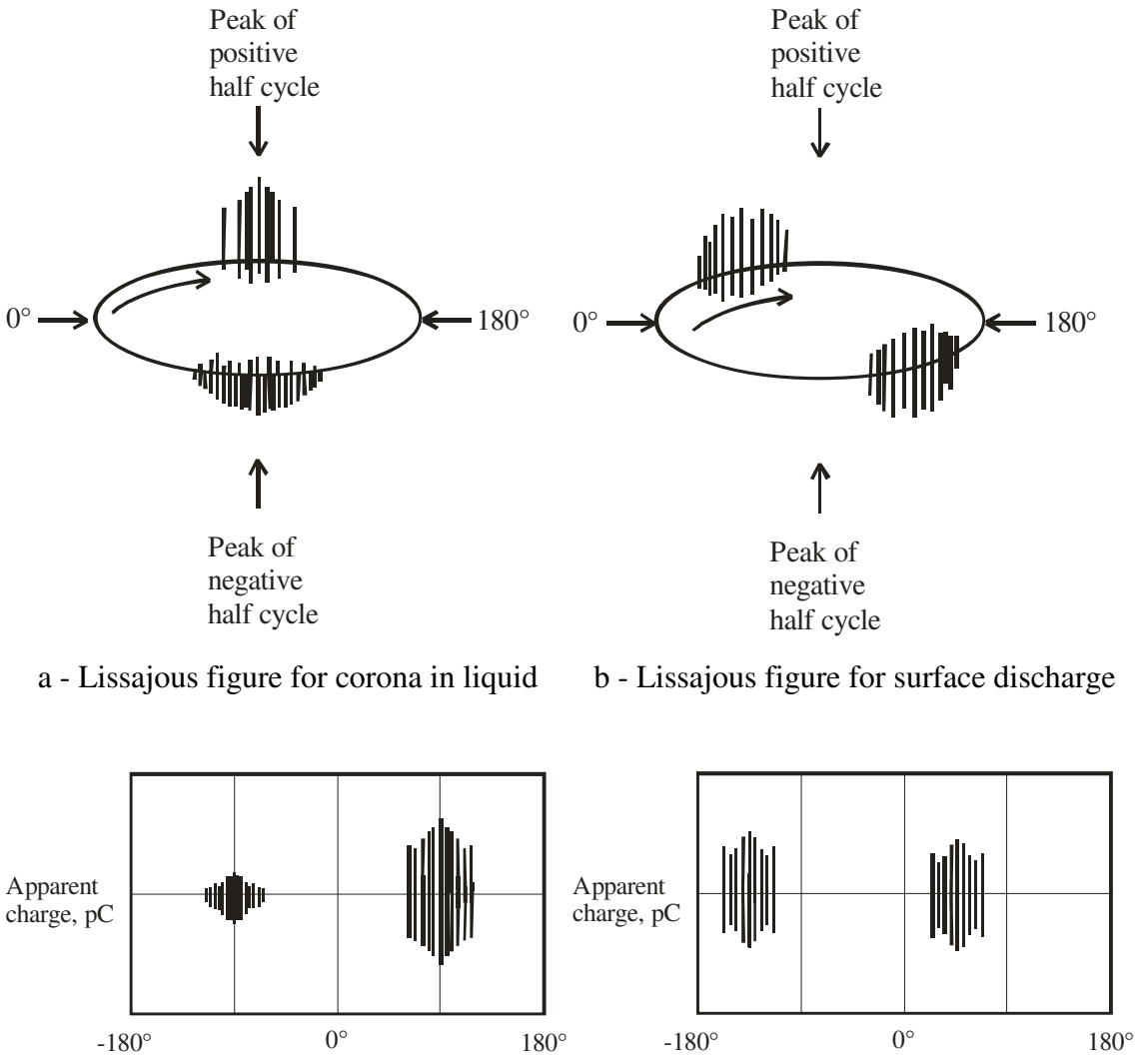

a - Lissajous figure for corona in liquid

b - Lissajous figure for surface discharge

c - ϕ-q plot for corona in liquid

d - ϕ-q plot for surface discharge

Figure 3.7 Typical Lissajous figures and ϕ-q plots for two types of PD

PD occurs at locations where a dielectric discontinuity coincides at a region of high electric stress. The three phase transformer has associated with it a time varying electric field which is the result of the interaction of the individual phase electric fields. Tracking and treeing are recognised signs of PD activity. This degradation has been identified in Chapter 1 to occur in the inter-phase region and bushing turrets. It infers that these constructional features are located in regions of high electrical stress leading to the possibility of an interaction between the construction feature and the general electric field. An overview of the transformer insulation structure is examined to find possible sites where and when the greatest electrical stress may occur.

3.6 Large transformer model using Finite Element Analysis

The insulation system of a large transformer operates in a multi-factorial environment comprising a time varying electro-magnetic field and thermal distributions which are a function of changing external loads and other factors such as the diurnal change in ambient conditions. The insulation is subjected to the ageing process which is the long term change of the material and system properties over time. Finally, the system is subjected to constant mechanical vibration at the operating frequency. The accurate modelling of such a practical large transformer is a complex time consuming task. However, given that the aim is to study the field distribution in the inter-phase barrier region, a simplified model has been developed by ignoring the thermal, mechanical stresses and the ageing processes. In addition, there are too many minor geometrical details occurring in a real transformer necessitating dimensional simplifications. For example, the inter-phase pressboard barrier was modelled with a single pressboard of equivalent thickness instead of a multilayered pressboard oil sandwich and only the electric field due to the high voltage series coils was considered.

3.6.1 Model characteristics

The model dimensions were based on proprietary information from a 400kV 1000MVA autotransformer in current production. The model considers a simplified arrangement of three phases in line separated by single (thick) sheets of pressboard forming the two inter-phase barriers with the overall internal dimensions of 7m x 2.5m x 2.8m. The wire frame outline is shown (Figure 3.8) with the phases 1, 2 and 3 taken as from left to right.

The model constants were programmed with the dielectric parameters of new oil and pressboard thus neglecting the effects of ageing. The voltage variables for the three phases were programmed with rated phase voltage of 230kV and 120° electrical phase shift with the peak voltage occurring mechanically in the centre of each phase coil. The volt drop per turn over the series coil was accounted for by programming a linear decrease in the voltage formulae in the model boundary conditions menu.

The voltage coils are cylinders placed adjacent to a plane surface which creates a divergent geometry. The electrical field at the surface of each barrier board is not uniform but varies both in time and position due to the physical arrangement and also due to the interaction between the time varying electrical fields from the adjacent voltage coils. Figure 3.9 shows the changing sequence of three dimensional electric fields showing the equi-potential (also known as iso-surface) contours for the model over ½ cycle at 30° elec. intervals and at rated voltage. (Note: the equi-potentials show the peak electric field distribution represented by a scale ranging from $3.6kVm^{-1}$ to $2.6MVm^{-1}$ corresponding to the change in colour spectrum from blue to red respectively with $1.6MVm^{-1}$ represented by the yellow contour). The central region of the barrier board along the major axis and the vertical edges of the barrier board closest to each winding are subjected to the greatest electrical stress as indicated by the red contour surfaces. The pressboard surface is therefore subjected to a peak electrical stress once every half cycle which is at 60° elec. and 240° elec. in the case of the region between phases 1 and 2.

An interesting event occurs at 90° later in time (i.e. at 150° and 330° in the case of the inter-phase region between phases 1 and 2) when the electric field reverses polarity promoting a sweeping effect along the surface of the pressboard. This is visualised in Figure 3.10 which is the 2D FEM model zoomed into the inter-phase region between phases 1 and 2 showing the streamlines (also known as flux lines) over the cycle from 144° elec. through to 154° elec. (i.e. a 556μs time span). This sweeping action is reported by Vincent et al. [136] as electrohydrodynamic movement during their study on carbon particle contamination.

The FEM shows that the transformer insulation structure is subjected to a dynamic electrical field which varies in both time and magnitude. Polarisation and charge emission is associated both with dielectric discontinuities and high electric stress. This raises the question as to how the changing electric field may affect space charge generated within the transformer such as say on one of the surfaces of the inter-phase barrier boards.

The model also revealed that it is only necessary to consider two adjacent voltage coils to simulate the field interaction on the inter-phase pressboard rather than three phases because the electrical field associated with one outer phase has little effect on the interaction at the barrier board between the centre phase and the other phase. This simplified the development of the laboratory experiment as only two high voltage supplies were required for the test facility to generate the two phase driven electrical fields.

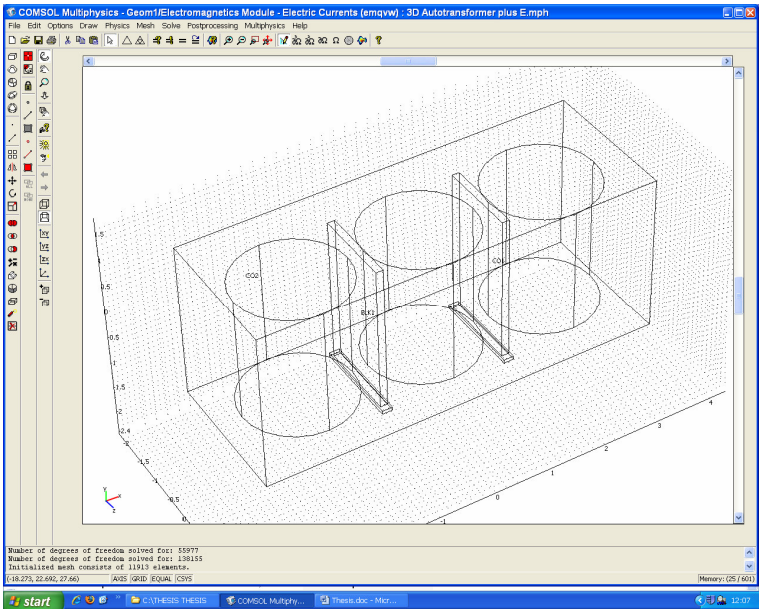

Figure 3.8 Basic wire frame model of 1000MVA 3 phase transformer in COMSOL

3.7 Summary

This chapter has considered the electrical charging processes and their interaction within a large transformer due to the structure of the transformer. The main electrical processes are polarisation and space charge development within dielectric materials and charge emission from conductors. The construction of a large transformer means that there are many possible sites for dielectric discontinuities and changes in insulation

material shape and form. The interaction between electrical stress and the transformer structure causes polarisation and space charge development whilst defects within the structure can lead to charge emission if conductors are exposed through insulation damage. Electrical charge damages insulation over time with high energy fast streamer processes leading to rapid dielectric breakdown of both solid and liquid insulation whilst partial discharges lead to a slower degradation of solid insulation known as treeing or surface tracking. Static electrification due to oil flow across pressboard has been identified as another charge generation process but no link has previously been made with polarisation even though both mechanisms are interfacial phenomena with similar factors.

The measurement of partial discharge is identified as a useful tool for the assessment of insulation condition. The basic theory of PD and its measurement using the electrical method were outlined as this is the preferred investigative tool for this project. The equipment and set-up for PD measurement was described as well as the expected PD patterns for corona discharge in liquid and surface discharge along a solid liquid interface.

Tracking along the oil pressboard interface is identified as the creeping discharge resulting from surface discharges. Historically, tracking is associated with the air-solid interface and no standard method for how to measure tracking on the liquid-solid interface was found.

A simple model of a three phase transformer has shown that the inter-phase barrier region is subjected to peak electric stress twice every cycle. This is due to the interaction of the time varying electric field (itself the result of the interaction of two phase related electric fields), on the divergent transformer structure. A hypothesis is proposed which suggests that space charge at the pressboard surface may be influenced by this general electric field. The next chapter describes the experimental apparatus constructed to test this hypothesis.

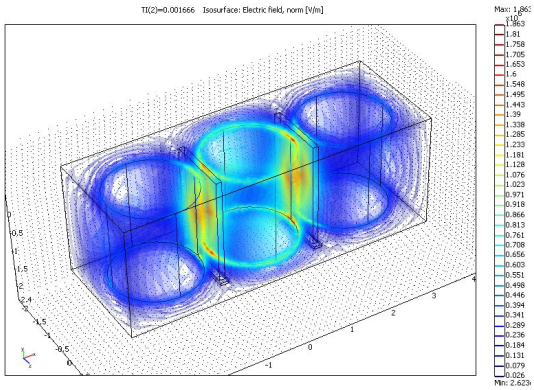

a - Model at time t0 + 30° elec.

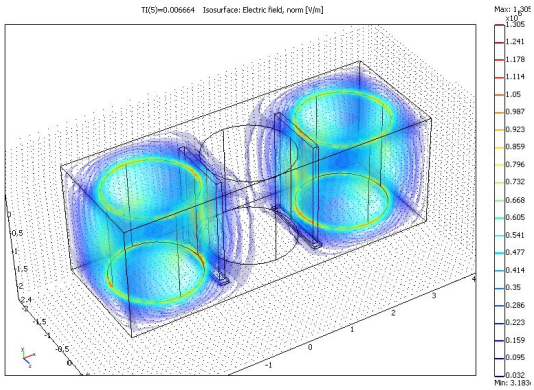

d - Model at time t0 + 120° elec.

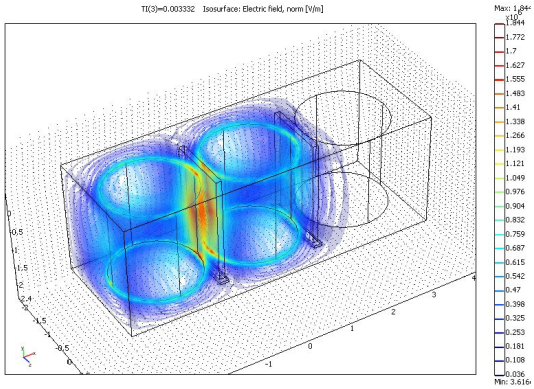

b - Model at time t0 + 60° elec.

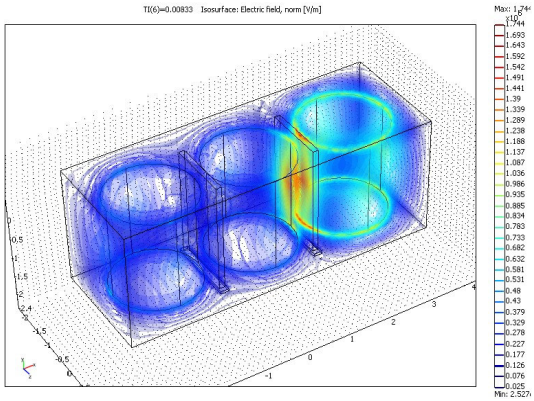

e - Model at time t0 + 150° elec.

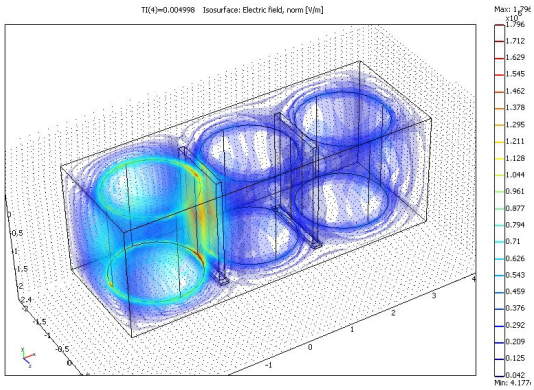

c - Model at time t0 + 90° elec.

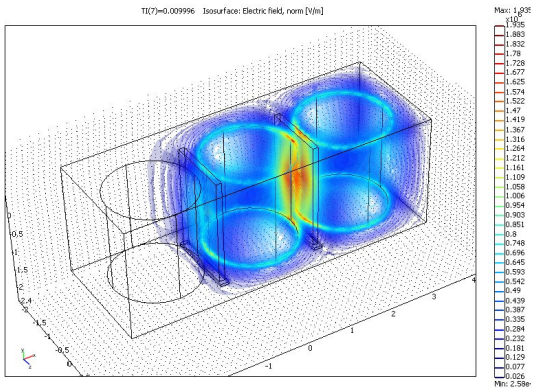

f - Model at time t0 + 180° elec.

Figure 3.9 3D COMSOL model showing the changing equi-potential field over ½ cycle as a result of the interacting phase electric fields

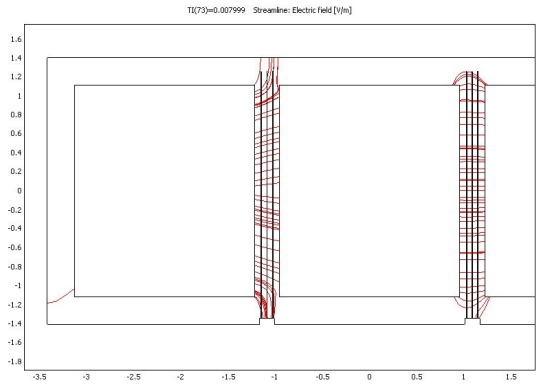

a - Model at time t0 + 144° elec.

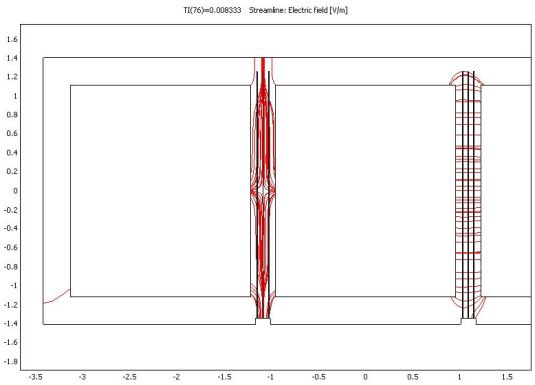

d - Model at time t0 + 150° elec.

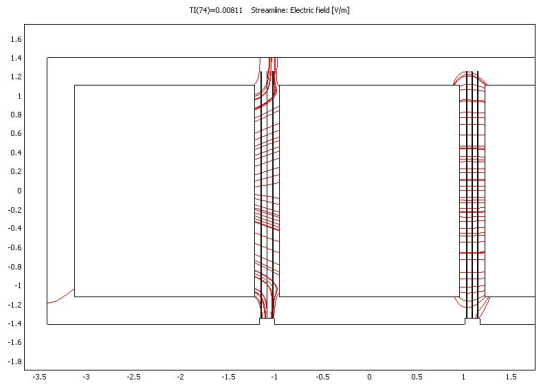

b - Model at time t0 + 146° elec.

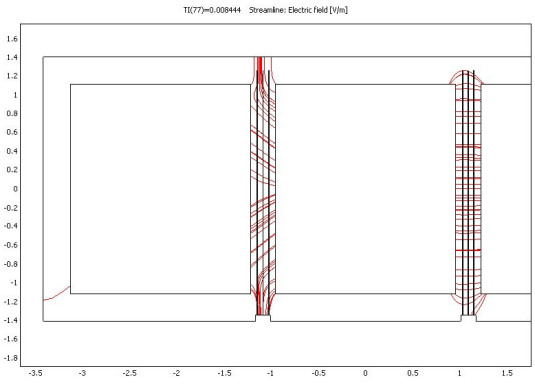

e - Model at time t0 + 152° elec.

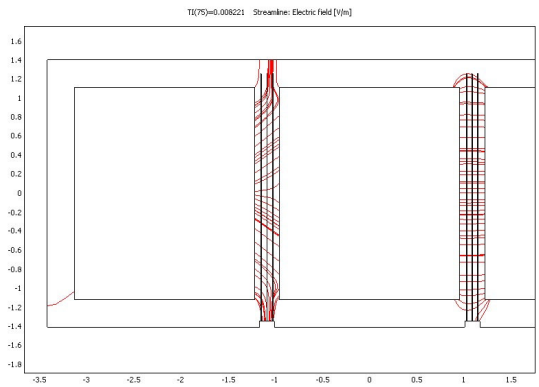

c - Model at time t0 + 148° elec.

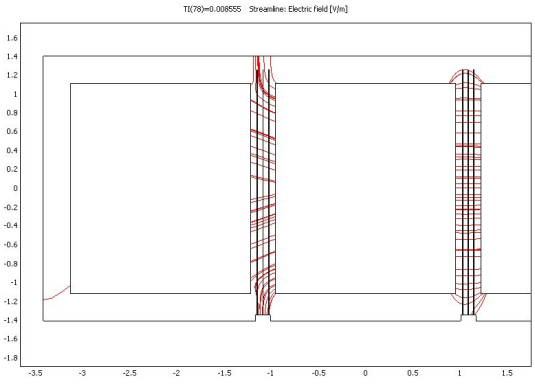

f - Model at time t0 + 154° elec.

Figure 3.10 2D COMSOL model (3 pressboards) showing streamlines reversing due to reversing electric fields at t0+150° elec.

Chapter Four

The experimental facility

The primary function of any high voltage experimental apparatus is to provide a contained environment in which repeatable experiments can be undertaken safely and reliably. The secondary function is the application of the process parameters to the test specimen. In realising a model of the inter-phase region, the experimental apparatus is required to meet the following interrelated functions:

- Contain and process a large volume (400 litres) of transformer oil.
- Contain the inter-phase model.
- Apply vacuum to the test cell in order to condition the pressboard.
- Control the temperature of the oil from 20° to 60°C (±3°C – considered an acceptable tolerance to replicate stable conditions within a transformer).
- Collect/store measurements of temperature and vacuum.
- Apply and vary two independent high voltage sources to the inter-phase model.
- Generate a localised space charge.

4.1 Experimental facility up-grade

A test platform, originally designed for a study on RVM techniques, was donated by National Grid to form the core of the experimental facility but found to be in an unserviceable condition. The following development was undertaken to upgrade the test platform to meet the project goals:

- Design and implementation of a new logic control using AlProWin software for the programmable logic controller (PLC).
- Design and implementation of a new user interface using LOOKOUT software.
- Replacement of the temperature probes from 2-wire to 4-wire type.
- Design and modification of the pipe work to allow additional fluid flow options.
- Re-positioning of the vacuum pump above the level of the test cell in order to avoid the problem of sucking oil into the vacuum pump.
- Rewiring of the valve position indicators.
- Replacement of gaskets to improve vacuum performance and fluid containment.
- Replacement/addition of thermal lagging to improve the thermal properties.
- Addition of a pump to circulate the oil and to improve the heating cycle response and temperature distribution of the oil.
- Addition of a mechanical safety valve to the test cell.
- Design and specification of the new cover plates.
- Procurement of 71kV rated horizontally mounted bushings.
- Design/implementation of an earth plan to provide earth protection for the PLC.
- Re-wiring of the control panel circuitry in line with electrical modifications.
- Tracing of the PLC circuitry to document the control circuit.
- Development of an independent bi-phase supply.
- Design and implementation of the barrier board model.

Appendix A documents the mechanical and electrical schematics with mechanical block diagram, pipe work arrangement, component locations and the PLC control circuitry.

4.2 Technical overview

The test platform consists of six elements:

- The autonomous system logic control and data acquisition run by the independent PLC.
- The user interface on a separate PC which allows user command and control (but not programming) of the PLC.
- The conservator which acts as the oil reservoir and expansion tank.
- The test cell chamber which carries the bushings, inter-phase model and discharge source.

- The FilterAll oil purifier plant.
- Bi-phase supply.

The apparatus replicates the general arrangement of a large transformer in that it comprises two chambers; the lower chamber (the test cell) and, located above it, the conservator (Figure 4.1). The test cell holds the barrier model and carries the bushings through which high voltage is applied to the barrier model. Oil is moved around the system by means of a system of pipes and manually operated valves using the purifier as the pumping mechanism. The oil is heated in the test cell using the 5kW trace heating element coiled around the chamber exterior. The PLC manages the functions of safe heating of the oil, fluid transfer and monitoring of the system temperature and valve positions. The PLC measures the test cell pressure and temperatures by an array of sensors fitted around the chamber. The valve positions are detected by means of micro-switches fixed to the pipe valves. The test cell is fitted with an independent mechanical safety valve set to 45kPa gauge pressure.

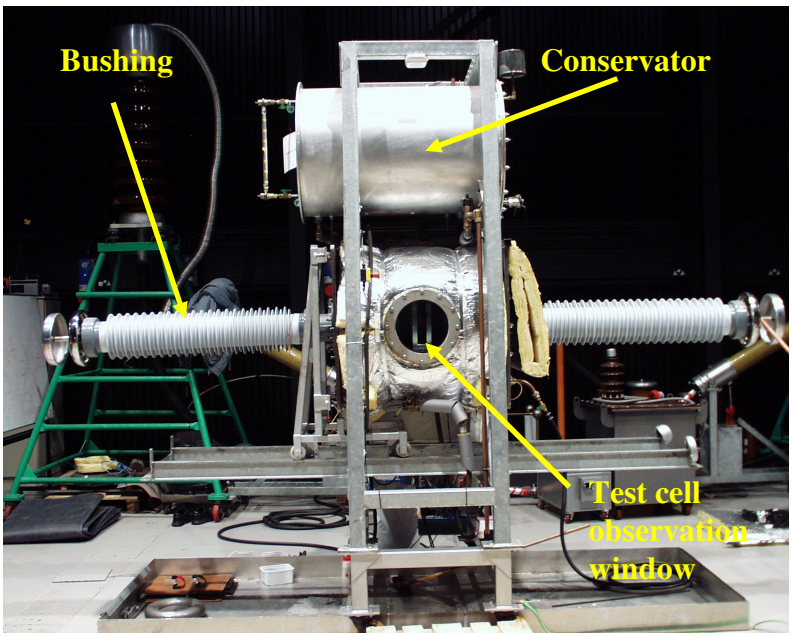

Figure 4.1 Side elevation of test cell showing observation window, conservator and bushings

The apparatus measures approximately 1m x 4m x 4m with the conservator having a capacity of 425litres and the test cell a volume of 370litres. The extra volume of the conservator allows for expansion/contraction of oil during heating cycles and storage of the oil when access is required to the test cell chamber. The test cell is filled with oil

from the conservator using gravity feed with the test cell under vacuum. User control of the system is achieved through the user interface. The user interface continuously accesses the PLC data and displays the system condition via mimic diagrams.

4.2.1 System logic control overview

A block diagram of the system logic control is given in Figure 4.2. The system is controlled by the AutoLog 2000s PLC programmed with bespoke software developed as part of the development phase. The function of the PLC is to:

- Monitor the system to avoid any dangerous conflict in term of excess temperatures/pressures or incorrect valve positions which could result in an elevated temperature or fluid spill.
- Collect and store the temperature and pressure profile of the test cell.

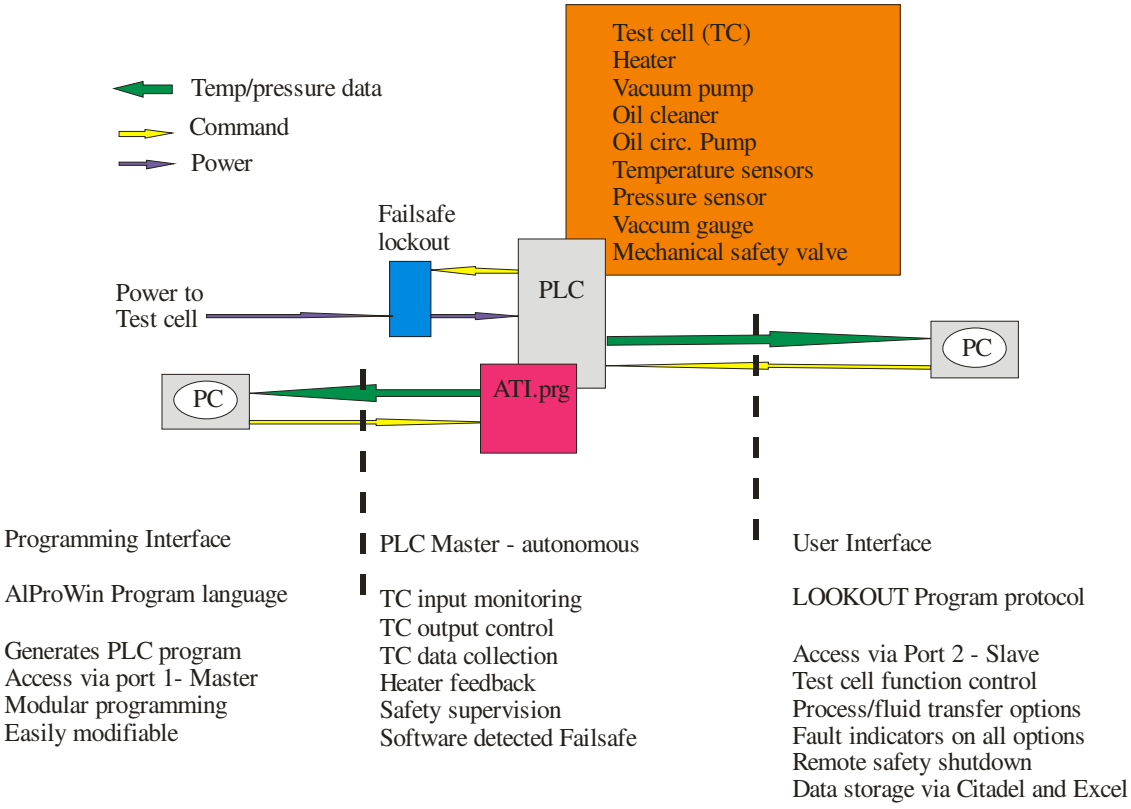

Figure 4.2 System logic control block diagram

The software continually monitors the system status by means of position indicators on the manually operated valves, temperature/pressure/level sensors fitted to the test cell and temperature/level sensors fitted to the conservator. The system status information is logged and presented to the operator via the user interface and control of the system is

through the user interface. A second separate interface is used to programme the PLC using AlProWin programming software.

4.2.2 PLC software overview

The PLC software autonomously drives the system by means of a continuously cycling control loop programmed as a series of modules. Immediately after start-up, the two communication ports of the PLC are configured with the communication data port set-up parameters. Key test cell temperatures, pressure and emergency stop status are checked by a Failsafe module in the program. The failsafe module initiates a program shutdown should the temperature or pressure be out of the control limits or an emergency stop detected. Following this successful initialisation sequence, the program makes an acquisition of temperatures, pressure and valve position data before dropping into the continuous process/fluid transfer decision loop. Within this loop, the PLC checks for the mode command and switches between “Process” mode and “Fluid Transfer” mode as appropriate.

During each program cycle, a failsafe check is performed to monitor the temperature/pressure sensors on the test cell, the smoke detectors and the emergency stop signals (either direct hardware activated or through the user interface). Any detected fault condition prompts the PLC to an immediate shut-down. The temperature/pressure profile of the test cell is collected during each program cycle and the software performs continuous logic checking to ensure that the correct sequence of valves is set for the desired operation or the set-point temperature in the test cell is maintained according to the requested process. The PLC software collates the sensor position data into a memory store and reflects the system status back to the user interface which is displayed as mimic diagrams. If a valve is incorrectly set for the programmed processor, the temperature out of limit, or the pressure is not correct, the software initiates a process stop and indicates the incorrect element on the fault indictors in the mimic diagrams. The use of fault indicators is one of the key safety features of the PLC as a process stop is initiated if any of the parameters are incorrectly set for a particular mode. The PLC refuses to allow the process to continue and the fault condition is flagged up to the user by an audible alarm and the incorrect setting highlighted on the user interface mimic diagrams.

4.3 System functions

The test platform allows nine processing operations to be performed. These operations are selectable from the user interface and divided into two modes termed “Process” or “Fluid Transfer” mode. The Process mode is considered to be more hazardous as it involves the application of heat or vacuum to the test cell. (Appendix A gives a Truth Table of the valve operations for the various processes.)

4.3.1 Process mode

The following functions are available in Process mode:

- Filling of the test cell under gravity.
- Heating and circulation of the oil in the test cell via the oil circulation pump.
- Vacuuming of the test cell (without oil) to condition the pressboard before introducing the bulk oil by filling under vacuum in Fluid Transfer mode.
- Continuous circulation of the oil in the test cell.

When under the heating cycle, the software allows an acceptable temperature input only if the value is the greater than ambient temperature and less than 90°C.

4.3.2 Fluid transfer mode

The following functions are available in Fluid Transfer mode:

- Filling the conservator from a barrel.
- Filling the conservator from the test cell (emptying the test cell).
- Filling the test cell from the conservator under vacuum.
- Drainage of the test cell back to a barrel.
- Circulation/purification of the oil via the conservator.

4.4 User interface

The user interface is implemented using National Instruments LOOKOUT software. This software provides the user access to the PLC to initiate the requested processes. The user interface displays the system status via mimic diagrams using real-time data provided by the PLC using 200 input/output (I/O) data points. The mimic diagrams show the valve conditions in each mode whilst the indicator panel shows the apparatus status (Refer Appendix A for the mimic diagrams). Temperature/pressure data is stored

using National Instruments “Citadel” which is accessed using a structured query language (SQL) database access tool. The data can also be downloaded in real-time using comma separated variable format (.csv) which can be read using Excel.

4.5 Oil conditioning plant

Oil is moved around the system using the dedicated FilterAll plant (Figure 4.3). In the same time, the plant conditions the oil by the sequential process of pre-heat, mechanical filtration and vacuum separation shown by the block diagram (Figure 4.4).

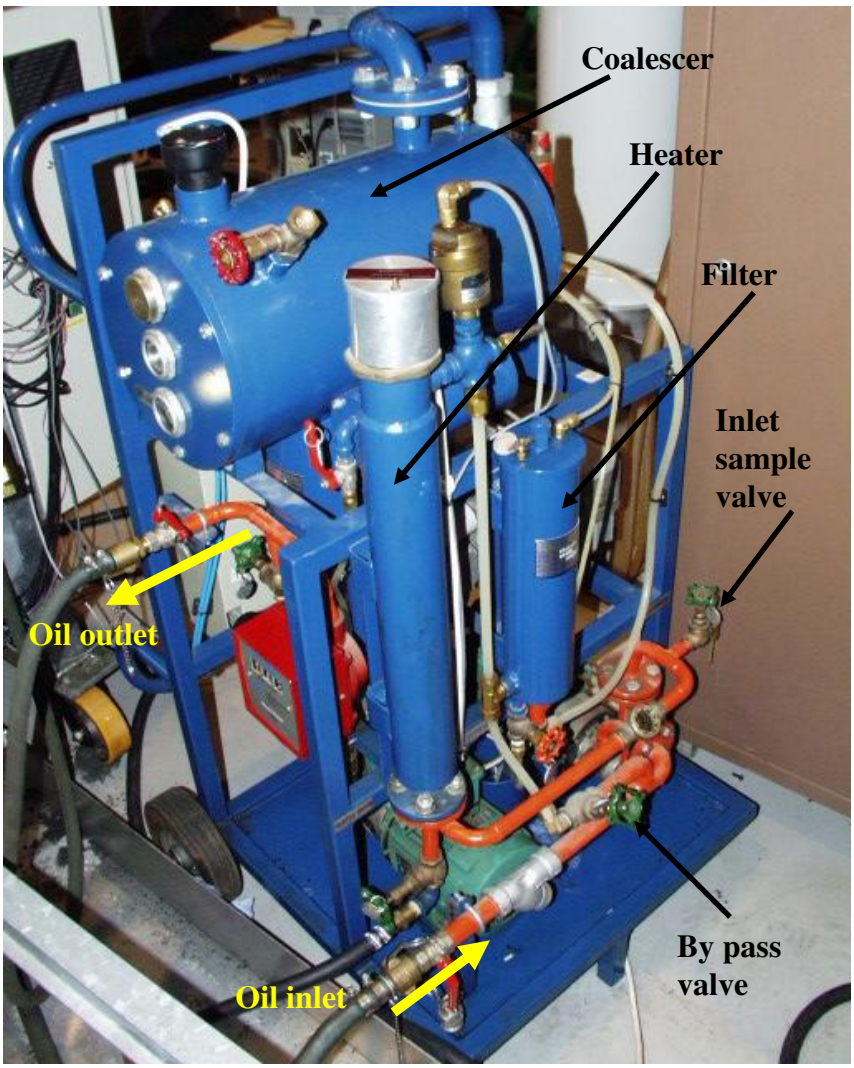

Figure 4.3 Oil conditioning unit

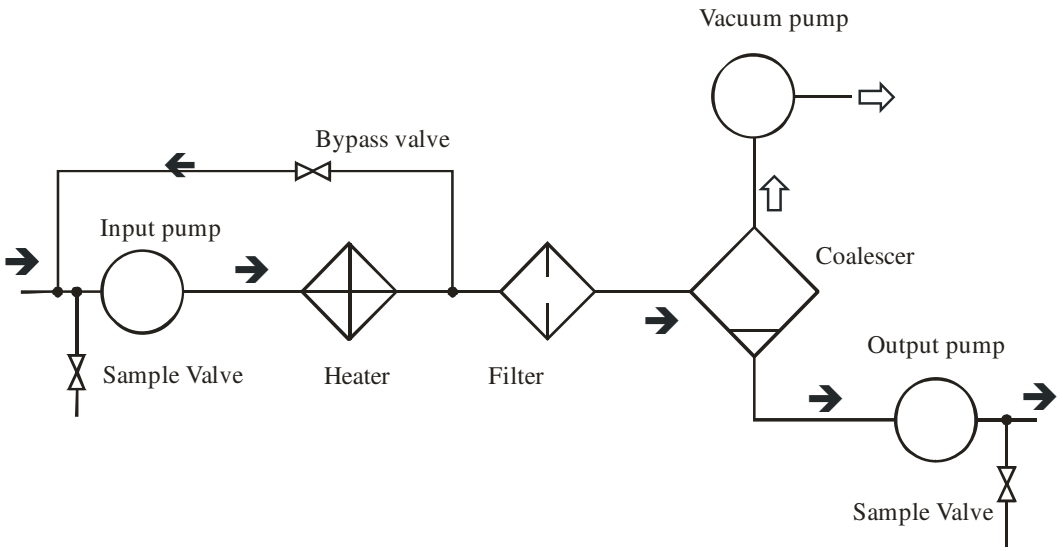

Figure 4.4 Oil conditioning unit block diagram

The input pump draws oil from the conservator or test cell and feeds the oil through the pre-heater at 60°C in order to lower the viscosity. The oil is pumped through the fine mesh filter to remove particulates before being injected into the vacuum coalescer. The vacuum coalescer is a combined two stage process where the heated (thinned) oil is injected into fine wire mesh situated inside the vacuum chamber (~0.2kPa absolute). As the heated oil, (with a lowered surface tension), is forced through the mesh, the mesh increases the oil surface area and allows moisture and gases to be drawn from the oil which are extracted using the vacuum pump. The liquid falls to the bottom of the coalescer from where it is taken by the outlet pump and returned to the system. The FilterAll has a maximum rated process capacity of 300 lhr^{-1} of oil. Throughput is adjusted by means of the bypass valve around the heater. It was found that, with reduced throughput of 120lhr^{-1}, a consistent level of 8 ~10ppm of moisture remaining in the oil could be achieved. Oil samples are drawn from both the input side of the input pump and the output side of the output pump to verify moisture extraction.

4.6 High voltage objectives

The upgrade to enable 200kV phase to phase working required the following:

- The choice of HV oil-air bushings
- The design and manufacture of new test cell end plates in order to mount the HV oil-air bushings.
- Knowledge of the design parameters of the inter-phase region in order to be able to propose a scaled model for the electrode array.

The first two elements interact in that the choice of the HV oil-air bushing dictated the design of the end plates and vice versa. The choice of the oil-air bushing also dictates the useful working space left inside the test cell.

4.6.1 HV oil air bushings and end plate design

The function of the bushings is to allow the high voltage to be applied through the wall of the test cell into the working space. The bushings themselves must be partial discharge free and the oil end must be sufficiently small to provide a useful working volume in the test cell. Commercially available bushings minimise the cost and lead-time by avoiding the need for a custom design. A standard bushing (Trench type 110HC595) was chosen which fulfilled these requirements. The bushings were supplied with cylindrical corona shields which could be removed leaving a variable working space of 224mm maximum between the electrodes. This allows a variety of electrode shapes and spacing profiles to be adopted which will be discussed in Chapter 5.

The decision process for the choice of bushing involved a complementary design for the end plate as well as a dimensional check for air clearances to the metallic parts of the test platform around the bushings. The criterion was that air clearances from the bushing end should not be less than the clearance distance from the corona disk along the length of the bushing to the test cell end plate (1.3m approx). Three end plate designs were considered; a flat plate and two turreted designs (15° and 30° from the horizontal). The flat plate design became the preferred option as this allowed the optimum air clearance distance as well as being easier to manufacture. The choice of a non-turreted design was made easy by the ability of the oil-air bushing to be mounted horizontally.

The requirement for the end plate is to hold the bushing and remain rigid under the normal operating temperature and pressures. Structural steel 20mm thick to standard S355 J2G3 BS EN 10025 Parts 1 & 3 (BS 4360 Grade 50 D) was chosen as this offered the required rigidity and intrinsic mechanical strength.

The air clearance to ground required that the test platform be raised by 300mm from its original state. The main criterion for the height extension is that the structure should

support the mass of the test cell when carrying 400 litres of oil. The total mass was estimated at 1100 kg approximate. The design was based on the use of 80 mm square box structure as used in the platform. (Refer Appendix B for the mechanical drawings for the HV upgrade elements.)

4.7 Concept for the inter-phase barrier model

The following elements were required to simulate the inter-phase barrier region:

- A means of holding sheet(s) of pressboard to form an oil-pressboard sandwich.
- A bi-phase supply to provide the independent high voltage sources.
- Two electrodes, to replicate the two phases.
- A discharge source and earth placed close to the pressboards to provide the space charge.

The electrodes and discharge source are detailed in the next chapter.

4.7.1 Pressboard holder

The sheets of pressboard are suspended in the chamber by means of four lugs positioned on a carrier ring centred in the test chamber (Figure 4.5). The lugs and mechanical fixings are made from insulating material to ensure that the pressboard holder is itself not a source of PD activity. The carrier ring is centred in the chamber by means of axial struts one of which is mechanically fixed to the chamber wall to provide a solid earth connection.

To model the inter-phase barrier, two pressboards are used in an oil sandwich arrangement. The test sample (pressboard 1.5 mm thick conditioned to pre-defined moisture content) is placed centrally between the two corona disks when the test cell is closed. A second board (3 mm pressboard conditioned to 0% moisture) is fixed to the specimen holder leaving an oil gap of 6 mm between it and the test pressboard. The second board acts as a guard to prevent inter-electrode flashover occurring in the event of discharge activity punching through the test pressboard.

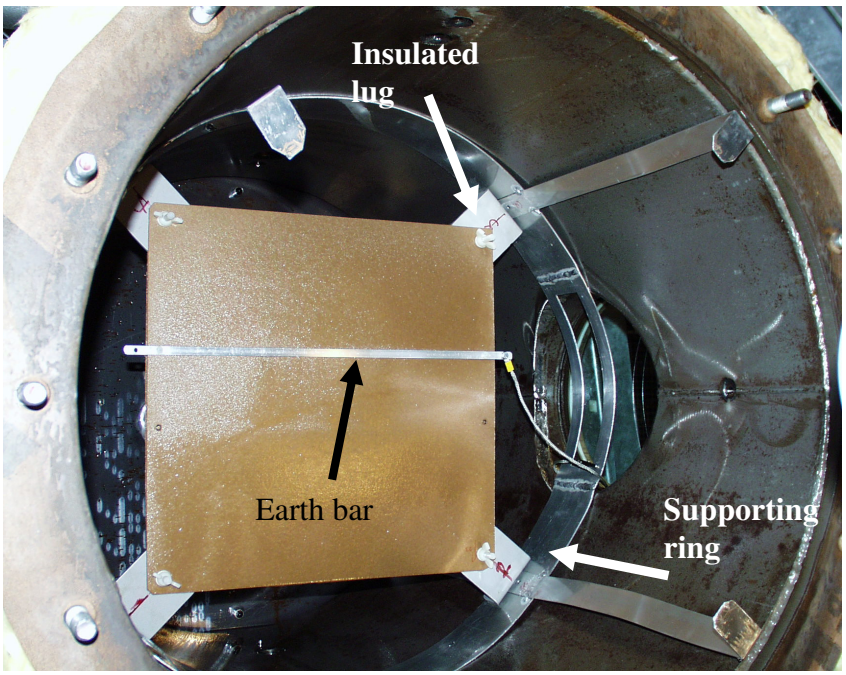

Figure 4.5 Internal view of test cell showing carrier ring, pressboard and earth bar

A bare aluminium strip is clamped to the pressboard sheet and earthed by means of a copper braid to the carrier ring to form the earth bar. This earth bar represents the tank support on which the inter-phase pressboard is usually mounted and completes the model of multilayer barrier board.

4.7.2 Bi-phase supply

Figure 4.6 shows the block diagram of the bi-phase supply which enables two independent voltage controlled sources. The three phase mains supply is fed through a Reo-Pruftechnik control cabinet which provides a single phase noise free source for the 380V/200kV Haefely transformer. The high voltage output is taken through one bushing to the bare electrode plate and becomes the reference voltage (V_1). At the same time, this voltage is applied to the discharge source placed on the surface of the pressboard which creates a localised electric field. The level of V_1 is controlled using the Haefely operating terminal OT247. The second source is generated by means of a low voltage variable phase generator the output of which is amplified through a power amplifier. The output of the amplifier is applied to the 240V/100kV Agea Kull transformer. The high voltage from the transformer is taken through the second bushing to the other electrode plate and becomes the control voltage (V_2).

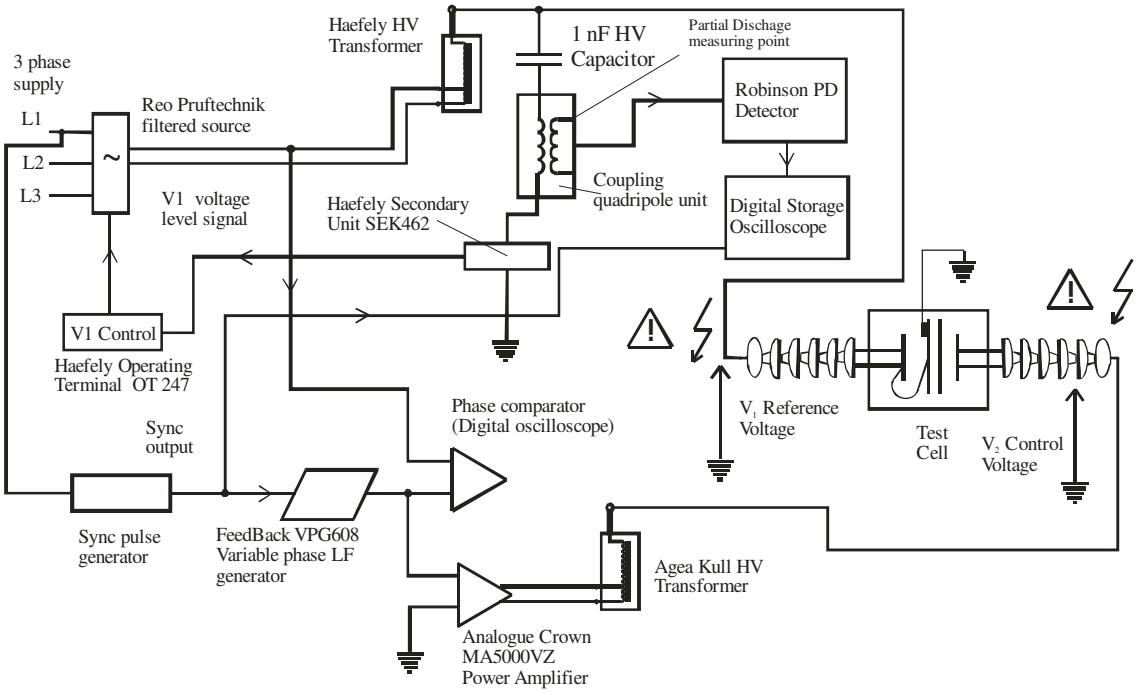

Figure 4.6 Block diagram of the bi-phase supply

The variable phase generator is free running and is phase locked to V_1 by means of the synchronisation pulse generated from L_1 of the 3 phase supply. The level of V_2 is controlled using the power amplifier gain control. The phase with respect to V_1 is controlled using the phase control on the variable phase generator. By this means, V_2 can be varied in amplitude and phase, ϕ, from 0° through to 360° elec. with respect to the reference voltage V_1. The two high voltages on the parallel electrode plates interact to form a general electric field. By adjusting the phase and amplitude of V_2 with respect to V_1, various general field configurations can be simulated which will be discussed in Chapter 5. The Robinson PD detector and digital storage oscilloscope are used to detect PD inception and extinction and to collect PD persistence plots and corresponding ϕ-q-n plots as described in §3.5.

Both the Haefely and the Agea-Kull transformers were proven PD free to their rated values giving a noise floor of 2pC. The power amplifier proved to be noisy with broad band noise level in excess of 50pC. The noise picked up by the Robinson is a function of the closeness of the control electrode to the reference electrode. This limits how closely the electrodes can be placed with respect to each other and thus the level of through stress which can be put on the pressboard. The other problem with the Robinson detector is due to the gain resolution setting (Figure 4.7).

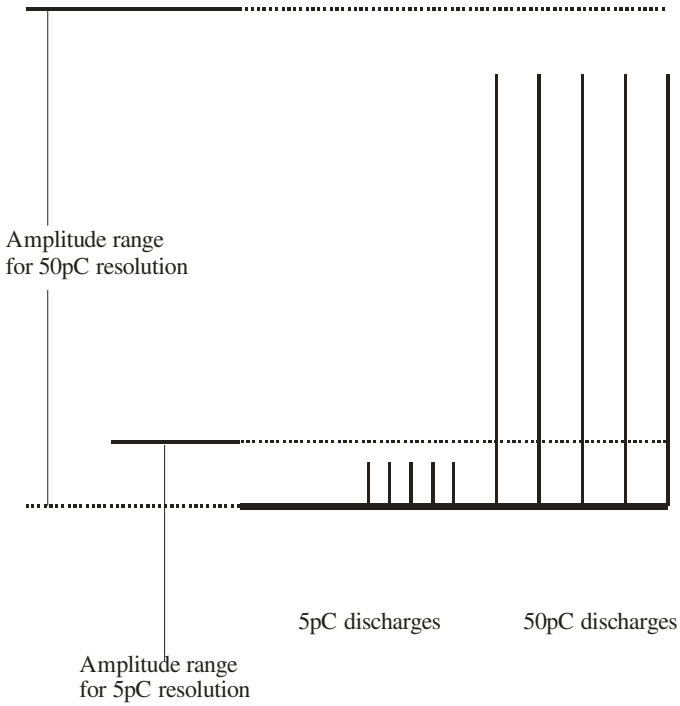

Figure 4.7 Diagrammatic representation of gain resolution

When the gain setting is set to detect (say) discharge in the range 0-10pC, any discharge greater than 10pC is clipped. Conversely, when the gain setting is set to detect discharge in the range 0-100pC, any discharges greater than 100pC are clipped and those less than 10pC become part of the background noise floor which is subsequently masked out in the bespoke ϕ-q-n plot generation algorithm. This explains why ϕ-q-n plots show regions of clipping at the range extremes. The gain resolution problem was overcome by taking sequential measurements at increasing gain settings to build a picture of the ϕ-q-n profile over several decades of charge level.

4.8 Test cell performance

The test cell provides the environment to house the inter-phase barrier model and allows two processes to be applied to specimens under test. These are the vacuum and heating processes. The vacuum process is used to impregnate the pressboard with oil and the heating process sets the temperature of the test cell. The processes are not used together and thus the process to impregnate pressboard with oil is different to the industrial process as described in §2.3.1. The vacuum impregnation process without heat ensures the impregnation of pressboard with oil whilst leaving the moisture content largely un-changed.

4.8.1 Vacuum process

Figure 4.8 shows the resulting vacuum profile under a typical vacuum cycle. The pressure inside the test cell chamber is reduced from atmosphere to approximately 2kPa absolute within 30 minutes.

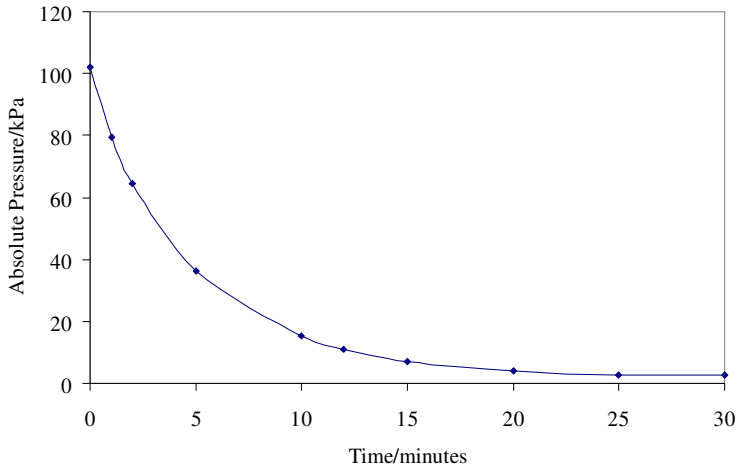

Figure 4.8 Test cell vacuum cycle

4.8.2 Effect of the vacuum process on pressboard moisture content

The industrial vacuum/heating process is designed to reduce the water content in the pressboard to a minimum whilst the transformer is impregnated with oil. This has the twin goals of removing all moisture with a target of 0% moisture remaining (accepted at around 0.5%) and to ensure that all air is eliminated from the pressboard and other voids in the transformer. This process takes advantage of the phenomenon of vapour pressure where water readily evaporates when the pressure is reduced below the vapour pressure of the liquid at the system temperature and the industrial process uses heat to accelerate the process. However, the industrial process conflicts with the experimental goal of impregnating pressboard whilst retaining a defined moisture level. This raised the issue of needing to understand the effect of the vacuum process on the moisture content of pre-conditioned pressboard of a defined size (450mm x 450mm) and thickness (1.5mm) representing approximately 330gram dry mass per pressboard.

Process time is the control parameter. The vacuum pump takes 30 minutes to reduce the vacuum to approximately 20mbar absolute. This was set as the limit for the vacuum process as a prolonged vacuum thereafter just continues to extract moisture. After the vacuum cycle, a further defined time (approximately 10 minutes) is required for air to be

re-introduced into the chamber to enable the pressboard to be extracted and the mass re-measured. The experiment was conducted by applying vacuum for the defined time of 30 minutes to pressboard at pre-conditioned moisture content (determined by mass over dry mass), and then extracting the pressboard without oil impregnation to see the change in mass. The masses were measured using a digital balance with an accuracy of ±0.03 gram thus obviating the need for error bars in any measurement.

Figure 4.9 shows the change in mass ~ pressboard moisture content under the vacuum cycle. It indicates that pressboard, dried to less than 2% moisture content, increases in moisture content when under this process. The increase in moisture is on account of the dead-times in the process and the process time itself, during which the pressboard attempts to regain moisture equilibrium with moisture in the air. The dead times are the 5 minutes it takes to place the pre-conditioned pressboard in the chamber and to seal the chamber and, following the vacuum process, the 10 minutes taken to break the vacuum by refilling with atmospheric air, unsealing the chamber and extracting the board. Additionally, the board undergoes a conflicting process of moisture take-up from the atmospheric air and the vacuum process which is extracting moisture and air during the vacuum process.

The rate of moisture absorption on a dry (0%) board is indicated by Figure 4.10. This shows that dry board re-absorbs 4 grams in 45 minutes (the complete cycle time). This represents 1% increase moisture and explains the cross over point at 3% shown in Figure 4.9. (The equilibrium would vary according to the relative humidity of the air). However, when pre-conditioned pressboard is oil impregnated, the second dead-time is no longer applicable. To uncover the effect of the oil impregnation process without impregnating the pressboard with oil, the experiment was repeated using dry (zero grade) air during the refill process to eliminate the effect of moisture re-absorbance during the refill dead time.

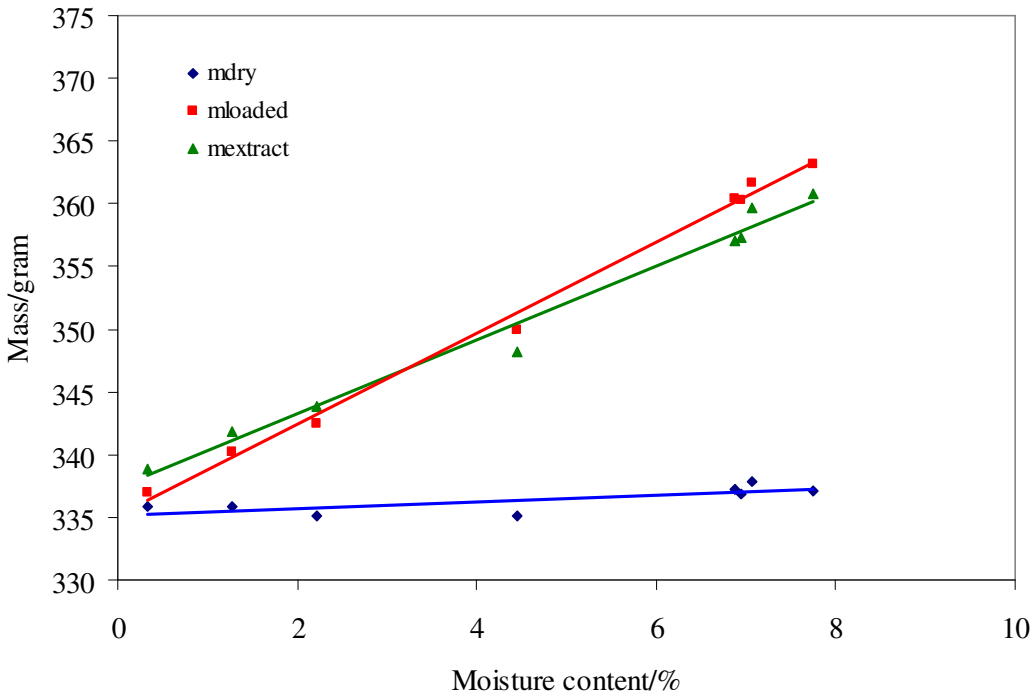

Figure 4.9 Mass ~ pressboard % moisture content: vacuum/atmospheric air cycle

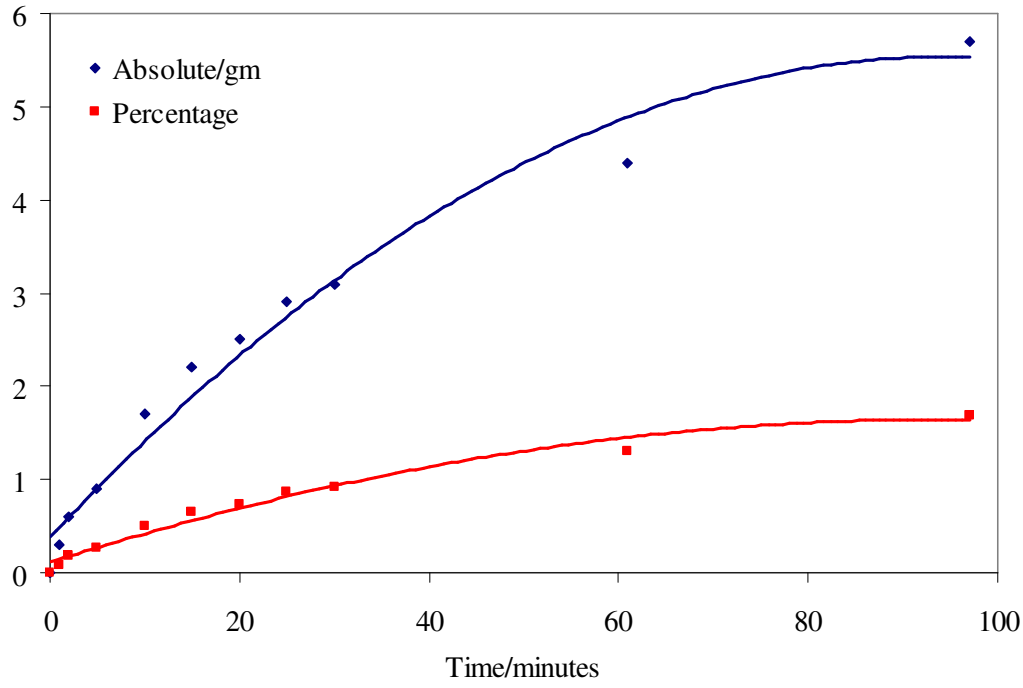

Figure 4.10 Rate of absorption of moisture for 1.5 mm thick pressboard dried to 0% moisture content and placed in normal atmospheric air (65%RH)

Figure 4.11 shows the change in mass ~ pressboard moisture content under the dry air refill cycle. It indicates a reduced change in moisture content from the initial moisture content for moisture content above 0.5%. The slight increase in moisture below 0.5% is caused by the initial absorption of moisture by the very dry board during the few

minutes that the board is being sealed in the test cell and in the initial stages of the vacuum process. Figure 4.12 shows families of curves using multiple boards at constant thickness confirming that the moisture extraction process is surface area dependent

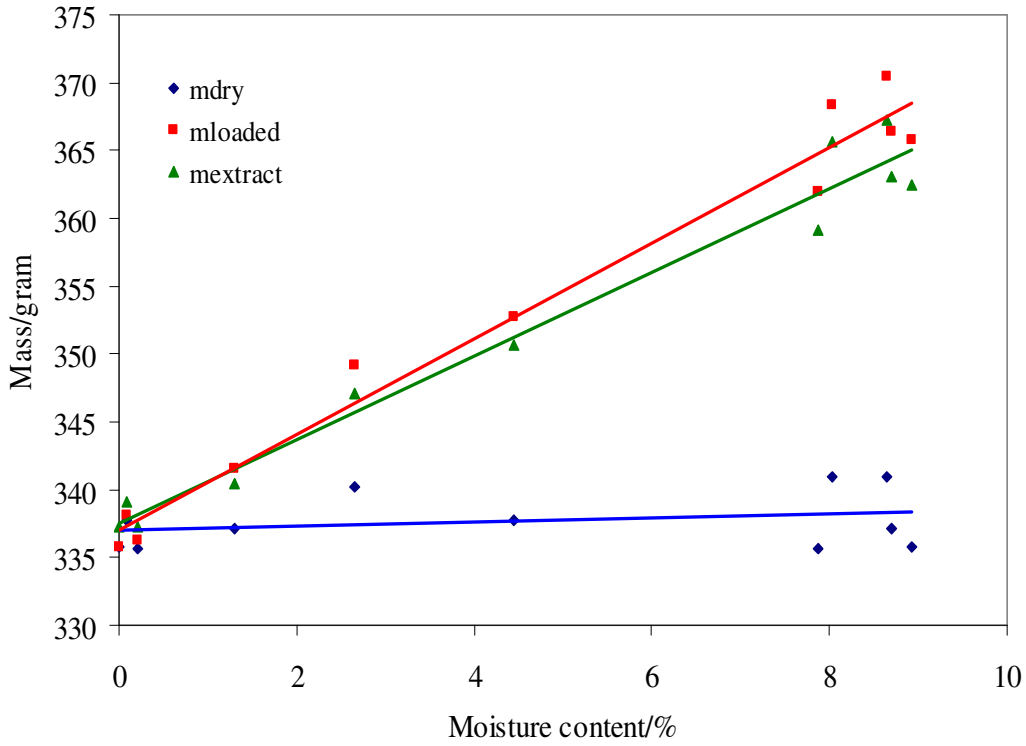

Figure 4.11 Mass ~ pressboard % moisture content: vacuum/dry air cycle

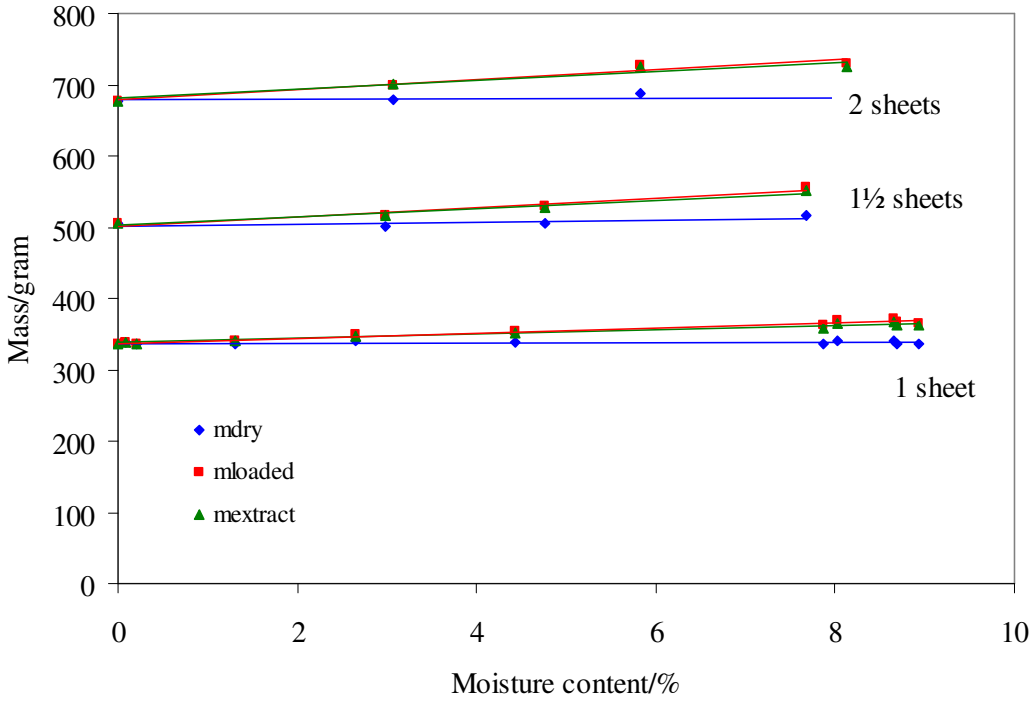

Figure 4.12 Mass ~ pressboard % moisture content: vacuum/dry air cycle for multiple pressboards (1, 1½ and 2 sheets)

The experiments confirm that pressboard with a pre-conditioned moisture content is affected by the specific test facility vacuum process. The pressboard undergoes moisture extraction caused by the application of the vacuum. The amount of moisture extracted is dependent upon the board surface area, the initial moisture content and the process time. By keeping the board mass and process time constant, the loss in board moisture is consistent and can be reasonably estimated. When using a single sheet of 1.5 mm board, the loss in moisture is less than 10% of the initial moisture content. In terms of the inter-phase barrier experiments, this represents an acceptable error. [Note: All quoted board moisture contents are the values as determined by board mass over dry mass and do not take into account the 10% loss incurred during the impregnation process.]

4.8.3 Heating process

The test cell is heated by means of the 5kW trace heating element surrounding the outside of the cylinder. Heat is transferred to the oil by direct conduction and an external pump is used to circulate the oil within the test cell in order to assist the internal convection currents arising in the oil due to temperature differential. The oil temperature within the test cell can be raised at a rate of 12~14°Chr^{-1} and the overall test cell temperature can be held stable to within ± 3°C. The temperature stability of the system relies on the thermal capacity of the oil volume and aided by the thermal insulation given by the double layer of 50mm thick industry standard Rockwool applied as a jacket around the test cell. In practice, to attain a desired test cell temperature, it was found best to offset the test cell set-point temperature (i.e. Tset) to 3~4° below the target test temperature. During the heating cycle, the heater switches off before the target temperature is achieved; the thermal mass of the system results in an overshoot which is damped by the continuous circulation to achieve the desired steady state test temperature within a reasonable time period of 30 minutes. The set point temperature is then adjusted to the desired value in order to maintain the temperature. Figure 4.13 shows the temperature profile across the vertical section of the test cell during an eight hour experiment during which it was required to hold the test cell temperature at 25°C. The temperature of the test cell is monitored by means of eleven PT100 thermocouples positioned around the chamber plus an additional one on the output of the oil circulation circuit. The temperature of the oil is monitored in three dimensions with the axial

vertical plane being the most significant as this gives the temperature profile of the oil between the oil inlet and outlet of the circulating path. Thermocouple TS02 positioned on the end flange is chosen as the set point measurement thermocouple because it is not in proximity to the heating coils and also gives a good indication of the temperature of the oil at the centre of the test cell.

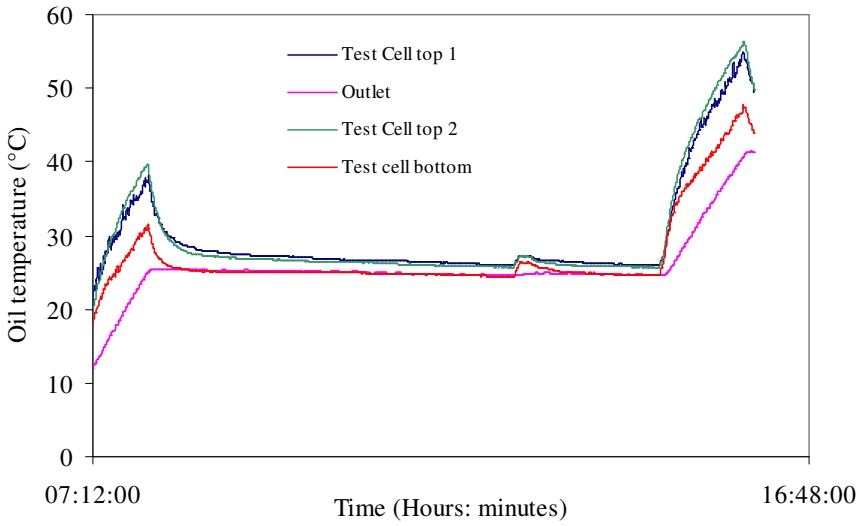

Figure 4.13 Cell temperature profile for set point of 25°C

4.9 Summary

A significant amount of engineering work was undertaken to create a test facility capable of representing the conditions of the inter-phase barrier region. This included the complete development of a new control system and user interface. Substantial refurbishments were made to the mechanical components of the system which included a re-design of the pipe work to improve system flexibility/temperature performance and replacement of gaskets to improve the vacuum performance. New end plates were designed to accommodate industry standard horizontally mounted bushings and to upgrade the test platform to high voltage working. Work was completed on documenting the electrical circuits and mechanical schematics of the test facility. The inter-phase barrier model was implemented using a pressboard oil sandwich to represent the barrier construction. It was determined experimentally that a controlled vacuum process had minimal effect on the moisture content of conditioned pressboard. The electrode design formed a key issue in the barrier model and the next chapter describes the work undertaken to the electrode system in the test cell to produce a reliable discharge source and to replicate the electric field conditions in the inter-phase barrier region using an independent bi-phase supply.

Chapter Five

The design of the barrier model

Surface tracking is the conducting path formed on the surface of the insulation material as a result of localised heat action caused by surface currents. A surface current is the drift of charge from a charge source under the action of an electric field which may be a general electric field or a locally enhanced field developed around a space charge. Localised space charge is generated in gas voids or from metal inclusions (floating discharge) as a result of partial discharges due to the action of a general electric field on the void or inclusion. The conventional way to create a localised space charge is to have a discharge source in the form of a sharp point (e.g. a needle) connected to a high voltage source. The geometry at the tip promotes the development of the space charge through Schottky field emission. However, the method of application is varied and several approaches have been adopted.

One approach is to implement a point-plane method [137,138,139,140]. This method produces a discharge source which is directed perpendicular to the surface rather than along it. Another approach is to use a parallel plane-plane method with pressboard placed perpendicularly between them and with a small point source created on the surface of one of the plane electrodes and adjacent to the pressboard [141]. This method overlooks the fact that the general field is not separated from the local field arising from the discharge source. In addition, the pressboard surface is parallel to the electric field

which is at variance to the inter-phase region where the pressboard surface is perpendicular to the general field. Between the two methods, the point plane approach appears at first glance to offer a better method of implementing a discharge source.

5.1 Problems found with the point-plane method

Samples of transformer board type TIV, 1.5mm thick and conditioned to 4% moisture were used in a point plane configuration with the needle tip of the discharge source placed vertical to the surface of the pressboard (Figure 5.2). The oil bath, approximately 600mm x 300mm x 150mm, is filled with 25 litres of clean dried Nynas Nytro 10GBN transformer oil [142]. Figure 5.1 shows persistence plots and corresponding ϕ-q-n plots for different levels of detector gain. The plots show corona discharge activity with the majority of activity occurring in the positive half cycle. The differences in amplitude and spread are due to the gain setting of the Robinson detector and illustrates the effect of gain selection as discussed in §4.7.2.

Figure 5.2 shows the effect of time on the discharge amplitude. In the time interval between 10 and 20 minutes, the discharge develops from low level discontinuous discharge in the positive half cycle to significant continuous discharge predominantly in the negative half cycle. At 25 minutes, the pressboard suffers puncture breakdown as evidenced by charring surrounded by the surface tracking features. Figure 5.3 shows close ups of the tracking marks on this sample and a second sample which verifies the problem of rapid punch through.

The point plane approach does produce tracking marks similar to those found by other investigators. However, the pressboard suffers rapid puncture rendering the experiments unpredictable in duration. In addition, the point-plane method doesn't adhere to the general principle for surface tracking where the discharge source and earth are on the same side as outlined in the CTI specification [132].

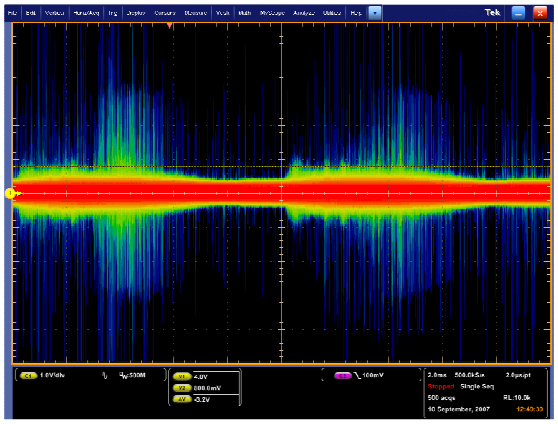

a - 5pC level persistence

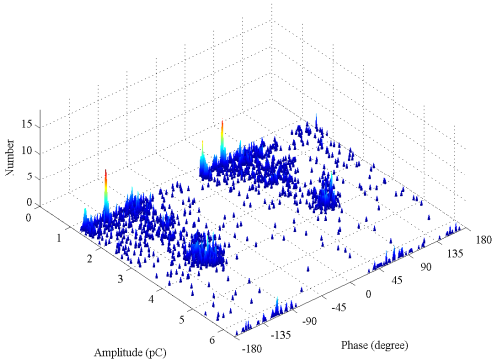

b - 5pC level ϕ-q-n plot

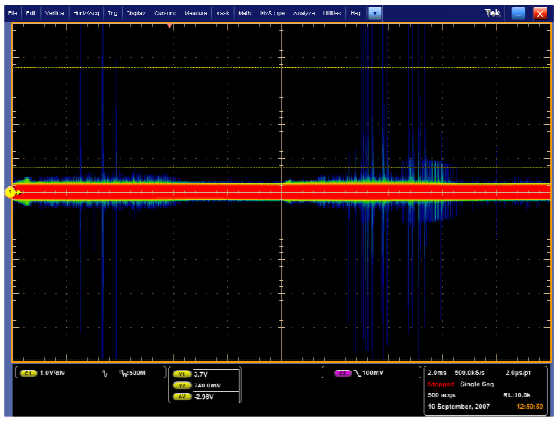

c - 50pC level persistence

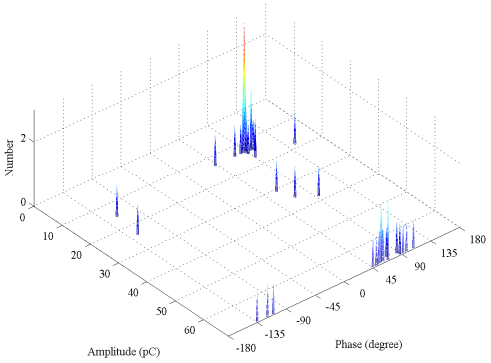

d - 50pC level ϕ-q-n plot

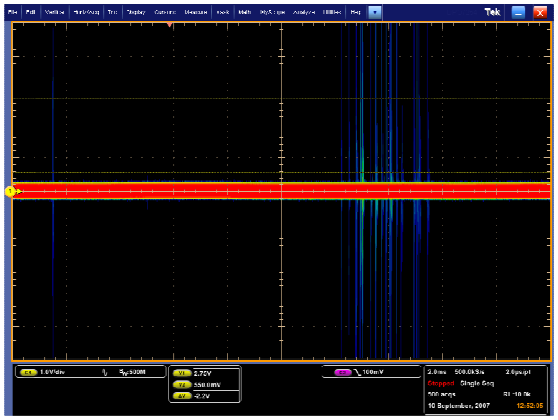

e - 500pC level persistence

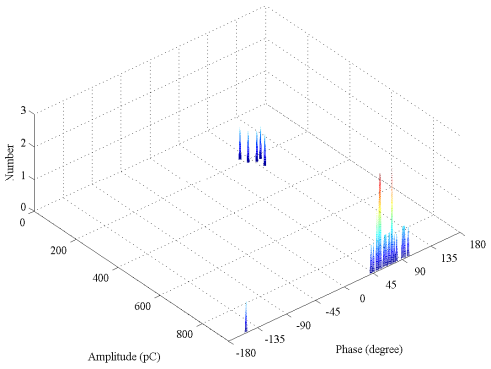

f - 500pC level ϕ-q-n plot

Figure 5.1 Point –plane persistence and ϕ-q-n plots at 20kV showing effect of Robinson gain selection

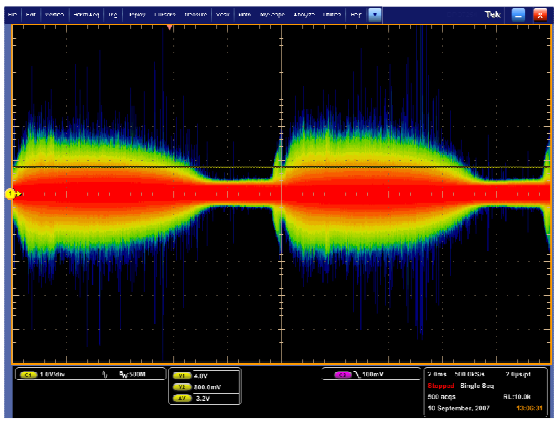

a - 5pC level - 10mins

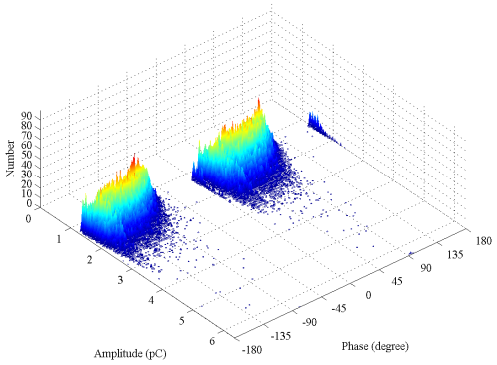

b - 5pC level ϕ-q-n plot at 10mins

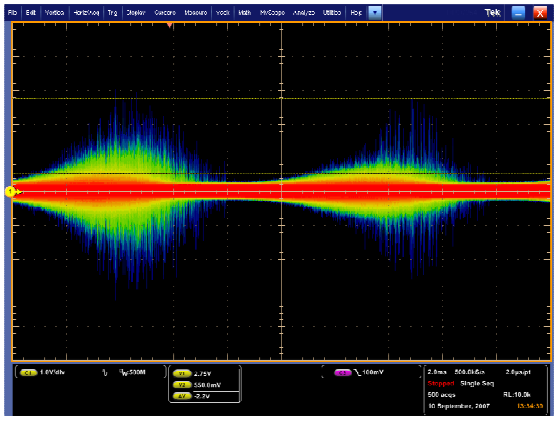

c - 500pC level - 20mins

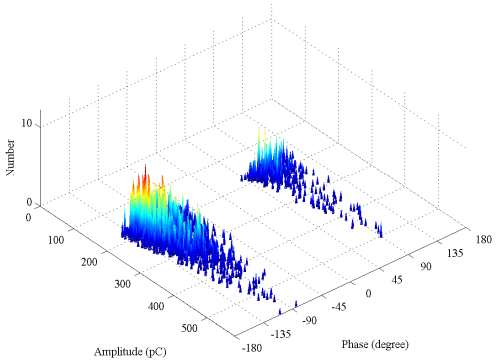

d - 500pC level ϕ-q-n plot at 20mins

e - Point-plane test set-up cross section.

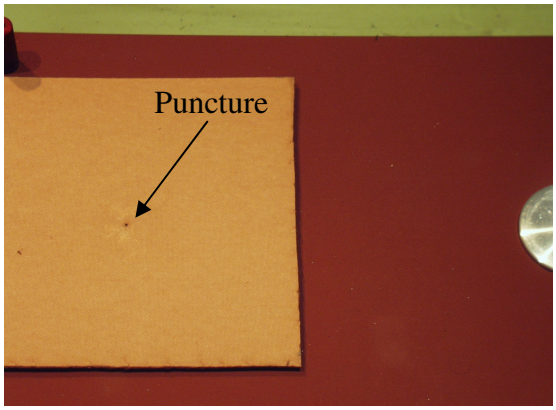

f - Pressboard 1 after 25 minutes

Figure 5.2 Point-plane apparatus, ϕ-q and ϕ-q-n plots at 20kV showing effect of time

The solution proposed to overcome the difficulties of the conventional approaches, is to modify the CTI configuration by using a needle discharge source placed nearly horizontal to the pressboard and at some distance from an earthed conductor also placed on the pressboard with the system immersed in oil. The acute angle of the needle ensures that space charge is directed along the surface rather than direct into the bulk of the pressboard. This method is termed the needle-bar method hereafter to distinguish it from the point-plane method.

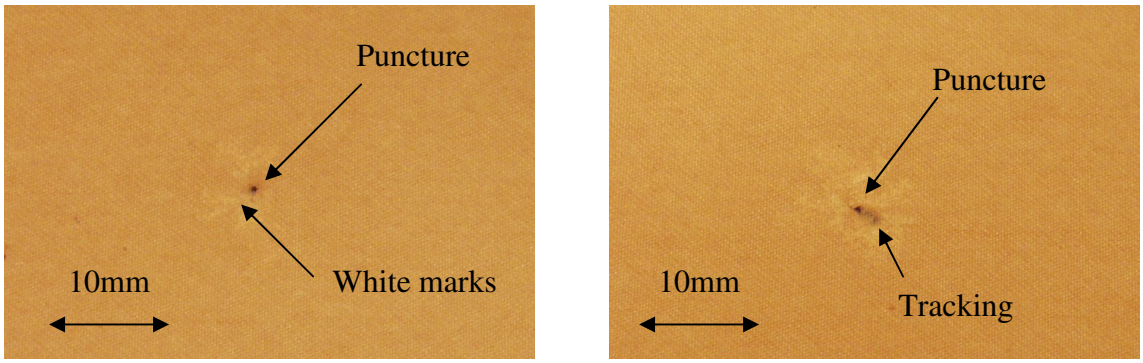

a - Puncture on sample 1 at 25 minutes b - Puncture on sample 2 at 15 minutes

Figure 5.3 Details of punch through and tracking marks on pressboard samples

5.2 Surface discharge using needle-bar method

A 450mm x 225mm sheet of 1.5mm pressboard was immersed into the bath. Two terminations were created in the pressboard at a distance of 300mm apart. One termination was earthed and connected to an un-insulated copper bar placed on the pressboard surface to form the earth bar. The other termination was attached to an external high voltage source and connected to the (tungsten) needle via a copper braid. This needle formed the discharge source. The needle was placed at an acute angle to the pressboard and perpendicular to the earth bar. The tip to earth gap was adjusted by means of a spacer removed after the distance has been set (shown 15mm in Figure 5.4).

5.2.1 Needle-bar method - effect of distance

To study the effect of separation distance, PD inception, PD extinction and surface flash-over voltages were obtained at fixed needle-bar distances ranging from 15mm to 55mm on un-aged pressboard pre-conditioned to selected moisture contents. The PD inception and extinction voltages were determined 5 times at each distance and the surface flash-over values determined 3 times to get statistical data. Finally, at each separation distance, the intrinsic oil voltage breakdown was obtained by removing the

pressboard. Figure 5.5 and Figure 5.6 show PD inception and extinction voltage, flash-over voltage and oil breakdown voltage (error bars at single standard deviation) for un-aged pressboard conditioned to 3.6% and 7.2% moisture content. Figure 5.7 shows the results using service aged board (moisture content approximately 2.5%).

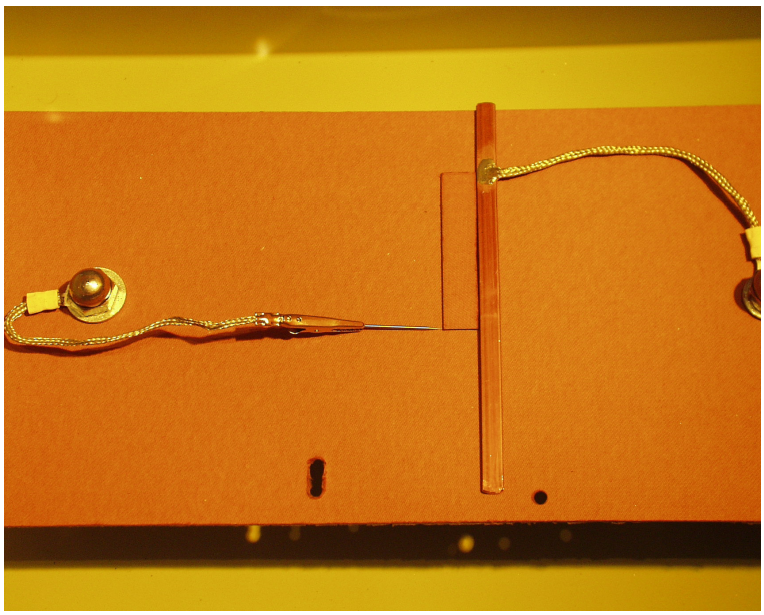

Figure 5.4 Overview of horizontal point-bar experiment apparatus showing method of adjusting the needle from the earth bar

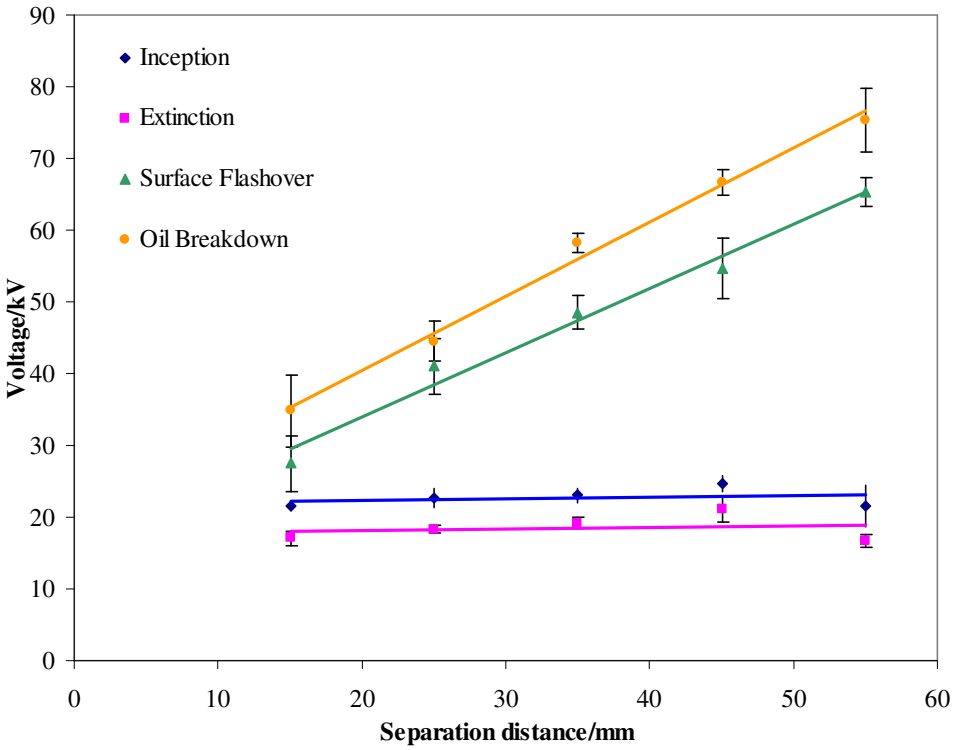

Figure 5.5 Breakdown, inception and extinction ~ distance - 3.6% moisture

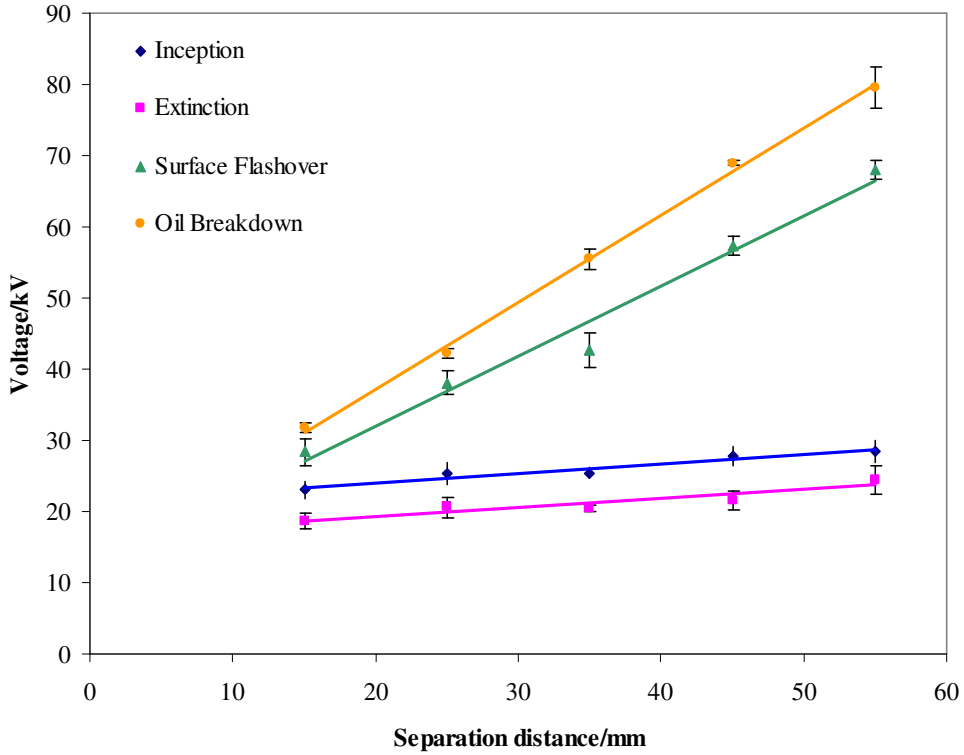

Figure 5.6 Breakdown, inception and extinction ~ distance - 7.2 % moisture

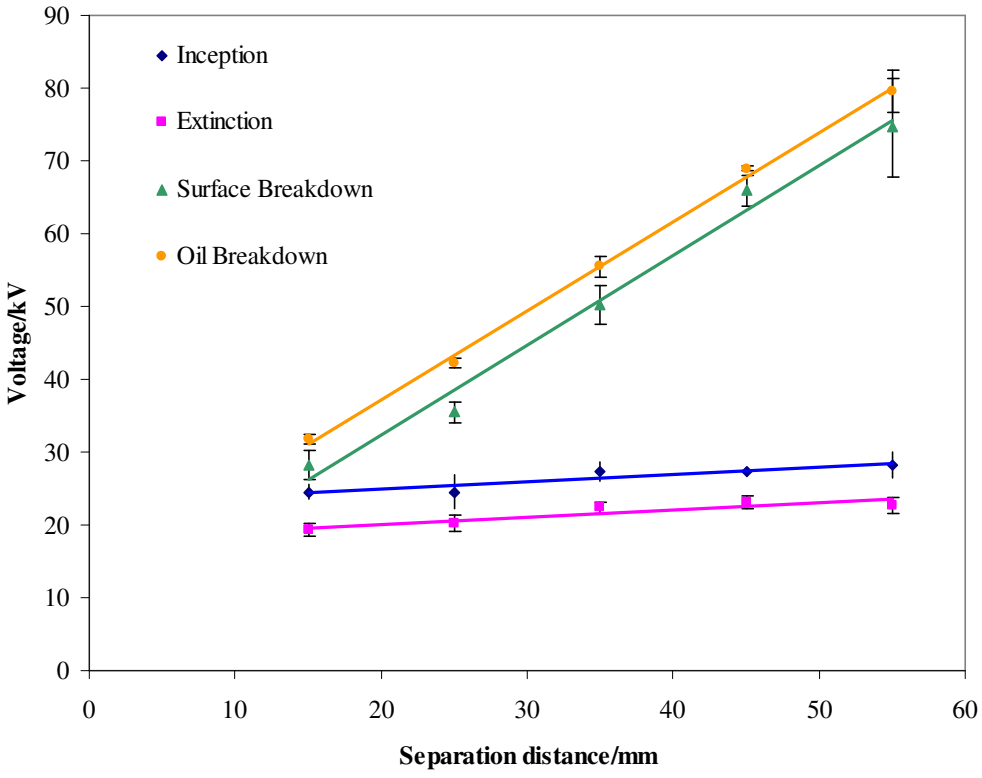

Figure 5.7 Breakdown, inception and extinction ~ distance - service aged

The graphs show that the PD inception and extinction values are insensitive to distance from the earth bar. This suggests that PD inception is due to the local field conditions

around the discharge source. On the other hand, the surface flashover and the intrinsic oil breakdown are sensitive with separation distance as both parameters increase with distance. This suggests that the bulk parameters are more dominant in these processes. With all board conditions, when the separation distance is greater than 15mm, sustained partial discharge occurs without flashover. The implication is that a local source of space charge can be sustained on the interfacial region and produce discharge which results in tracking damage.

Figure 5.8 shows ϕ-q-n plots at selected distances for un-aged board conditioned to 7.2% moisture and gaps of 35mm through to 55mm. Appendix C contains further series of ϕ-q-n plots ~ distance for pressboard conditioned to 3.6% moisture and service aged pressboard for source voltages of 25kV and 30 kV and at PD detector gain settings of 5pc, 50pC and 500pC.

The ϕ-q-n plots show two distinct patterns. One pattern shows single PD events occurring at the peak positive and negative half cycles with less frequent single PD events occurring at higher amplitudes around the peak positive cycle indicating corona discharge (e.g. Figure C.3 and Figure C.7). The second pattern shows broad PD activity occurring in the first half of each cycle which is evenly matched in amplitude which indicates surface discharge (e.g. Figure C.5 and Figure C.10) but also may include corona activity (e.g. Figure C.6). The two patterns may vary for a particular board condition which appears to suggest that the PD activity is switching from one form to the other (compare Figure C.10 with Figure C.12). In reality, this is a result of electrode distance and the localised conditions which cause the PD activity to start as either corona discharge or surface discharge and is also a function f the gain resolution.

5.2.2 Needle-bar method - effect of duration

The needle tip was positioned 35mm from the earth bar on pressboard conditioned to 7.2% moisture. A voltage of 25kV was applied (i.e. at a level above the PD inception voltage) for 12 hours. At regular time intervals a photograph of the resultant surface tracking was taken (Figure 5.9).

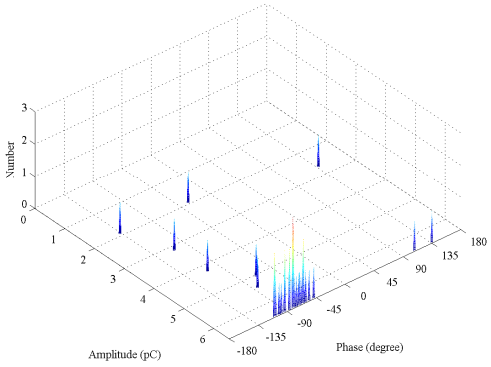

a - 20kV at 15mm distance

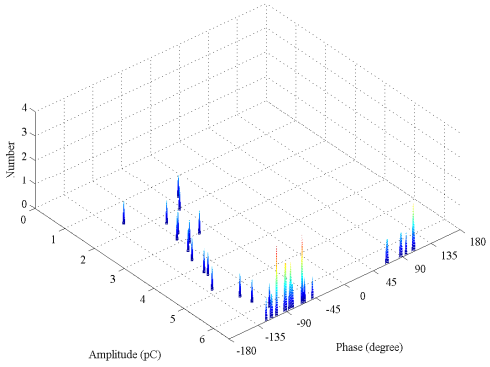

d - 25kV at 45mm distance

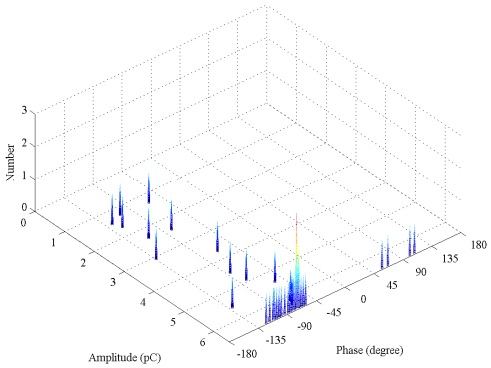

b - 25kV at 25mm distance

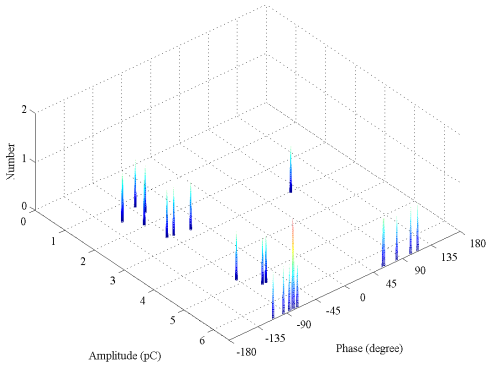

e - 25kV at 55mm distance

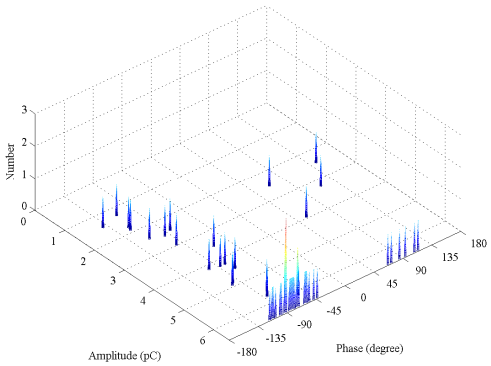

c - 25kV at 35mm distance

Figure 5.8 Series of ϕ-q-n plots ~ distance for oil bath containing virgin pressboard conditioned to 7.2% moisture. Robinson set to 5pC resolution

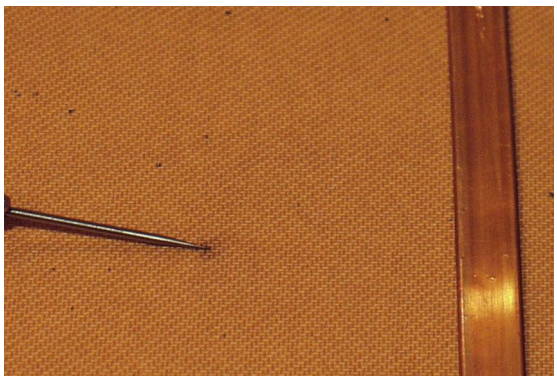

a - after 3 hours

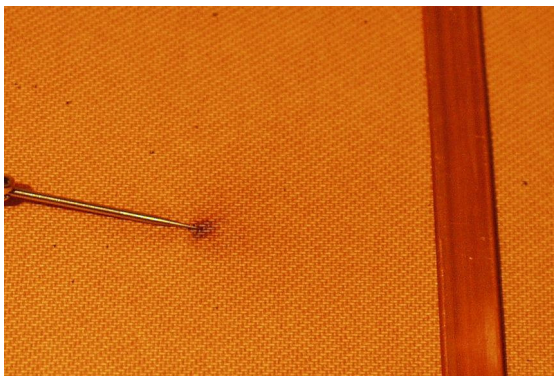

c - after 9 hours

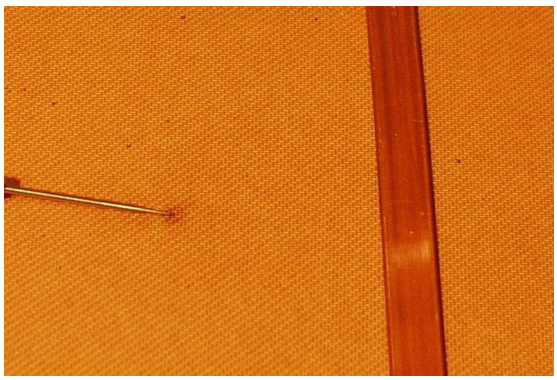

b - after 6 hours

d - after 12 hours

Figure 5.9 Time lapse sequence for pressboard with 25kV at 35mm

At 25kV, a discolouration develops around the tip and develops slightly with time. There is a suggestion of a drift in the carbonisation track towards the earth bar after 12 hours.

A second board, conditioned to 7.2%, was subjected to 30kV for 15 hours with a stop of 60 hours duration after 9 hours. Figure 5.10 shows the corresponding photograph sequence at 3 hourly intervals. At the increased level of 30kV, white marks appear after 3 hours of applied voltage with characteristic tracking lines clearly visible after 6 hours. The white marks suggest evidence of a drying action as these marks “disappeared” when the voltage was removed for 60 hours (weekend) only to reappear soon after the voltage was re-applied. After 15 hours, a significant pattern of white marks and tracking lines were established with a drift towards the earth bar clearly visible.

.

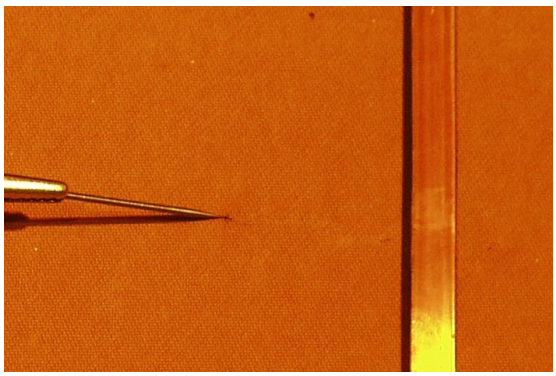

a - after 3 hours

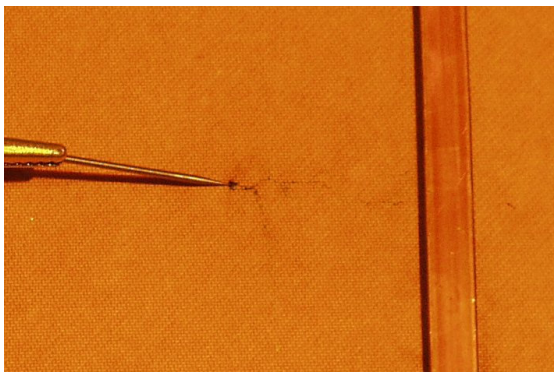

d - after 60 hour stop

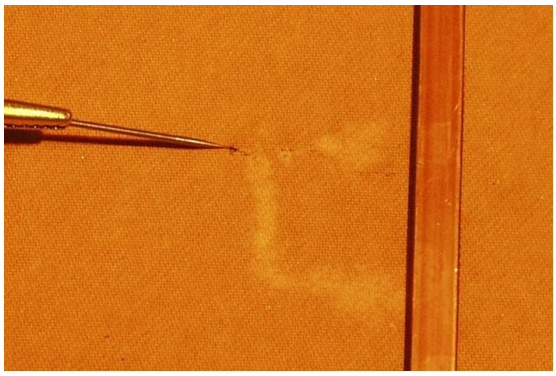

b - after 6 hours

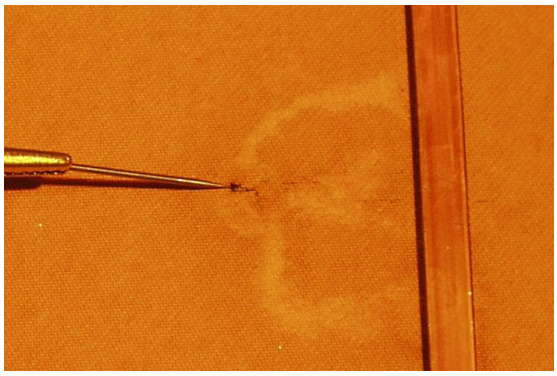

e - after 12 hours

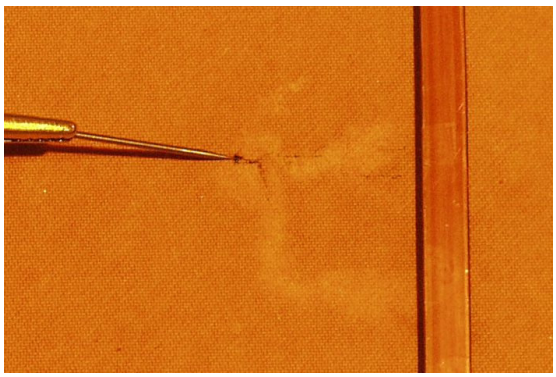

c - after 9 hours - experiment stopped.

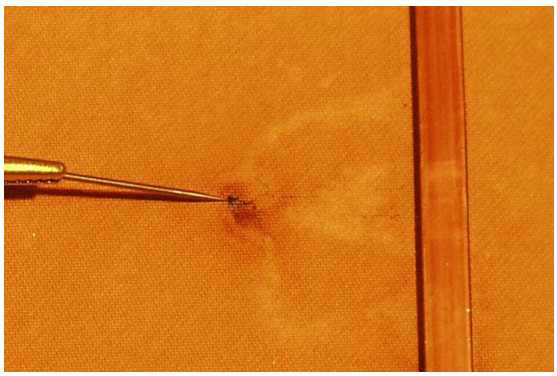

f - after 15 hours

Figure 5.10 Time lapse sequence for pressboard with 30kV at 35mm

The photo sequences indicate that duration and applied voltage are significant factors in tracking damage suggesting that the resultant damage is a voltage x time function. The figures show that tracking can be established and sustained over relatively long periods producing surface damage but without leading to surface flash-over or breakdown.

The experiment shows the clear advantage of the needle bar method over the conventional point plane method. A discharge source positioned on the surface creates partial discharges directly onto the insulation surface and causes surface discharge as evidenced by the tracking marks. The method is repeatable and sustainable for a comparatively long time without causing a breakdown event which would stop the experiment.

5.2.3 Visual observations during the breakdown process

During the experiments to determine the surface flash-over point, the breakdown processes could be followed through four distinct events as shown diagrammatically in Figure 5.11. The first event occurs at the point of PD inception when there is no *visual* indication of activity but PD is known to be established as evidenced by recorded PD activity. The second stage occurs when a corona glow develops around the discharge tip upon increasing the voltage level into the sustained PD discharge region. The corona glow is a sign that ionisation and secondary avalanche is taking place [123]. As the voltage level is increased further, a third stage occurs when thin streamers are observed from the earth bar and some audible crackling is heard. The fourth stage is the actual breakdown event which occurs suddenly but too rapidly to be observed by eye. The lack of significant tracking marks suggests that this process occurs just above the pressboard surface and justifies the term surface flash-over and is associated with the bulk liquid medium.

All breakdown events were recorded to occur on the positive half cycle which supports the observation of Lungaard that breakdown with positive streamers occur at lower voltages than with negative streamers [123]. The explanation is that, in the positive half cycle, the positive tip attracts negative charge which falls into the positive tip thus extending the region of positive space charge. The process continues in an expanding outward direction thus advancing the positive tip which attracts more negative charges from an ever increasing volume [122]. In the case of the negative half cycle, the negative tip promotes the development of an outwardly propagating negative space charge which then shields the tip thus effectively reducing the field strength at the tip tending to depress field emission. Alternatively, a higher energy (i.e. voltage) is

required to advance the space charge to achieve breakdown with a negative tip, so, a positive tip breakdown always occurs before a negative tip breakdown.

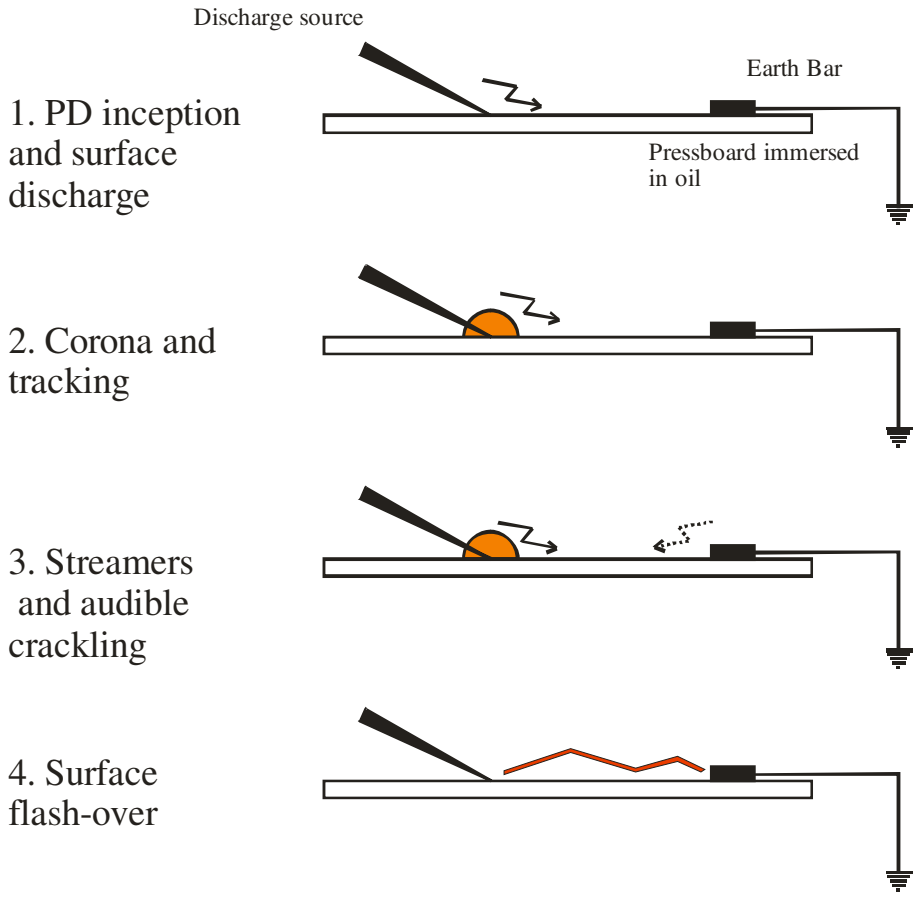

Figure 5.11 Representation of surface flashover by stages

The prolonged process of PD activity and corona during the second stage leads to localised heating which dries out the pressboard and then results in charring of hydrocarbon molecules forming tracking marks seen on the surface of the pressboard. The activation energy for mineral oil (at 0.3 to 0.7eV) is lower than that for pressboard (at 0.9eV [143]). This suggests that the tracking marks on the pressboard are more likely due to oil pyrolysis rather than that of the cellulose and that the tracking occurs at or just below the surface.

5.2.4 Discussion on needle - bar experiment

The results from the needle - bar experiment justify the criticisms of the conventional point - plane and plane - plane methods by respectively solving the problem of pressboard punch through and by providing a mechanism whereby an isolated space

charge may be generated and applied to a surface. Moreover, the following conclusions can be drawn.

Surface tracking can be sustained for a comparatively long time without surface flash-over or breakdown. An operational zone exists which is a function of geometry (i.e. gap distance) and voltage which allows partial discharge to take place without breakdown. The degree of damage due to the surface tracking is clearly a volt x time product as it depends upon the energy level (i.e. voltage) and duration. Finally, the presence of the pressboard affects the inherent withstand margin for direct breakdown through the bulk oil by depressing the voltage at which flashover occurs and collaborates the research of Lundgaard [144]. In this work, Lundgaard proposes that the voltage depression is due to field enhancement in the oil caused by the higher permittivity of the pressboard but his apparatus used a general field configuration at high voltage to generate the discharge. The results from the needle bar experiments show that the service aged pressboard (smoother in texture) depresses the withstand voltage less than the virgin pressboard. This suggests that the surface condition is the significant factor in the depression of surface flashover. (The resolution in the results for 3.6% moisture and 7.2% moisture is not sufficient to be able to determine the effect of the moisture content on voltage depression).

Figure 5.5, 5.6 and 5.7 show similar trends for the onset of PD activity with distance from the earth bar suggesting that pressboard moisture content and board contamination are not the significant factors for the onset of PD. However, the (smooth) contaminated board doesn't depress the surface flash-over as much as the rougher virgin pressboard indicating that the surface roughness plays a more significant role than contamination in the flash over process.

The real importance of the needle -bar experiment is that it reveals an operational zone in which sustained partial discharge can be maintained without flashover. The approach is to adjust the distance of the discharge source from earth such that partial discharge occurs whilst maintaining the distance from the earth sufficiently large enough to avoid flashover over a wide range of voltage level.

One document reported evidence from an inter-phase barrier failure that the barrier boards had warped and touched the high voltage coils (of an early design which did not use outer insulation wraps over the series coil) [16]. The implication is that the movement may have damaged the paper wraps and exposed the copper of the high voltage coils thus forming a discharge source from bare metal. It is thus reasonable to use a needle discharge source for the mechanism of space charge generation rather than any other. It is also reasonable to associate (i.e. connect) the discharge source to one of the voltage sources just as space charge developed from such a defect in the transformer is associated with the high voltage coil. This is the concept used to design the discharge source in the barrier model in order to understand the behaviour of space charge in the interactive field.

5.3 Barrier model design concept

The objective for the barrier model is to represent the three dimensional volume of the inter-phase region (as shown in Figure 3.8) to include two adjacent series voltage coils and the oil-pressboard sandwich of the inter-phase barrier.

The inter-phase barrier is modelled by two planar aluminium disk electrodes, perpendicular to the axis of the test cell with an oil-pressboard sandwich positioned centrally in between. Each disk electrode represents the outer surface of adjacent high voltage series coils (Figure 5.12). The discharge source, formed from a strip of copper fitted with a tungsten needle, is connected to one of the electrodes and introduced into the working space (Figure 5.13). This electrode (and the discharge source) is termed the reference electrode, V_1. The second electrode, termed the control electrode V_2, is energised from the bi –phase supply. A bare earthed aluminium bar placed on one pressboard is also introduced into the space between the disks. The reference electrode and the discharge source are thus energised simultaneously. When the voltage is sufficiently high to cause charge emission at the discharge source, localised space charge is formed at the oil pressboard interface. At the same time, the electric field from each planar electrode interacts to form the general electric field.

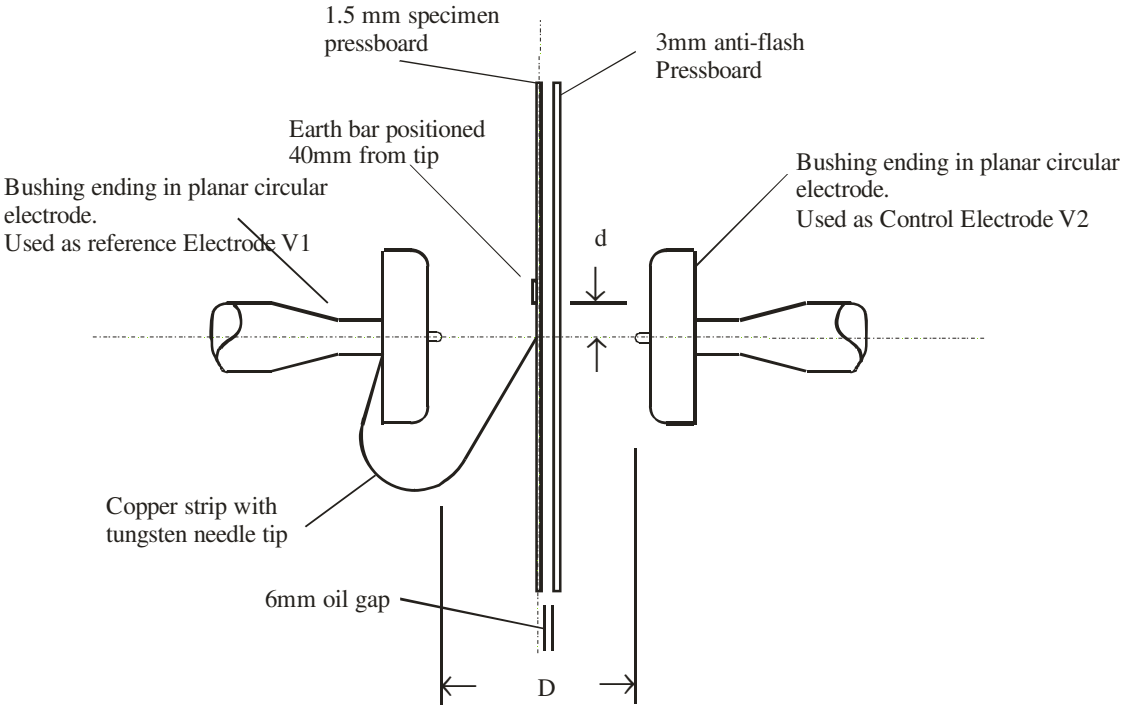

Figure 5.12 Schematic cross section of inter-phase barrier model

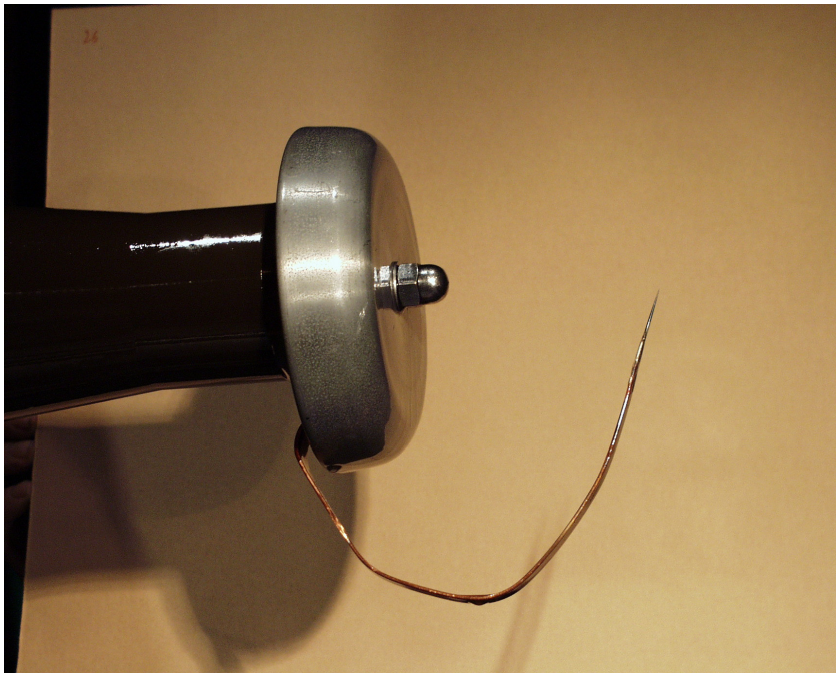

Figure 5.13 Actual reference planar electrode and discharge source

The barrier model is designed to ensure that PD activity occurs only at the discharge source. The following steps were undertaken to achieve this. Firstly, the electrodes and earth bar were ensured to be smooth thus making discharge through field emission unlikely from these areas. In addition, the electrodes and earth bar were fitted un-insulated as additional applied insulation could result in oil wedges/ cavities leading to

unintentional sources of PD. Finally, a known weak link is effectively created by deliberately inserting a sharp needle into the system and this defines the position from which the PD will originate. The electrode system (without discharge source) was confirmed PD free up to the bushing rating of 71kV.

5.4 The interaction of time varying electric fields

The electric field created around each electrode is a function of the applied voltage, the electrode shape and the spatial arrangement between the electrode and other conducting components. The two individual electric fields interact throughout the volume space to form a time varying general electric field. This general field has associated with it a temporal and a spatial component. The temporal component is a function of the phase, ϕ, and the amplitude of the two individual time varying electric vectors. The corresponding spatial component is a function of the position in space within the three dimensional volume relative to the each electrode and the other conducting components. The time varying nature of the general electric field becomes significant when it interacts with a mechanical surface such as at the oil pressboard interface.

The interacting temporal and spatial components are more easily understood by treating them separately. Considering the phase barrier (Figure 5.12) as a two dimensional (2D) model in the vertical plane (x-y) with the following assumptions: the individual time varying electrical fields are derived from sinusoidal voltages applied to the electrodes with the electrical phase angle ϕ at 120°elec. There is electrical and spatial symmetry in the y axis and the z axis (i.e. the axis out of the paper) and the pressboard is centred between the electrodes in the y-z plane. The voltage and electric field vectors follow the conventional counter-clockwise rotation with the "East" direction defined as 0°elec. for the reference voltage vector. The electric potential at any point in space (i.e. the general electric vector) is then the vector sum of the individual voltage vectors using the principle of superposition. Figure 5.14 shows the temporal vector model at any point within the 2D space with the control voltage, V_2 lagging the reference voltage, V_1, by the phase angle, 120°. In this case, the resultant electrical vector for the general field leads the reference vector by 30° elec.

The electric stress at any point is defined as the electrical gradient, i.e.:

$$E = -V / d \qquad (5.1)$$

where V is the electric potential difference over a corresponding mechanical distance d. The minus sign denotes that the electric stress is in the opposite direction to the electric potential vector and indicates the physical direction that a free negative charge would take.

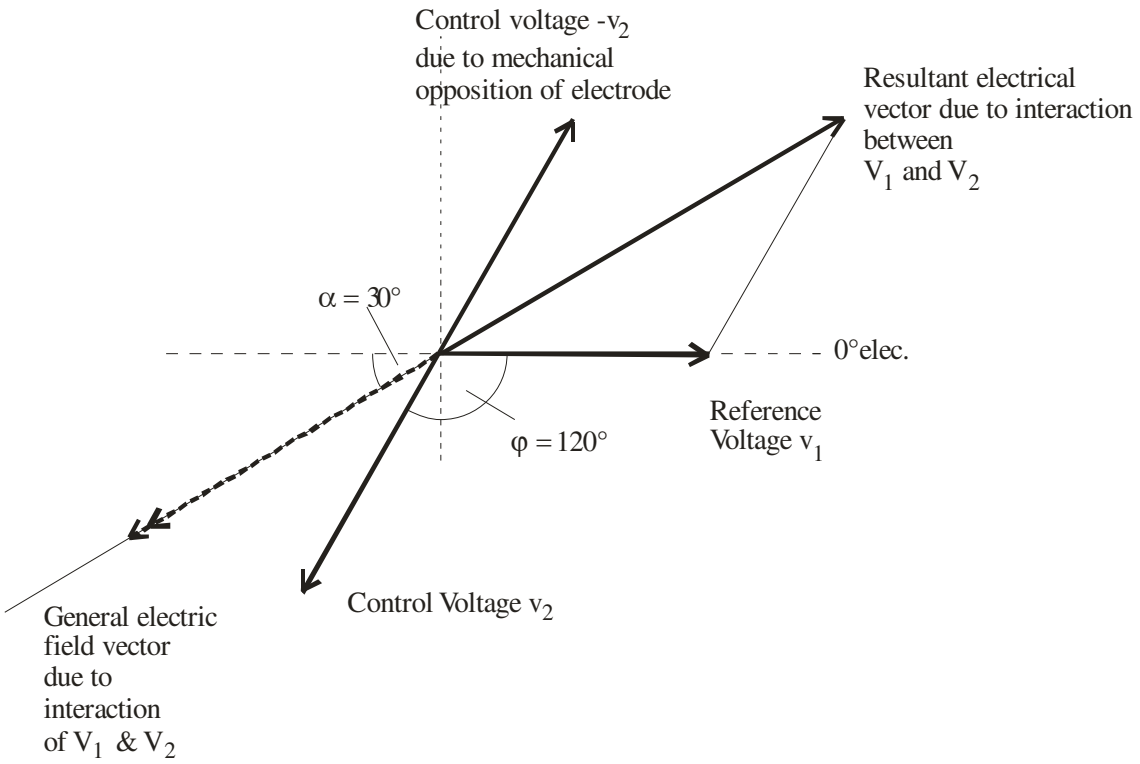

Figure 5.14 Temporal phasor diagram of voltage interaction showing resultant general electric field

In this case, the general electric field lags the reference voltage by 150° elec. in the time domain and is illustrated in Figure 5.15. A general electric vector is set up which is a function of the magnitude of the individual electric vectors and the phase difference between them. However, equation (5.1) clearly shows that the electric stress is associated with the spatial domain. Therefore, the mechanical spacing must be taken into account when defining the electric stress.

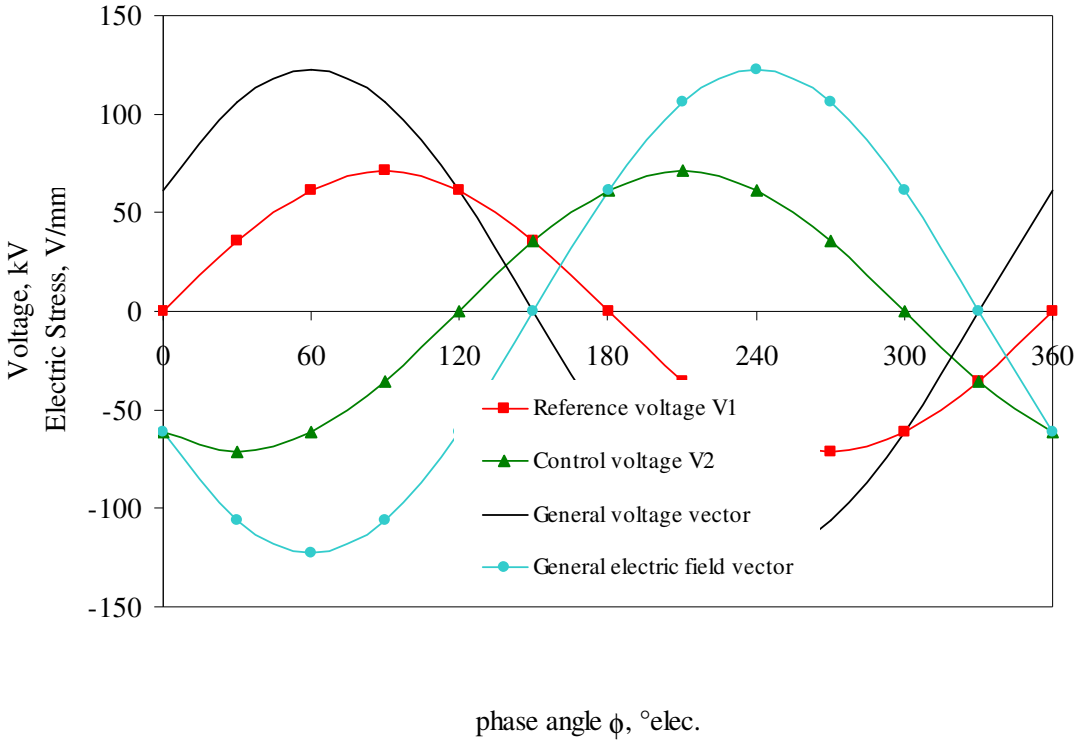

Figure 5.15 Time domain plot of voltage and electric field vectors related to electrical phase angle

5.4.1 Moving from the temporal domain to the spatial domain

For the phase barrier model, with the pressboard parallel to the planar electrodes, the mechanical direction for maximum through electrical stress in the pressboard is when the electrical stress vector is at 90° in the spatial domain. Therefore, when moving from the temporal domain to the spatial domain, the electric field must be rotated by 90° anticlockwise to take into account the attitude of the pressboard in the y axis (Figure 5.16) in order to determine the electric stress. When the general electric field is perpendicular into the surface of the pressboard, the resultant electric stress is the through stress with an associated maximum through stress. When the general electric field is aligned with the surface the resultant electric stress is the creep stress with an associated maximum creep stress. In the case of the barrier model at 120° elec. phase difference, the parallelism of the pressboard to the plane electrodes and the orthogonality of creep and though stress means that the peak through stress is in phase with the general electric field (at 60°elec.) and the peak creep stress field occurs 90°elec. in time later (i.e. 150°elec. referenced to V_1) and is shown in Figure 5.17.

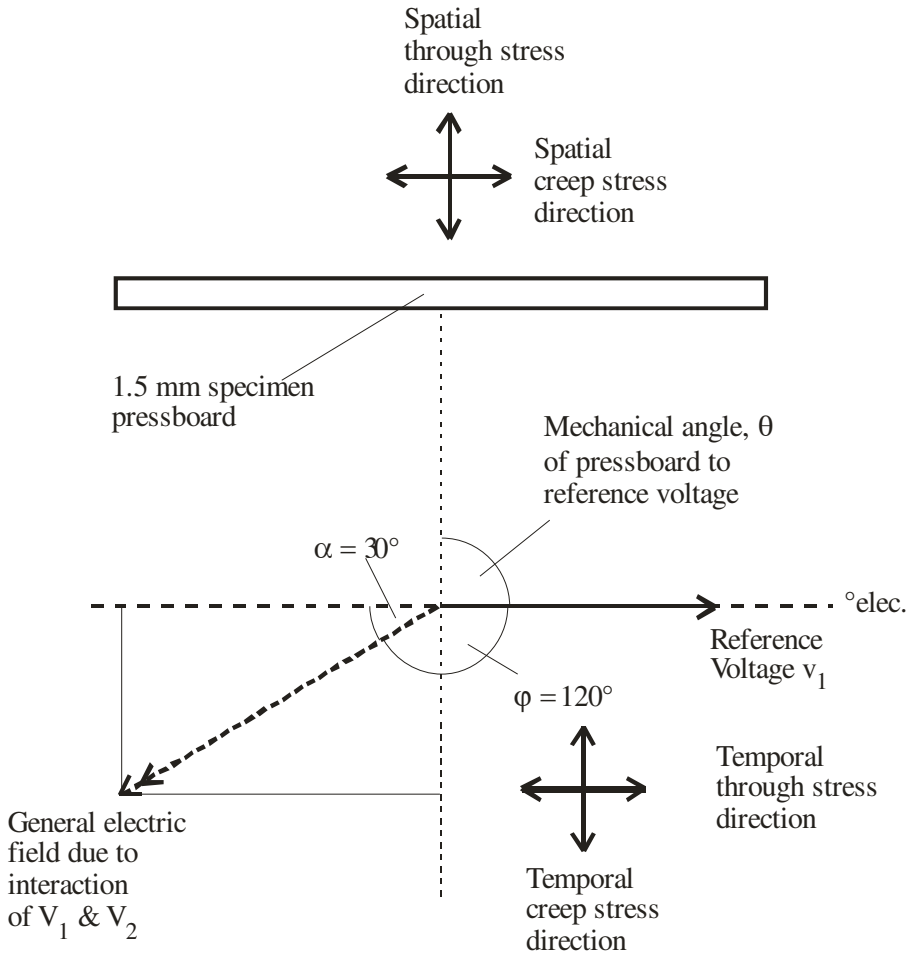

Figure 5.16 Spatial phasor diagram showing electrical stress resolved into two orthogonal components

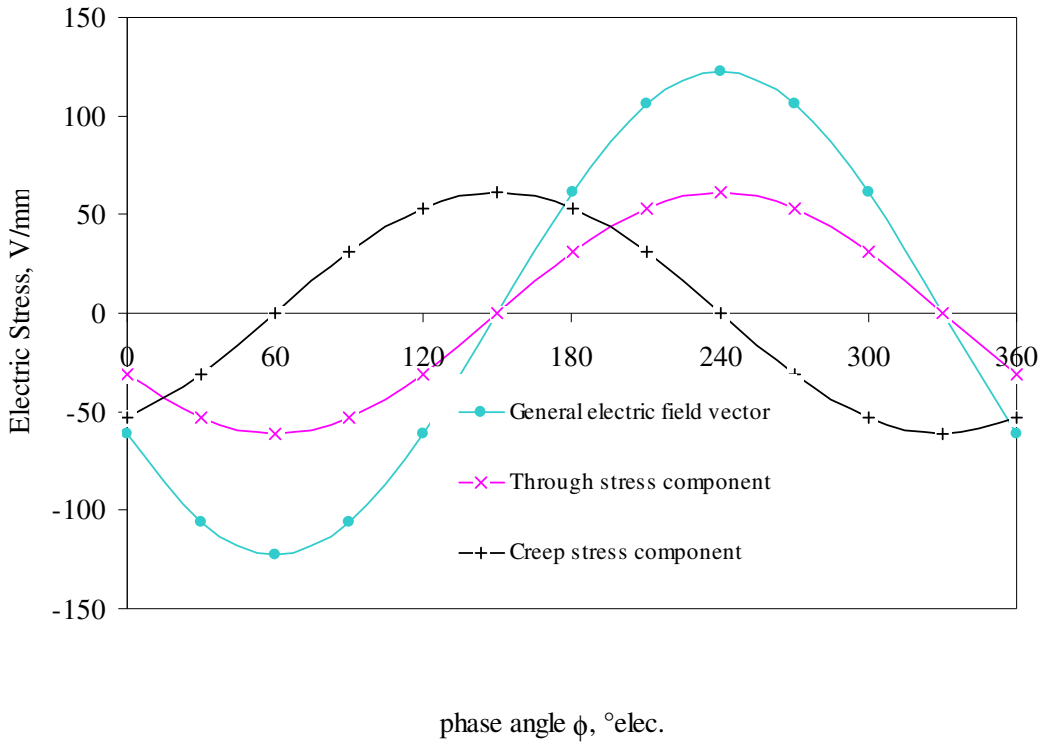

Figure 5.17 Time domain plot of stress showing time relationship of maximum creep and through stress with the general electric field vector

The implication is that the spatial attitude of a surface positioned within a time varying electric field needs to be taken into account to determine at what point during the electrical cycle the maximum creep stress or through stress occurs. Also, the directionality of the electric stress suggests that electric stress affects electrical charge at the interface in two different ways; the through stress enhances the polarisation at the interfacial layer whereas the creep stress promotes a drift of surface charge away from the high field region which describes the mechanism for creeping discharge.

The 2D time domain plots can only show the changing nature of the electric stress and not the magnitude because the magnitude of the electric field stress is directly linked to the spatial domain through equation (5.1). This may be variable according to the stress direction. The general electric field vector exists all the time as the time varying potential vector which is changing in direction. It is the instantaneous electric potential at the point in question and the spatial distance between the point in question and another point in the direction of the general electric field which determines the magnitude of stress. The implication of this is that the magnitude of the electric stress in two orthogonal directions can be completely different depending upon the mechanical profile. This makes electric stress analysis very difficult for complex geometries without the aid of FEM packages. Figure 5.17 shows equal creep and through stress for illustrative purposes only. The creation of the general electric vector is determined by the magnitudes and phase relationship of the individual electric vectors and this enables the derivation of a range of general electric fields.

5.4.2 The creation of two special general electric fields

The previous analysis considered a simplified model with 120° elec. phase difference between the voltage vectors. A combined general temporal and spatial phasor diagram is shown in Figure 5.18. The spatial creep stress is (using vector notation):

$$\overrightarrow{e_{creep}} = \left|\overrightarrow{e_1} + \overleftarrow{e_2}\right|_V \tag{5.2}$$

$$\overrightarrow{e_{creep}} = \left|\overrightarrow{e_1} - \overrightarrow{e_2}\right|_V \tag{5.3}$$

Similarly, the through stress or perpendicular stress is:

$$\overrightarrow{e_{through}} = \left|\overrightarrow{e_1} + \overleftarrow{e_2}\right|_h \tag{5.4}$$

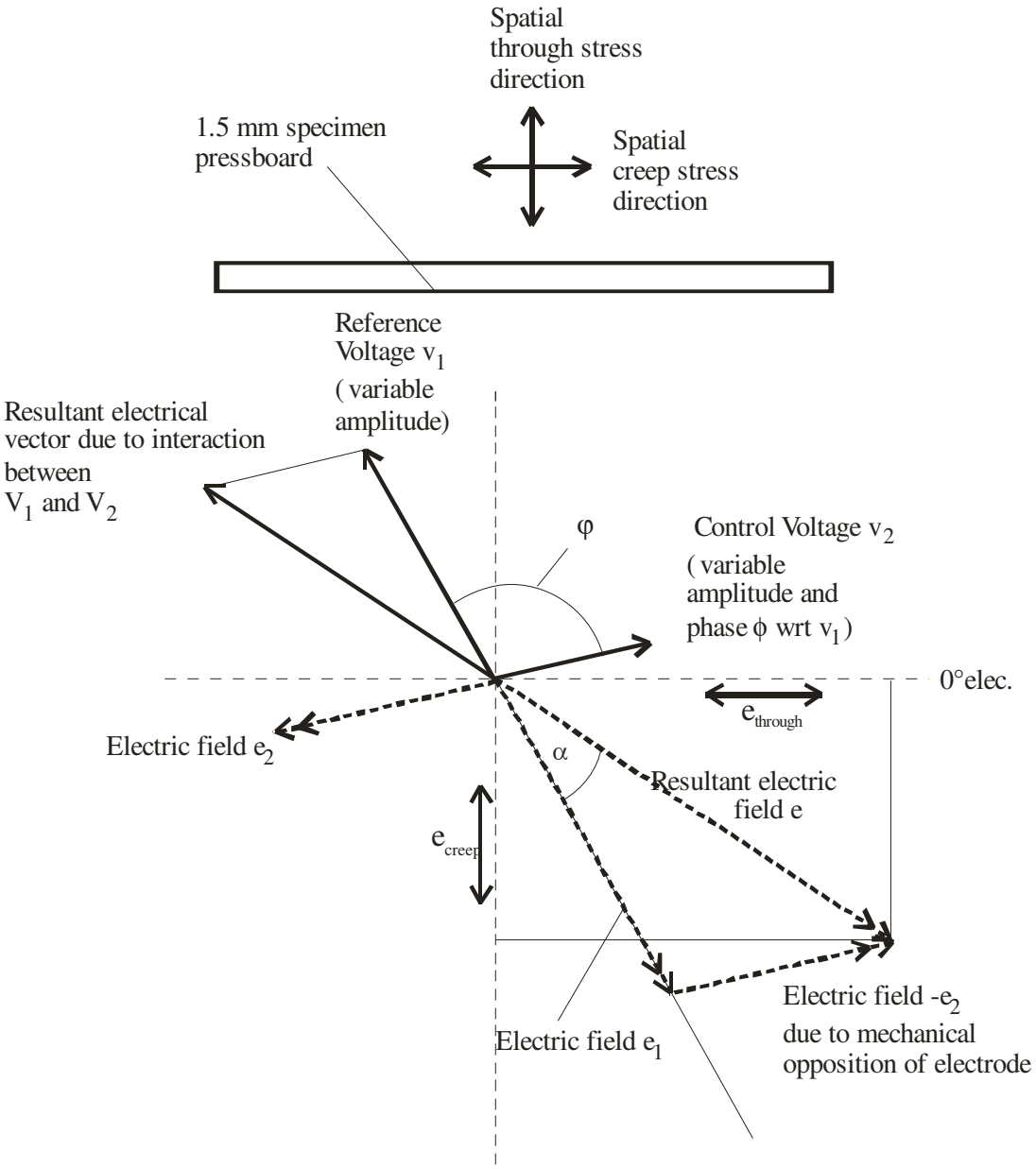

Figure 5.18 Combined temporal/spatial vector diagram for general condition

$$\overrightarrow{e_{through}} = \left|\overrightarrow{e_1} - \overrightarrow{e_2}\right|_h \qquad (5.5)$$

When the two voltage vectors are identical in amplitude and phase (i.e. $\phi = 0°$ and $V_1=V_2$, then $\overrightarrow{e_2} = \overrightarrow{e_1}$

$$\overrightarrow{e_{creep}} = \overrightarrow{e_{through}} = 0 \qquad (5.6)$$

showing that there is no electric stress due to the absence of a general field. Similarly, when the two voltages are in anti-phase (i.e. $\phi = 180°$ and $V_1=V_2$, then $\overrightarrow{e_2} = -\overrightarrow{e_1}$)

$$\overrightarrow{e_{creep}} = 2\left|\overrightarrow{e_1}\right|_v \qquad (5.7)$$

$$\overrightarrow{e_{through}} = 2\left|\vec{e_1}\right|_h \qquad (5.8)$$

Under this condition, the creep stress and the through stress are both at the maximum values for the applied voltages and 90° out of phase.

5.4.3 The electrical stress profile in a large transformer

The creep stress and the through stress thus vary not only in time but also according to position in 3 dimensional space with the respective maxima occurring 90° out of phase but acknowledging the fact that the maxima may be completely different due to the mechanical spacing in the stress orientation. In the case for a large 3 phase transformer with the electrical phase difference, ϕ at 120°elec., the maximum through stress occurs at 60° elec. and the maximum creep stress occurs at 150° elec.; (i.e. when the general electric field is reversing polarity). The FEM (i.e. Figure 3.9) has already shown that maximum electrical stress occurs along the vertical axis of the pressboard and at the top and bottom edges under these conditions but this representation doesn't differentiate through and creep stress which can be shown by cross sectional plots.

Figure 5.19 gives plots of through stress and creep stress along the vertical surface of the inter-phase pressboard at 60° elec. and 150° elec. respectively using both 2D and 3D FEMs. These show that, under normal conditions, the maximum through stress at the pressboard centre is 1200Vmm^{-1} and occurs at 60° elec. The maximum creep stress is 100Vmm^{-1} and occurs at the pressboard edges and at 150°elec. showing the time, magnitude and directional variance nature of creep and through stress.

5.4.4 The electrical stress profile in the test cell model

In the test cell, the through stress and creep stress can be altered either by adjusting the voltage on the electrodes and/or adjusting the electrode separation distance. Table 5.1 shows the predicted maximum creep stress (at board edge) and through stress (at board centre) for normal 120° phase operation derived from a 2D FEM of the test cell at selected electrode voltages and separation distances, (where V is bushing rated voltage of 71kV and D_{max} is 183mm between the electrodes) and compared against the creep stress and through stress predicted from the 2D FEM of the 3 phase transformer (Figure 3.10).

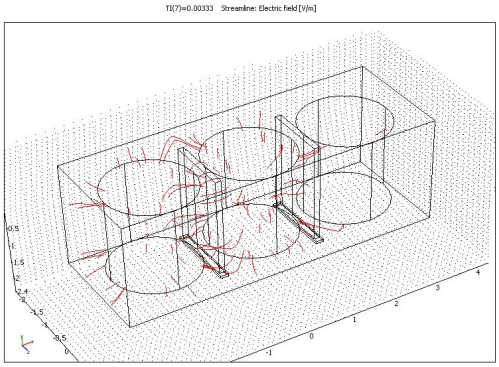

a - 3D model at 60° elec. showing streamlines

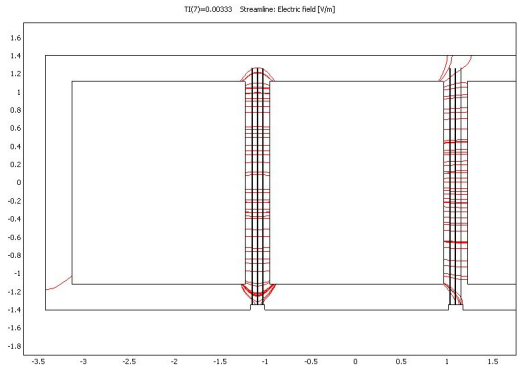

b - 2D model at 60° elec. showing streamlines

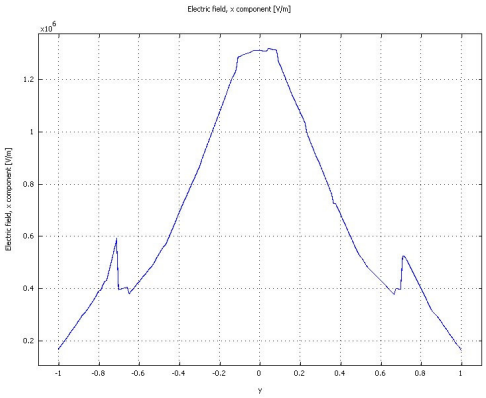

c - (3D) through stress: y direction at 60°

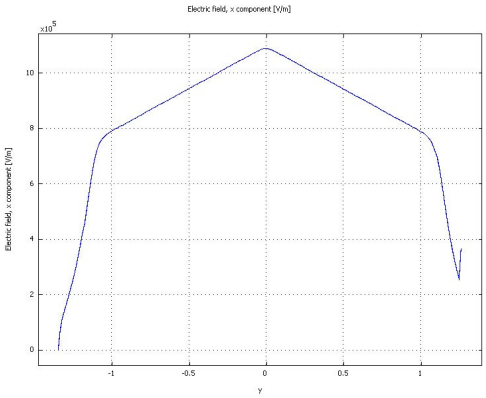

d - (2D) through stress: y direction at 60°

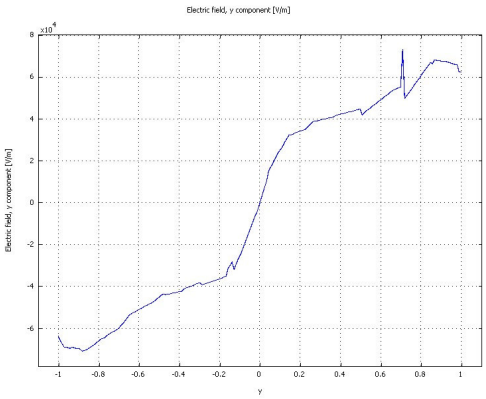

e - (3D) creep stress: y direction at 150°

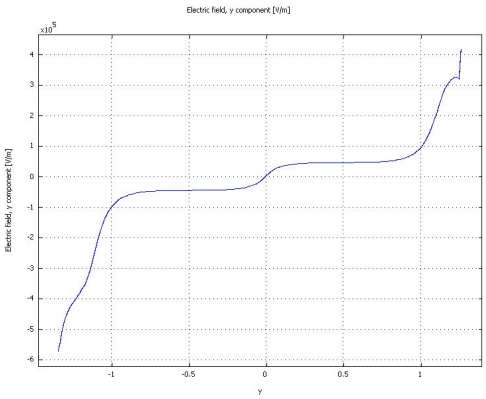

f - (2D) creep stress: y direction at 150°

Figure 5.19 Comparison of through stress and creep stress using 2D and 3D FEM

Table 5.1 Comparison of maximum predicted through stress and creep stress between 1000MVA and test cell at various test cell options

	1000MVA Transformer	**Test Cell**				
Scale factor	**Rating**	**Rating**	**½ V**	**½ D**	**¼ D**	**Mimic**
Line Voltage (kV)	400	123	61	123	123	43
Phase Voltage (kVrms)	231	71	35	71	71	25
Phase-phase (mm)	266	183	183	92	46	46
Pressboard height (mm)	2600	450	450	450	450	450
P/b centre to earth (mm)	1300	375	375	375	375	375
Max. through stress* (V/mm)	1100	815	405	1600	3000	1000
Max. creep stress** (V/mm)	40	150	80	190	200	70

*Max through stress occurs at board centre
**Max creep stress occurs at board edge

The FEM approach indicates that the test cell gives a good approximation of "normal" field conditions of the 3 phase transformer when the electrodes are spaced at ¼ the maximum distance and the voltage applied to the electrodes is 25kV (i.e. one third the bushing rating). However, for the series of experiments, the electrodes were set to maximum distance to explore the effect of a weaker general field acting on a discharge source placed on the pressboard to explore the effect of the general field on space charge. The earth bar to discharge source distance, d, is set to 40 mm in order to avoid potential influence from the creep stress at the fringes of the pressboard. Figure 5.20 gives a FEM snapshot of the test cell without earth bar at 140° elec. (i.e. just before conditions of maximum creep stress and field reversal) showing that the maximum creep stress occurs at the edges as indicated by the streamlines. Figure 5.21 is the FEM snapshot under the same conditions, but with the earth bar inserted, showing that the earth bar creates its own local conditions but is outside the area of fringing.

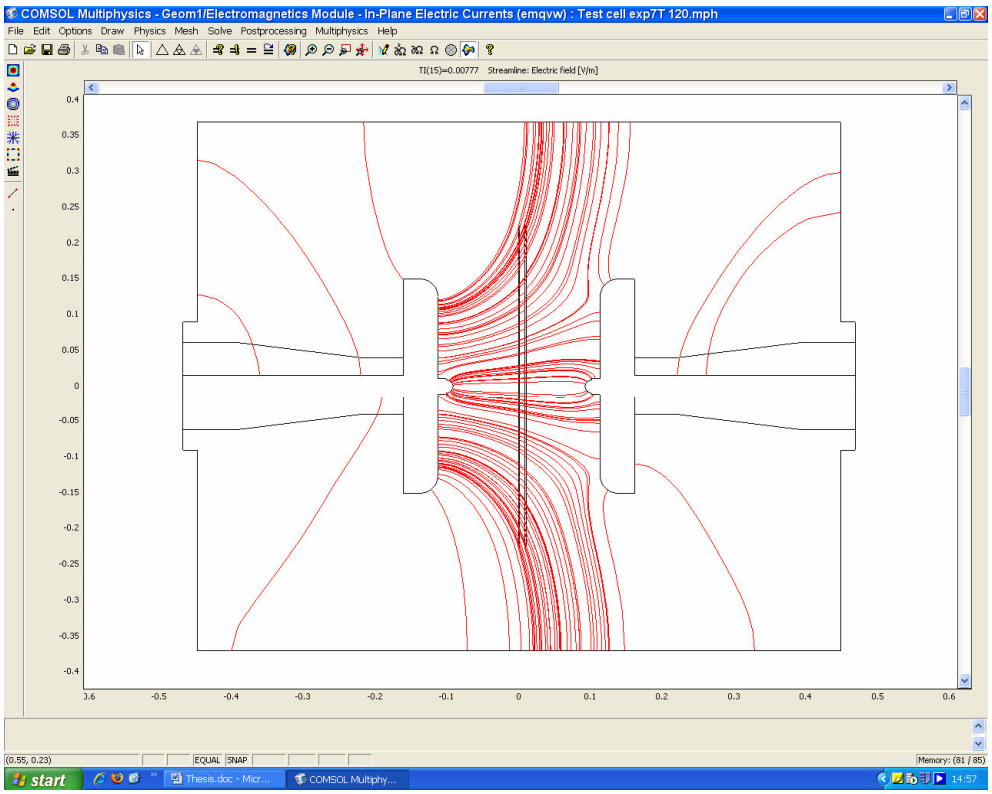

Figure 5.20 2D FEM of test cell at maximum electrode spacing and 25kVrms showing streamlines at 140° elec.

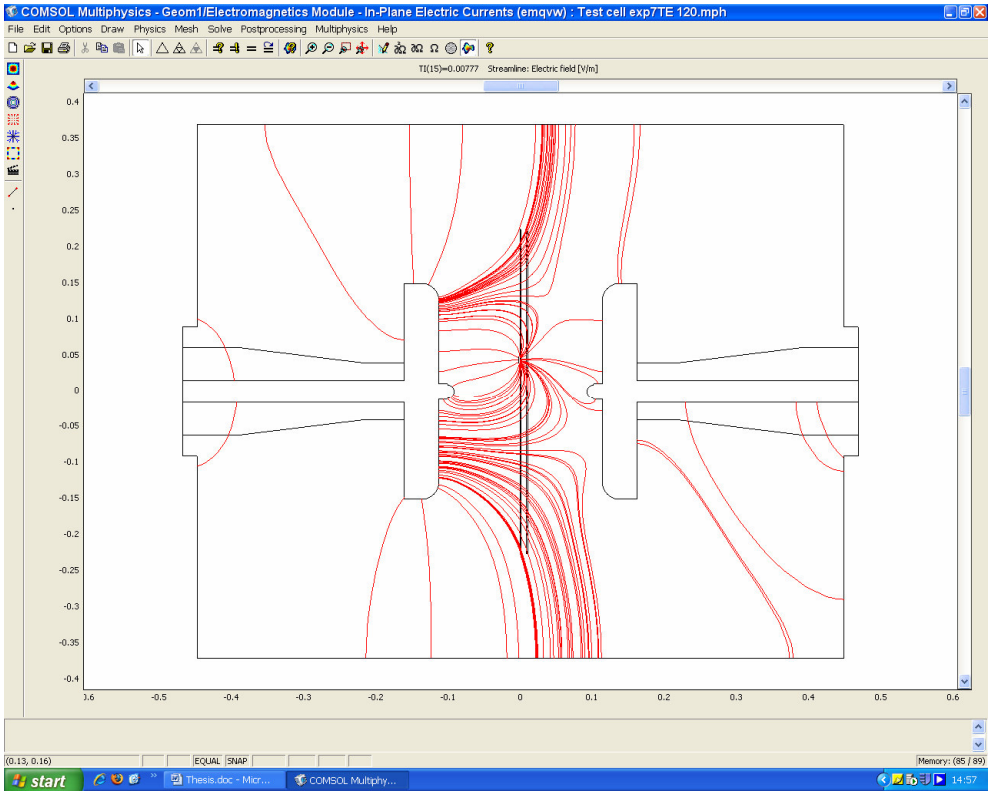

Figure 5.21 2D FEM of test cell at maximum electrode spacing and 25kVrms showing effect of earth bar at 140°elec.

Creep stress is therefore a major issue in regions of tight geometry and under conditions where the electric field cuts the geometry at sharp angles such as voltage coil end insulation [145].

An infinite number of interactions are possible between the local field (arising from the discharge source) and the general field, itself a result of the interaction of the electric fields from the two electrodes. However, three particular cases are considered to explore the effect of the general field on surface discharges arising from the discharge source.

5.5 Test cell configurations

Figure 5.22 shows the configuration when both electrodes have the same amplitude and phase. The electric fields are mechanically opposed due to the physical arrangement of the electrodes. The interacting electric fields result in a null general field. Space charge is subjected solely to the local field from the discharge source and acts towards the earth bar along the surface of the pressboard.

Figure 5.23 shows the configuration when one electrode is grounded. Space charge is subjected to the interaction of the local field from the discharge source with the uniform time varying general field derived from one electrode to earth.

Figure 5.24 shows the configuration where the general field is the result of the interaction between electric fields from the control and reference electrodes when there is a phase difference, ϕ, but with amplitude equal at $A_2=A_1$.

The general field is a result of the interaction of the two fields with an infinite number of solutions depending upon the phase angle difference, ϕ (shown as 120° lagging in Figure 5.24). As the phase difference increases from 0° to 180° the general field changes from the null field (as in Figure 5.22) until, at the phase difference of 180° (i.e. in anti-phase), a general field is formed enhanced by a factor of 2 over the situation as in Figure 5.23.

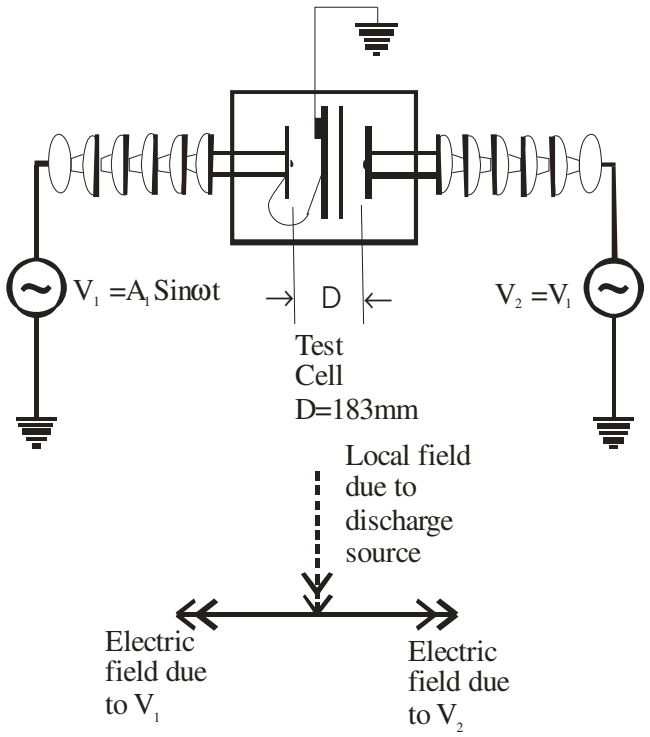

Figure 5.22 Interaction of electric fields resulting in no general field

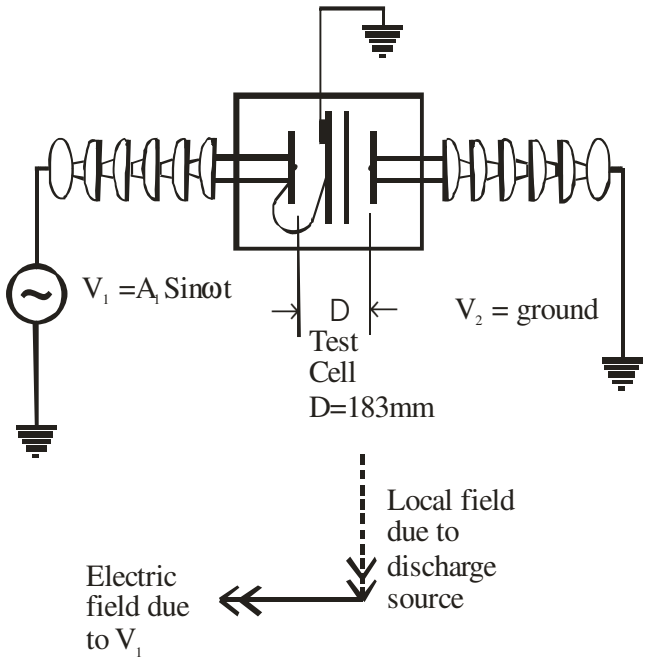

Figure 5.23 Fixed general field due to electric field from V_1 alone

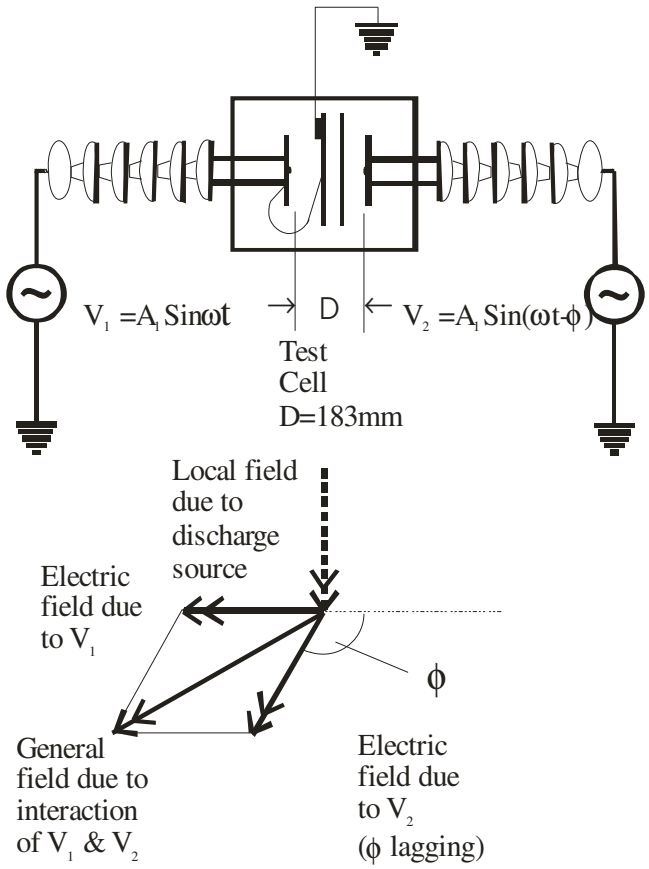

Figure 5.24 General field due to interaction of electric fields from V_1 and V_2

Table 5.2 shows the predicted electrical stress on a point on the pressboard which is mid way between the discharge source and the earth bar. At any condition, the resulting general field has a through component and a creep component acting on the local field. Table 5.2 shows that the creep stress due to the general field acting on the discharge source is negligible under all conditions and thus the creep stress is only due to the local stress field associated with the discharge source. At the same time, the through stress acts on the localised field according to the general field conditions. However, in comparison to the typical electric stress of $7kVmm^{-1}$ necessary at the discharge source to create discharge through field emission, the through stress acting on the localised field (typically $300Vmm^{-1}$) is relatively small. The particular cases when ϕ is 120° lagging or 120° leading are significant, as these configurations replicate the general field conditions existing within the two inter-phase barrier regions of a transformer.

Table 5.2 Comparison of maximum predicted through stress and creep stress for standard test cell under various test configurations.

	Test Cell Model	**Experiment**				
		$V_1=V_2=0$	**$V_2=0$**	**$V_2=V_1\angle\phi$**		
General field phase	**120°**			**60°**	**120°**	**180°**
Line Voltage (kV)	43	43	43	43	43	43
Phase Voltage (kVrms)	25	25	25	25	25	25
Phase-phase (mm)	183	183	183	183	183	183
Pressboard height (mm)	450	450	450	450	450	450
P/b centre to earth (mm)	40	40	40	40	40	40
Through stress* (V/mm)	285	0	165	165	285	330
Creep stress* (V/mm)	5	0	5	8	5	0
Local through stress* (V/mm)	0	0	165	165	280	330
Local creep stress* (V/mm)	0	510	530	550	520	510

* Through stress and creep stress at halfway point between discharge source and earth bar

5.6 A new model for the oil-pressboard interface

Pressboard is classed as a solid material. The use of the word "solid" conveys the sense of a homogenous and dense material, but pressboard is in fact a light fibrous and porous material. This explains why an impregnation process is necessary as this removes moisture and gasses from the fibrous structure and refills the interstices with oil molecules. The measure of impregnation is defined by the oil absorption which is taken to be 13% typically for transformerboard TIV [29] though it varies according to material and surface finish [146]. After the impregnation process, the oil pressboard insulation medium forms a composite insulation structure, the interface of which appears to change abruptly from bulk pressboard to the bulk oil. Current research on static electrification at the oil/pressboard interface focuses on the chemistry of pressboard rather than mechanical surface features such as porosity and surface roughness which are only mentioned in passing [147].

A visual study of the surface of pressboard reveals that the situation is actually rather more complex. Pressboard is manufactured in a range of surface finishes from smooth (i.e. calendered) to a textured cloth finish [34]. Standard TIV transformerboard (as used in the experiments), is made with a textured finish characterised by a fine array of

dimples approximately 0.7mm x 0.2mm x 0.1mm deep (Figure 5.25). At a higher magnification the fibrous structure on the surface becomes more obvious (Figure 5.26).

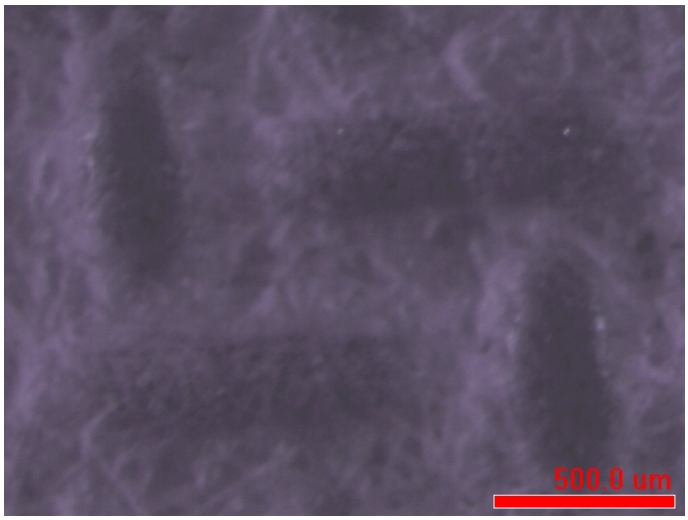

Figure 5.25 Surface morphology of dry pressboard at 50X magnification

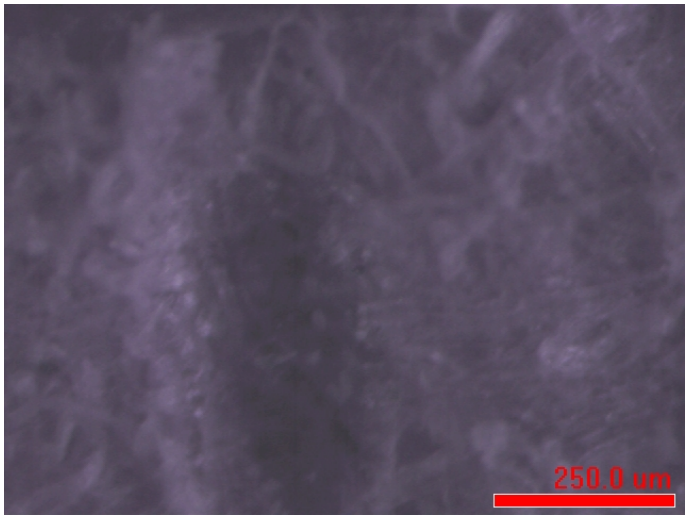

Figure 5.26 Surface morphology of dry pressboard at 100X magnification

The oil-pressboard interface is in reality not a “clean” edge but rather a transition region comprising a heterogeneous region between the bulk oil/pressboard composite and the bulk oil. In this transition region, the ratio of oil changes from the typical value (i.e. the bulk value of oil adsorption, say 13%) towards 100% as the material structure changes from the bulk oil/pressboard composite medium to the oil medium forming a

heterogeneous oil/pressboard zone further complicated by the presence of the dimples. The liquid boundary layer resides just outside this transition zone.

The classical mechanical model, with non-polar solid and liquid molecules (such as the mineral oil and pressboard), describes the liquid boundary layer due to the weak Van de Waals forces between the covalent molecules. The liquid molecules, closest to the "solid" medium, stick to the solid and form the so-called "no-slip" layer which is the Stern layer in the GCS model (thus linking the EDL model to the mechanical model). These molecules are fixed and there is a gradual transition from stationary oil molecules to the flowing oil molecules in the free stream with the region in between forming the boundary layer. The boundary layer is small in thickness for laminar flow and increases in thickness for turbulent flow. The rough surface increases turbulent flow and the thickness of the boundary layer whereas a smooth surface diminishes the turbulence and hence the thickness of the boundary layer. The mechanical model of the oil pressboard interface may be better described as a liquid boundary layer containing the no-slip layer next to a heterogeneous transition region which merges into the bulk homogenous oil/pressboard composite structure (Figure 5.27).

The EDL model describes a homogenous solid surface with the EDL existing at a thickness of no more than one or two molecules next to it [111]. The visual inspection suggests that the interface is actually more complicated in the case of the porous interface between oil and pressboard. The results from the needle-bar experiment confirm the complexity and suggest that two different mechanisms may work at the interface depending upon the energy level of the discharge source.

The experiments show that surface discharges and flashover occur in a non-flow fluid environment as the oil is stationary over the pressboard. (This does not mean that oil flow is not also an enhancing factor as this has been demonstrated experimentally for static electrification by Zhang [107]). The tracking, (which progresses away from the discharge source and is a function of energy level and time as evidenced by the duration experiment), is clearly the result of the electronic action in the pressboard at the layers just below the surface suggesting that the tracking is primarily associated with the transition region.

The flashover which occurs at higher energy levels from the discharge source happens just above the surface suggesting that it is associated with the oil boundary layer next to the pressboard. The rougher surface of textured pressboard has thicker boundary layer/EDL (i.e. the interfacial layer) which allows more charge to accumulate for a given voltage and explains why flashover results at a lower voltage than would occur with the same separation using the smoother surface. This suggests that there are two possible paths available for charge transport along the interfacial layer i.e. one which uses the oil EDL and another which uses the heterogeneous oil/pressboard transition zone.

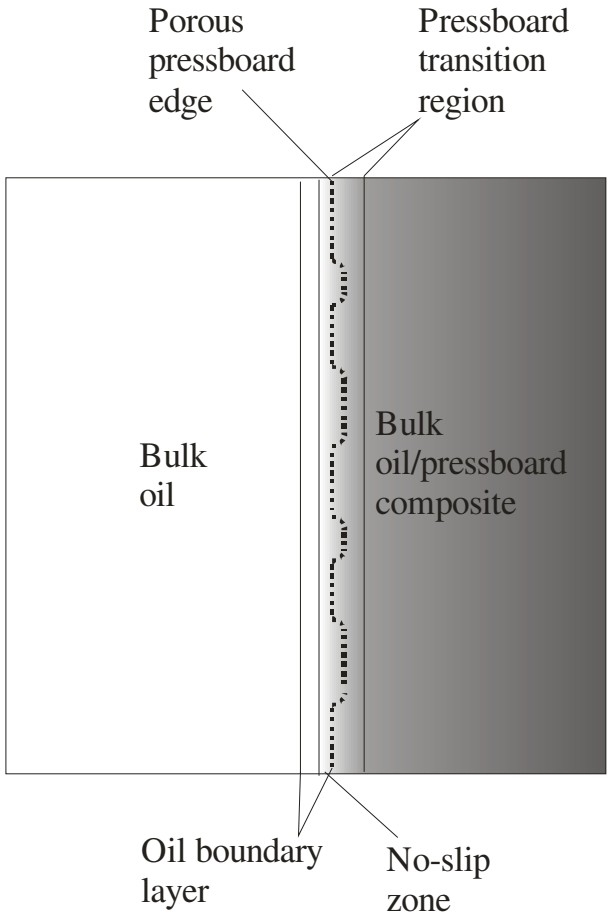

Figure 5.27 Boundary layer model of oil pressboard interface

5.7 Summary

This chapter has answered two technical questions revolving around the design of the discharge source and the test cell inter-phase model. The first question is how to reliably create surface discharge without undue damage to the specimen under test. The second question relates to how do two electrical fields interact and the effect of the general field on a dielectric discontinuity such as created by an oil pressboard interface.

The first question was answered by reviewing the conventionally accepted methods to create surface tracking. These were found wanting and a totally new approach had to be developed. The new approach overcame the problems of board puncture and general field effects exhibited by the conventional methods. The new approach showed that an ionising discharge source, when placed in close contact at the oil pressboard surface, results in PD and surface discharges leading to surface tracking but without immediately leading to breakdown. The results of these experiments lead to three significant conclusions.

The first is that the degree of damage due to PD is time and voltage level dependent. This means that surface tracking can be established and sustained on the oil-pressboard interface for a considerable time without electrical breakdown thus solving the first question.

The second conclusion is that the inception/extinction of the PD is insensitive to the gap distance from earth suggesting that surface discharge is a local phenomenon associated with the interaction of high electric field strength on a defect. Surface flash-over and intrinsic oil voltage breakdown are sensitive to the gap distance indicating that these are mechanisms associated with the bulk material properties.

The third is that the presence of the solid surface depresses the intrinsic voltage withstand of the bulk oil medium so that surface flash-over occurs at a lower value than the bulk medium properties would predict. The evidence of damage from tracking and surface flash-over suggests that these events occur at two different layers associated with the oil pressboard interface structure and that the structure of the surface plays a role in the level of voltage depression.

The morphology of the oil pressboard interface along with the conventional views on boundary layer and EDL theory was re-examined in the light of these results. This indicated that the interface is more complex than the conventionally accepted simple liquid solid interface due to the texture and porosity of the pressboard. A new oil-pressboard boundary layer model was proposed which explains the difference between tracking and surface flashover. Tracking damage is caused by drying out the pressboard

and then pyrolysis of the oil molecules embedded in the pressboard transition region suggesting that it is primarily a sub-surface effect associated with the transition zone. Surface flashover is a general process which occurs just above the surface of the pressboard suggesting that it is associated primarily with the oil in the EDL.

The second question relating to the electric field interaction was answered by developing a vector model the results of which supported the FEM of a large transformer in comparison to the test cell model. The vector model indicated that the general electric field has an interacting temporal and a spatial component associated with it. The temporal component is a function of the magnitude and phase of the applied voltages. The spatial component is a function of the directionality of the temporal component and the mechanical aspect in this direction. When the general electric field interacts with a solid interface, the directionality of the electric field and the attitude of the interface determine whether the effect is either through stress or creep stress which are always 90°elec. out of phase. Finally, maximum creep stress is shown to occur during the transition in phase of the electric field and at spatial regions where the general electric field is highly divergent.

When the vector model was applied to the test cell, it showed that a complete range of general electric fields could be created. Three specific configurations were considered and are chosen as the basis for the test cell experiments. The next chapter considers the effect of the surface discharges on pressboard in the barrier models as a function of phase difference, temperature, moisture content and board condition.

Chapter Six

Experiments using the discharge source in the barrier model

The oil-bath experiments identified three factors necessary for the development of surface tracking on pressboard. The first is the distance of the discharge source from the earth bar. It is necessary to choose a value which is greater than the distance where PD inception can immediately lead to surface flash-over. The second parameter is the voltage x time product. The voltage must be sufficiently high to initiate PD inception and promote tracking damage within a reasonable time frame. Finally, the voltage must not be too high to result in surface flash-over at the distance chosen. The duration experiment showed that a source voltage of 30 ~ 35kV with the discharge source located 35 ~ 40mm from the earth bar produces tracking after 6 hours. These factors were taken into when configuring the test cell to model the inter-phase barrier region.

6.1 Experimental objectives

The objectives of the experiment were to investigate the following conditions over a temperature range of 20° to 60°C:

- Onset of PD activity caused by the local field alone.
- Onset of PD activity caused by the interaction of the through general field (through stress only) on the local-field.

- Effect on the local field PD activity with the interaction of the general field which is changed as a result of phase change between the electrode field sources.
- A duration experiment at room temperature (20°C) to assess the time effect of PD activity where the general field is a product of the two electrode fields at 120° phase difference (i.e. simulating field conditions inside the barrier region).

The experiments were conducted on new pressboard conditioned to 3.6% moisture, 7.2% moisture and a pressboard sample taken from the outer series coil insulation wrap of a service transformer. (Viscometric tests on samples of the service aged board showed that, although the board has been taken from a transformer in service for 30 years, the pressboard "appeared un-aged" with an average DP value of 970 [148]. This is not an unsurprising result as the samples were taken from a disassembled transformer during an industrial scrapping procedure where the reason for the scrap was due to a tap changer fault and not due to major insulation degradation. In addition, although it was certain that the pressboard was taken from the outer series coil insulation wraps, it was not possible to be sure that the pressboard had been operational in the region of the highest electric stress. However, the fact that the pressboard is in a service aged condition (albeit not aged using the DP definition) could be interpreted as having a specimen of contaminated "un-aged" pressboard.

The experiments were conducted using the bi-phase arrangement as depicted in Figure 4.6 using the electrical method and equipment as described in §3.5 to measure PD. The noise floor of the system was determined to be 1~2pC up to the bushing rating of 71kV. Valid PD was considered to be detected (i.e. PD inception) when pulses with amplitude of approximately 5pC were regularly observed. (This is a weakness of the system as the data gathering relies on continuous visual observation and subjective judgement of sustained PD activity. For this reason, at each measurement point, five sets of data for PD inception voltage (V_{iv}) and PD extinction voltage (V_{ex}) were taken.) Data for the ϕ-q-n plots were mostly collected just after the point of PD inception to avoid sustained or heavy PD activity which could lead to conditioning of or damage to the pressboard. The exception was when duration experiments were being undertaken with the recording of sustained or heavy PD activity being the objective. All ϕ-q-n plots are referenced to the applied reference voltage V_1.

6.2 Effect of temperature on PD activity due to the local field

The configuration, as depicted in Figure 5.22, was used with the control electrode (V_2) connected to the reference electrode (V_1). The voltage was increased from 0V to V_{iv}. Five sets of corresponding V_{iv} and V_{ex} data were noted for each temperature following achievement of system temperature stability. In this arrangement, there is no general field and electrical discharges are transported along the oil/pressboard interface under the action of the local field associated with the discharge source.

Figure 6.1, Figure 6.2 and Figure 6.3 respectively show the PD inception and extinction voltages due to the local field alone on the pressboard surface as a function of system temperature and with new pressboard conditioned to moisture content of 3.6% and 7.2% and service aged pressboard. The dotted lines show the results from a second data collection exercise.

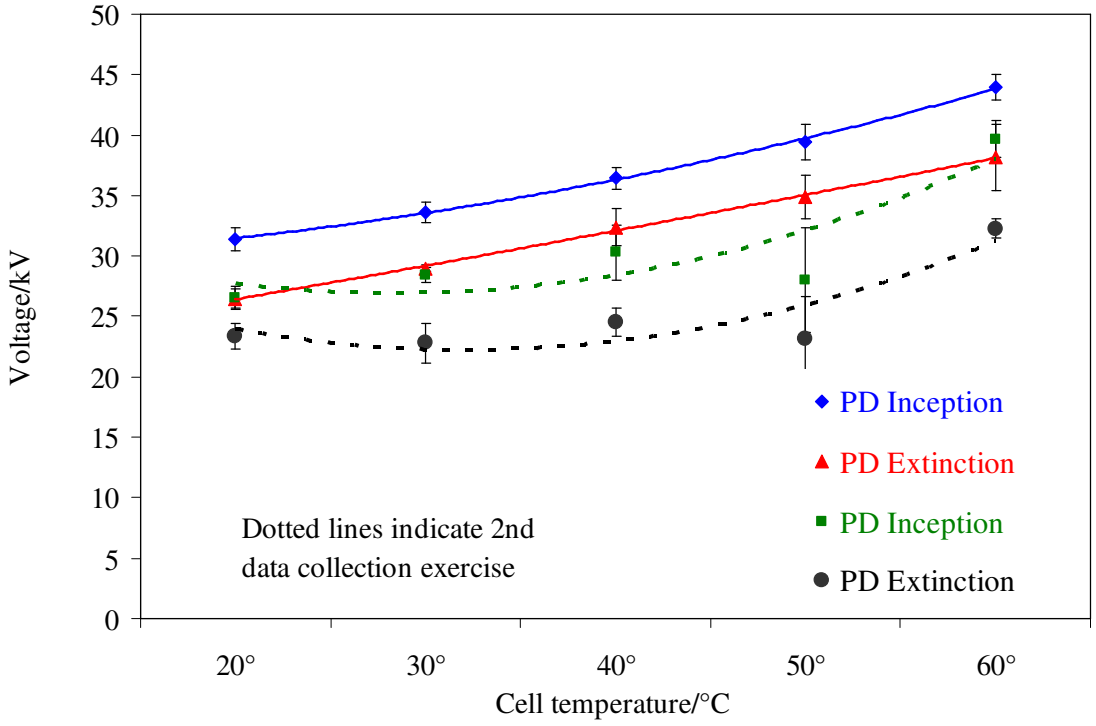

Figure 6.1 Inception and extinction voltage ~ system temperature for local field at 3.6% moisture (two temperature cycles)

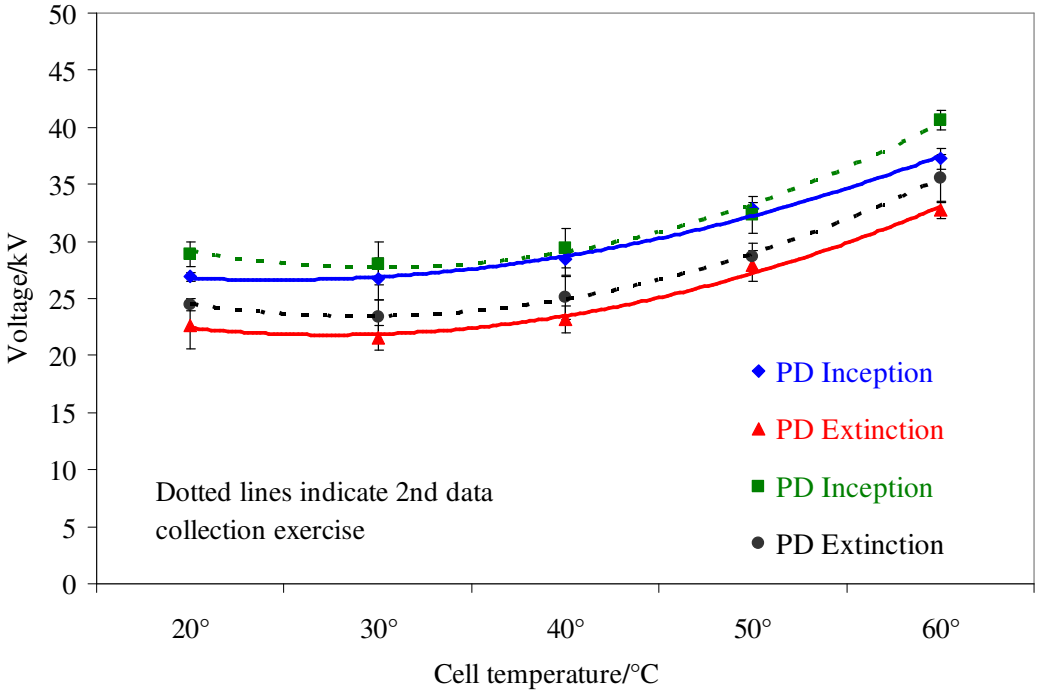

Figure 6.2 Inception and extinction voltage ~ system temperature for local field at 7.2% moisture (two temperature cycles)

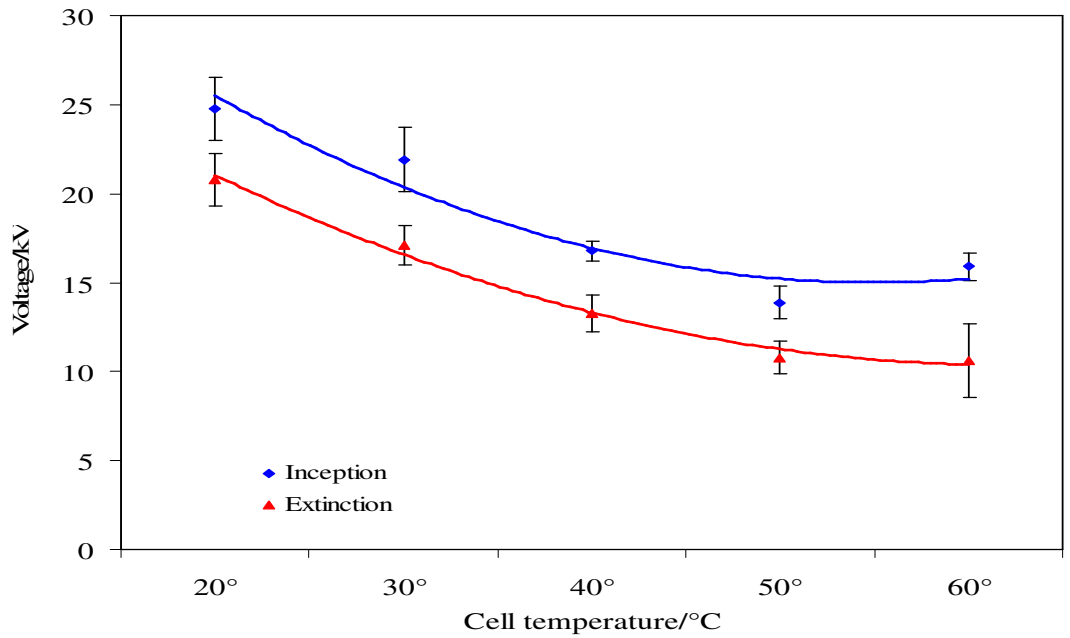

Figure 6.3 Inception and extinction voltage ~ system temperature for local field using service aged pressboard

6.3 Effect of temperature on PD activity due to the local field with the interaction of a fixed general field.

The arrangement as depicted in Figure 5.23 is used where the control electrode (V_2) is earthed and the reference electrode (V_1) varied from 0V to V_{iv}. Five sets of corresponding V_{iv} and V_{ex} data were noted for each temperature following achievement of system temperature stability. Electrical discharge is transported along the oil pressboard interface under the interaction of the local field and the fixed general field developed between the electrodes with the control electrode earthed.

Figure 6.4, Figure 6.5 and Figure 6.6 respectively show the PD inception and extinction as a function of system temperature and with new pressboard conditioned to moisture content of 3.6% and 7.2% and service aged pressboard.

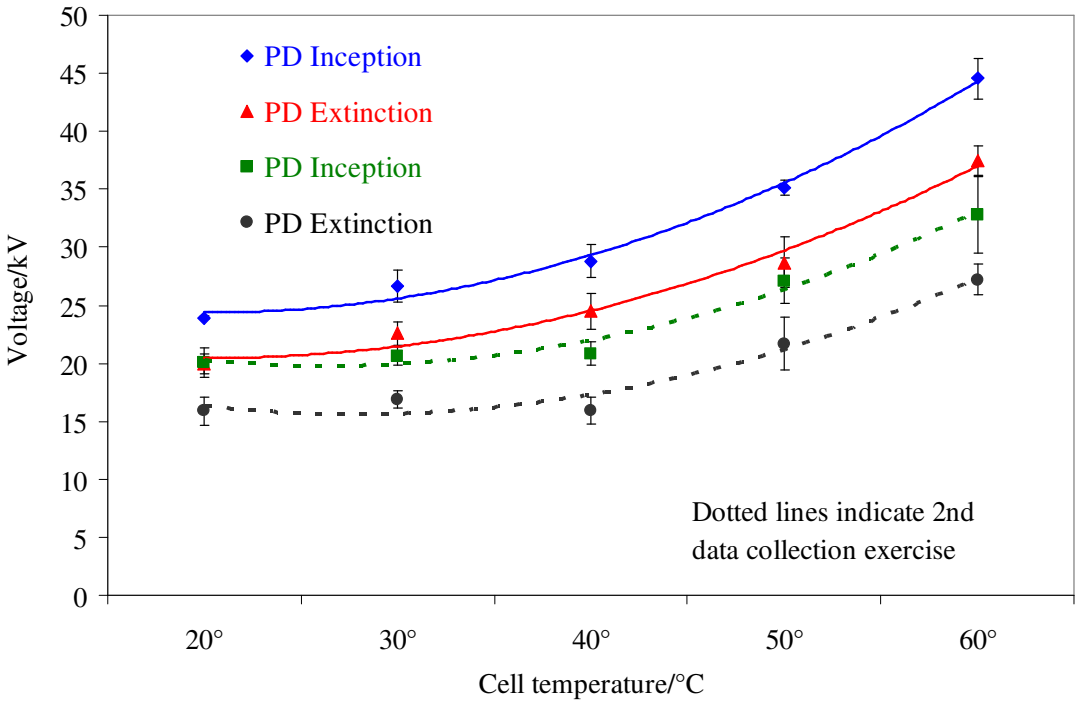

Figure 6.4 Inception and extinction voltage ~ system temperature for local – fixed general field interaction at 3.6% moisture (two temperature cycles)

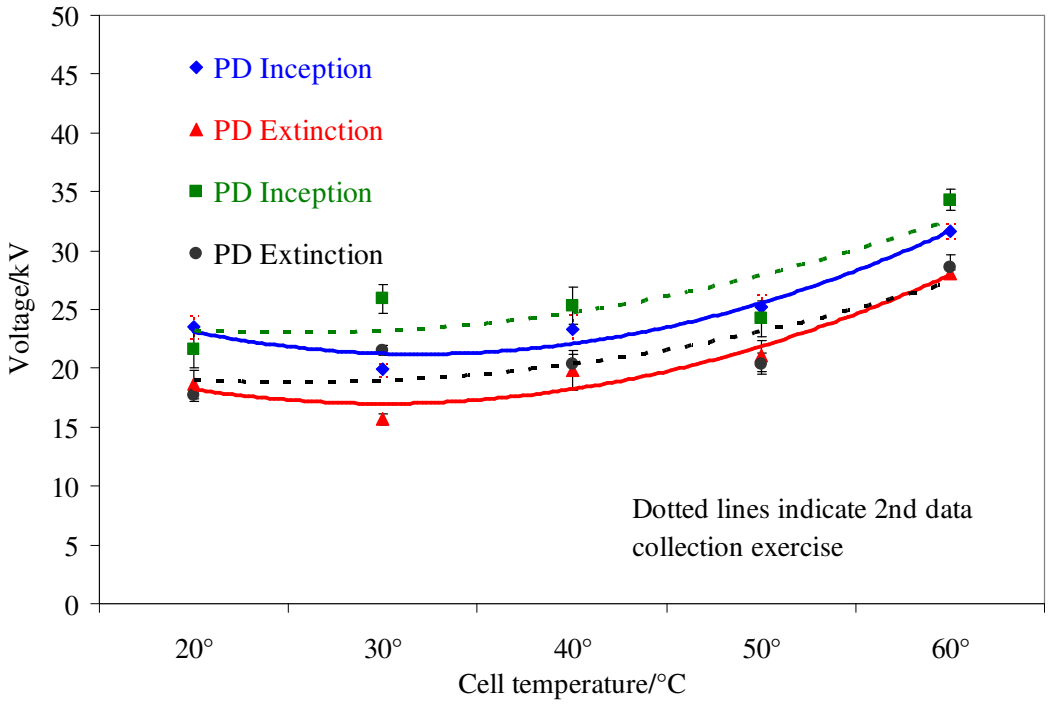

Figure 6.5 Inception and extinction voltage ~ system temperature for local – fixed general field interaction at 7.2% moisture (two temperature cycles)

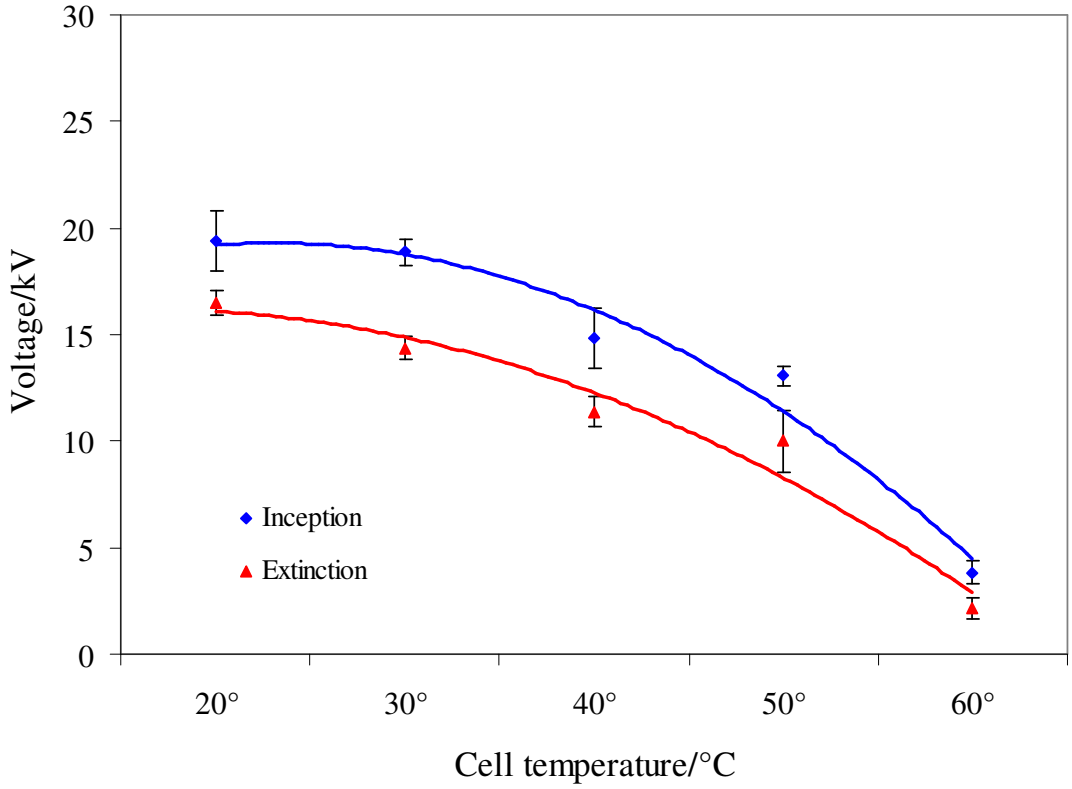

Figure 6.6 Inception and extinction voltage ~ system temperature local – fixed general field interaction using service aged pressboard

The figures reveal the effects of temperature and electric field interaction and board contamination on surface discharge. Figure 6.1, 6.2, 6.4 and 6.5 show a positive trend

with temperature meaning that surface discharge is harder to initiate with increasing temperature. Both oil and pressboard conductivity increase with temperature [149, 150] which implies that PD inception voltage should fall with increasing temperature and this is shown by the result using the service aged board. The variance from the expected result for the new pressboard is explained by the large oil to pressboard ratio (1100:1 %w/w). As the temperature increases from 20°C to 60°C, moisture migrates from the pressboard into the oil leaving a drier pressboard. The Fabré-Pichon curves indicate that most of the moisture moves from the pressboard into the oil in the test cell. (In a large transformer, the oil to pressboard ratio is more like 10:1 %w/w and so the relative mass of moisture which moves into the oil is negligible). This result suggests that the moisture in the pressboard is the first initiator of surface discharge in an otherwise un-contaminated pressboard. The second data collection results (dotted) show different inception and extinction voltages suggesting some localised conditioning of the pressboard around the discharge source.

When comparing the null field condition to the interacting fixed general field condition (i.e. Figure 6.1 to Figure 6.4 and Figure 6.2 to Figure 6.5), it is seen that the onset of PD (i.e. surface discharge activity) occurs at a lower voltage with the interacting fixed general field than with the null field at all temperatures. The explanation is that the fixed general field, due to the 90° mechanical orientation with the local field, is enhancing the localised space charge due to polarisation in the transition region resulting in PD activity at a lower energy level. When comparing the responses for pressboard conditioned to 7.2% moisture against the responses for pressboard conditioned to 3.6% moisture, (i.e. Figure 6.4 to Figure 6.1 and Figure 6.5 to Figure 6.2) the PD onset for the 7.2% board occurs at lower voltage levels. This suggests further that the increased moisture content is enabling surface discharge at a lower energy level due to the increased availability of negative charge carriers from the polar moisture molecules. Finally Figure 6.3 and Figure 6.6 show the effect of board contamination due to the service aged board. In this case, the figures show a negative trend with temperature meaning that the surface discharge is easier to initiate due to the wider availability of negative charge from the contamination embedded in the pressboard. The ϕ-q-n plots at 40°C and 50°C (Figure 6.7) for the fixed general field interaction condition show broad discharge at significant amplitude indicating that the response is

due to the contamination rather than temperature. The service aged board is relatively un-aged in terms of DP value and this suggests that board contamination is more significant than moisture for the onset of surface discharge due to the presence of more locally available charge providers.

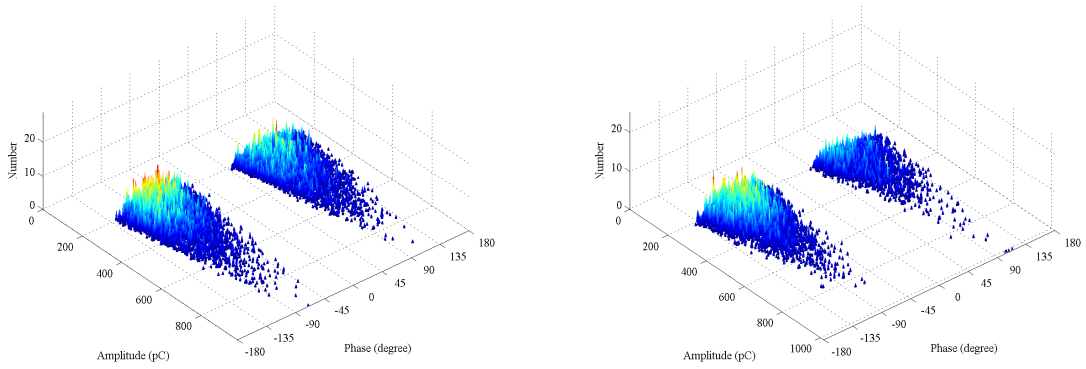

a - System temperature at 40°C

b - System temperature at 50°C

Figure 6.7 ϕ-q-n plots for service aged pressboard with general field condition at 15kV and Robinson at 500pC resolution

6.4 Effect of phase change in the general field on PD activity

The arrangement as depicted in Figure 5.24 is used where V_1 and V_2 (in-phase) are simultaneously increased to a value above the average PD inception voltage (as determined in the experiment with a null general field). The phase of V_2 with respect to V_1 is then changed in fixed steps to 60° lag, 120° lag, 60° lead, 120° lead and finally 180°. At each phase difference, ϕ-q-n plots of discharge are recorded. In this test, with V_2 equal to V_1 but at different phases, a changing general field is developed between the reference and control electrodes The two conditions of 120° lag and 120° lead are significant as these two conditions replicate the normal operational conditions as found in the inter-phase barrier region. PD and surface discharge activity is already present due to the discharge source local field and therefore this experiment measures the change in PD activity due to the enhancement of the local field caused by a variation in the general field between the control and reference electrodes.

Figure 6.8 through to 6.11 shows the ϕ-q-n plots for 3.6% moisture board under temperature conditions of 20°C and general -field phase differences of 0°, (i.e. in phase) and 60° lag, 120° lag, 60° lead, 120° lead and finally 180° (i.e. anti-phase) and for 2

different phase voltages each at 2 Robinson gain settings. (The figures are interpreted by scanning the ϕ-q-n plots anti-clockwise in the following sequence: in-phase, 60°lag, 120°lag, 120°lead, 60°lead and then anti-phase.)

Appendix D contains PD activity persistence and corresponding ϕ-q-n plots for 3.6%, 7.2% moisture and service aged boards at discrete temperature intervals. The following *general* trends are apparent from the ϕ-q-n plots:

- At any particular condition of temperature and $V_{control}$, the intensity of PD activity is substantially increased between in-phase and anti-phase conditions.
- At any particular condition of temperature and $V_{control}$, the intensity of PD activity is substantially increased between in-phase and 120° lag (or lead) conditions.
- For the new pressboard, as the temperature is increased, $V_{control}$ must be increased to enable PD activity thus confirming the temperature effect in Figure 6.1 and Figure 6.4 for the null general field and Figure 6.2 and Figure 6.4 for the fixed general field.
- The PD activity occurs at the peak of the first and third quadrants confirming corona associated with the discharge source.

The enhancement of PD due to the change in general field is explained by the polarising action of the general field at the interfacial region. Figure 6.12 shows a cross section of the test cell under a null general field. In this condition, the interfacial layer is subjected to the local field from the discharge source which polarises the liquid molecules associated with the EDL in the vicinity of the discharge source. This suggests that charge transport is through the fixed pressboard transition region arising from the ionisation of polar water molecules. As the system temperature is increased, moisture migrates from the pressboard requiring a higher energy level to initiate ionisation.

When the general field is applied (such as when the control electrode is earthed - shown in Figure 6.13) the polarisation at the interfacial layer is enhanced allowing greater ability for charge transport: the greater the field strength of the general field (as when the control electrode is in anti-phase with respect to the reference electrode), the greater the polarisation at the interfacial layer.

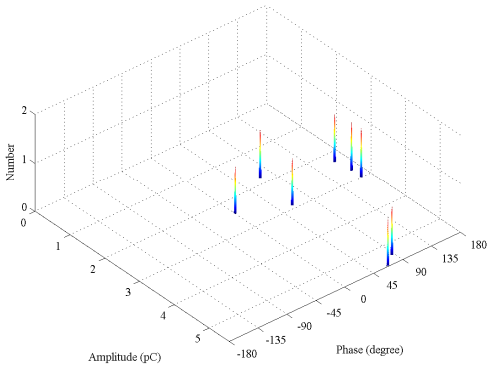

a - $V_{control}$ in phase with V_{ref}

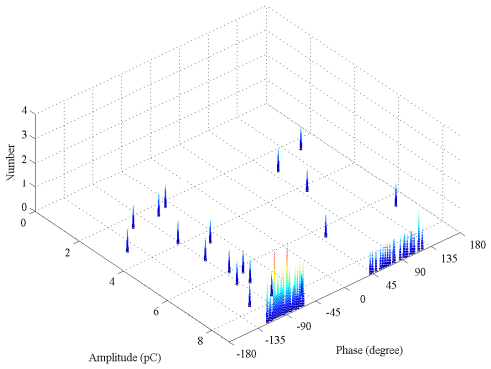

f - $V_{control}$ in anti-phase with V_{ref}

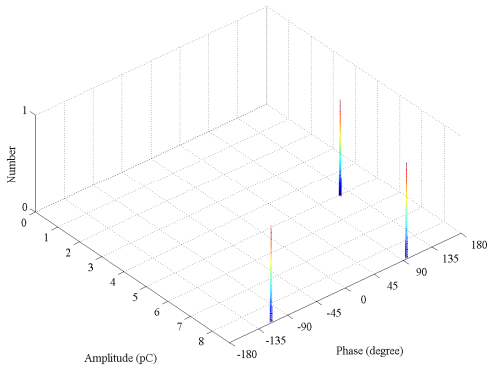

b - $V_{control}$ 60° lag with V_{ref}

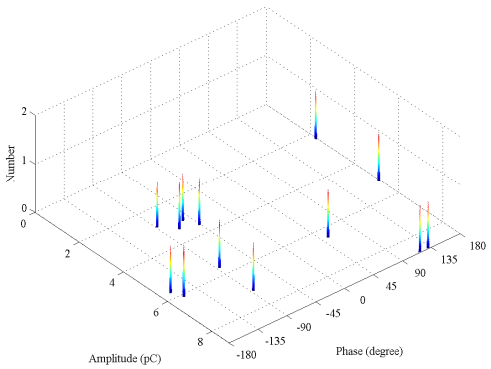

e - $V_{control}$ 60° lead with V_{ref}

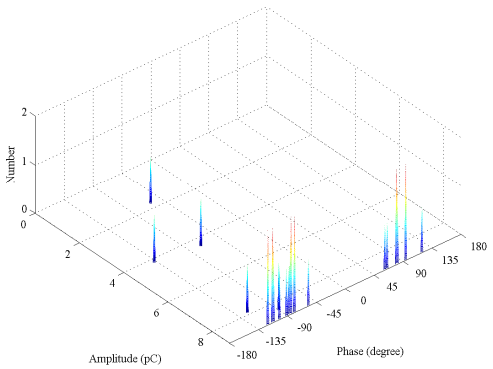

c - $V_{control}$ 120° lag with V_{ref}

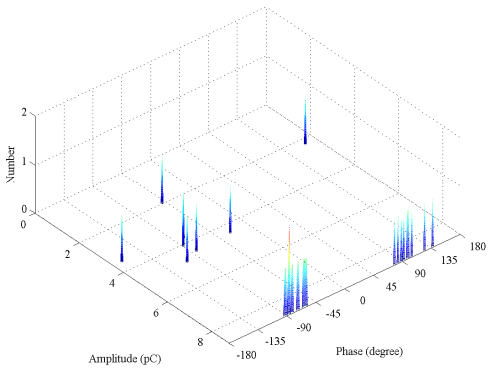

d - $V_{control}$ 120° lead with V_{ref}

Figure 6.8 Series of ϕ-q-n plots ~ phase change of $V_{control}$ at 25kV for virgin pressboard conditioned to 3.6% moisture and at 20°C. Robinson at 5pC resolution

No plot taken as no discharge detected

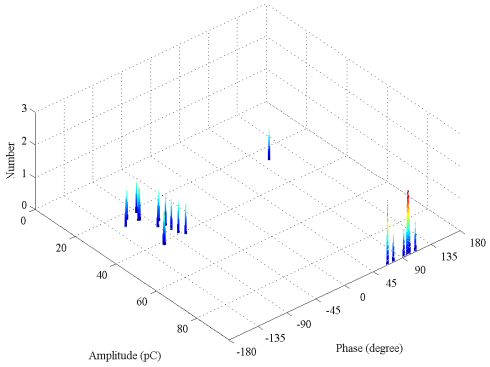

a - $V_{control}$ in phase with V_{ref}

f - $V_{control}$ in anti-phase with V_{ref}

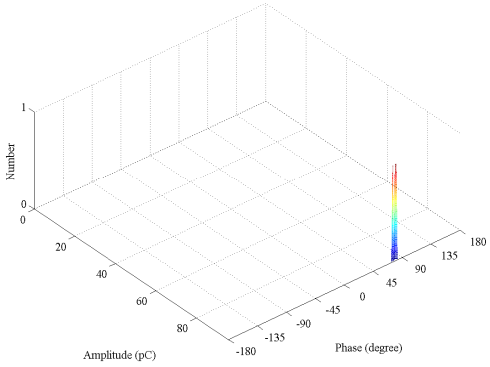

b - $V_{control}$ 60° lag with V_{ref}

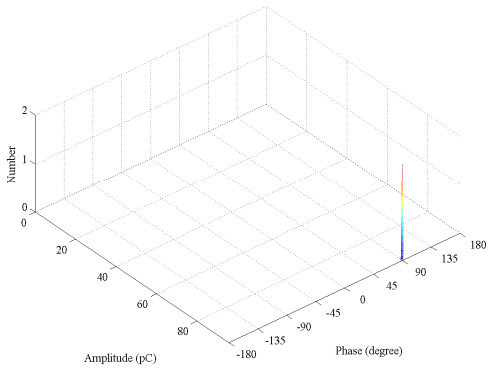

e - $V_{control}$ 60° lead with V_{ref}

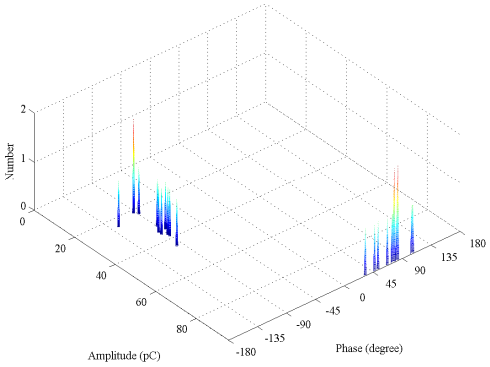

c - $V_{control}$ 120° lag with V_{ref}

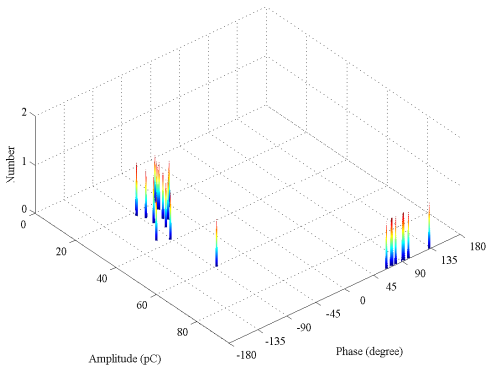

d - $V_{control}$ 120° lead with V_{ref}

Figure 6.9 Series of ϕ-q-n plots ~ phase change of $V_{control}$ at 25kV for virgin pressboard conditioned to 3.6% moisture and at 20°C. Robinson at 50pC resolution

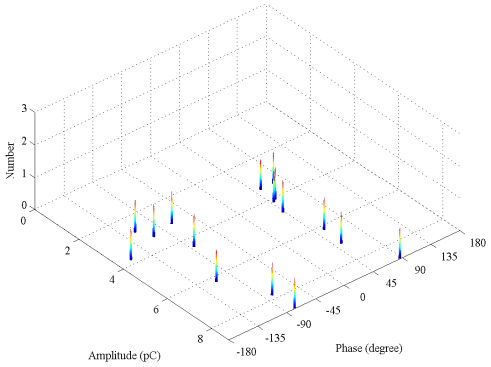

a - $V_{control}$ in phase with V_{ref}

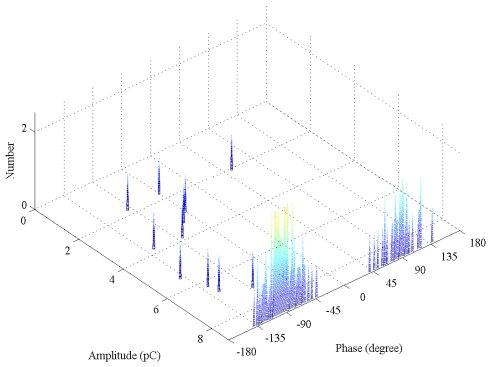

f - $V_{control}$ in anti-phase with V_{ref}

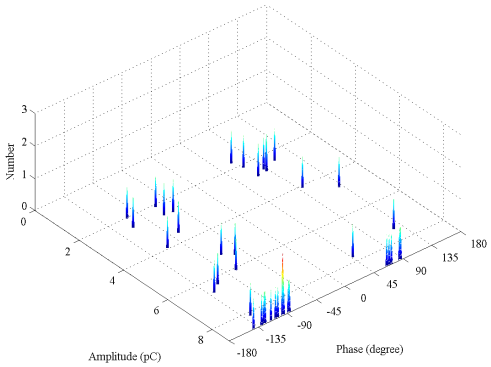

b - $V_{control}$ 60° lag with V_{ref}

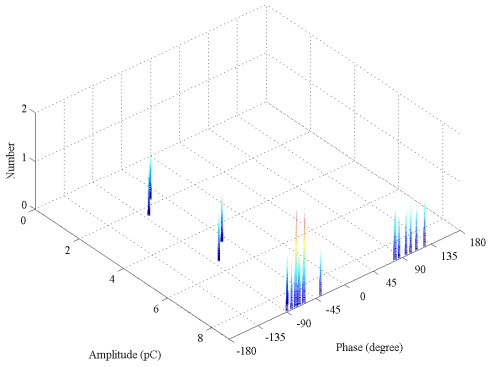

e - $V_{control}$ 60° lead with V_{ref}

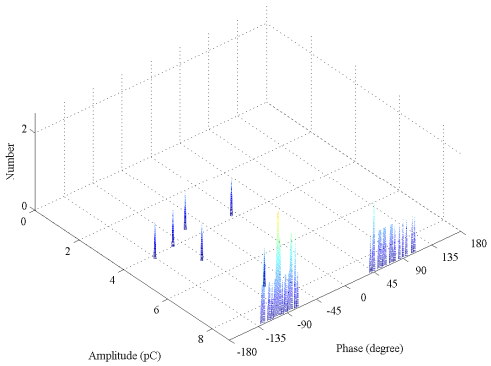

c - $V_{control}$ 120° lag with V_{ref}

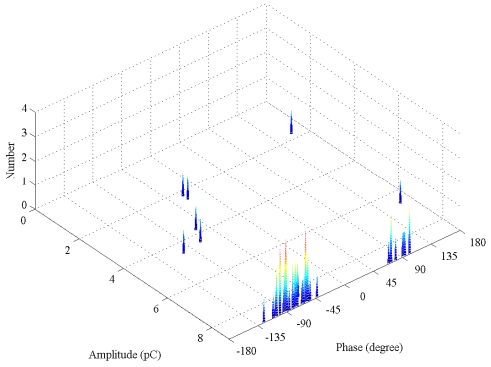

d - $V_{control}$ 120° lead with V_{ref}

Figure 6.10 Series of ϕ-q-n plots ~ phase change of $V_{control}$ at 30kV for virgin pressboard conditioned to 3.6% moisture and at 20°C. Robinson at 5pC resolution

No plot taken as no discharge detected

a - $V_{control}$ in phase with V_{ref}

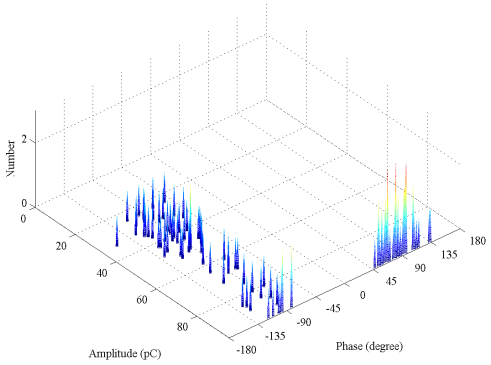

f - $V_{control}$ in anti-phase with V_{ref}

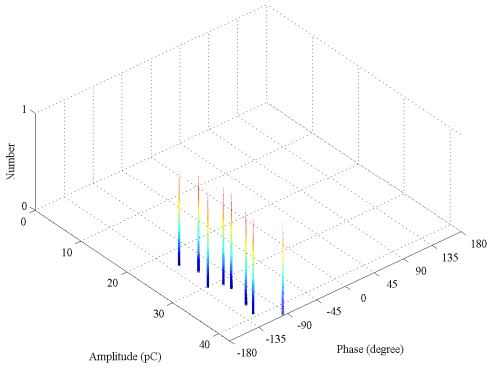

b - $V_{control}$ 60° lag with V_{ref}

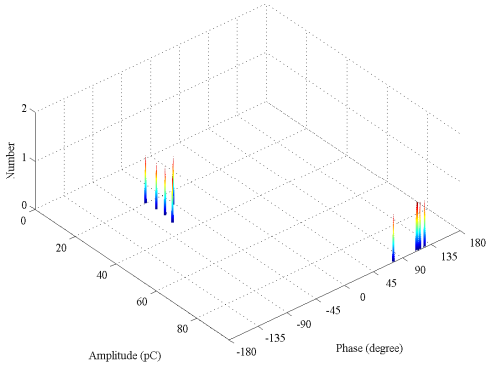

e - $V_{control}$ 60° lead with V_{ref}

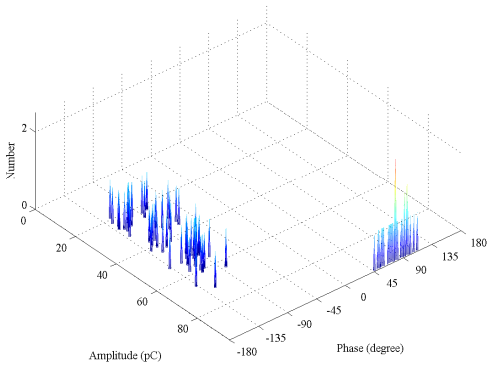

c - $V_{control}$ 120° lag with V_{ref}

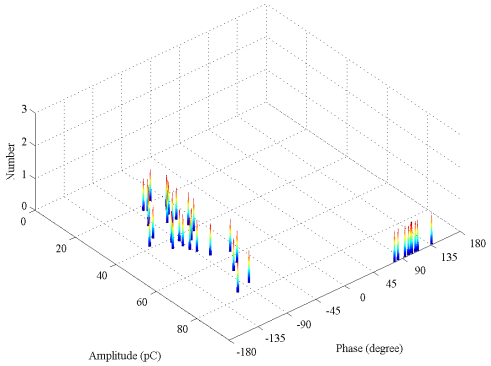

d - $V_{control}$ 120° lead with V_{ref}

Figure 6.11 Series of ϕ-q-n plots ~ phase change of $V_{control}$ at 30kV for virgin pressboard conditioned to 3.6% moisture and at 20°C. Robinson at 50pC resolution

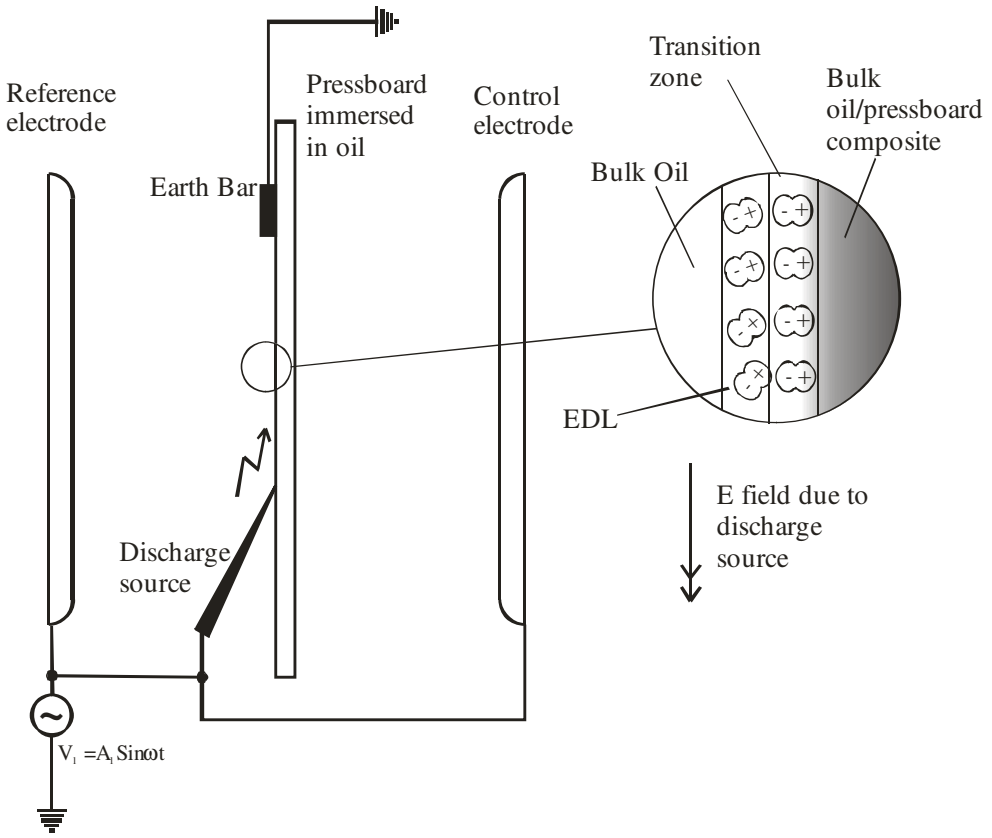

Figure 6.12 Diagrammatic representation showing effect of local field on the interfacial layer

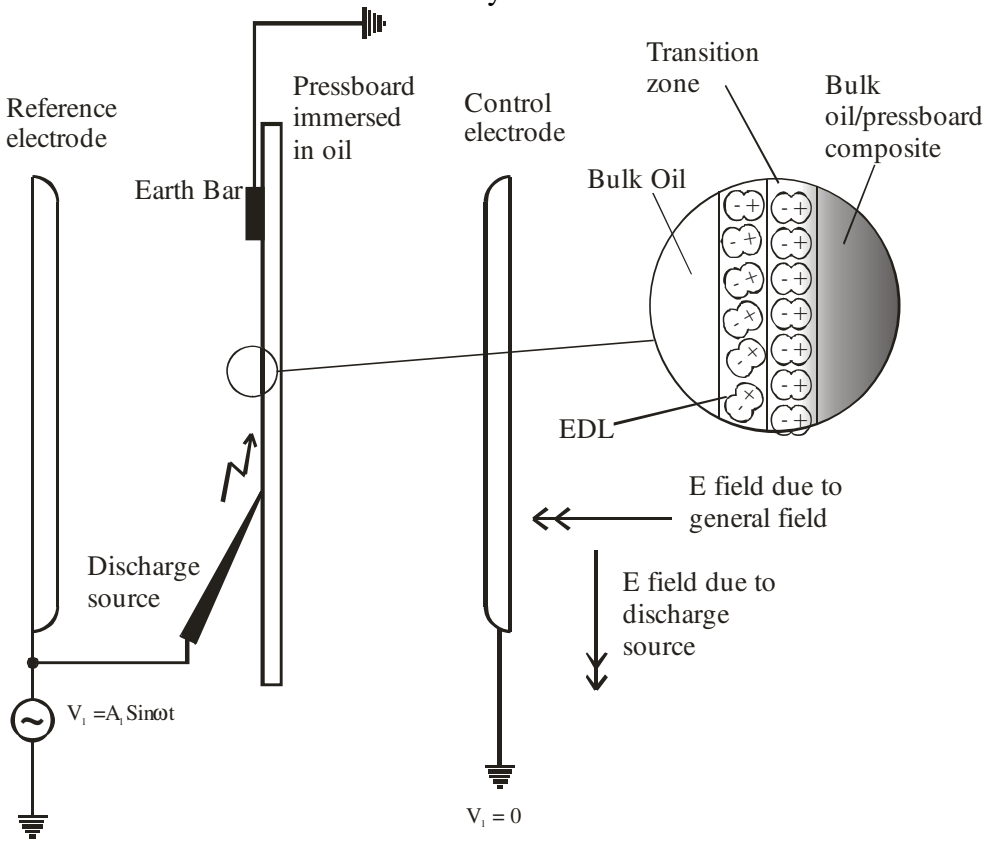

Figure 6.13 Diagrammatic representation showing enhancement of the interfacial layer due to the interaction of the general field and local field

This explains why the intensity of the discharge increases as the general field is applied with increasing polarisation. This suggests that charge is injected into the interfacial layers when the through stress is at a maximum, (i.e. signified by PD occurring around the peak of the cycle) and the resulting space charge is then relaxed through the interfacial layers by the sweeping motion occurring as the electric field changes direction 90° elec. thereafter in the cycle. The in-phase charge injection is associated with the resistive current and the quadrature component, due to the charge relaxation, is associated with the imaginary component of capacitive current.

6.5 Effect of duration of PD activity due to a local field under general field conditions of 120° elec. phase difference

The arrangement as depicted in Figure 5.24 was used where V_1 and V_2 (initially in-phase) were set at 30kV (i.e. above the average inception voltage for PD to occur as determined in test 1). The phase of V_2 was changed to 120°lag and the voltage applied for 5 hours after which the voltage on each electrode was increased to 35kV and applied for a further 7 hours. New pressboard conditioned to 3.6% moisture was used.

Figure 6.14 through to Figure 6.18 show the ϕ-q-n plots at selected time intervals and at different gain setting of the Robinson detector for continuous discharge at 35kV and 120° lag and temperature 20°Cfor virgin pressboard conditioned to 3.6%. The figures are interpreted by scanning the ϕ-q-n plots in a vertical line at the hour mark. In this way, an impression of the charge activity is gained. At some point between 4 and 6 hours, PD becomes more intense which suggests a sudden degradation of the insulation around the discharge source. In addition, the type of PD activity has changed from single discharge events around the peaks of the discharge voltage, associated with corona (Figure 6.8 to Figure 6.11), to more broadly spread discharge over the first and third quadrants associated with surface discharge. The explanation is that the drying out of the pressboard has been completed and the degradation of the pressboard surface in the transition region through pyrolysis of the oil molecules is underway. This was confirmed when the pressboard was extracted 16 hours following completion of the experiment. Figure 6.19 and Figure 6.20 show the tracking developed on the surface of the pressboard after the full time interval of 12 hours.

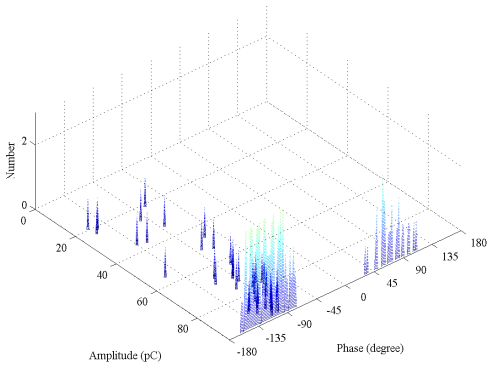

a - Robinson at 50pC resolution

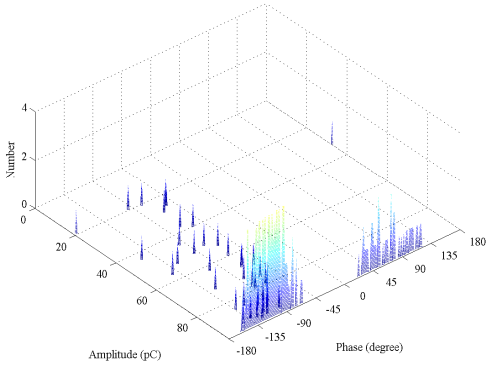

a - Robinson at 50pC resolution

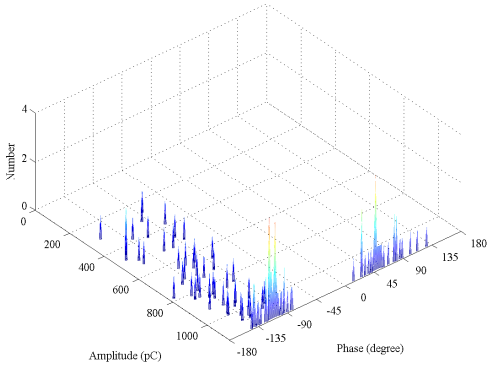

b - Robinson at 500pC resolution

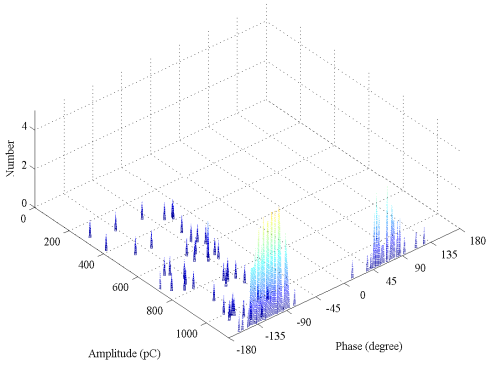

b - Robinson at 500pC resolution

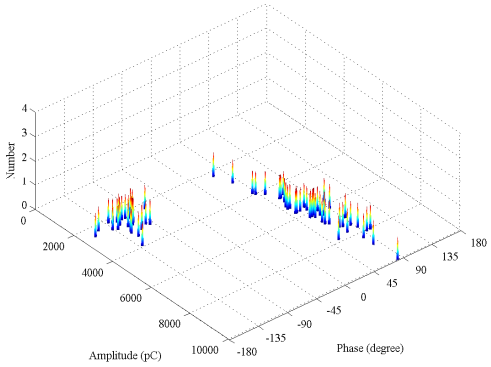

c - Robinson at 5000pC resolution

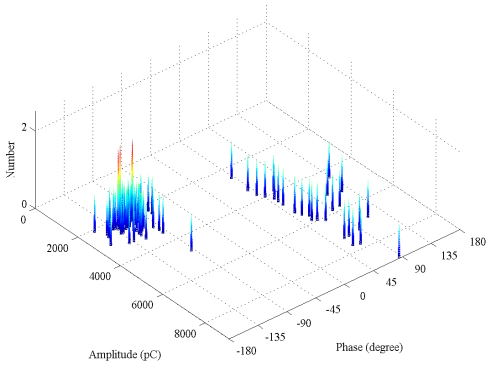

c - Robinson at 5000pC resolution

Figure 6.14 ϕ-q-n plots at 1 hour

Figure 6.15 ϕ-q-n plots at 2 hours

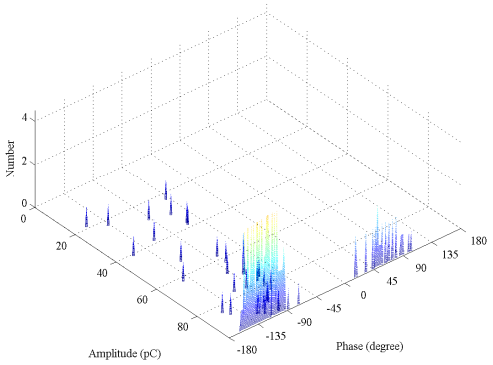

a - Robinson at 50pC resolution

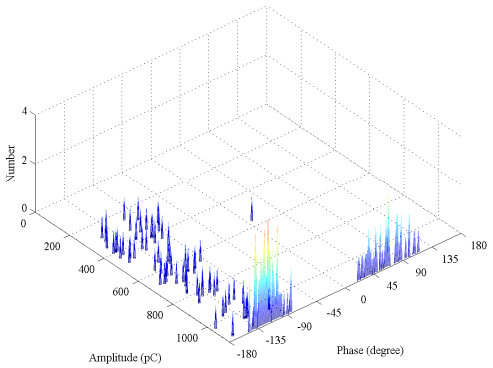

b - Robinson at 500pC resolution

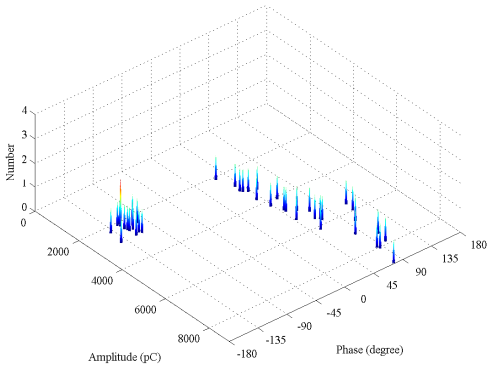

c - Robinson at 5000pC resolution

.

Figure 6.16 ϕ-q-n plots at 4 hours

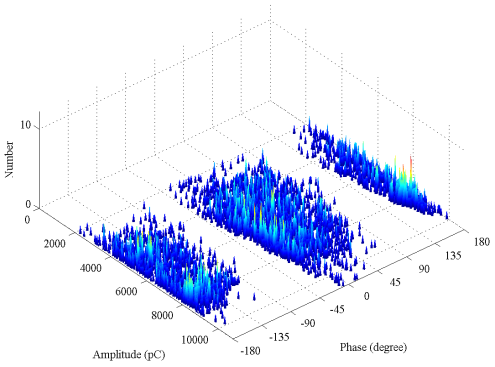

a - Robinson at 5000pC resolution

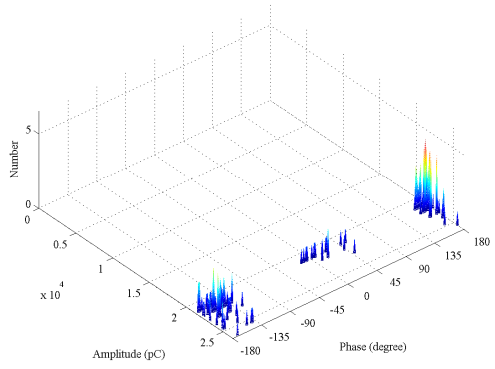

b - Robinson at 50000pC resolution

Figure 6.17 ϕ-q-n plots at 6 hours

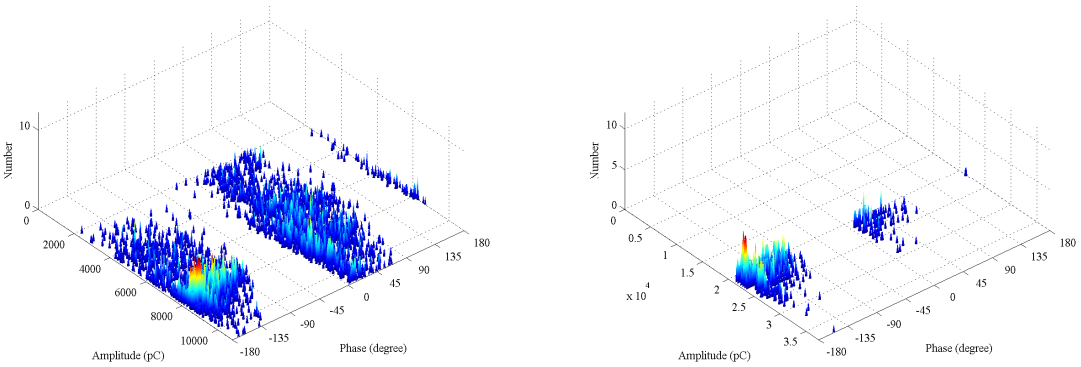

a - Robinson at 5000pC resolution

b - Robinson at 50000pC resolution

Figure 6.18 ϕ-q-n plots at 7 hours

No white marks are seen on the pressboard because the pressboard was extracted 16 hours following cessation of the experiment thus allowing the pressboard to re-attain moisture equilibrium in the locality of the discharge. However, the tracking is clearly more directional and of greater length than the tracking patterns obtained from the needle bar experiment (Figure 5.10) indicating the influence of the general field.

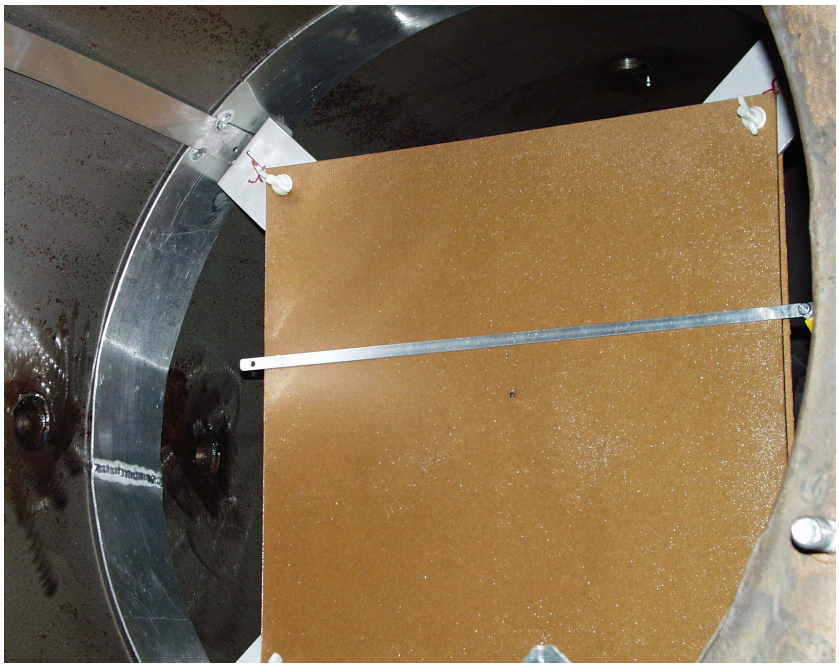

Figure 6.19 Pressboard in test cell after 12 hours showing tracking to earth bar

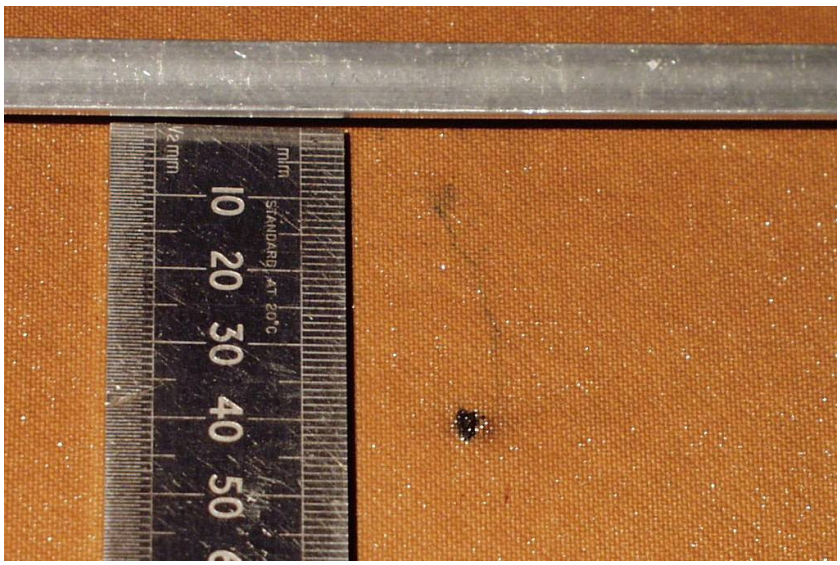

Figure 6.20 Zoom showing detail of tracking

6.6 Summary

A series of experiments have been undertaken using the inter-phase barrier model comprising a pressboard oil sandwich and two planar electrodes representing the high voltage series coils of a transformer. The experiments explored the action of the general field produced by the interaction of the electric fields from the electrodes on discharge activity (created by a discharge source positioned on the surface of the conditioned pressboard).

The inception and extinction of PD is a complex function of board condition, system temperature and the general field induced by the phase difference on the system electrodes. For a non-contaminated board, the level of discharge is affected by both moisture content and by temperature with an inverse relationship with temperature. In this case, surface discharge is suppressed at the higher temperatures due to the migration of moisture out of the pressboard requiring higher voltage to initiate PD inception. For a contaminated board, the level of discharge is affected by both the degree of contamination and by temperature with a positive relationship with temperature. In this case, surface discharge is enhanced at the higher temperatures due to the increased conductivity requiring lower voltage to initiate PD inception. When any discharge activity is present, the intensity is enhanced with the interaction of a general field. The increase in intensity is explained by an increase of the interfacial polarisation at the oil pressboard interface due to the interaction of the general field.

Chapter Seven

Experiments using a floating discharge

A floating discharge may occur around a conducting particle isolated within the insulation medium (i.e. the conducting particle is neither connected to the high voltage nor the earth) when it is subjected to an intense electric field. (The term "isolated" will henceforth be used to avoid confusion of the term "floating" in the context of a liquid medium). PD pattern activity is characterised by discrete discharges occurring on both halves of the applied waveform but in advance of the voltage peaks (i.e. in quadrants 1 and 3 of the applied voltage) and the discharge magnitude is insensitive to the applied voltage [135]. This chapter revisits the experiments undertaken in the oil bath and the test facility to first examine the effect of an electric field on the isolated conducting particle under the conventional test methods.

7.1 Effect of general electric field on non-fixed conducting particles

The oil bath equipment was set up in the plane - plane configuration (Figure 7.1) with pressboard (conditioned to 3.6% moisture) covering the earth plane and 10 non-fixed conducting particles (1 to 3mm in length cut from a 1.5mm diameter welding rod) arranged in a tight group on the pressboard layer. The top electrode was set at a distance of 35mm from the particles and voltage applied. Figure 7.2 shows the resulting PD inception and extinction voltage with oil gap distance and Figure 7.3 shows corresponding ϕ-q-n plots with electrode distance.

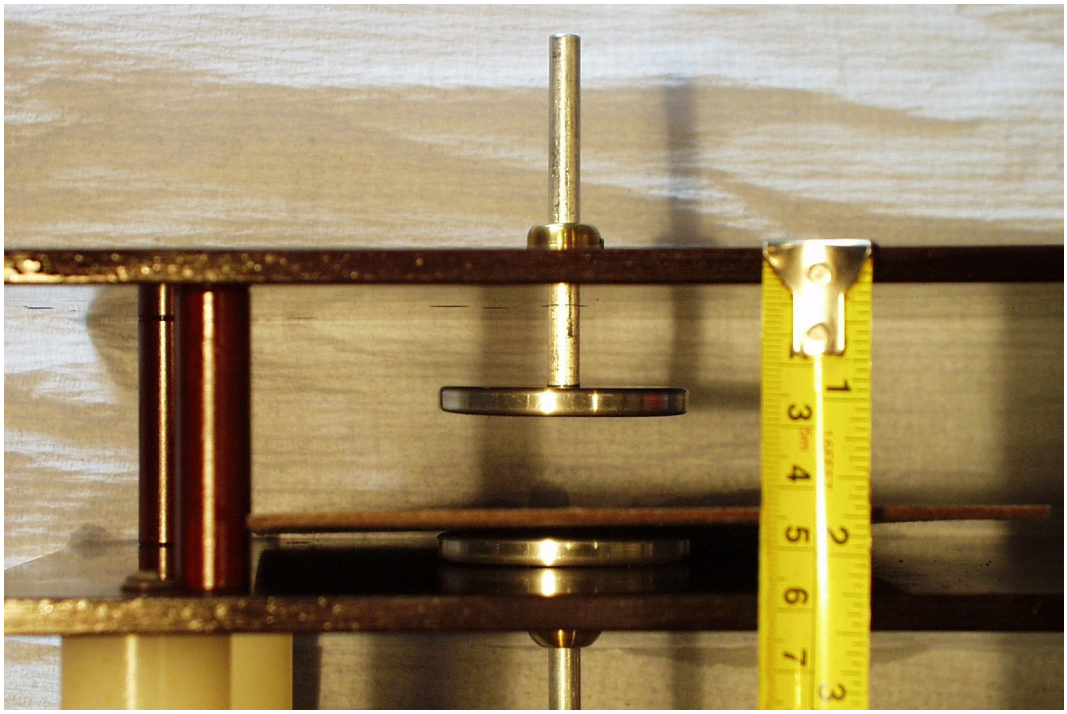

Figure 7.1 Plane-plane configuration

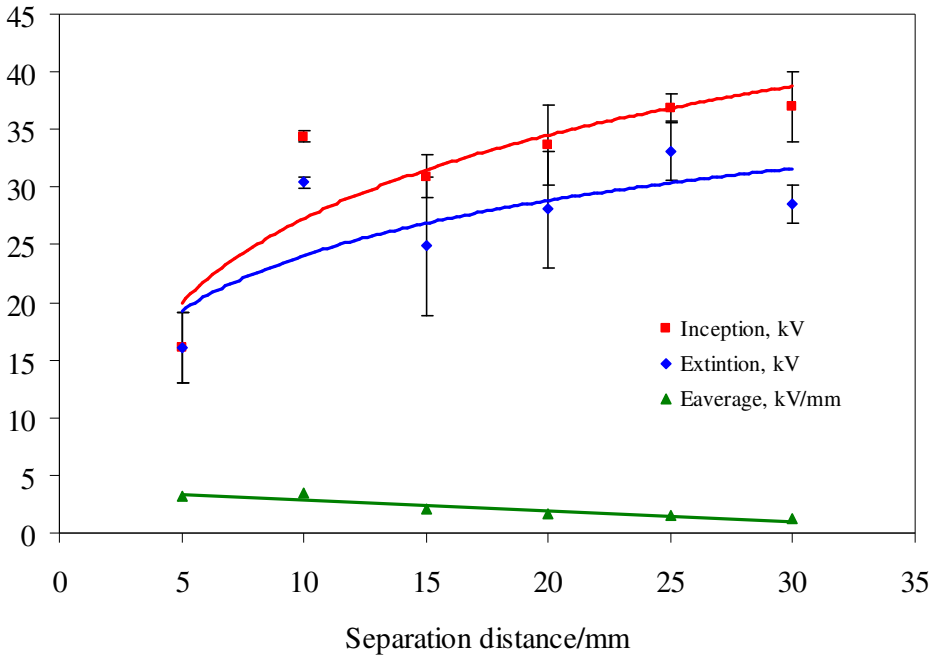

Figure 7.2 PD inception and extinction with gap distance for plane-plane electrode system using pressboard with 3.6% moisture

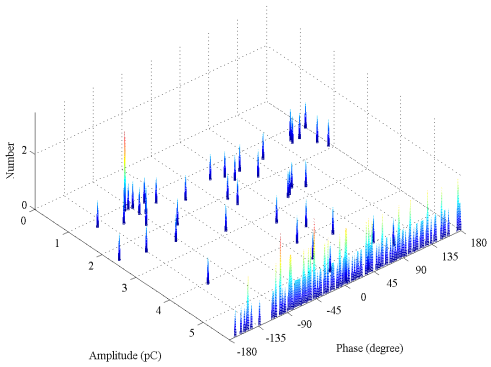

a - 5mm distance, 13.7kV

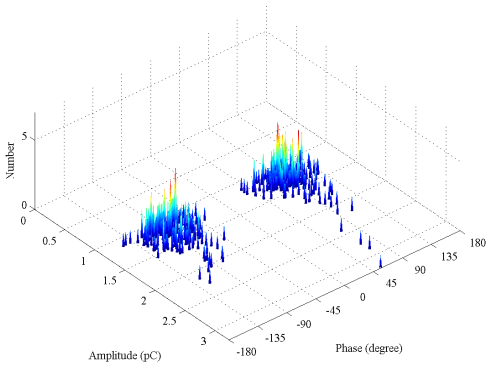

d - 20mm distance, 37.3kV

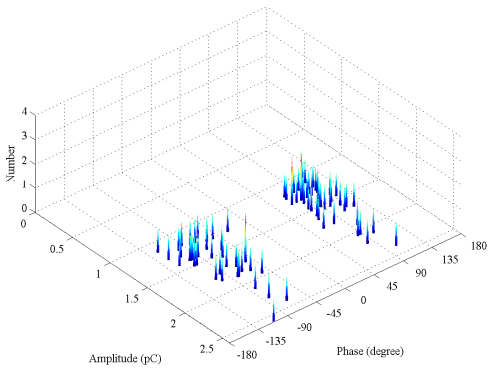

b - 10mm distance, 34.1kV

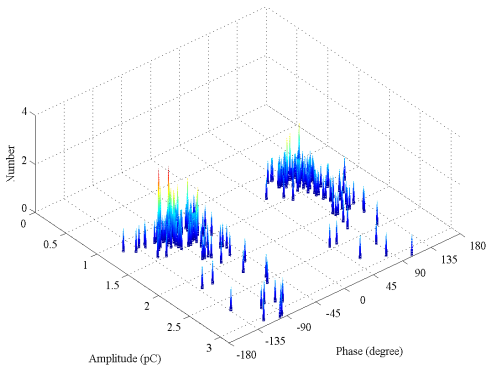

e - 25mm distance, 37.5kV

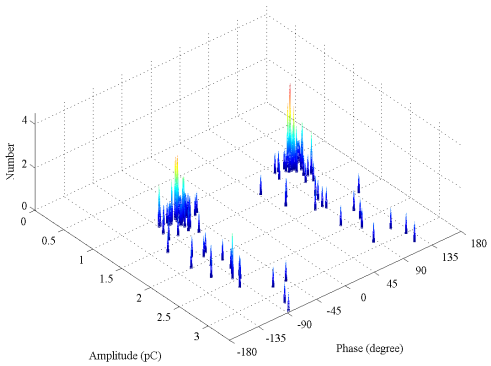

c - 15mm distance, 29.3kV

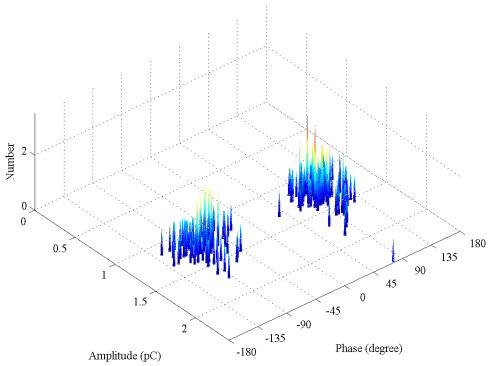

f - 30mm distance, 36.1kV

Figure 7.3 Series of ϕ-q-n plots ~ distance of top plane electrode at room temperature for virgin pressboard conditioned to 3.6% moisture (floating discharge). Robinson set to 5pC resolution

Figure 7.2 shows that an average electric field greater than 1.2kVmm^{-1} initiates PD which occurs at the peaks (Figure 7.3) but also in advance of the peaks suggesting a combination of corona activity and floating discharge rather than floating discharge alone. As the plane electrodes are brought closer together (and taking into account the fall in inception voltage), the average electric fields in both the oil and the pressboard

change as the oil:pressboard ratio is increased (with the effective electric field strength in the oil always greater than 1.2kVmm^{-1} (Figure 7.4)).

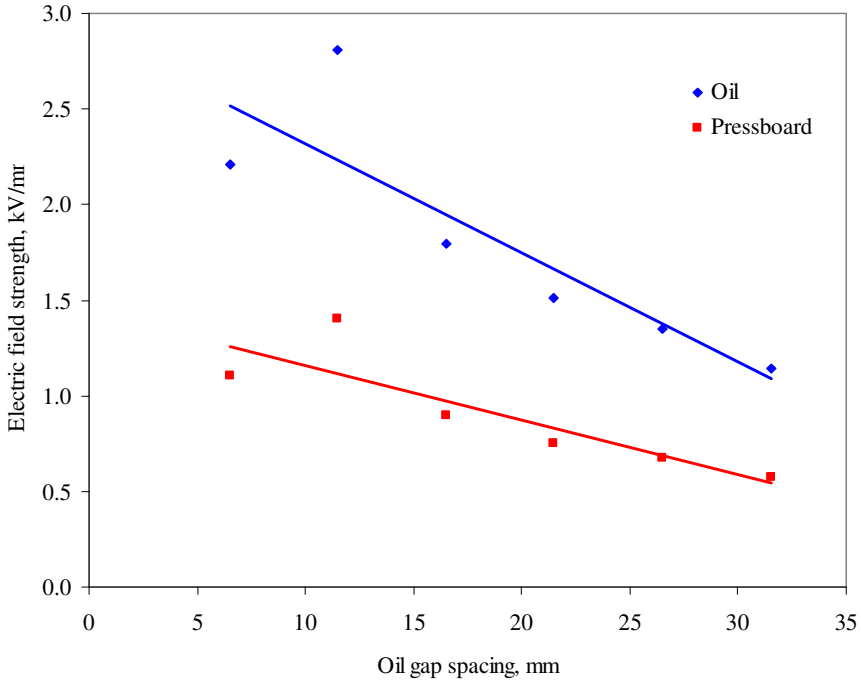

Figure 7.4 Change in electric field strength ~ distance taking into account the PD inception voltage

When the voltage is increased significantly above the inception voltage, a single intense period of PD activity occurs which ceases after a short time (1 -2 seconds) and does not restart even with increasing applied voltage. The cause is revealed when the experiment apparatus is disassembled and the particles are found to have scattered (Figure 7.5) towards the edges of the plane electrode where the creep stress is the greatest due to the fringing effect. The movement of the particles is due to the electrophoresis (more commonly termed electro-kinetics under the general umbrella of electro-hydrodynamics) where the electric field interacts with the EDL around the particle to move the particle into the region of least electric stress (Figure 7.6).

The problem of using non-fixed isolated conducting particles is self evident and three-fold. Firstly, no discharge is evident unless the average field exceeds 1.2kVmm^{-1} which means that high field strengths or closely spaced electrodes are required. Secondly, the movement of the particles due to electro-kinetic action makes sustained discharge difficult to implement with free moving particles. Finally, repeatable results are difficult to obtain when using a number of different sized particles as it is impossible to

return all the particles to the exact same positions following the electro-kinetic action. This explains the wide spread in the error bars as indicated in Figure 7.2. The plane-plane method is shown to be inadequate in the study of "floating" discharge.

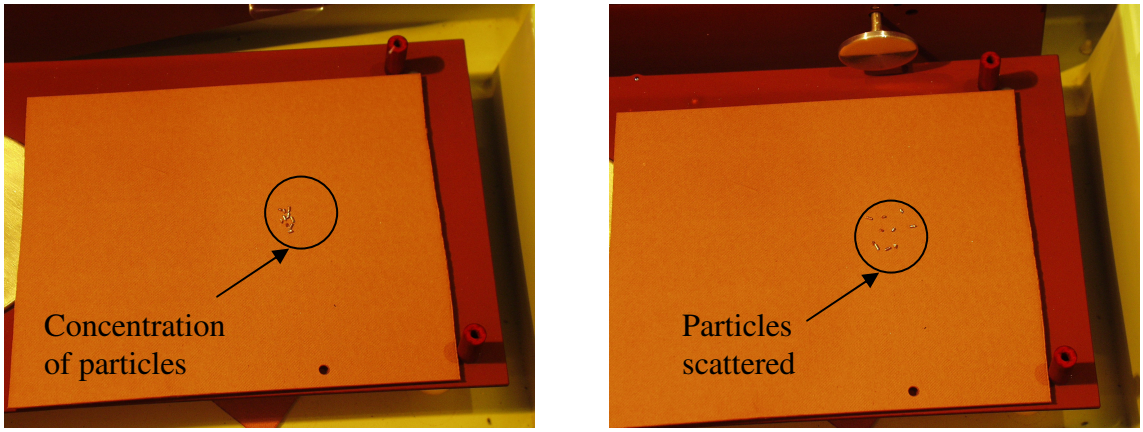

a - Particles – before energising

b - Particles – scattered after energising

Figure 7.5 Plane-plane configuration showing electro-kinetic effect on loose particles

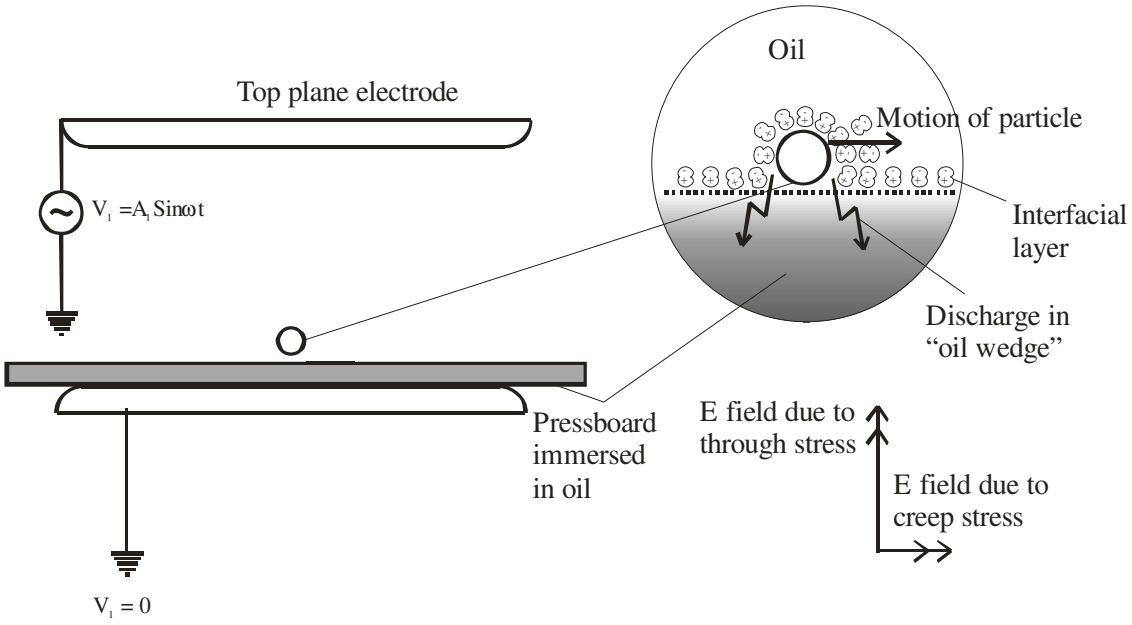

Figure 7.6 Electro-kinetic action on particle due to creep stress component

7.2 The effect of isolated conducting particles on flash-over voltage

The needle-bar experiment (as used in Figure 5.4) was re-configured with the particles placed in a tight group and positioned half way between the discharge source and earth bar. Figure 7.7 shows the effect of source distance from the earth bar on PD inception, extinction and surface flash-over compared with the values as measured without the particles (dotted lines). Figure 7.8 shows ϕ-q-n plots against the effect of distance and

voltage level. These show discharges occurring in the first and third quadrants of the cycles thus confirming "floating" discharge activity.

The graph shows that the presence of the isolated conducting particles depresses PD inception, extinction and surface flashover. At the gap distance of 55mm, PD inception, extinction and surface flash-over values are similar to the values obtained without the presence of the particles. This confirms that the effect on the particles is due to the proximity to the discharge source. At the gap distance of 55mm, it was observed that all the particles had been pushed by electro-kinetic action towards the earth bar. The creepage distance had effectively been restored and explains why the surface flash-over value and PD inception voltages are restored to the values before the addition of the particles.

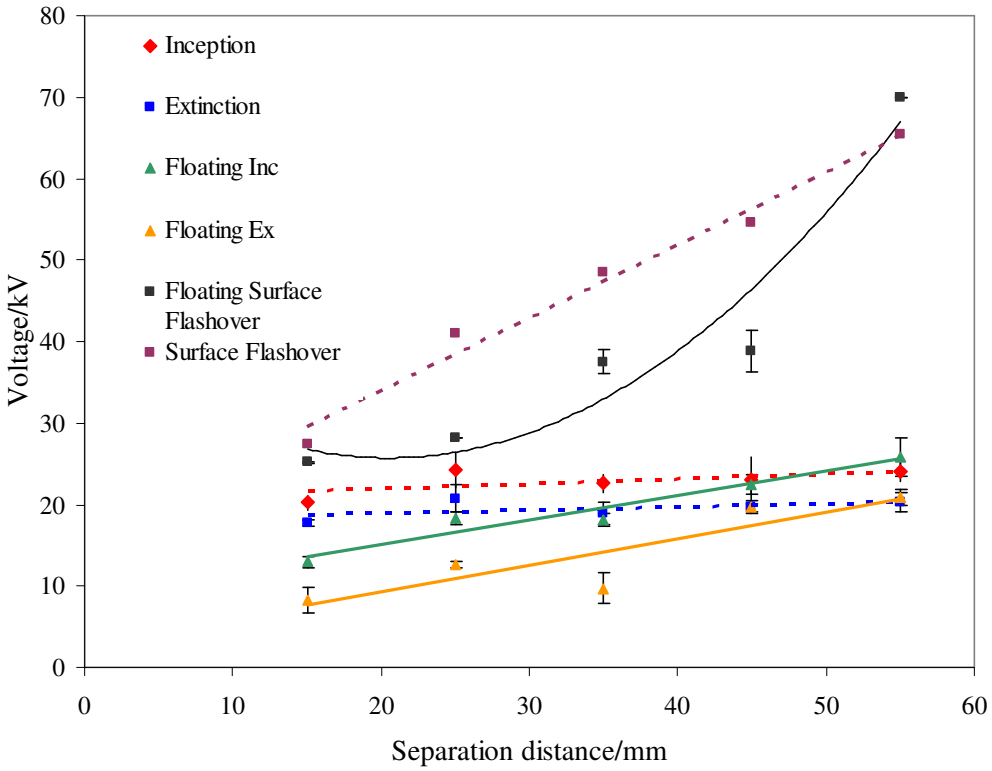

Figure 7.7 PD inception, extinction and surface flash-over with gap distance for needle-bar system using pressboard with 3.6% moisture

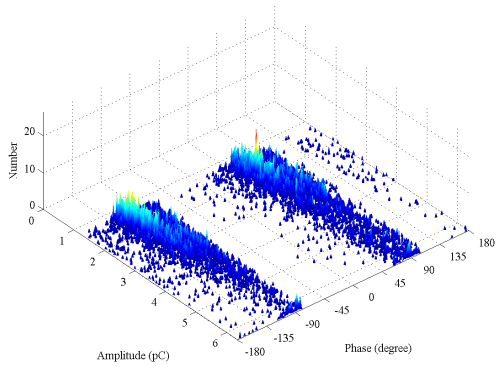

a - 25mm distance, 20kV, 5pC

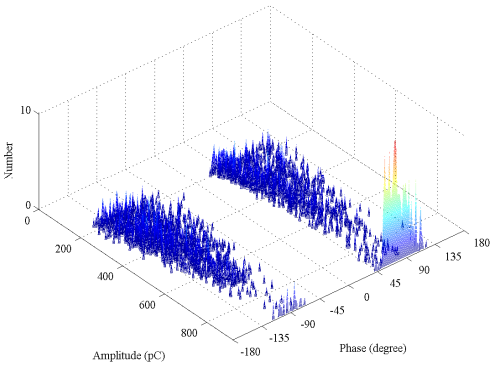

c - 45mm distance, 25kV, 500pC

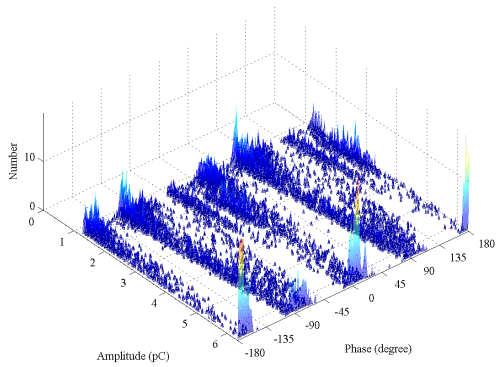

b - 35mm distance, 20kV, 5pC

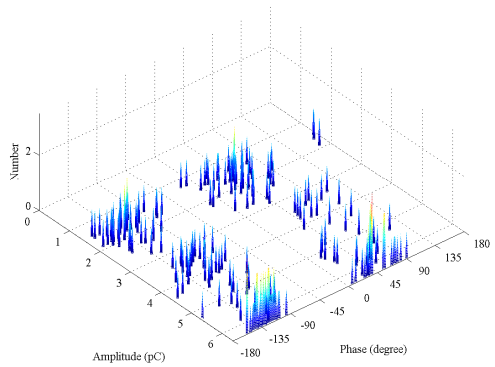

d- 55mm distance, 30kV, 5pC

Figure 7.8 ϕ-q-n plots ~ distance of needle from earth bar at room temperature for virgin pressboard conditioned to 3.6% moisture and floating discharge

7.3 Summary of oil bath experiment - isolated conducting particles

The oil bath experiments, using both the plane-plane method and needle-bar methods, show that an isolated conducting particle influences PD activity only when in a high electric field. Non-fixed particles create difficulties as regards repeatability due to particle movement and the non-regularity of the particles. The problem of fixing an isolated conducting particle onto vertical pressboard was overcome by using a square of silver loaded conductive paint (10mm x 10mm) positioned midway between the discharge source and earth on pressboard conditioned to 3.6% moisture (Figure 7.9)

7.4 Effect of temperature on PD activity due to the local field

The test cell was arranged as shown in Figure 5.22 with the isolated conducting particle positioned between the discharge source and the earth bar. The PD inception and extinction voltage with temperature is given in Figure 7.10 and associated ϕ-q-n plots given by Figure 7.11.

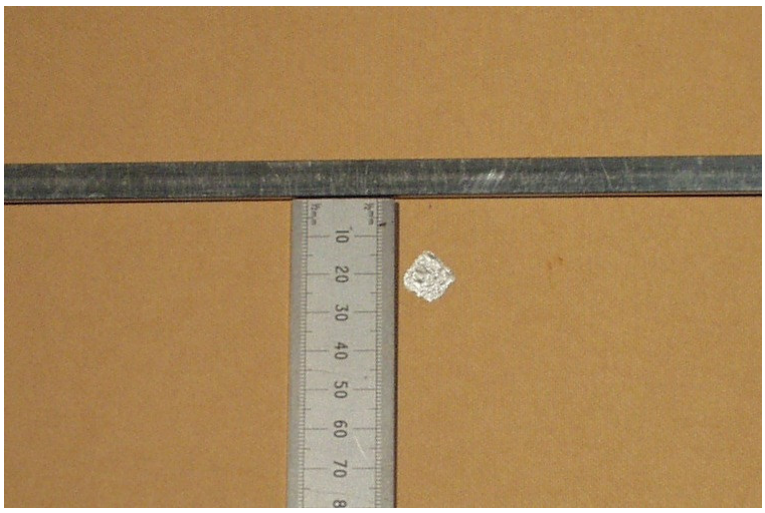

Figure 7.9 Pressboard showing conductive paint

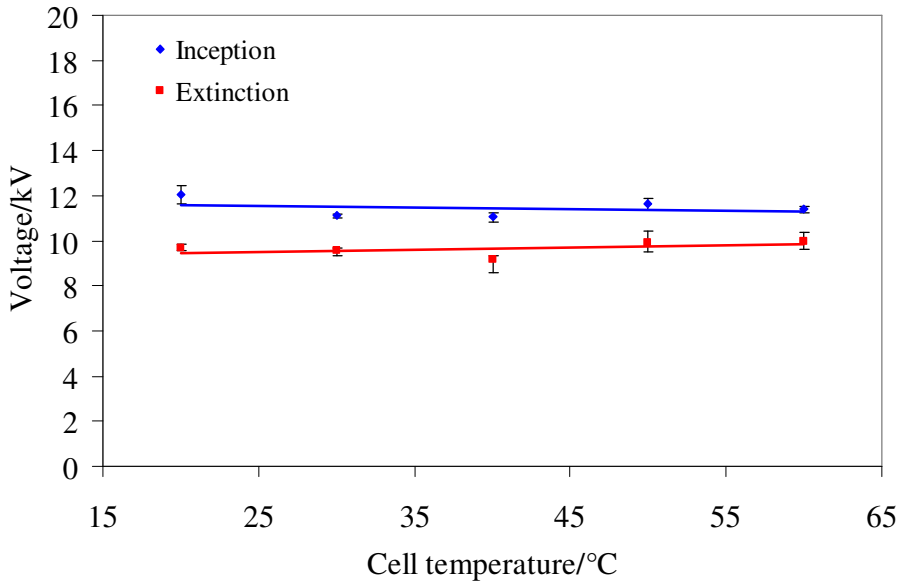

Figure 7.10 Inception and extinction voltage ~ system temperature for local field on isolated particle on pressboard at 3.6% moisture

7.5 Effect of temperature on PD activity due to the local field with the interaction of a fixed general field.

The test cell was arranged as shown in Figure 5.23 with the isolated conducting particle positioned between the discharge source and the earth bar. The PD inception and extinction voltage with temperature is given in Figure 7.12 with associated ϕ-q-n plots given in Figure 7.13. At 50°C, flash-over occurred at 45kV before any PD was registered and the experiment was discontinued thereafter.

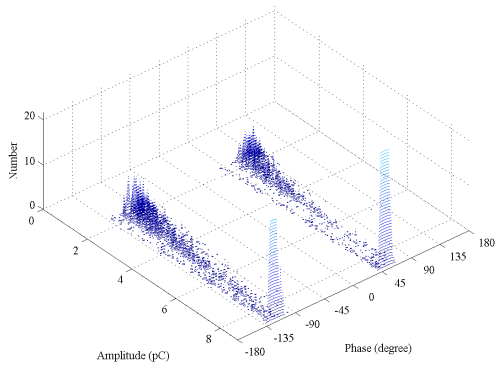

a - 12.5kV at 20°C

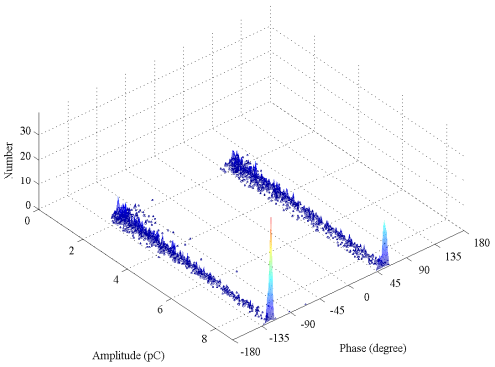

d - 12.5kV at 50°C

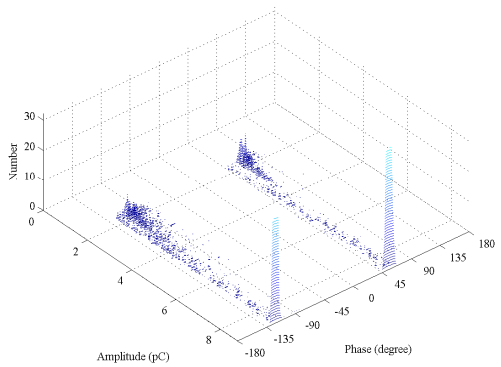

b - 12.5kV at 30°C

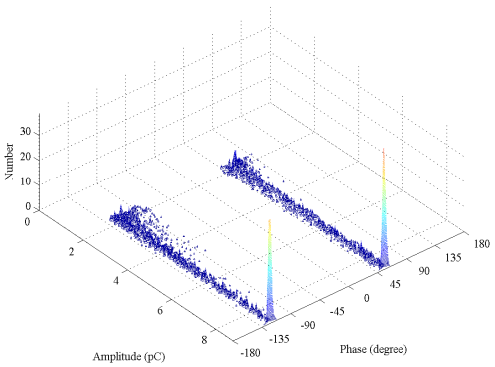

e - 12.5kV at 60°C

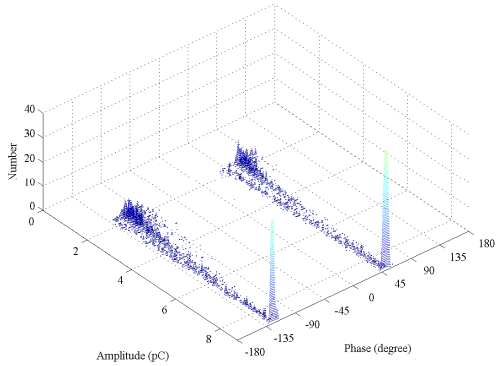

c - 12.5kV at 40°C

Figure 7.11 Series of ϕ-q-n plots ~ temperature for virgin pressboard conditioned to 3.6% moisture and floating discharge, test cell configured for null general field. Robinson set to 5pC resolution

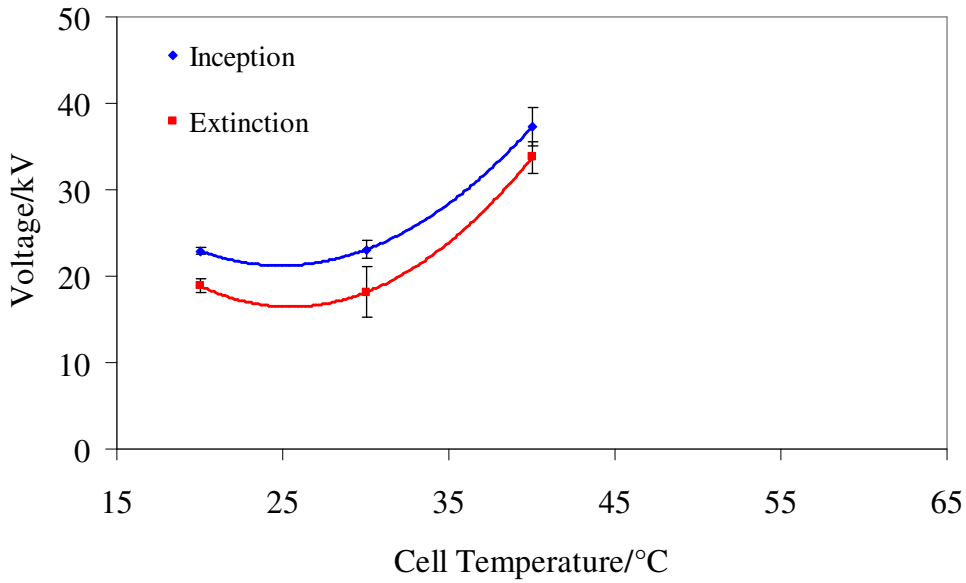

.

Figure 7.12 Inception and extinction voltage ~ system temperature for localised – general field interaction with 3.6% moisture in pressboard

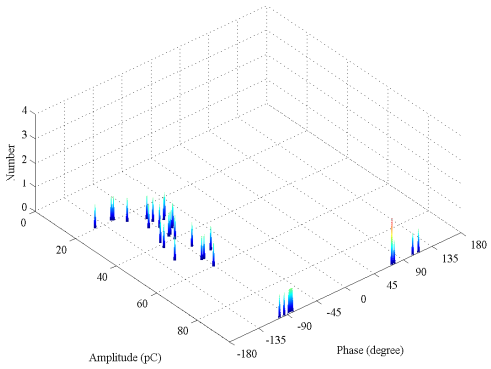

a - 25kV at 20°C

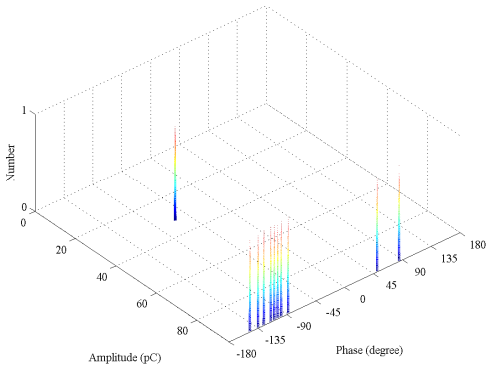

c - 40kV at 40°C

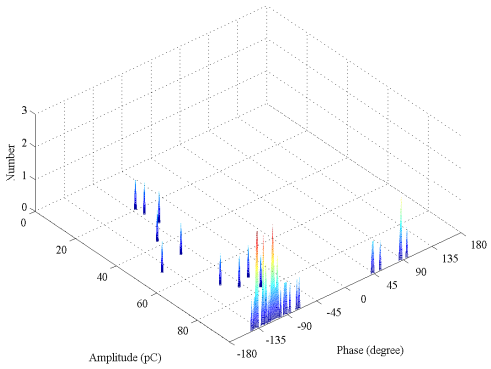

b - 30kV at 30°C

Figure 7.13 Series of ϕ-q-n plots ~ temperature for virgin pressboard conditioned to 3.6% moisture and floating discharge, test cell configured for fixed general field. Robinson set to 50pC resolution

7.6 Effect of phase change in the general field on PD activity

The test cell was arranged as shown in Figure 5.24 with the isolated conducting particle positioned between the discharge source and the earth bar and with the voltage set to 20kV on each electrode. The ϕ-q-n plots for 3.6% moisture board under general -field phase differences of 0°, (i.e. in phase) and 60° lag, 120° lag, 60° lead, 120° lead and finally 180° (i.e. anti-phase) for system temperature conditions of 20°C through to 60°C are shown in Figure 7.17 through to Figure 7.21 at the end of the chapter. The figures show that PD onset is directly influenced by the phase difference of the control electrode from the reference electrode.

7.7 Discussion of results

The results from the test cell experiments with the isolated conducting particle do not follow the results found with the corresponding experiments described in Chapter 6. Firstly, in the case of the null field, the onset of PD activity occurs at lower voltage and no significant response of PD inception is found with temperature (c.f. Figure 7.10 with Figure 6.1). In the case of the fixed general field with respect to earth, a significant response is found with temperature with flashover occurring at 50°C (c.f. Figure 7.12 with Figure 6.4). Finally, in the case of the phase change experiment, PD activity remains stable but PD inception tracks the phase change of the control electrode with respect to the reference electrode. This is in contrast to the results obtained without the isolated conducting particle where the intensity of PD activity is related to the phase change but the onset remains associated with the reference electrode (c.f. Figure 7.17 through Figure 7.21 with The presence and proximity of the isolated conducting particle has altered how the general field interacts with the discharge source because the isolated fixed conducting particle acts as a region of charge storage.

In the case of the null general field, PD inception appears to occur at a lower voltage (10kV level compared to 20kV level). In reality, because of the small separation distance (10mm approximately), the local creep field strength between the discharge source and the isolated particle (as calculated by the FEM) is much greater (of the order of 1.3kVmm^{-1}) compared to the field strength in the same region without the isolated particle (280Vmm^{-1}). The ϕ-q-n plots (Figure 7.11), characteristic of floating discharge,

suggest that PD activity is caused by currents circulating between the discharge source and the conducting particle (Figure 7.14).

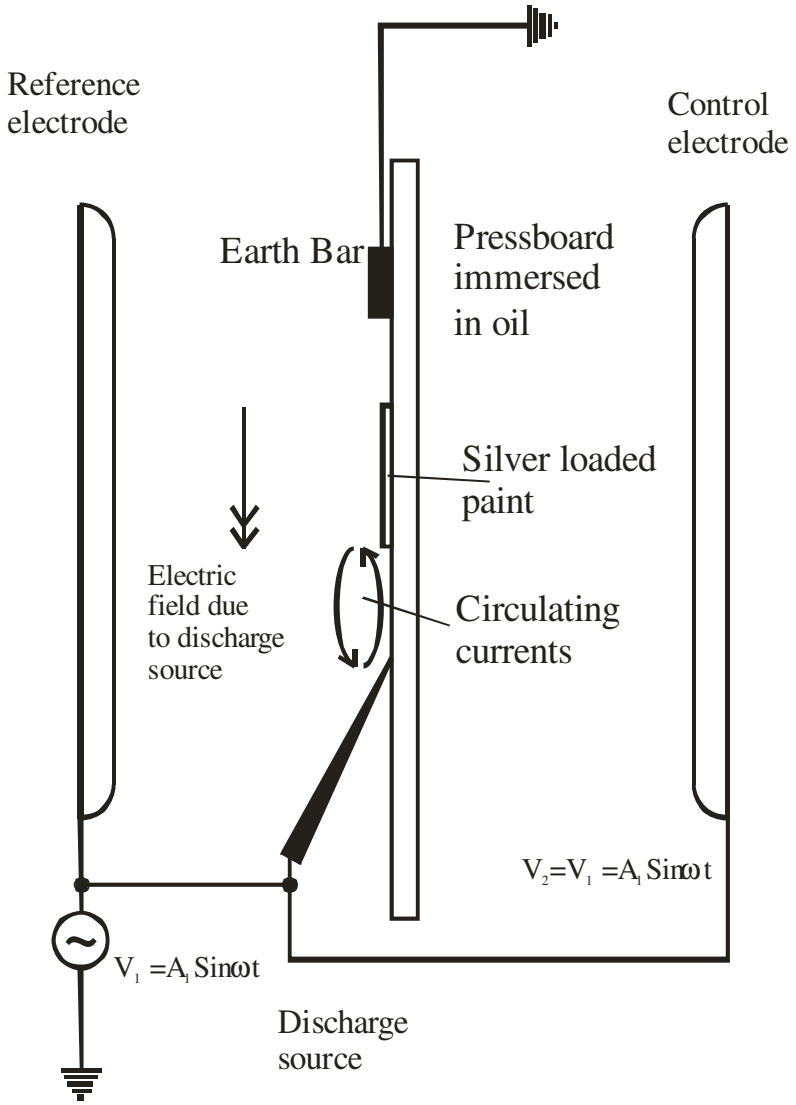

Figure 7.14 Diagrammatic representation of surface discharge from isolated conducting particle in null field

The lack of PD activity, around the peaks of the ϕ-q-n plots, indicates the absence of ionisation or corona. This explains why PD inception is not influenced by temperature because the PD is not initiated by moisture. It is unaffected by any change in pressboard conductivity due to moisture migration as a result of the temperature change. This suggests that the charge transport due to the surface discharge occurs in the oil boundary layer above the pressboard rather than in the pressboard transition region.

In the case of the fixed general field, the ϕ-q-n plots (Figure 7.13) show discrete discharges occurring around the peaks which indicate corona activity rather than surface discharge activity. As the system temperature was raised, it was necessary to increase

the voltage level in order to achieve PD inception indicating similar moisture migration from the pressboard as found in the experiments documented in Chapter 6. At 50°C, flash-over from the discharge source occurred before PD inception was established and this explains the end of the PD inception and extinction characteristic at 40°C in Figure 7.12. In this configuration (Figure 7.15), the fixed general field is established in the same time as the localised field from the discharge source.

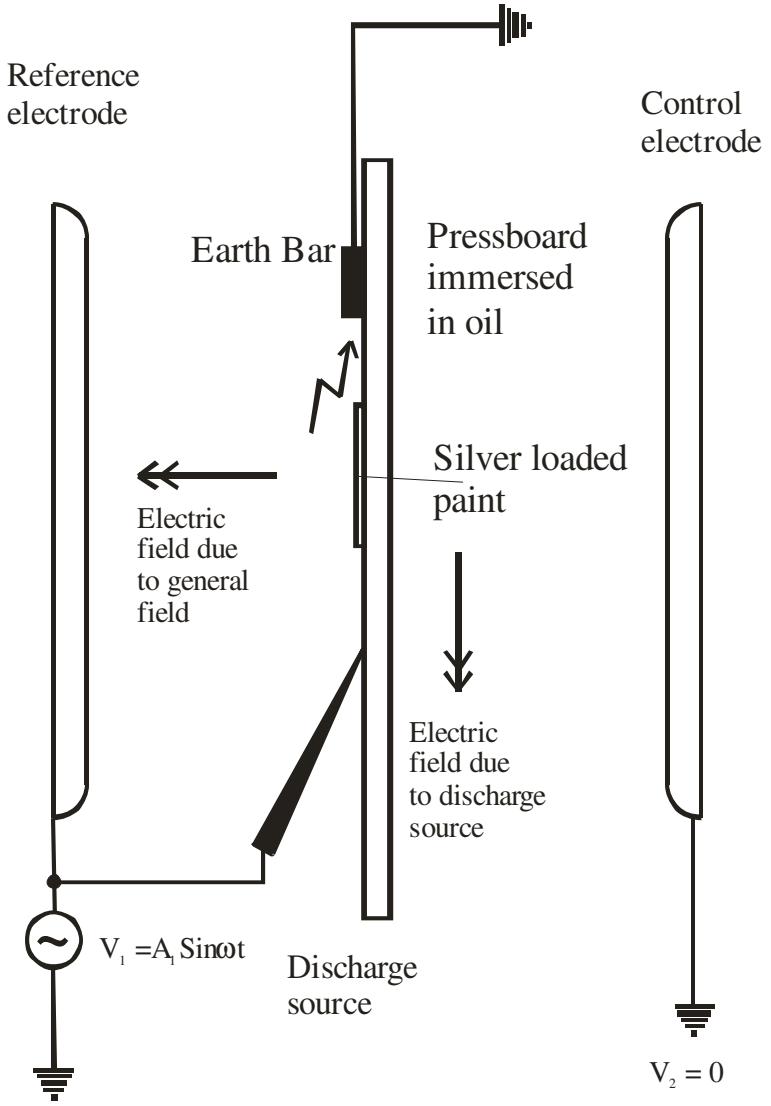

Figure 7.15 Diagrammatic representation of partial discharge from isolated conducting particle in fixed general field

The interfacial layer in the pressboard between the discharge source and the isolated particle (in this case the silver loaded paint mark) is enhanced resulting in the development of space charge between the discharge source and the isolated particle. PD inception is dependent upon the proximity of the isolated particle to the discharge source which effectively reduces the creepage distance to earth. Flash-over results at a

lower voltage than expected taking into account the changing moisture profile with increasing temperature as the system temperature is raised.

In the case of a variable general field (Figure 7.16), with the voltage set higher than the inception voltage, sustained surface discharges always occurs as evidenced by PD patterns in the first and third quadrant of all ϕ-q-n plots in Figure 7.17a through to Figure 7.21a . These indicate circulating currents similar to that obtained in the null field condition. When the general field is varied from 0° through to 180°, the intensity of PD associated with the circulating currents remains unchanged though the phase relationship tracks exactly the change in the phase difference between the individual fields. The surface discharges were established during the null general field condition and then the variable general field is applied. Because the ratio of local creep field strength to general creep field strength is of the order 5:1, the application of the general field has little effect on the circulating currents already established in the EDL other than to change the phase relationship. The implication of this result is that care needs to be taken in the interpretation of PD patterns recorded under the condition of interacting electric fields. The phase relationship between the interacting fields needs to be known otherwise the PD patterns for one type of activity (in this case surface discharge) may be misinterpreted as PD pattern for a different type of activity (e.g. corona).

7.8 Summary

A series of experiments have been undertaken using isolated fixed and non-fixed conducting particles. In the case of non-fixed isolated particles, the particles will move towards the region of highest creep stress under electro-kinetic action balanced by mechanical forces of gravity, fluid viscosity and friction. If the isolated particle is fixed, then the creepage distance between the discharge source and earth is reduced by forming a conducting region on which charge can accumulate. The results indicate that the conducting particle plays a charge storage role when the local field is higher than $1.2 kVmm^{-1}$ or when it is within the sphere of influence from a discharge source. In this situation circulating currents can be set up between the fixed conducting particle and the discharge source which are transported in the oil layer above the pressboard. The magnitude of the circulating currents is not enhanced by the general field because they are the result of the local creep stress. Surface current activity is indicated by resolved

PD activity in the first and third quadrants which is unaffected by temperature and general field intensity. Care must be taken when interpreting the surface discharge PD patterns under conditions of an interacting field as the phase relationship between the fields influence the phase distribution of the surface discharge PD pattern.

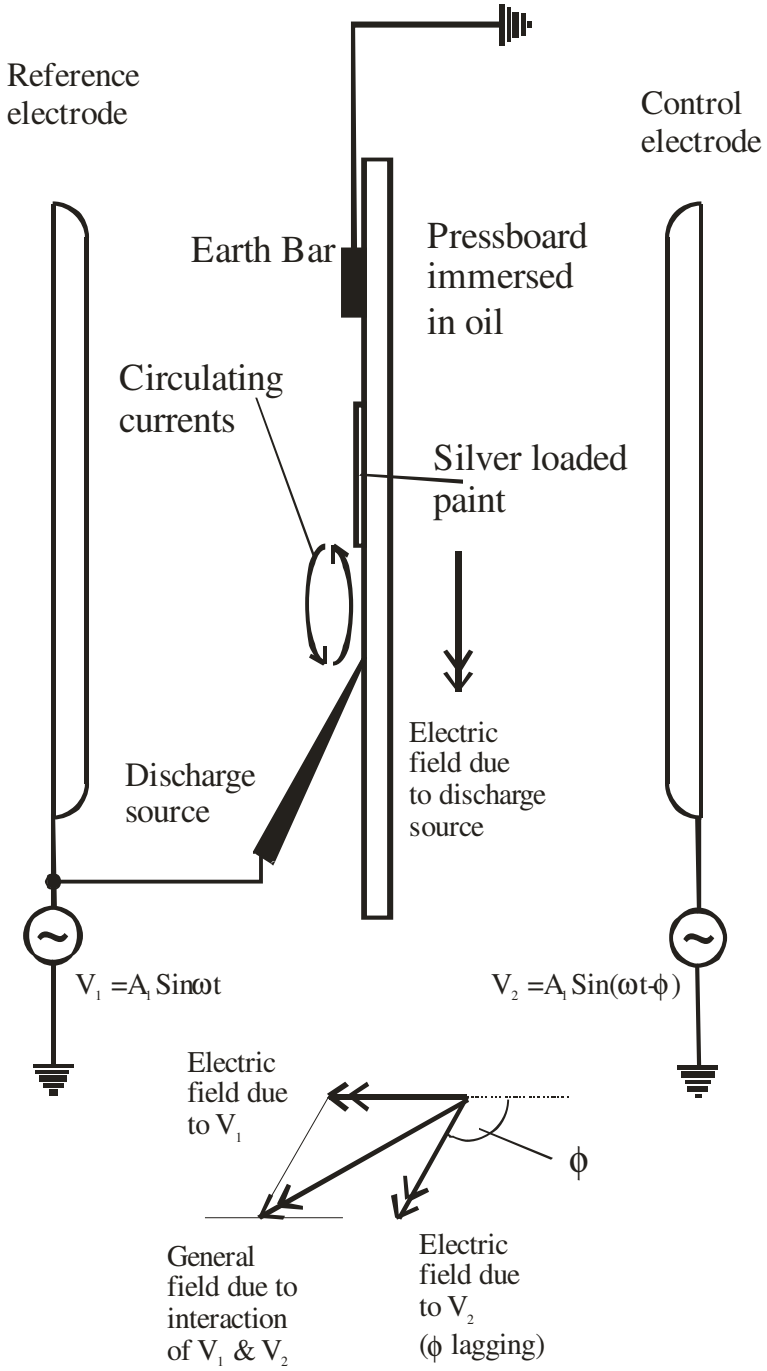

Figure 7.16 Diagrammatic representation of surface discharge from isolated conducting particle in variable general field

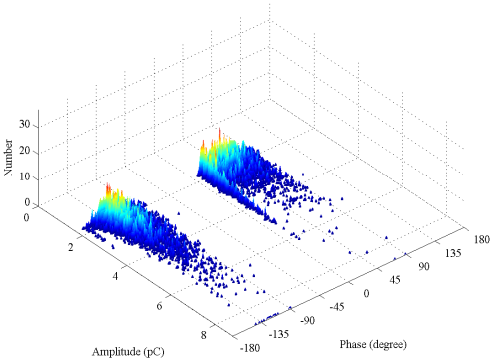

a - $V_{control}$ in phase with V_{ref}

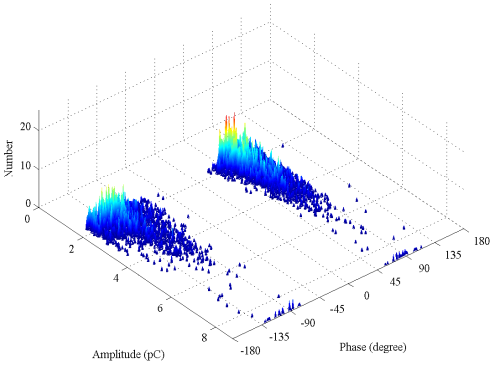

f - $V_{control}$ in anti-phase with V_{ref}

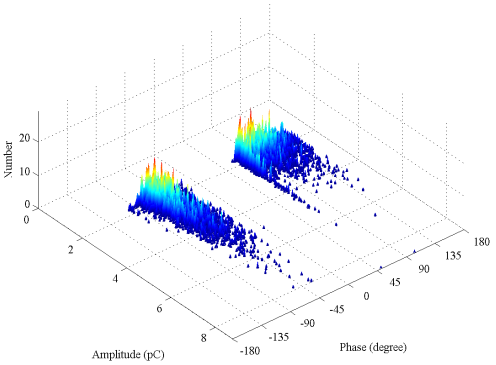

b - $V_{control}$ 60° lag with V_{ref}

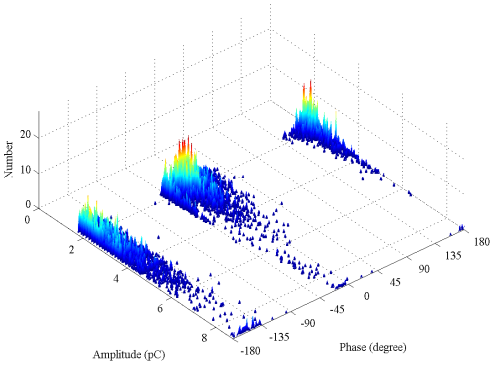

e - $V_{control}$ 60° lead with V_{ref}

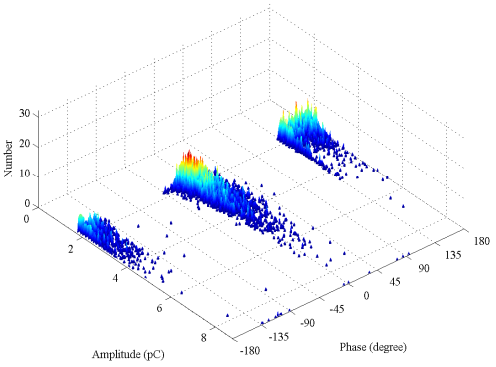

c - $V_{control}$ 120° lag with V_{ref}

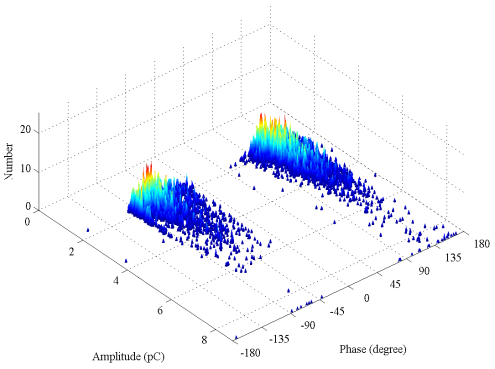

d - $V_{control}$ 120° lead with V_{ref}

Figure 7.17 Series of ϕ-q-n plots ~ phase change of $V_{control}$ at 20kV for virgin pressboard conditioned to 3.6% moisture and at 20°C and floating discharge. Robinson set to 5pC resolution

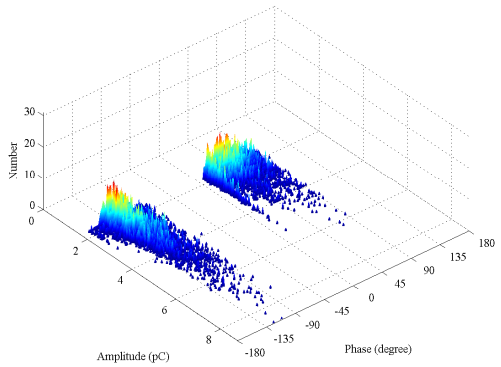

a - $V_{control}$ in phase with V_{ref}

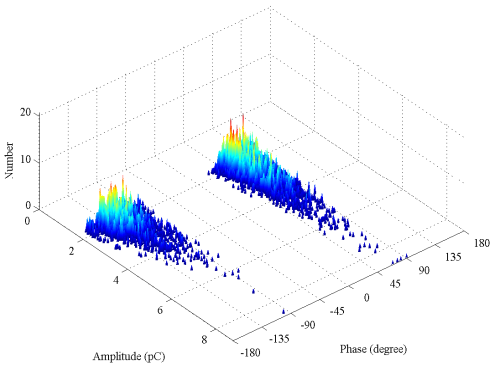

f - $V_{control}$ in anti-phase with V_{ref}

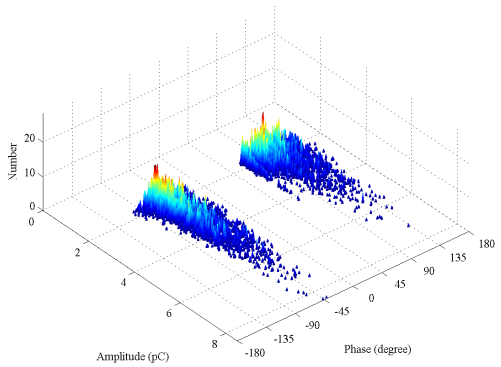

b - $V_{control}$ 60° lag with V_{ref}

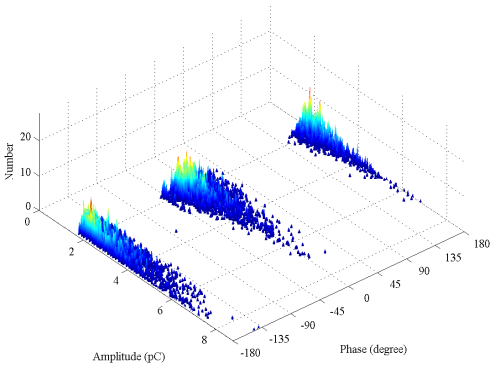

e - $V_{control}$ 60° lead with V_{ref}

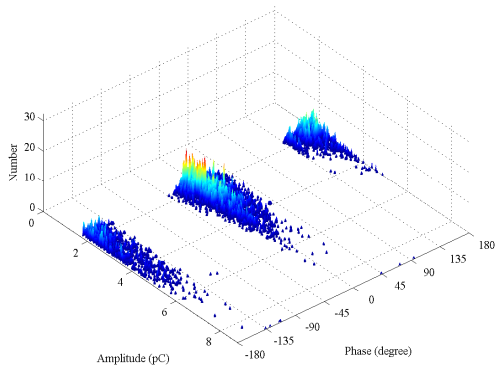

c - $V_{control}$ 120° lag with V_{ref}

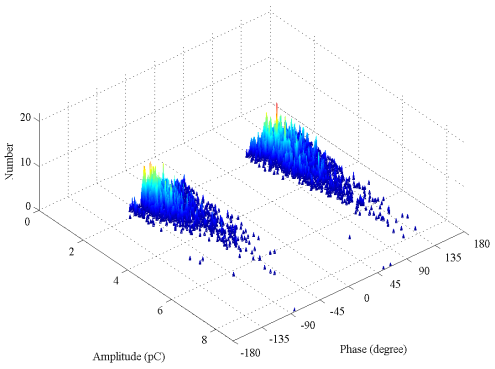

d - $V_{control}$ 120° lead with V_{ref}

Figure 7.18 Series of ϕ-q-n plots ~ phase change of $V_{control}$ at 20kV for virgin pressboard conditioned to 3.6% moisture and at 30°C and floating discharge. Robinson set to 5pC resolution

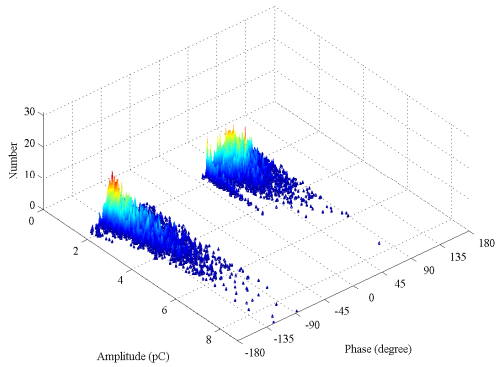

a - $V_{control}$ in phase with V_{ref}

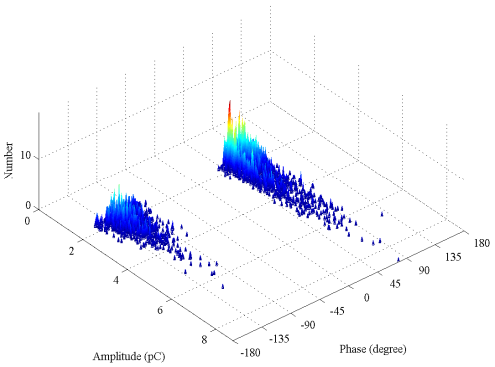

f - $V_{control}$ in anti-phase with V_{ref}

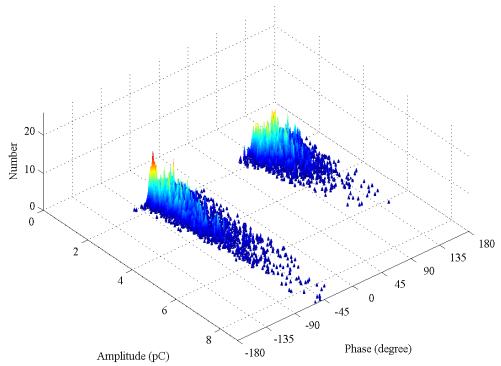

b - $V_{control}$ 60° lag with V_{ref}

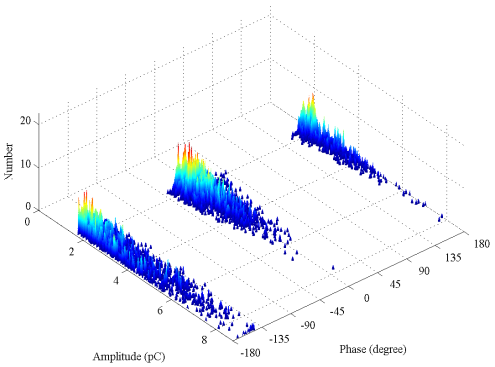

e - $V_{control}$ 60° lead with V_{ref}

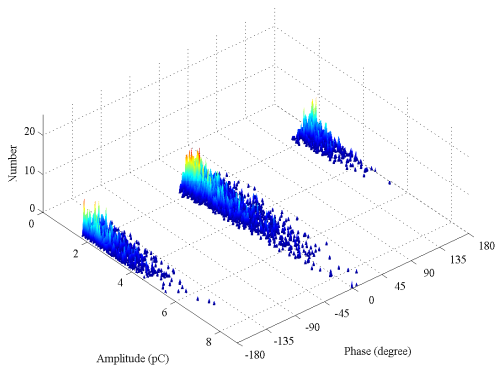

c - $V_{control}$ 120° lag with V_{ref}

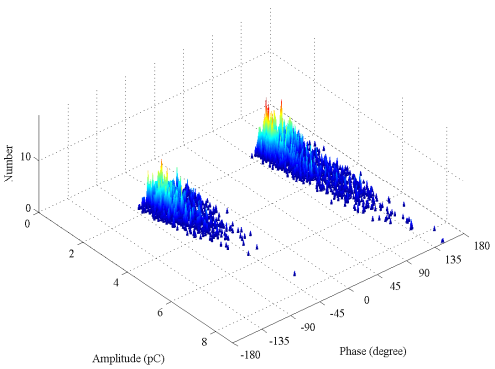

d - $V_{control}$ 120° lead with V_{ref}

Figure 7.19 Series of ϕ-q-n plots ~ phase change of $V_{control}$ at 20kV for virgin pressboard conditioned to 3.6% moisture and at 40°C and floating discharge. Robinson set to 5pC resolution

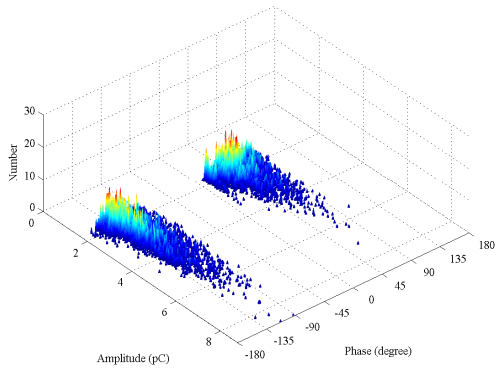

a - $V_{control}$ in phase with V_{ref}

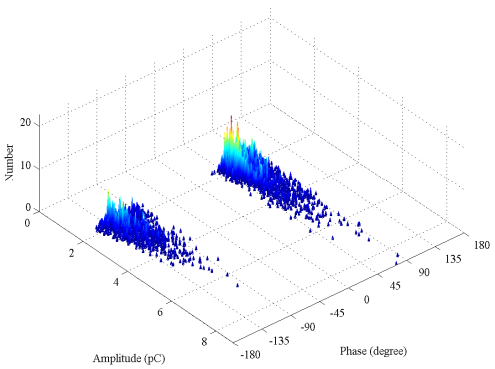

f - $V_{control}$ in anti-phase with V_{ref}

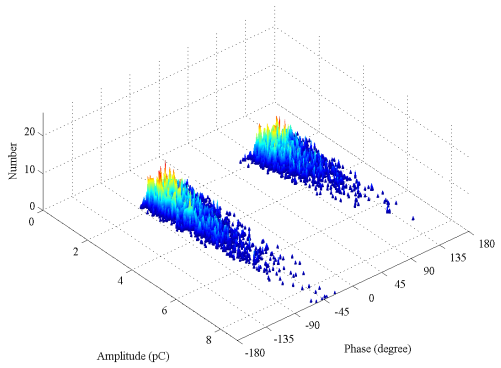

b - $V_{control}$ 60° lag with V_{ref}

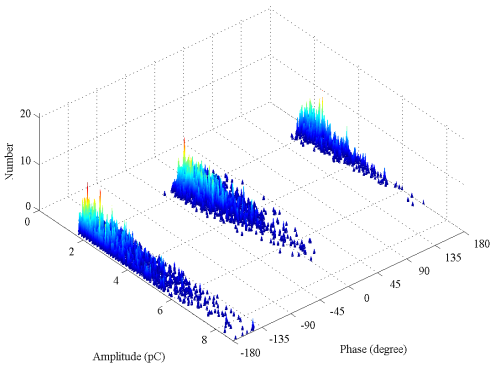

e - $V_{control}$ 60° lead with V_{ref}

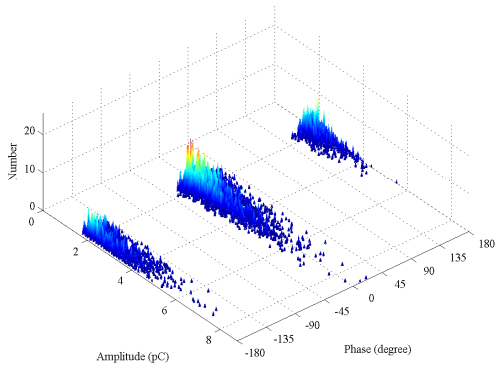

c - $V_{control}$ 120° lag with V_{ref}

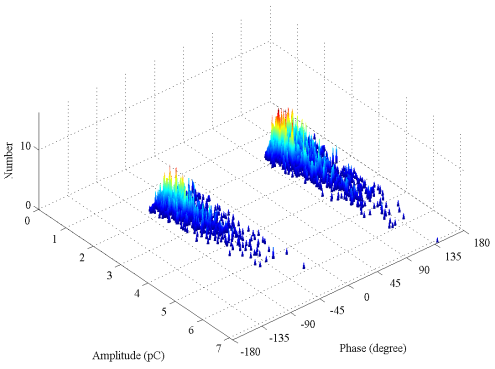

d - $V_{control}$ 120° lead with V_{ref}

Figure 7.20 Series of ϕ-q-n plots ~ phase change of $V_{control}$ at 20kV for virgin pressboard conditioned to 3.6% moisture and at 50°C and floating discharge. Robinson set to 5pC resolution

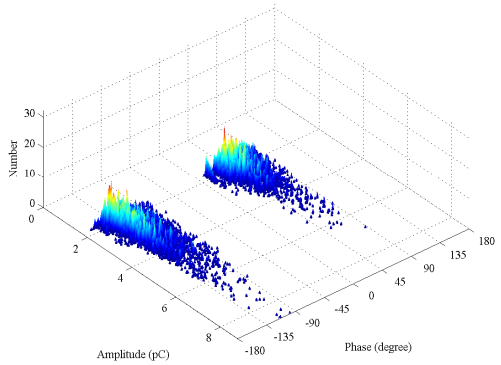

a - $V_{control}$ in phase with V_{ref}

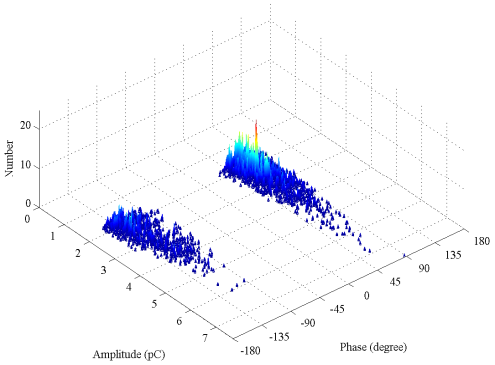

f - $V_{control}$ in anti-phase with V_{ref}

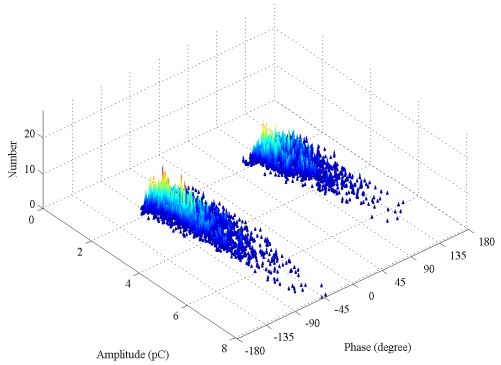

b - $V_{control}$ 60° lag with V_{ref}

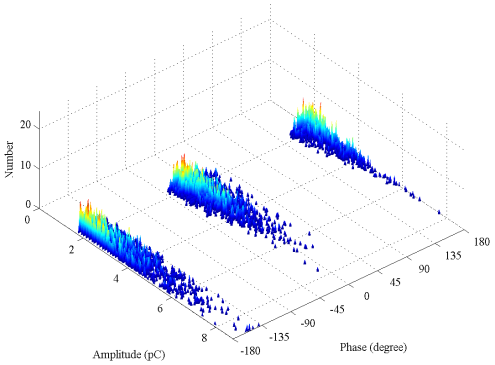

e - $V_{control}$ 60° lead with V_{ref}

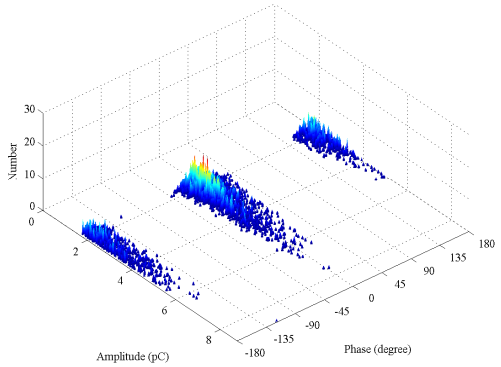

c - $V_{control}$ 120° lag with V_{ref}

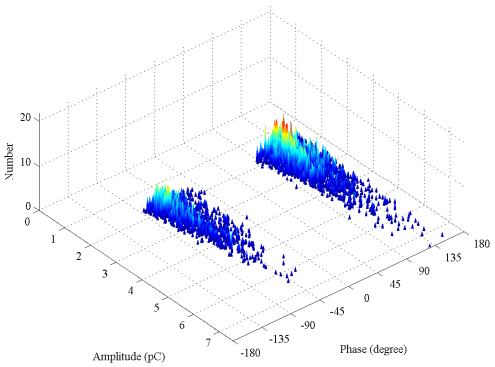

d - $V_{control}$ 120° lead with V_{ref}

Figure 7.21 Series of ϕ-q-n plots ~ phase change of $V_{control}$ at 20kV for virgin pressboard conditioned to 3.6% moisture and at 60° and floating discharge. Robinson set to 5pC resolution

Chapter Eight

Conclusions and recommendations

The development of the experimental facility formed a significant aspect of the project and involved the major renovation of an existing test platform. The refurbishments included the renewal of the system control and user interface, the re-design and implementation of new control circuitry and an earth plan, extensive plumbing and mechanical improvements, an up-grade to high voltage working and the conceptual design and implementation of the model for the inter-phase barrier including the design and implementation of an independent bi-phase supply.

The model of the inter-phase barrier necessitated an understanding of many technical aspects relating to liquid filled transformers, their design, manufacture, operation and maintenance. This included knowledge of the material science relating to mineral oil and paper, general construction techniques of large transformers, maintenance and diagnostic techniques, high voltage engineering principles including finite element modelling, the physics of electronic action and discharge and the many industrial standards relating to testing and materials. A host of elements have been brought together which has resulted in the development of novel concepts and enabled the mechanism for the enhancement of surface tracking in the inter-phase barrier region to be investigated in a systematic manner.

8.1 Achievements of project

The project has produced a large scale test facility which is technically novel in two respects. The first novelty is not the size of the facility (Lundgaard worked with a 600 litre facility in the 1980s), but the method by which the variable general electric field is created within the volume space by the interaction of two independent time varying electric fields from mechanically opposed electrodes. In the case where the electric fields are identical (i.e. same amplitude and phase), the resultant general field is a null field. The general field is varied simply by changing the phase relationship of the applied voltage to each of the electrodes. The bonus is that when the phase difference is 120° elec., the resulting field interaction replicates that occurring in the inter-phase barrier region. The second novelty is the method of implementing a directional discharge source to produce a localised space charge which can then interact with the variable general field developed between the electrodes.

The project also led to the development of a new approach to investigate tracking on solid materials in liquid media. Guidelines for the determination of tracking exist only for solid insulation in air. The conventional approaches, taken by many researchers, employ either the point-plane method or parallel plane methods. Both of these methods were shown in Chapter 5 to have limitations. The point-plane method is not practical for the study of surface discharge on pressboard due to the problem of rapid burn-through of the specimen under test; the parallel plane method makes it difficult to resolve the influence of the general field from the local field.

The novel concept was to modify the CTI approach and to implement the needle-bar method where the discharge source and the earth are on the same surface such that the discharge source is not influenced by a general field. This arrangement revealed that partial discharges from a discharge source are insensitive to distance from the earth bar; i.e. discharge is a localised phenomenon which can be influenced by a general field.

8.2 Discussion of results

The results from Chapter 5 show that, under elevated conditions of electrical stress, a local field develops around a high stress point resulting in corona discharge. Put another way, for PD to occur there must be the interaction of a high strength electric

field on a defect. This becomes surface discharge when the stress point is placed in proximity to a solid insulation surface. The surface discharge causes scorch marks (tracking) on the surface of the insulation. The surface damage is a function of a voltage x time product (and insulation material) and explains why surface discharge without insulation breakdown may exist for years as reported in the literature review. This approach uncovered three elements necessary for surface tracking i.e. a discharge source of sufficient energy which must be in proximity to a solid surface.

The results also show that the solid interface depresses the intrinsic level of voltage withstand along the surface plane which may be afforded by the volume of liquid insulation without the solid insulation. It effectively lowers the margin of safety which may be subjected to further degradation of the insulation through the general ageing mechanisms or contamination. The lowered margin of safety can be more easily overcome by an over-voltage resulting in surface flash-over. Under these conditions the insulation may break down at a value lower than the properties of the bulk insulation would predict.

The observation, that the depressed surface flash-over voltage is different for different surface textures, lead to a new interpretation of the interfacial layer as expanded in Chapter 5. With the contaminated pressboard, it should be expected that a flashover would occur at a lower voltage than with un-aged (new) pressboard. The results clearly show the opposite. Because the flash tests were undertaken quickly, (i.e. without time for a sustained discharge and conditioning to take place) the extra margin of voltage withstand afforded by the aged pressboard is due to the smooth surface condition as opposed to the textured surface of the new pressboard. The interpretation therefore proposes that the interfacial layer for oil-pressboard interface is not just the discrete boundary layer of oil adjacent to the "solid" pressboard (as assumed in many papers describing static electrification) but includes an extended transition region where the bulk oil merges into the bulk pressboard. The transition region is a function of the roughness and porosity of the pressboard in the region near the pressboard surface.

The experiments, described in Chapter 6, on the interaction of the null general field and the fixed general field with the localised discharge source show that both moisture and

contamination play a role in discharge initiation. The PD inception voltage response to temperature with new pressboard shows a positive relationship with temperature which is at variance with the expectation. The contaminated pressboard shows the expected negative relationship with temperature due to increased conductivity. The explanation for the difference is that, due to conditioning, the moisture equilibrium mechanism and the high oil:pressboard mass ratio, the new pressboard "dries out" with temperature making PD inception harder to initiate at the higher temperature whereas PD inception occurs at lower values for the service aged pressboard due to the increased conductivity at higher temperatures. This indicates that contamination is a more significant factor than moisture in PD inception.

Chapter 6 shows that the interaction of the general field on the interfacial layer enhances the polarisation of the interfacial layer and increases the surface discharge by increasing the transport of charge through the polarised transition zone of the interfacial layer. The enhancement is greatest when the interacting electric fields are in anti-phase but the condition of 120° elec. lagging or leading (i.e. the normal operational conditions inside the barrier region of a large transformer) will result in significant enhancement of any discharge.

Taking all these elements together, a mechanism for the development of surface tracking in the inter-phase barrier region can be proposed which is dependent upon the interaction of many factors. First of all, a discharge will only occur at a location where a high level electric field and a defect co-exist in the same volume space. This results in partial discharges through ionisation leading to the formation of space charge. If the discharge source is in proximity to an oil-pressboard interface then the space charge will interact with the interfacial layer at the surface of the pressboard leading to surface discharges. The chemical composition of the pressboard (i.e. moisture and contamination) and system temperature are all factors in determining the onset and magnitude of discharge. The moisture and contamination, through ionisation of polar molecules, provide sources of charge which can be readily transported through the interfacial layer. Contamination is more significant than moisture in determining the level of discharge and increased system temperature is another co-factor. If the discharge source is located in the inter-phase barrier region, then, the normal operating

conditions with the interacting field at 120° phase difference will sustain the surface discharge due to the enhancement of the interfacial layer. Put another way, due to the enhancing effect of the general field interaction in the inter-phase region, the discharge source will produce PD at a lower energy level than would otherwise occur. The electronic action through ionisation acts initially on the moisture and/or contamination and locally dries out the pressboard resulting in the evolution of H_2 and O_2 leading to a self sustaining process. Charring follows which is predominantly due to oil pyrolysis because the activation energy for oil is lower than that for pressboard. Supporting evidence comes from reported DGA analysis of working transformers as identified in Chapter 2 where it is known that hot spots result in the evolution of hydrocarbon gasses due to oil degradation. The tracking becomes a slowly developing feature due to the interfacial layer which acts as an effective conducting channel allowing tracking to progress just below the pressboard surface. However, the creep component of the general field is not a significant factor except at the coil ends as shown by the FEM models described in Chapters 3 and 5. The effect of the creep component of the electric field is to act as a background drift promoting the transport of charge carriers along the interfacial layer with a sweeping effect occurring as the electric field changes direction twice every cycle. Because of the mechanical arrangement of the cylindrical coils within the earthed frame, and with the peak voltage occurring on the central and outermost part of each cylinder, the sweeping action of the electric field, as it changes direction, is towards the nearest earth. This explains why a surface flashover, should it occur in the inter-phase region, is always directed downwards; this is the simply the nearest earth.

Sokolov, as highlighted in Chapter 1, identified three components for his model of creeping discharge; the first is a breakdown of the oil gap followed by surface discharge in oil across the barrier boards and, thirdly, “sparking within the pressboard” to grow the tracking path. The results have clearly shown that the surface discharge and creeping discharge are two aspects of the same phenomenon i.e. creeping discharge is the manifestation of surface discharge growing along the interfacial layer. The surface discharge is caused by ionisation due to the interaction of a high electric field on a defect. The sparking in the pressboard is initiated and sustained by moisture and other contamination in the pressboard. The interaction of the general field on the interfacial

layer promotes the process by enhancing the polarisation of the interfacial layer and providing the relaxation mechanism to sweep charge away along the interfacial layer. Thus, there remains only the first component to be answered (i.e. the mechanism of oil gap breakdown).

8.3 Lifetime extension

The project had a background secondary objective to answer a "big question" relating to large transformers i.e., how to extend the life-time of aged oil filled transformers. The results hint that there really isn't a single answer because a symptom may be the result of multitude of interacting factors. In addition, transformers exhibit many failure symptoms as identified by the numerous evolved diagnostic techniques.

The ultimate fate of an individual transformer is related to the cumulative sum of all the interactions it experiences and this is clearly recognised by the stress life model as illustrated in Chapter 1. Given a large enough population, general trends tend to become apparent over time as, say, a particular class of equipment succumbs to a particular failure mode as a result of an inherent material defect, or age related defect, which only becomes apparent over time. The term "old age" is used to classify the fate of an individual which can not be pinned down to a single root cause. The individual achieves an acceptable service life in economic terms but is considered to be uneconomical for further repair. It is said to be "worn out", though the actually demise may be as a result of a host of ailments occurring at the same time.

The lifetime surveys discussed in Chapter 1 show that a small percentage of items always fail unexpectedly and the root cause is a rare coincidence or interaction of a specific set of circumstances. (Occasionally, an unpredictable event will occur which is classified an Act of God and (usually) involves some natural cataclysm.) Finally, there is the class of failure where a small number of items fail inexplicably and for which initially there is no obvious root cause. In the case of large oil filled transformers, the industry strives to produce a quality level of product and service. The clear evidence for this, as seen in Chapter 1, is the low overall failure rate and that, by and large, there are relatively few instances of severe power outages or failure. This is the result of the interaction of good science, engineering design and quality manufacture which work

together to eliminate defects, enhance system and equipment capability to maximise the time before failure. Statistical techniques are used throughout the manufacturing and operational life to estimate the probability of failure under a specific cause. Many diagnostic techniques have been developed as outlined in Chapter 2 to monitor the changing condition of the equipment insulation but, none of these methods are yet sophisticated enough to predict exactly when a particular individual will fail. Condition assessment and regular maintenance are only tools used to prolong service life. In terms of unexpected failure, given enough post-incident investigation through the use of forensic analysis, the set of interactions may be uncovered and the results fed back to manufacturers in order to enhance the capabilities of future designs. As regards Acts of God; engineering analysis can only conclude that the original design specification has been exceeded by the pertaining environmental conditions. The point here is that general guidelines can be issued as part of an asset management strategy, but that specific issues have to be addressed on a case by case basis. Successful asset management of any network must include a program of maintenance and replacement balanced against the capital cost of the asset replacement and service disruption; this is the current approach taken by network operators as identified in Chapter 1.

In terms of answering some a specific issue of failure in liquid filled high voltage transformers, this project has achieved solid results by identifying the mechanisms for the initiation and sustaining of discharge in the inter-phase region and the role played by the interfacial layer with the interaction of the time varying electric fields. This has been obtained by the creation of a unique item of test apparatus as well as the development of a novel technique to study surface tracking. Lifetime can be increased by addressing specific issues one at a time but, along with research, maintenance and diagnostics, continuous product replacement must remain a key element in the asset management strategy because nothing lasts for ever.

8.4 Conclusions

A unique test facility has been developed which models the inter-phase barrier region of large transformers and enables independent voltages to be applied to conditioned pressboard in a temperature controlled environment. The novelty of the test facility is that it enables a general electric field to be created which is the result of the interaction

of two independent electric fields. In addition, a new approach has been developed to enable the study of surface discharge on an oil pressboard interface using only the local field from the discharge source. The oil bath experiments show that it is possible to maintain partial discharge without breakdown of the insulation for long periods, that there are distinct stages in the surface flash-over process and that surface condition plays an important role in the flash-over process. The study on surface tracking has shown that the degree of tracking damage is a function of the energy x time product of discharge. It explains why tracking can exist for a long time in a system without breakdown.

The results from the test cell experiment confirm that partial discharge is enhanced by the general field and that contamination is a more significant co-factor than moisture in this process. A major success is the creation of tracking within a short time frame on the surface of a pressboard layer due to a localised discharge source and the interaction of two independent electric fields. The results suggest mechanisms for two out of the three factors in Sokolov's model for the inter-phase barrier failure mode. One factor is the presence of a localised space charge. The space charge on the surface of the pressboard may promote surface discharges which are sustained for long periods leading to tracking damage but not necessarily leading to immediate failure. The normal operating conditions of the inter-phase region with the interaction of two adjacent electrical fields enhances the discharge by polarisation of the EDL and additionally sets up a general electric field drift component parallel to the surface of the pressboard which directs the tracking to the nearest earth. The presence of the EDL influences the voltage withstand capability of the bulk liquid along the surface of the pressboard. Flash-over may occur if the tracking damage is sufficient to degrade the intrinsic surface resistivity or an external over-voltage degrades the margin of safety for the voltage withstand of the oil/pressboard interface. The project has resulted in the development of two novel techniques both of which offer scope for further investigation into tracking and the EDL.

8.5 Recommendations for further work

The project had insufficient time to address the first factor in Sokolov's creeping discharge model (i.e. the oil gap flashover) and this is the next goal to be targeted.

However, a slight weakness in the barrier model must first be addressed. This is the use of parallel plate electrodes which means that the electric field strength is not as representative in vertical space as would occur from a real series winding due to the turns volt drop. This can be overcome by adopting shaped electrodes which mechanically compensate for the turns volt drop to give a more representative divergent electric field. A study of the oil gap discharge would be aided by visual analysis which could be achieved by the provision of high speed camera equipment to observe oil gap discharge through the test cell window.

The test facility could also benefit with the introduction of a noise free power amplifier for the bi-phase supply. For this project, the noisy power amplifier did not prove to be a problem as any PD from the amplifier was attenuated by the position of the Robinson pick-up. However, this limits how close the electrode can be brought in the inter-phase model and the resultant strength of the general field. The main disadvantage of the test cell is the time required for experimental setup which lends the equipment to being more suited for duration experiments rather than work requiring quick turnaround.

The development of the new approach to study surface discharge opens up a new avenue to explore with respect to the EDL. The feature of the needle-bar equipment is that is possible to set up experiments very quickly and which are physically accessible. The method is not just limited to an oil-pressboard interface but may be applied to *any solid insulation in any liquid or gaseous medium*. The apparatus would benefit from additional engineering work such as a transparent container to allow photographic recording of the processes from all angles and a mechanism to allow remote adjustment of the needle-bar gap. The key issues which should be top of the research agenda are effect of the morphology the pressboard surface (i.e. surface texture and texture orientation) on voltage depression, the influence of contamination (i.e. particulates and moisture) and the possible role of photo-emission in the surface tracking process. The interesting questions that need to be addressed relate to the thickness of the EDL with respect to the liquid boundary layer and how deep the EDL penetrates into the bulk material as a function of surface texture and material characteristics.

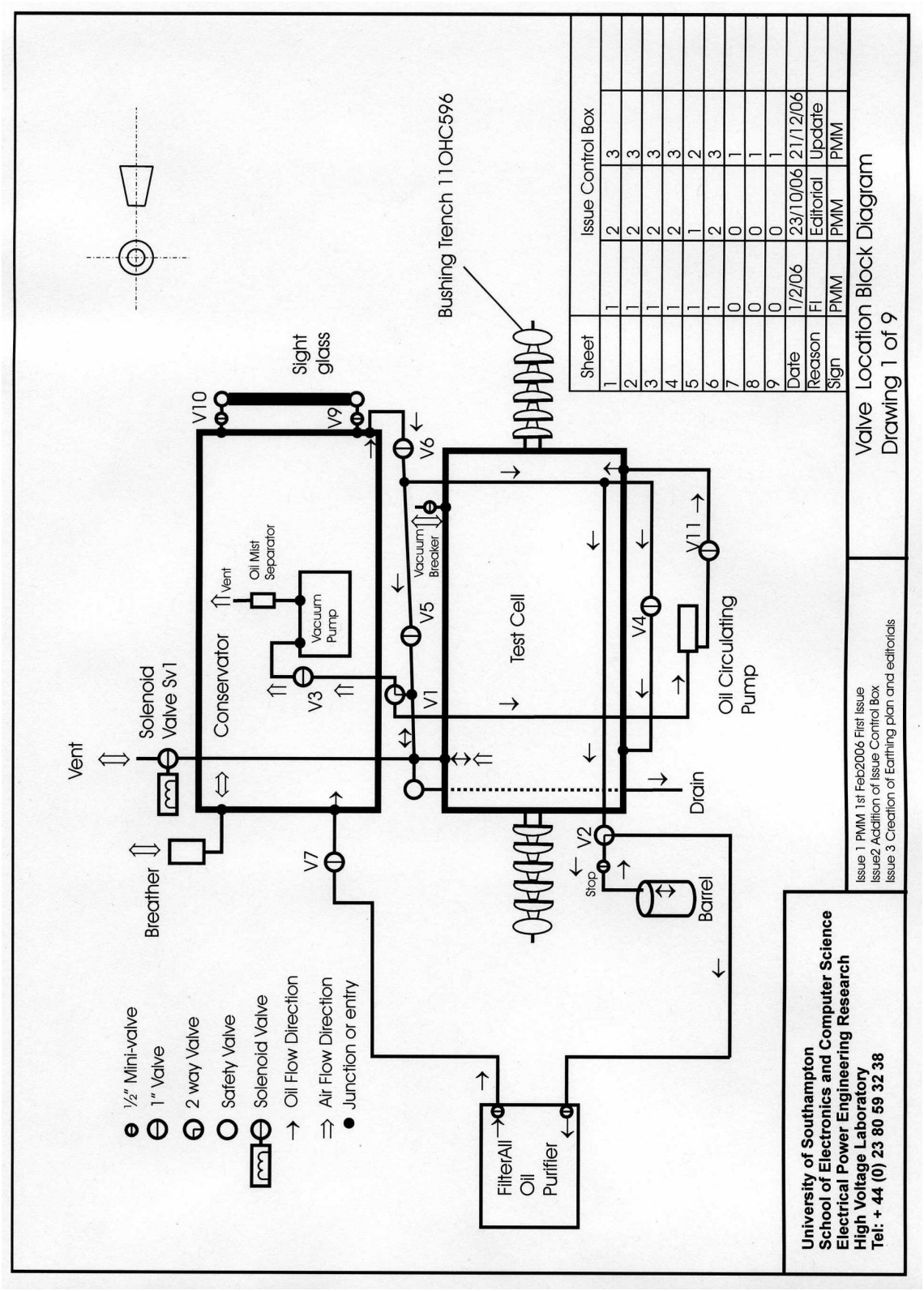

Figure A.1 Valve location block diagram

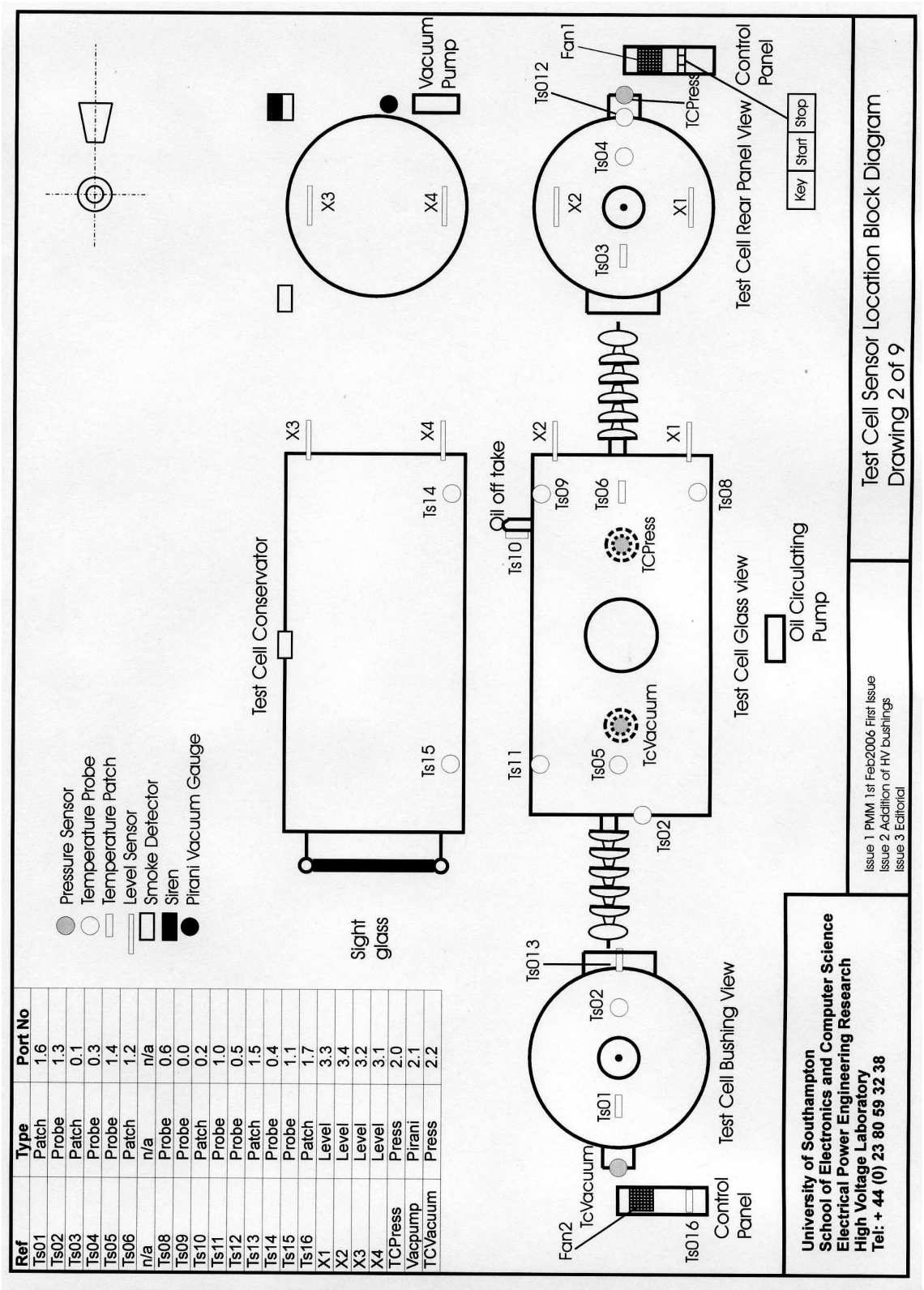

Figure A.2 Test cell sensor location block diagram

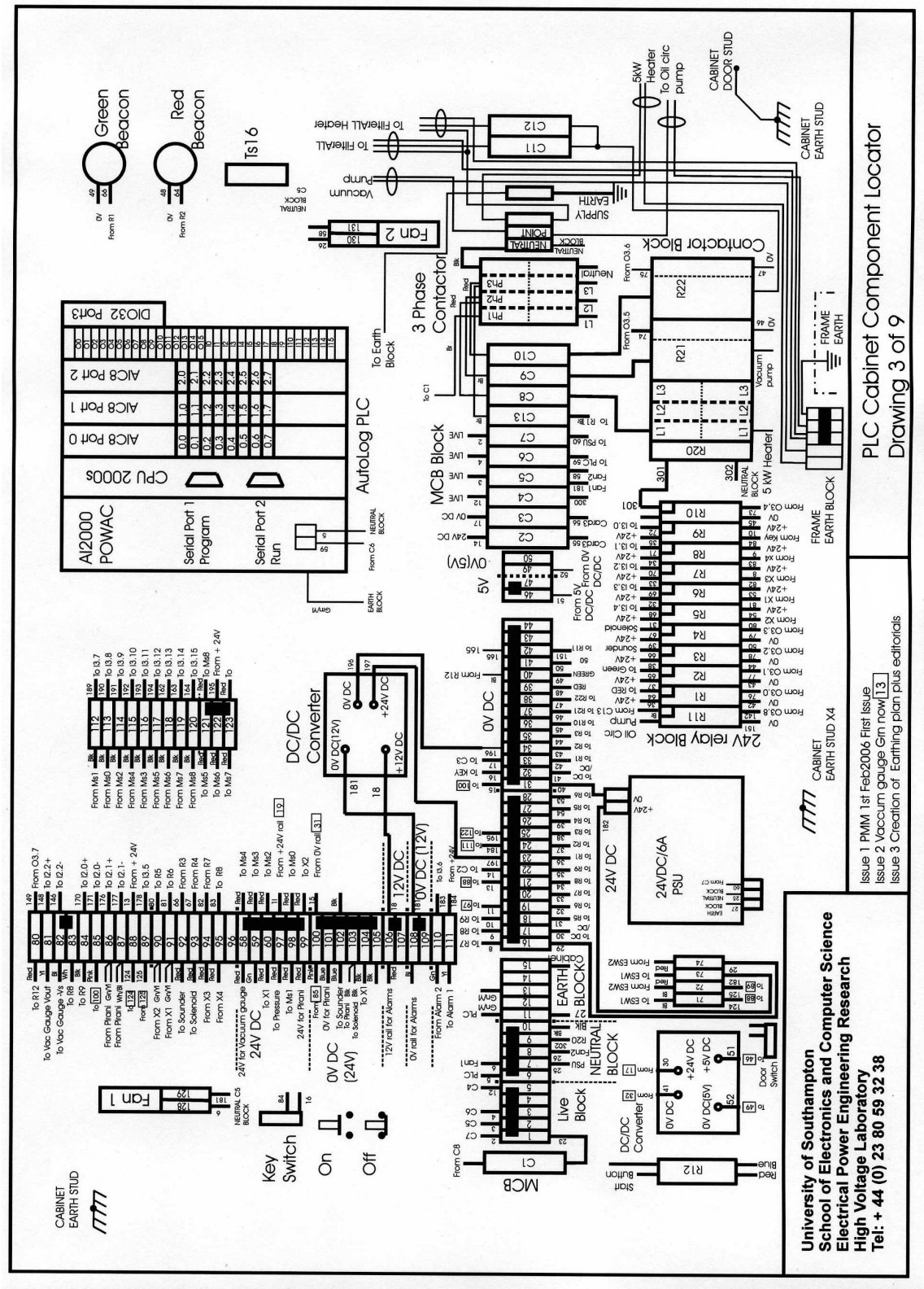

Figure A.3 PLC component location block diagram

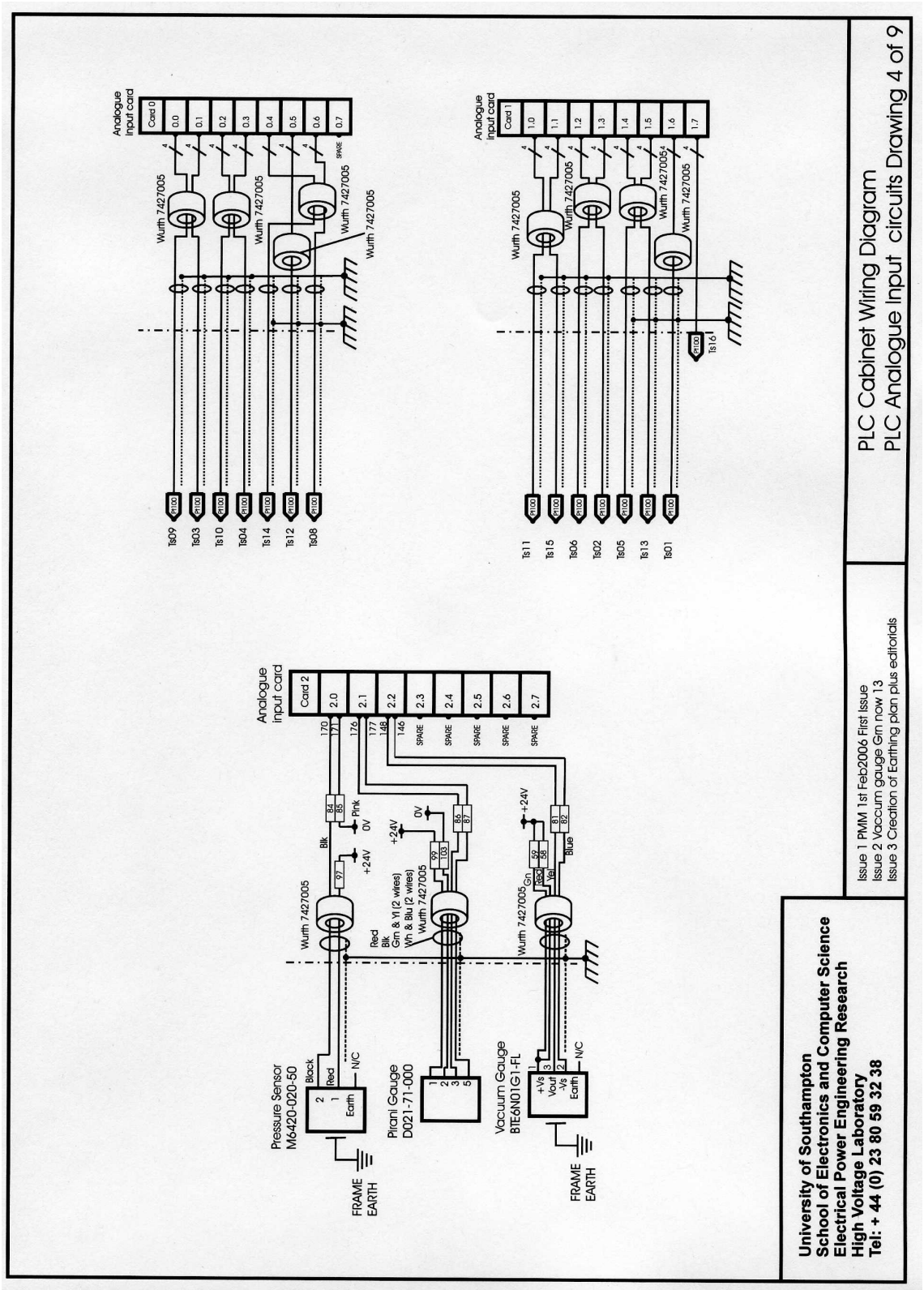

Figure A.4 PLC analogue input circuits

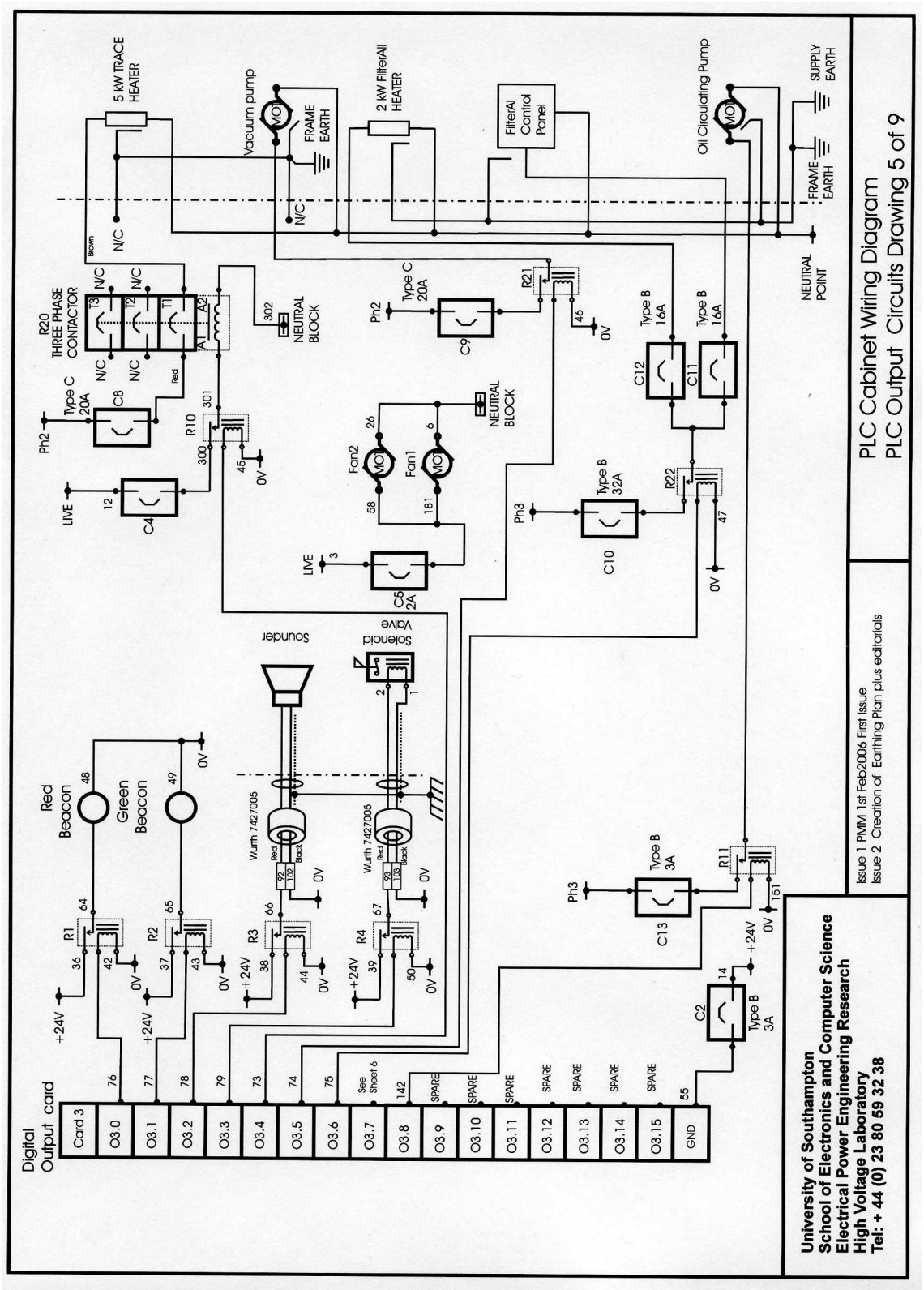

Figure A.5 PLC output circuits

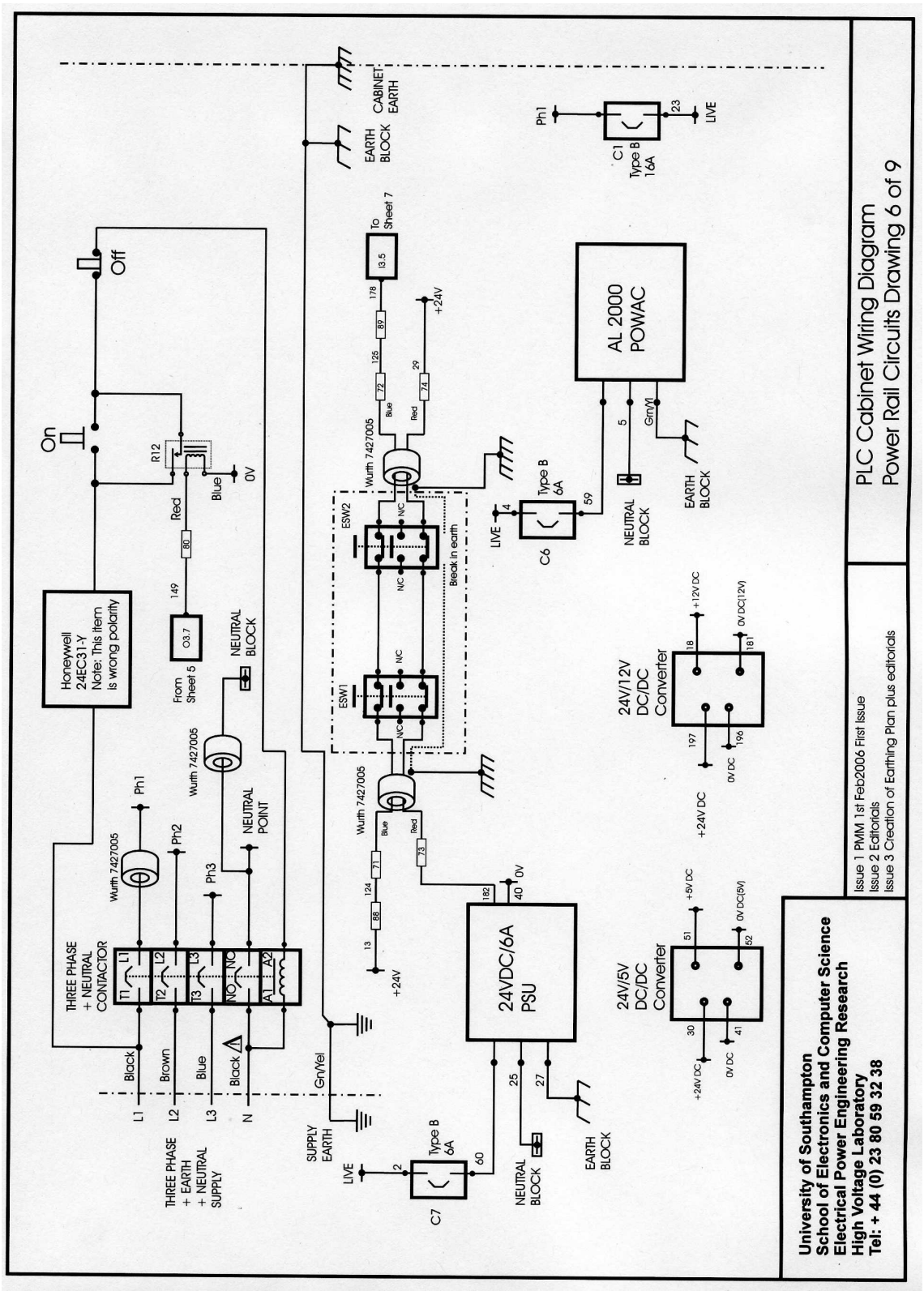

Figure A.6 PLC power rail circuits

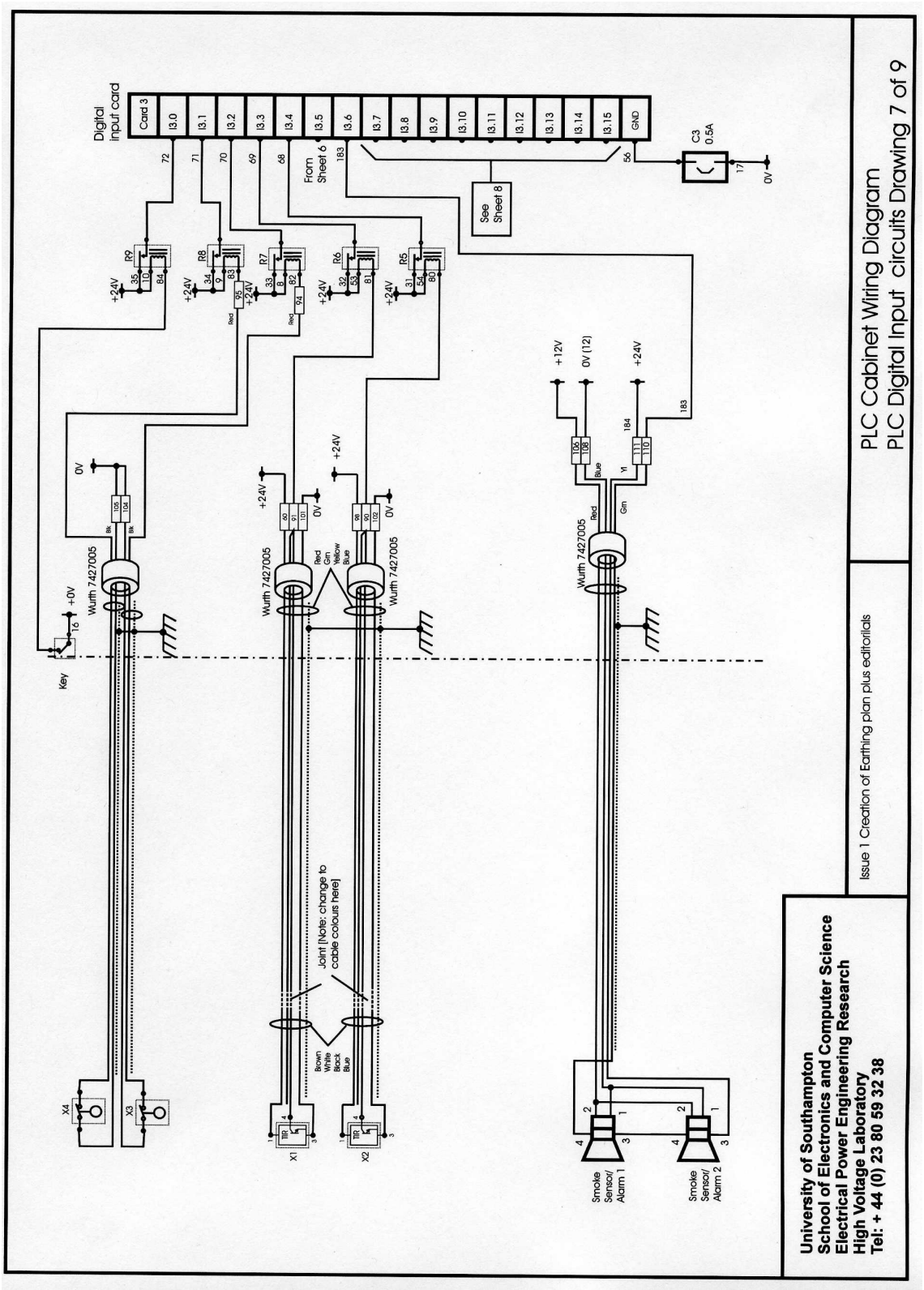

Figure A.7 PLC digital input circuits

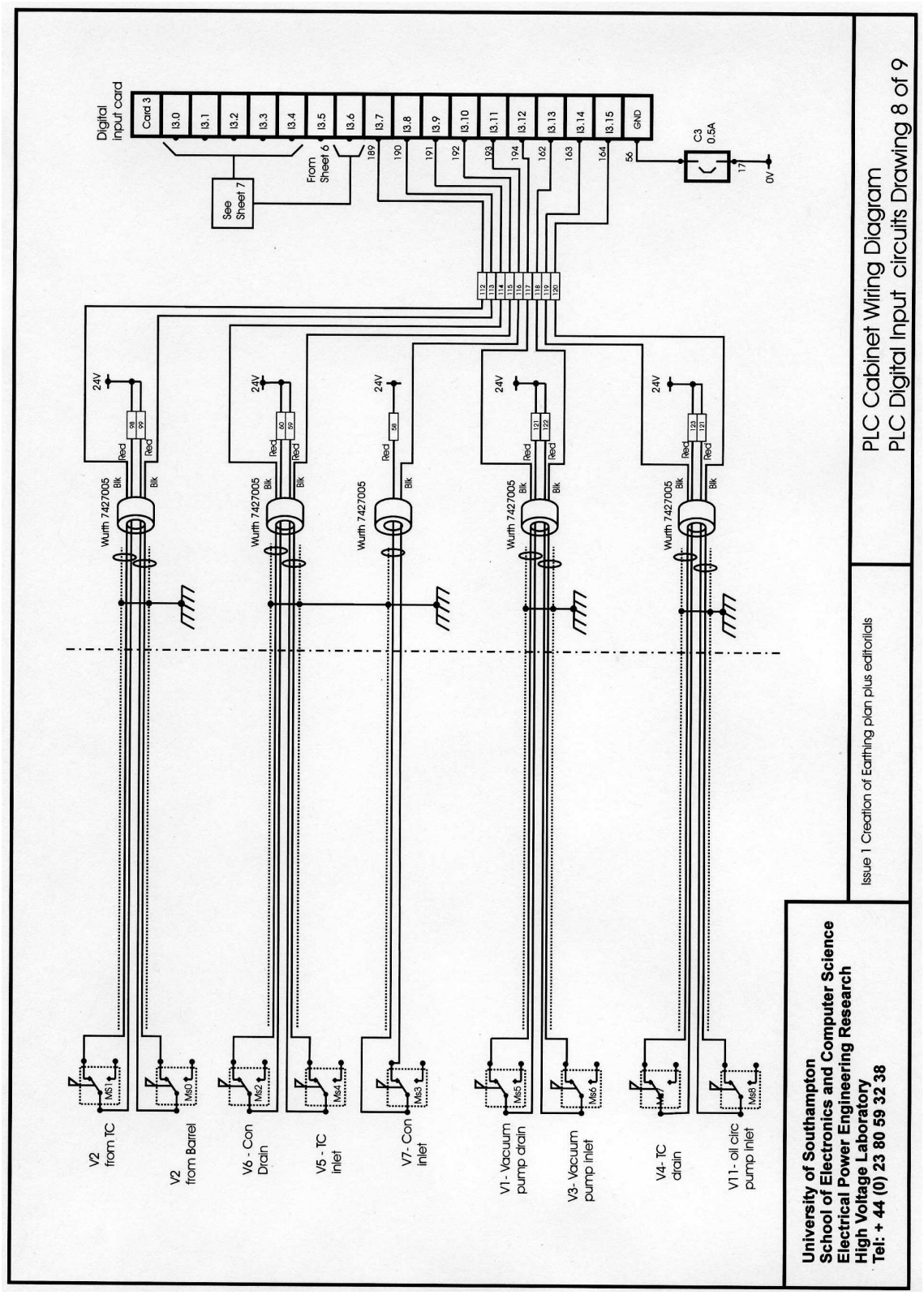

Figure A.8 PLC digital input circuits

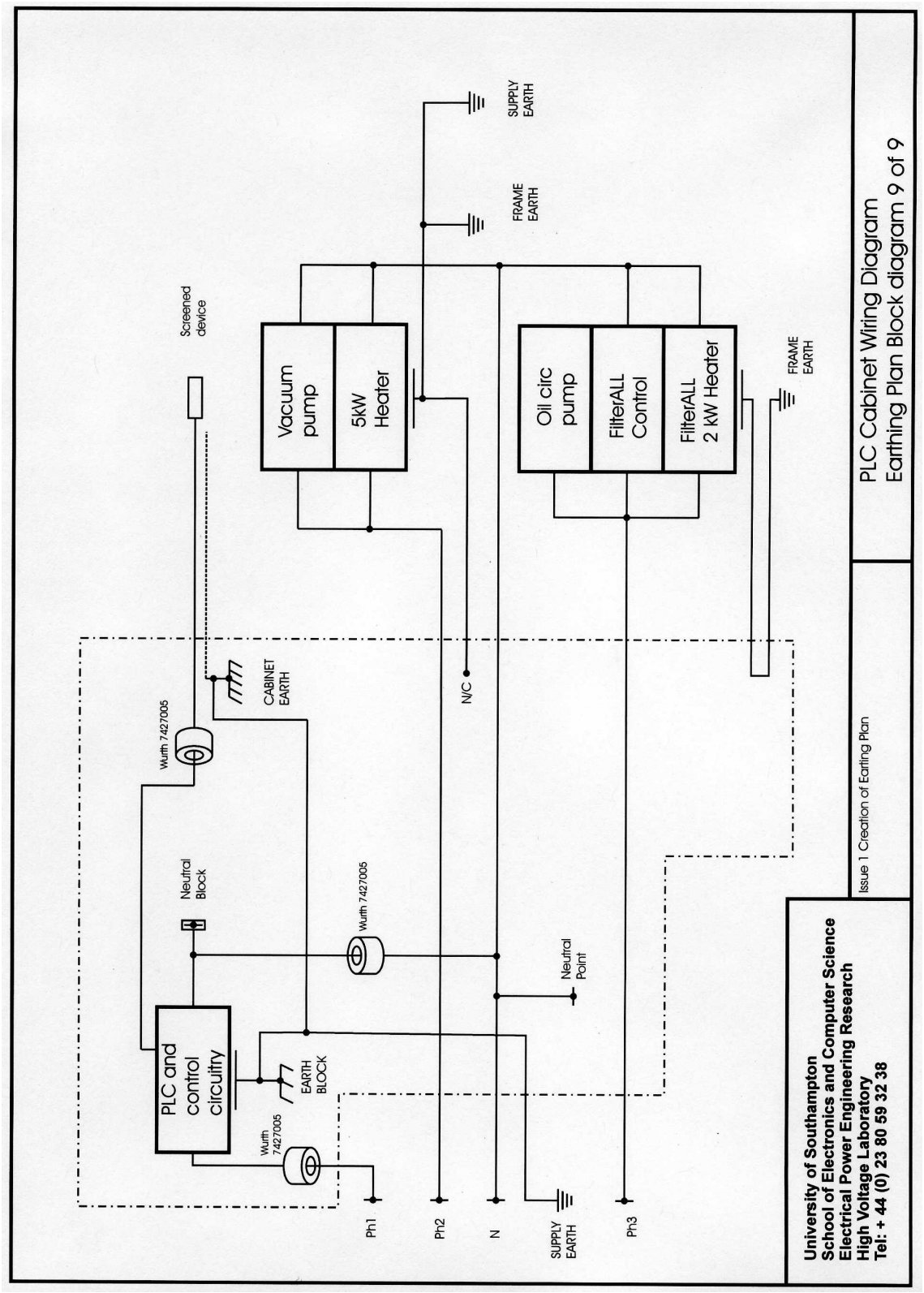

Figure A.9 PLC earth plan block diagram

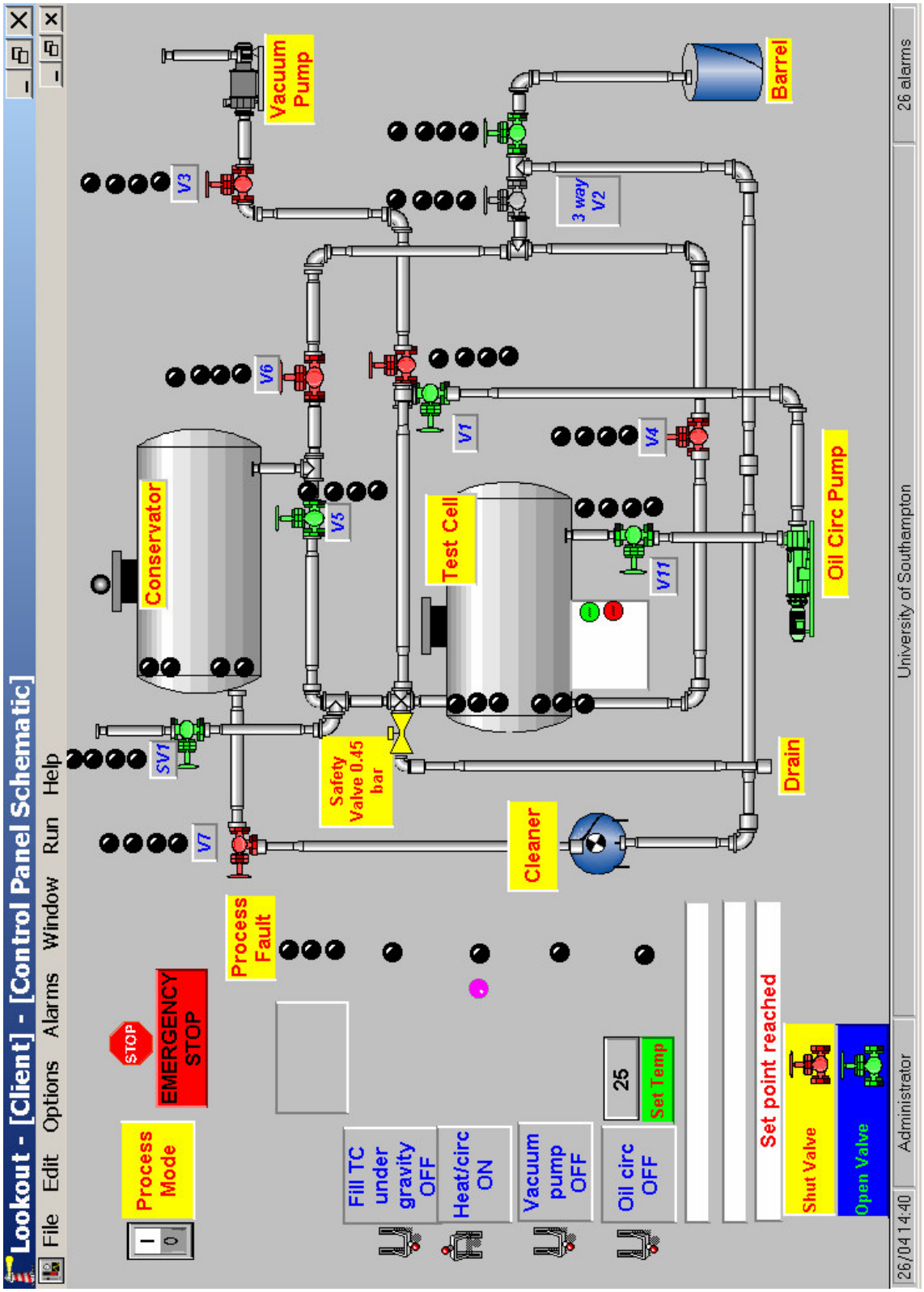

Figure A.10 System operation - Process mode mimic diagram

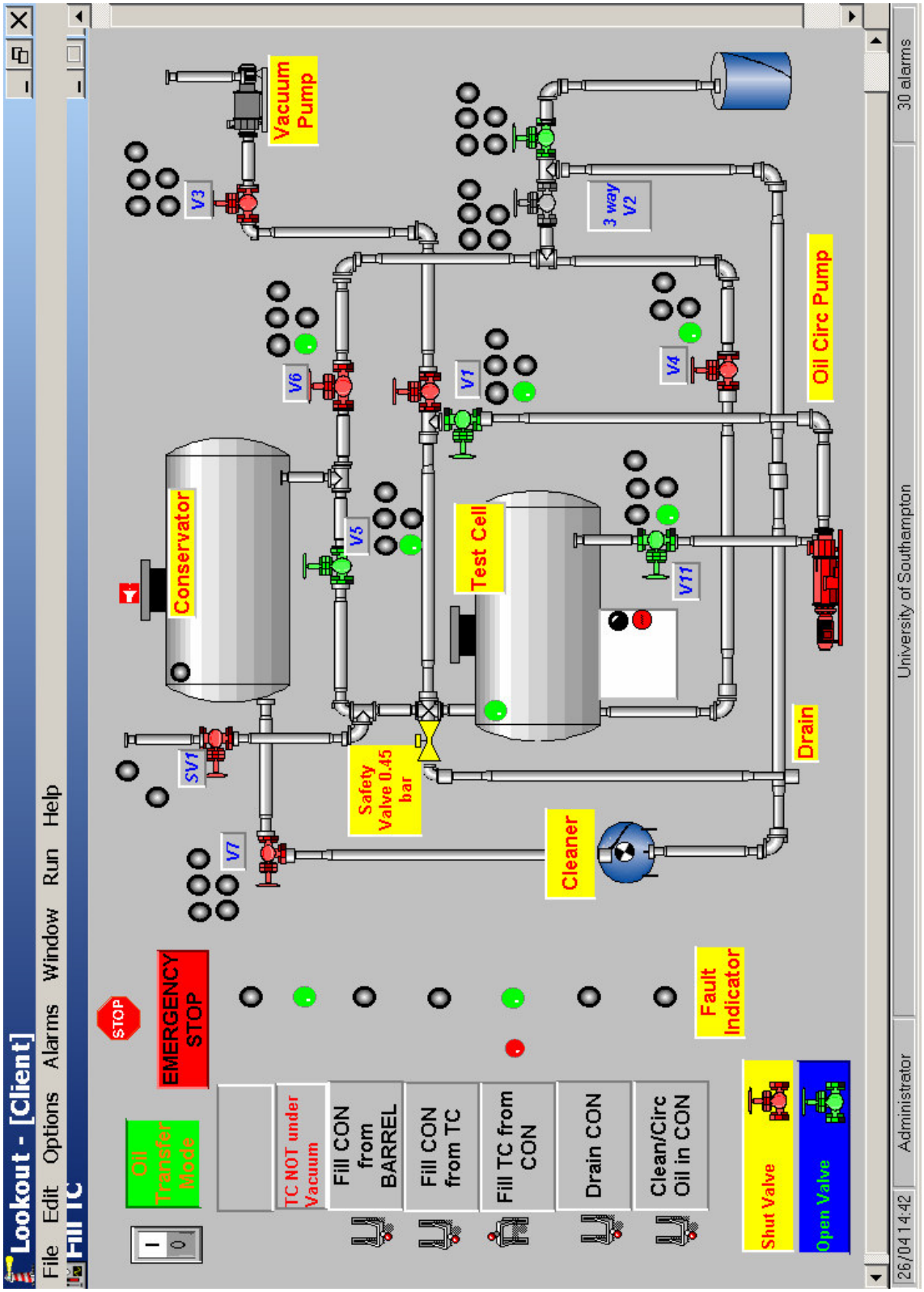

Figure A.11 System operation - Fluid transfer mode mimic diagram

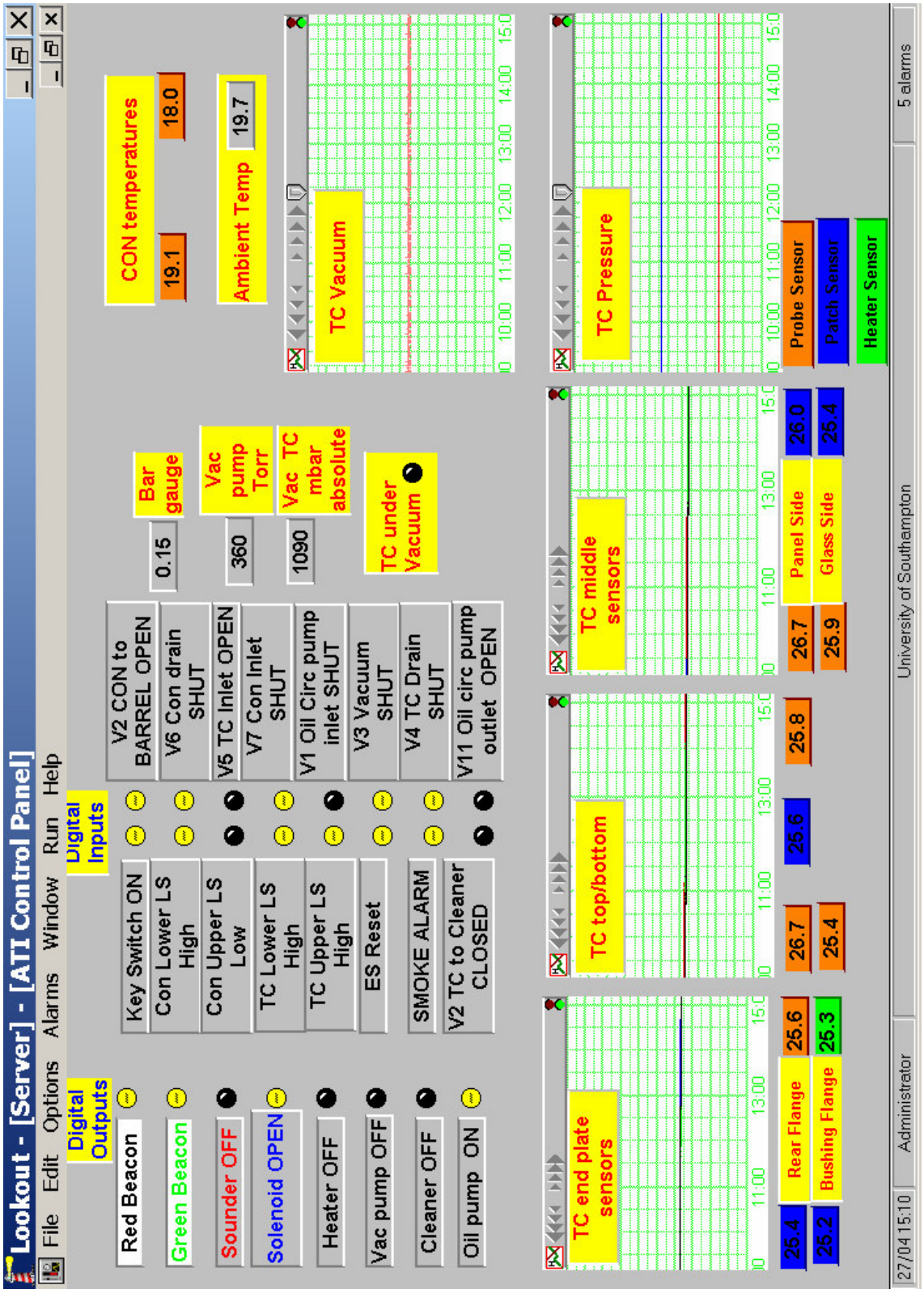

Figure A.12 System operation - Data display mimic diagram

Appendix A: System operation

Table A.1 Test cell valve truth table

Operation	Vac pump drain/circ V1 2way	2 WAY V2	Vac V3	TC drain V4	TC air vent Solenoid	TC Inlet V5	CON DrainV6	Con Inlet V7	Oil circ V11	TC Vacuum breaker	Oil Pump	FilterAll
Fill Conservator from Barrel	Vac	Barrel	C	C(X)	C(X)	C	C	O	C	C	OFF	ON
Fill CON from TC	Vac	TC	C	O	O	C	C	O	C	C	OFF	ON
Fill TC from CON under Vac	Vac	Barrel	C	O	C	C	O	C	C	C	OFF	OFF
Drain Conservator to Barrel	Vac	TC	C	C	C(X)	C	O	C	C	C	OFF	ON
CIRC OIL from CON via FilterAll	Vac	TC	C	C	C(X)	C	O	O	C	C	OFF	ON
Fill TC under gravity	Oil	Barrel	C	O	O	C	0	C	O	C	OFF	OFF
Heat/Circ oil TC	Oil	Barrel	C	C	O	O	C	C	O	C	ON	OFF
Vac TC (No Oil)	Vac	Barrel	O	C	C	C	C	C	C	C	OFF	OFF
Circ oil only	Oil	Barrel	C	C	O	O	C	C	O	C	ON	OFF
Microswitch/Relay	MS5	MS0/MS1	MS6	MS7	Solenoid	MS4	MS2	MS3	MS8	n/a	R11	R22
Digital I/O Port	I3.12	I3.8/I3.7	I3.13	I3.14	O3.3	I3.10	I3.9	I3.11	I3.15	manual	O3.8	O3.6
Issue 7 PMM 17/6/2008 Editorial update (C=closed; O =open; (X) = Don't care)												

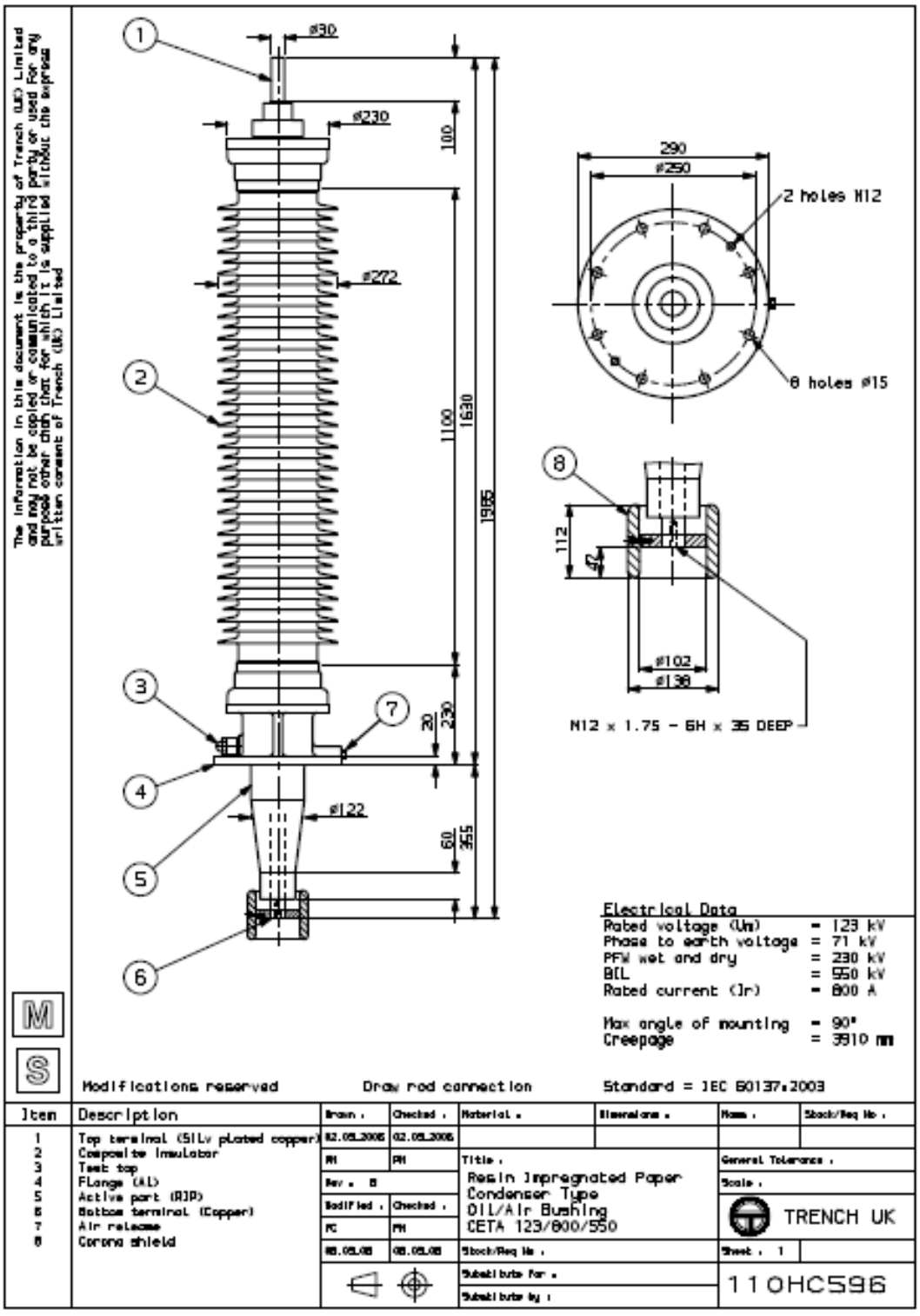

Figure B.1 123kV Horizontally mounted bushing

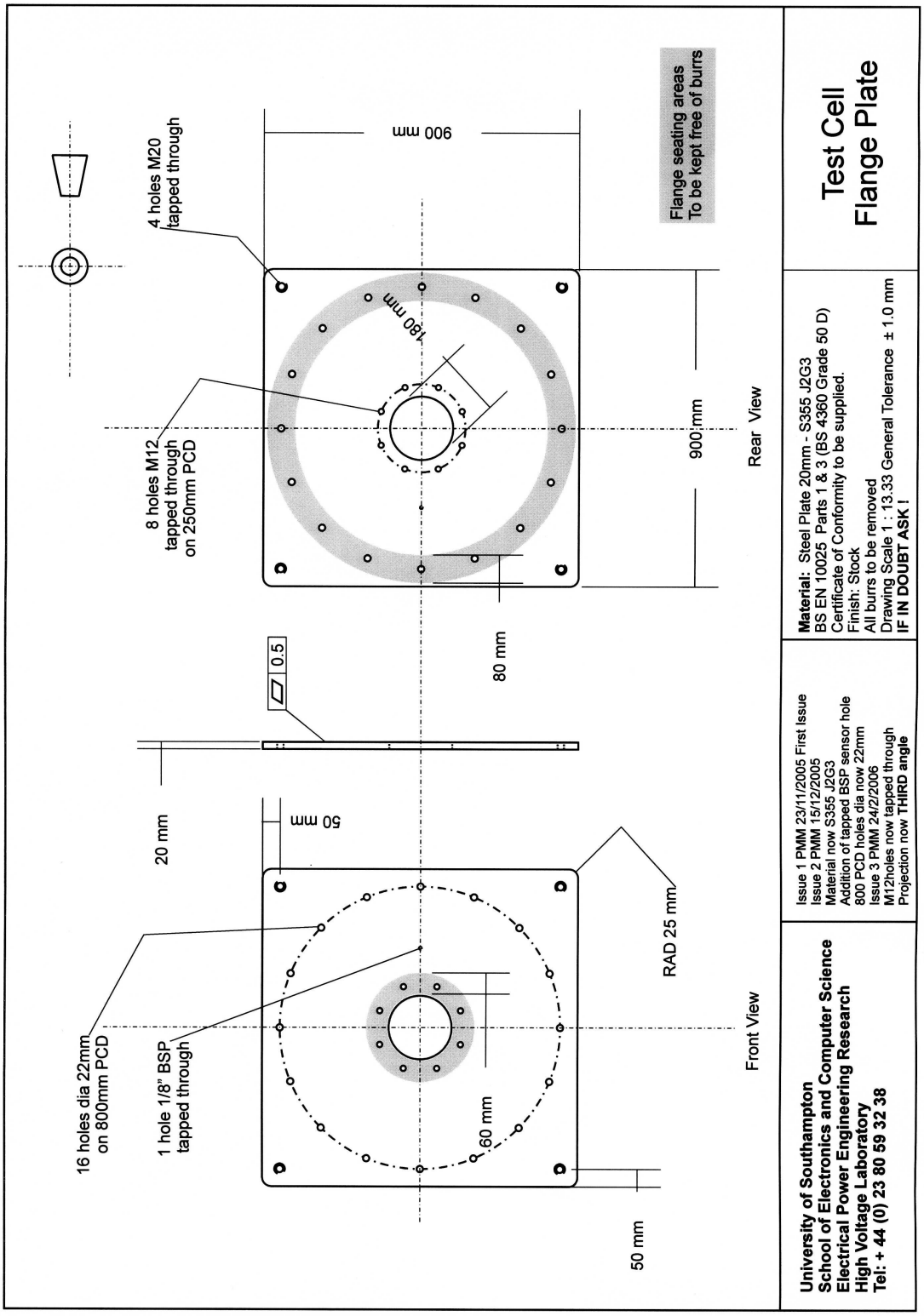

Figure B.2 Test cell end plate

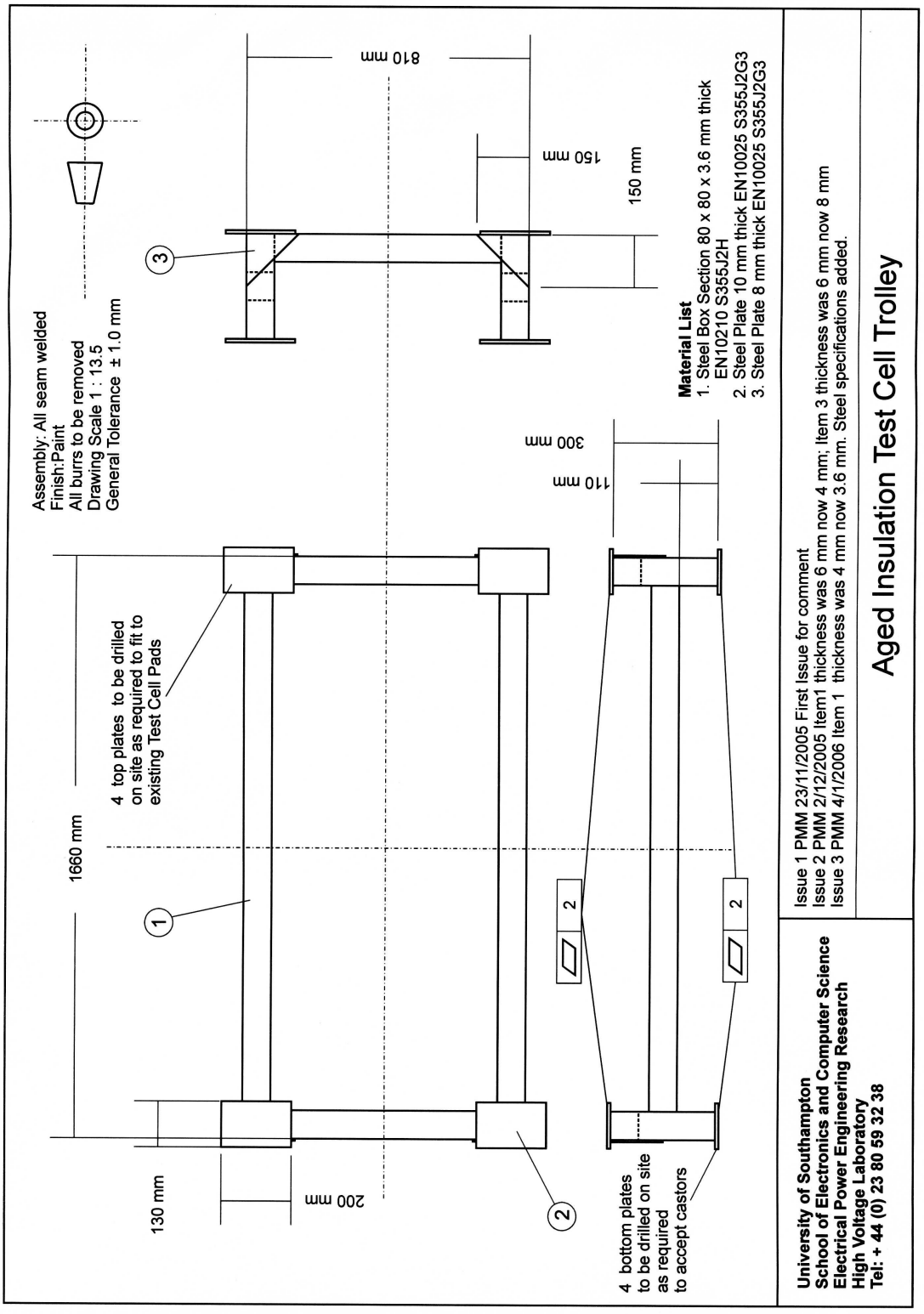

Figure B.3 Test cell trolley

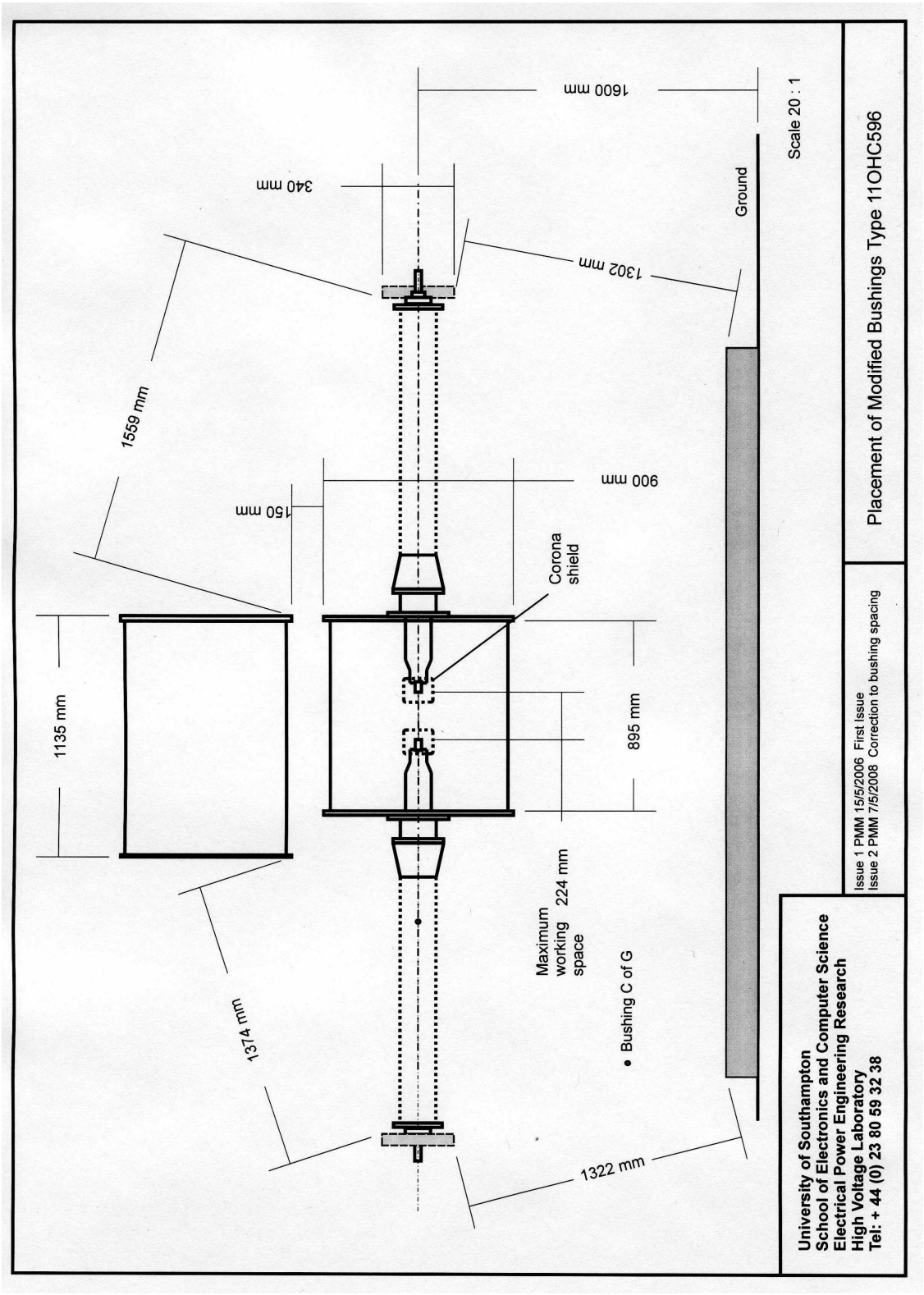

Figure B.4 Test cell cut –away overview (side elevation)

Appendix C: ϕ-q-n plots of voltage ~ distance for pressboard in oil bath

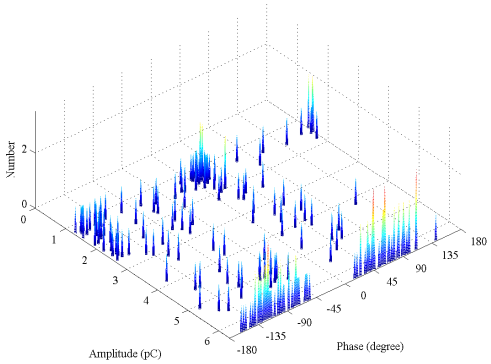

a - 20kV at 15mm distance

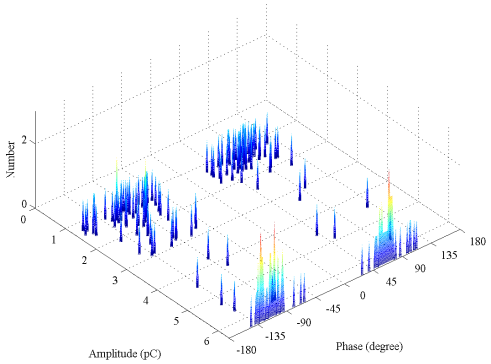

d - 25kV at 45mm distance

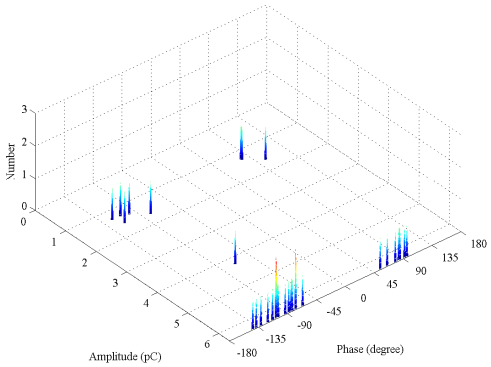

b - 25kV at 25mm distance

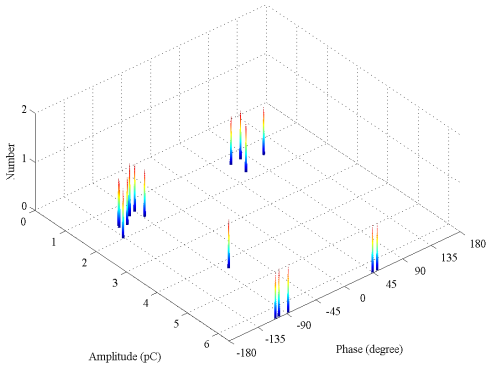

e - 25kV at 55mm distance

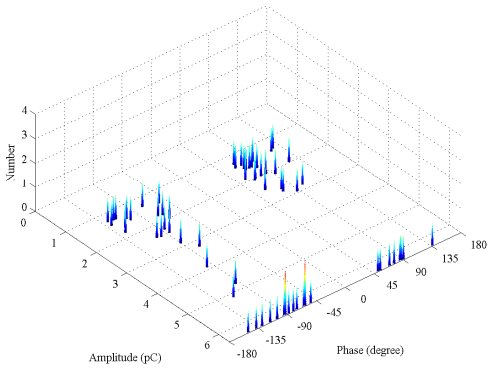

c - 25kV at 35mm distance

Figure C.1 Series of ϕ-q-n plots ~ distance for oil bath containing virgin pressboard conditioned to 3.6% moisture. Robinson set to 5pC resolution

Appendix C: ϕ-q-n plots of voltage ~ distance for pressboard in oil bath

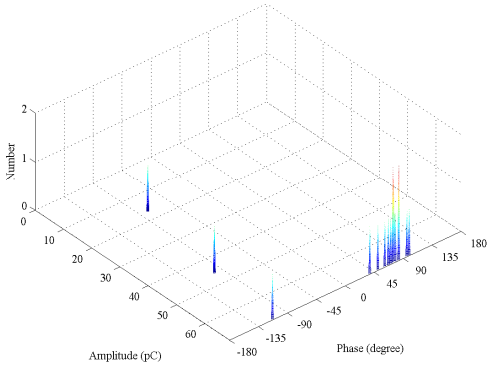

a - 20kV at 15mm distance

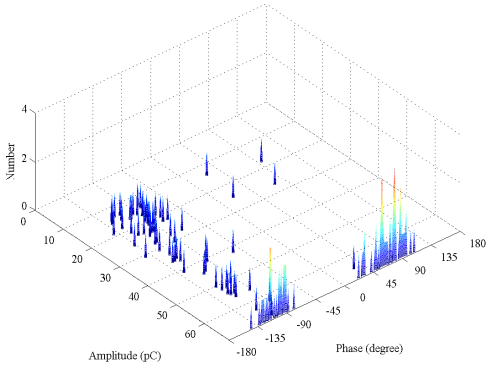

d - 25kV at 45mm distance

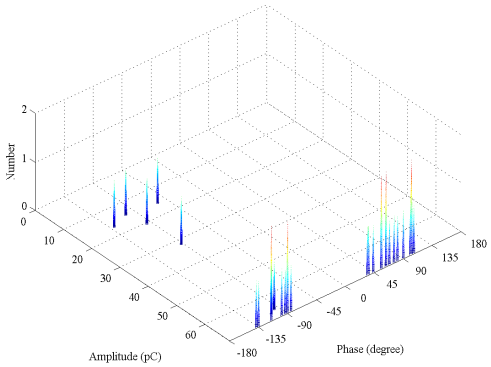

b - 25kV at 25mm distance

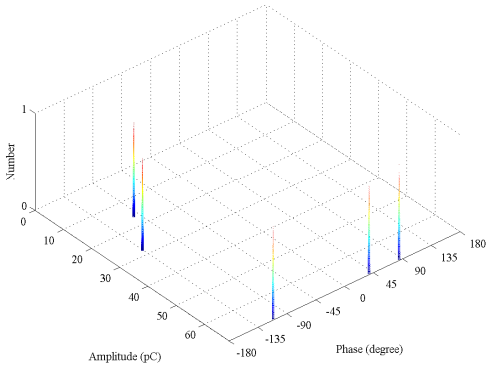

e - 25kV at 55mm distance

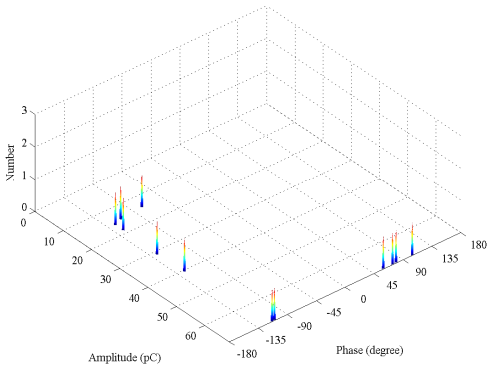

c - 25kV at 35mm distance

Figure C.2 Series of ϕ-q-n plots ~ distance for oil bath containing virgin pressboard conditioned to 3.6% moisture. Robinson set to 50pC resolution

Appendix C: ϕ-q-n plots of voltage ~ distance for pressboard in oil bath

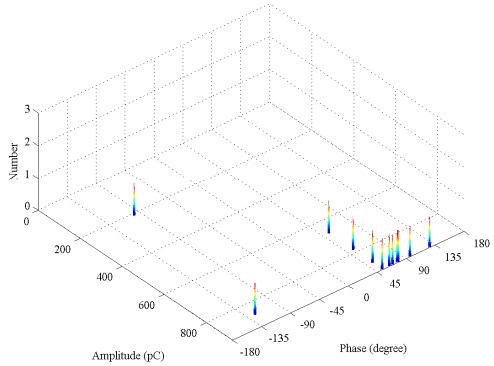

a - 20kV at 15mm distance

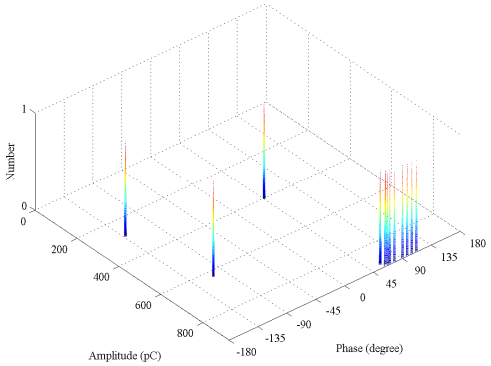

d - 25kV at 45mm distance

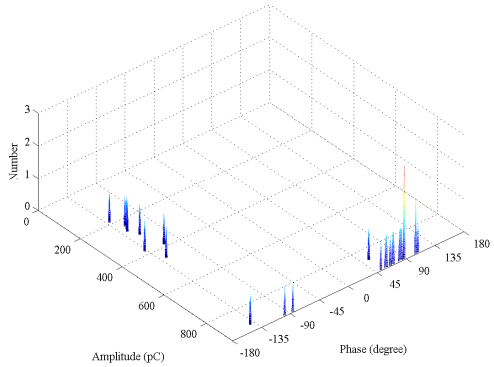

b - 25kV at 25mm distance

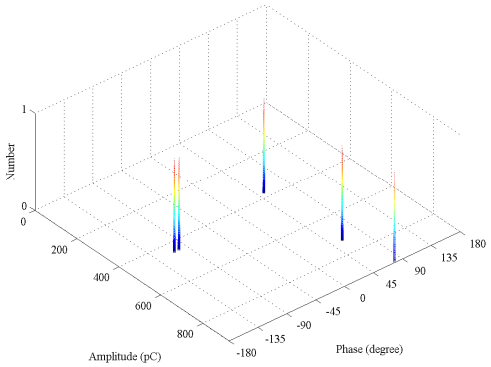

e - 25kV at 55mm distance

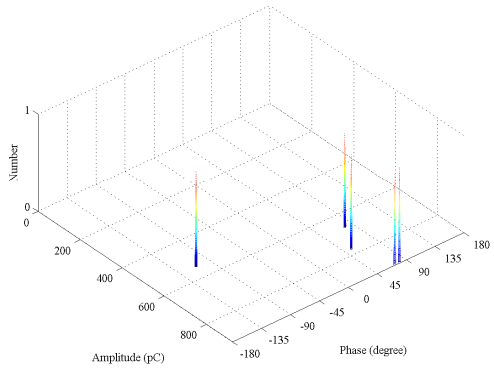

c - 25kV at 35mm distance

Figure C.3 Series of ϕ-q-n plots ~ distance for oil bath containing virgin pressboard conditioned to 3.6% moisture. Robinson set to 500pC resolution

Appendix C: ϕ-q-n plots of voltage ~ distance for pressboard in oil bath

No data taken at 15mm

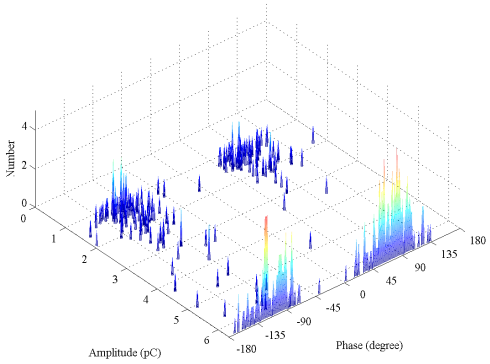

a - 30kV at 15mm distance

d - 30kV at 45mm distance

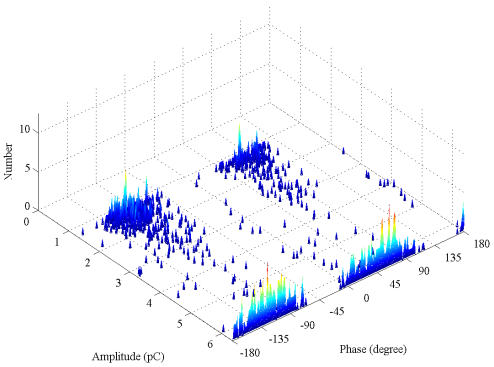

b - 30kV at 25mm distance

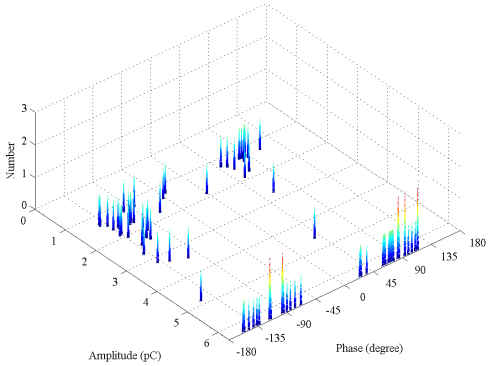

e - 30kV at 55mm distance

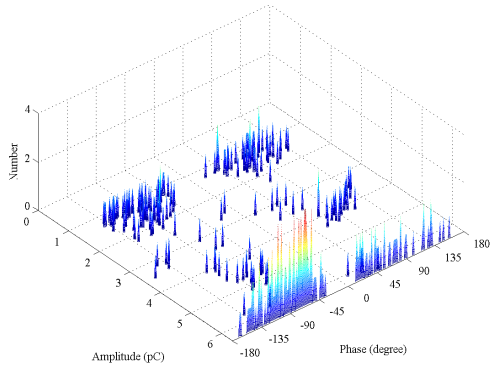

c - 30kV at 35mm distance

Figure C.4 Series of ϕ-q-n plots ~ distance for oil bath containing virgin pressboard conditioned to 3.6% moisture. Robinson set to 5pC resolution

Appendix C: ϕ-q-n plots of voltage ~ distance for pressboard in oil bath

No data taken at 15mm

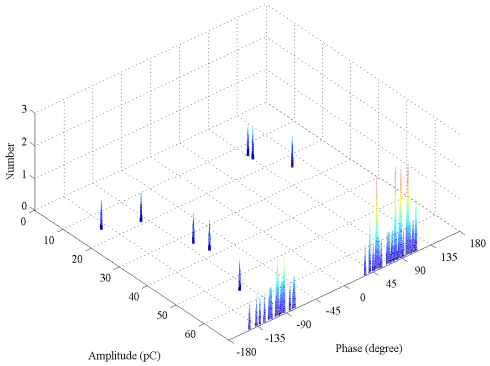

a - 30kV at 15mm distance

d - 30kV at 45mm distance

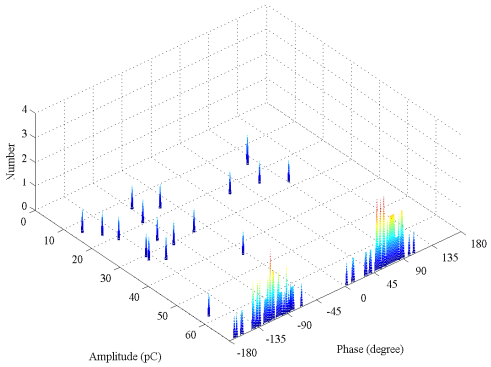

b - 30kV at 25mm distance

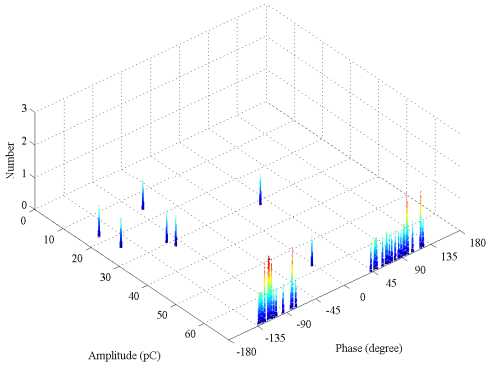

e - 30kV at55mm distance

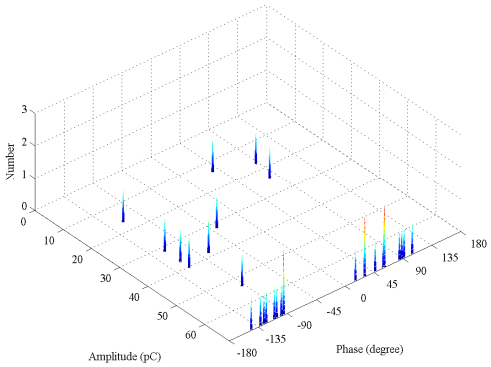

c - 30kV at 35mm distance

Figure C.5 Series of ϕ-q-n plots ~ distance for oil bath containing virgin pressboard conditioned to 3.6% moisture. Robinson set to 50pC resolution

Appendix C: ϕ-q-n plots of voltage ~ distance for pressboard in oil bath

No data taken at 15mm

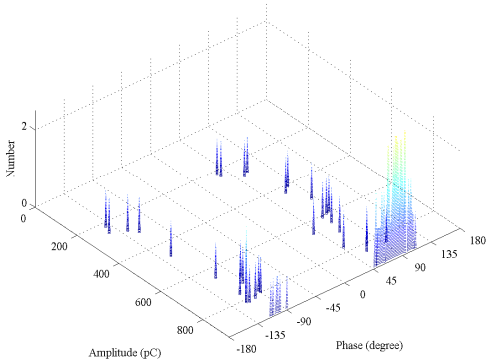

a - 30kV at 15mm distance

d - 30kV at 45mm distance

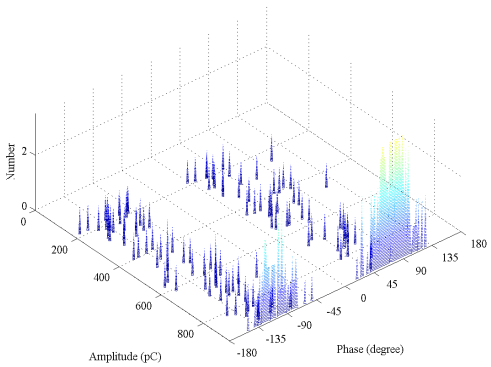

b - 30kV at 25mm distance

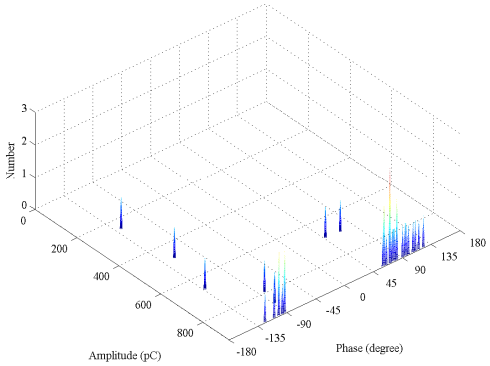

e - 30kV at 55mm distance

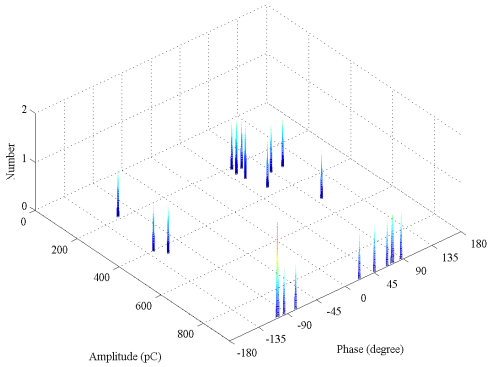

c - 30kV at 35mm distance

Figure C.6 Series of ϕ-q-n plots ~ distance for oil bath containing virgin pressboard conditioned to 3.6% moisture. Robinson set to 500pC resolution

Appendix C: ϕ-q-n plots of voltage ~ distance for pressboard in oil bath

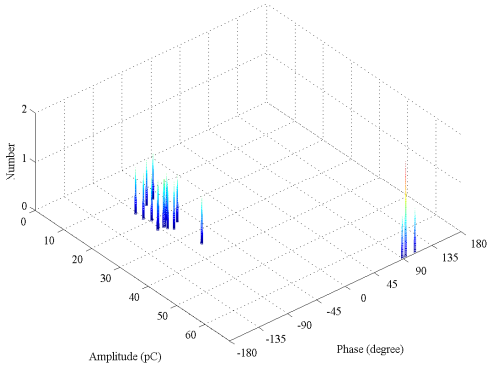

a - 20kV at 15mm distance

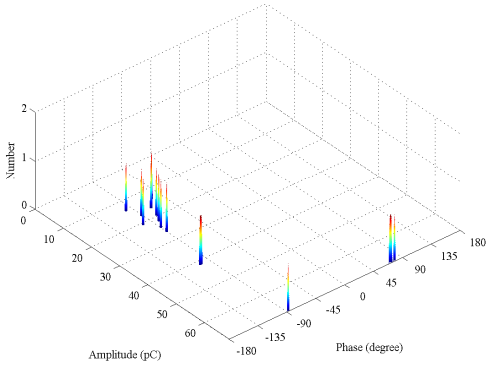

d - 25kV at 45mm distance

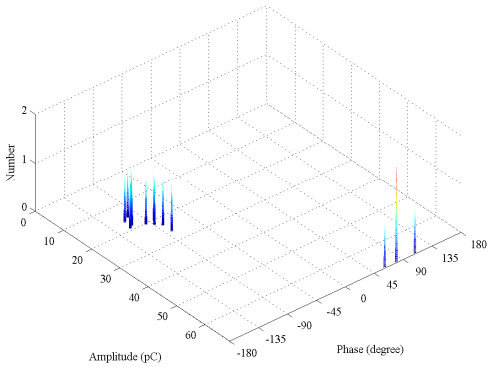

b - 25kV at 25mm distance

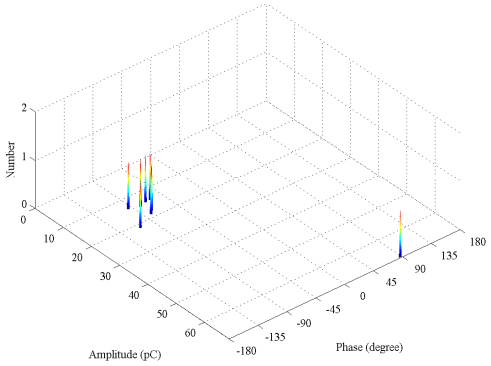

e - 25kV at 55mm distance

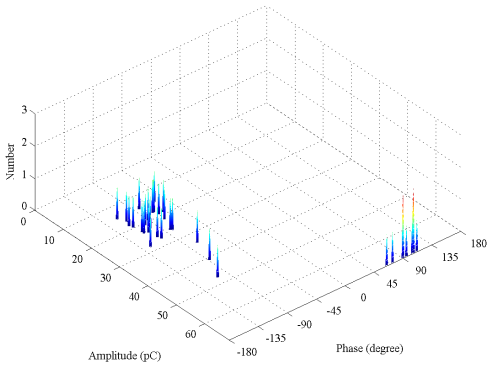

c - 25kV at 35mm distance

Figure C.7 Series of ϕ-q-n plots ~ distance for oil bath containing virgin pressboard conditioned to 7.2% moisture. Robinson set to 50pC resolution

Appendix C: ϕ-q-n plots of voltage ~ distance for pressboard in oil bath

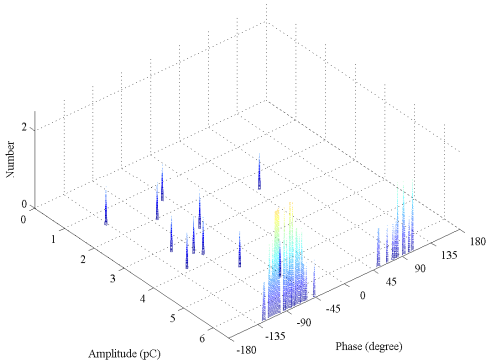

d - 30kV at 45mm distance

No data taken at 15 m and 25 mm distances as this was too near the surface flashover value

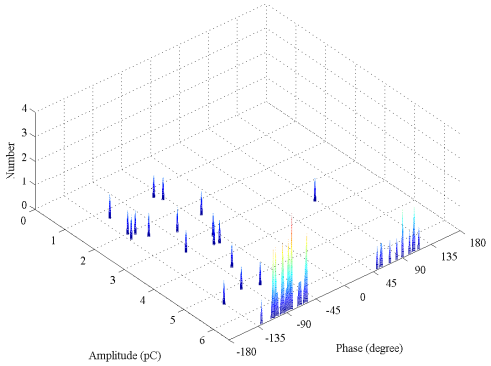

e - 30kV at 55mm distance

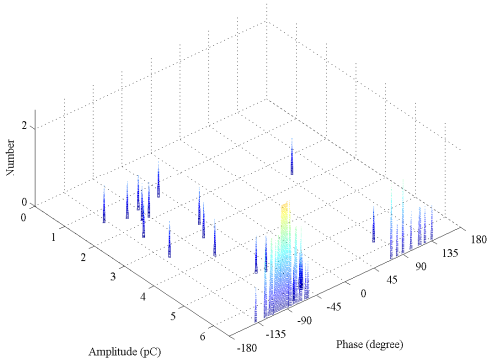

c - 30kV at 35mm distance`

Figure C.8 Series of ϕ-q-n plots ~ distance for oil bath containing virgin pressboard conditioned to 7.2% moisture. Robinson set to 5pC resolution

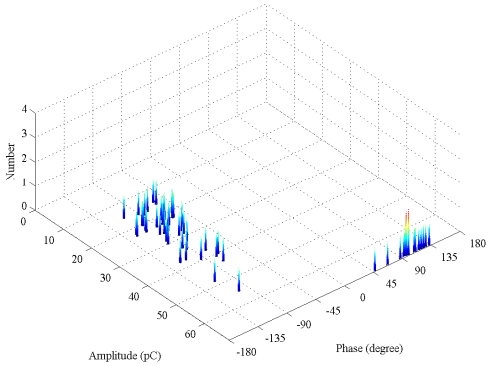

d - 30kV at 45mm distance

No data taken at 15 m and 25 mm distances as this was too near the surface flashover value

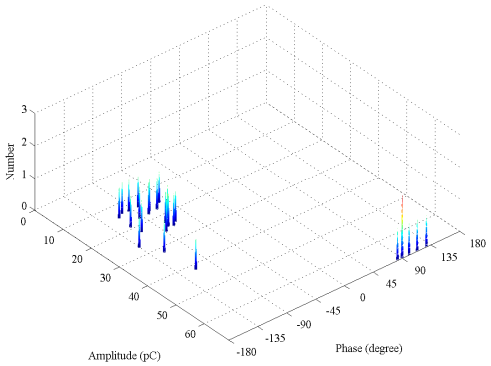

e - 30kV at 55mm distance

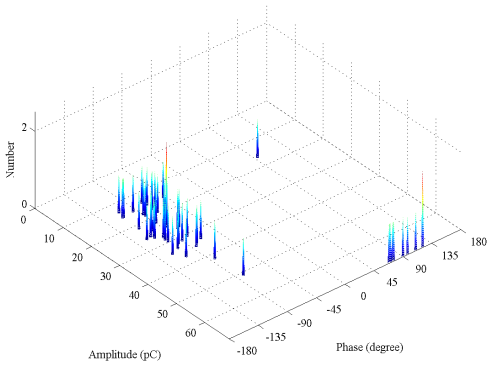

c - 30kV at 35mm distance

Figure C.9 Series of ϕ-q-n plots ~ distance at 30kV for oil bath containing virgin pressboard conditioned to 7.2% moisture. Robinson set to 50pC resolution

Appendix C: ϕ-q-n plots of voltage ~ distance for pressboard in oil bath

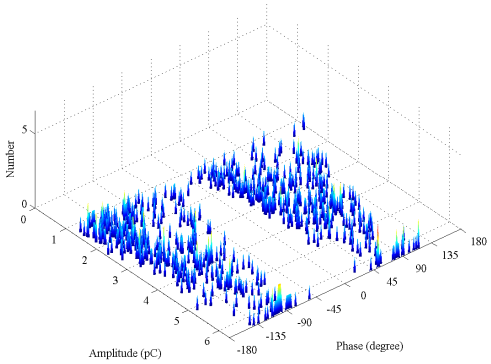

a - 20kV at 15mm distance

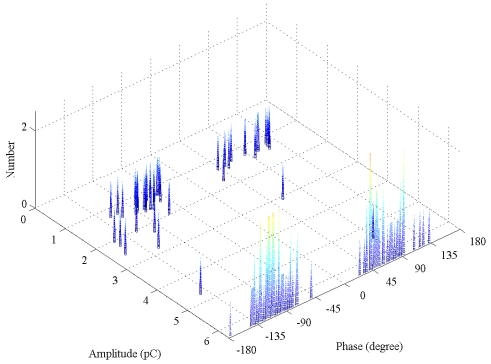

d - 25kV at 45mm distance

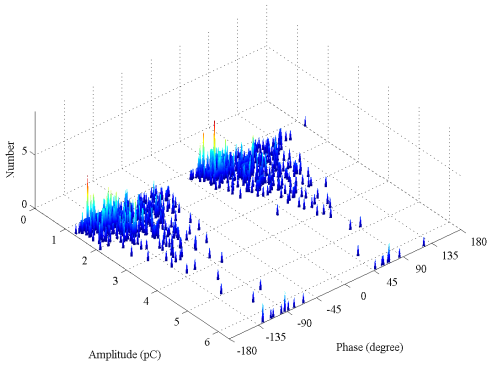

b - 25kV at 25mm distance

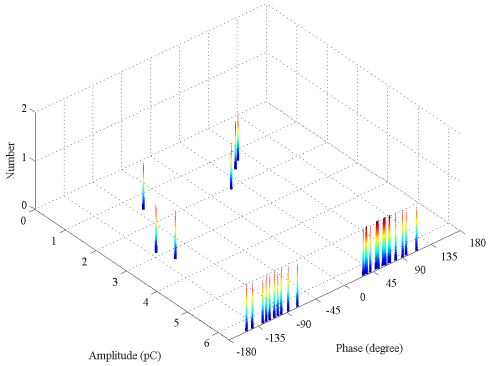

e - 25kV at 55mm distance

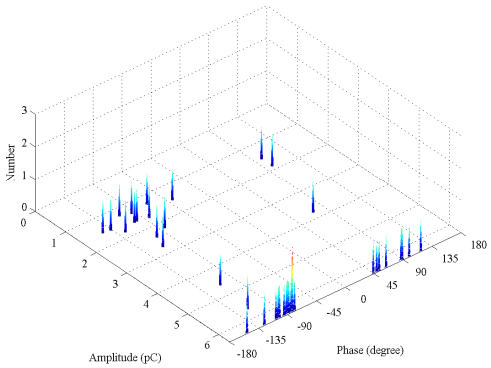

c - 25kV at 35mm distance

Figure C.10 Series of ϕ-q-n plots ~ distance for oil bath containing service aged pressboard. Robinson set to 5pC resolution

Appendix C: ϕ-q-n plots of voltage ~ distance for pressboard in oil bath

No data taken at 25kV

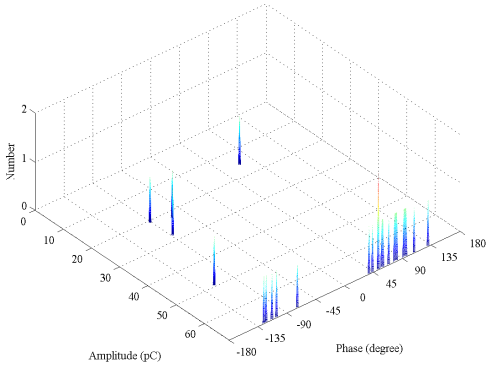

a - 25kV at 15mm distance

d - 25kV at 45mm distance

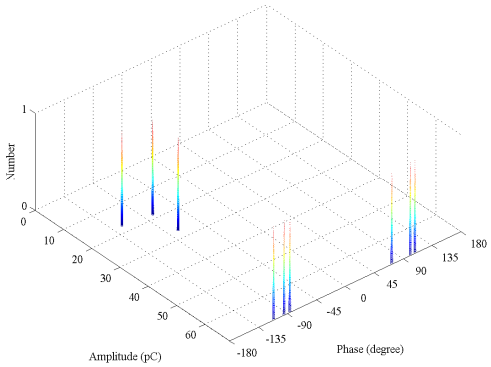

b - 25kV at 25mm distance

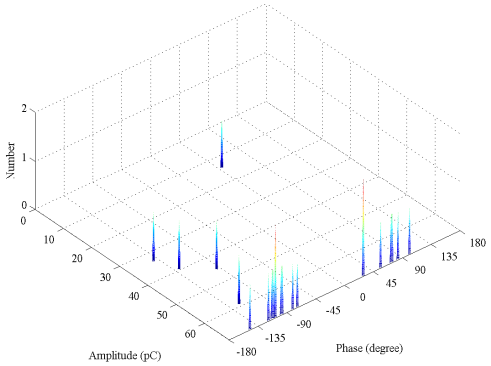

e - 25kV at 55mm distance

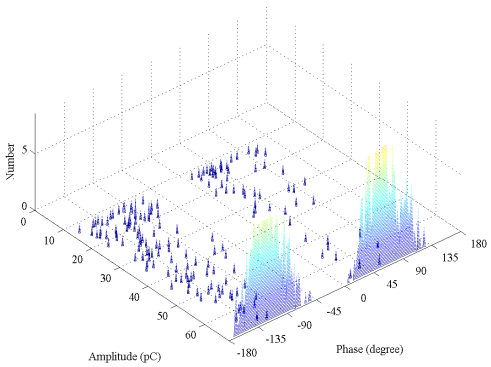

c - 25kV at 35mm distance

Figure C.11 Series of ϕ-q-n plots ~ distance for oil bath containing service aged pressboard. Robinson set to 50pC resolution

Appendix C: ϕ-q-n plots of voltage ~ distance for pressboard in oil bath

No data taken at 25kV

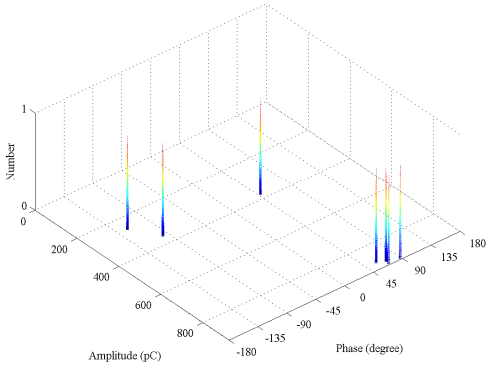

a - 25kV at 15mm distance

d - 25kV at 45mm distance

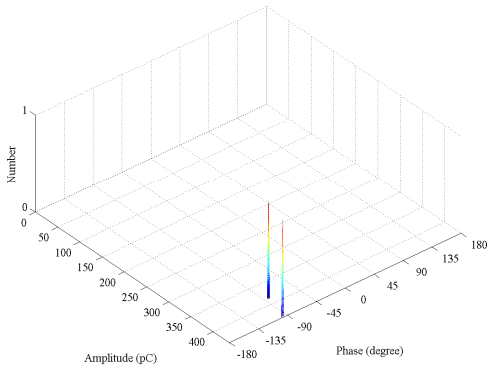

b - 25kV at 25mm distance

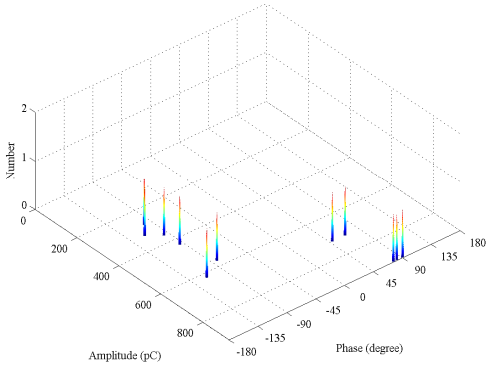

e - 25kV at 55mm distance

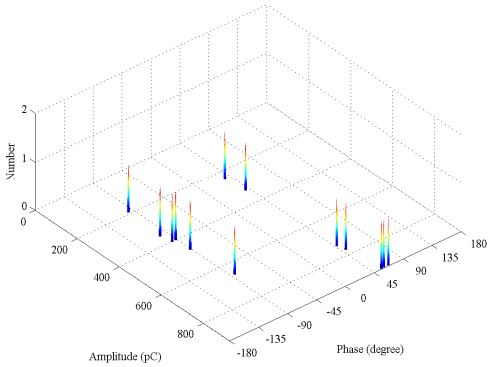

c - 25kV at 35mm distance

Figure C.12 Series of ϕ-q-n plots ~ distance at 25kV for oil bath containing service aged pressboard. Robinson set to 500pC resolution

Appendix C: ϕ-q-n plots of voltage ~ distance for pressboard in oil bath

No data taken at 30kV

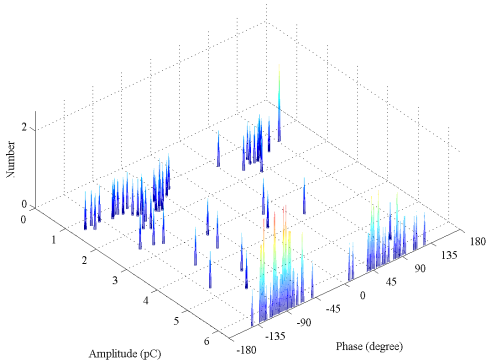

a - 30kV at 15mm distance

d - 30kV at 45mm distance

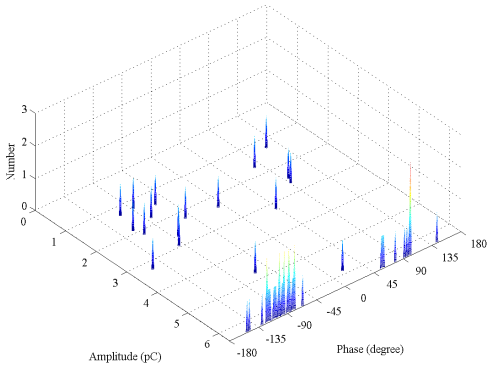

b - 30kV at 25mm distance

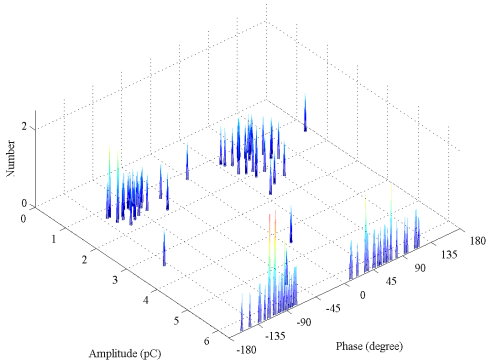

e - 30kV at 55mm distance

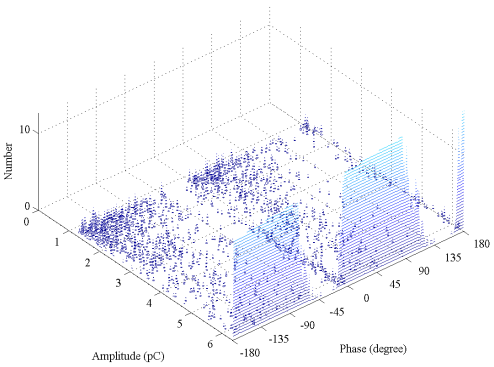

c - 30kV at 35mm distance

Figure C.13 Series of ϕ-q-n plots ~ distance for oil bath containing service aged pressboard. Robinson set to 5pC resolution

Appendix C: ϕ-q-n plots of voltage ~ distance for pressboard in oil bath

No data taken at 30kV

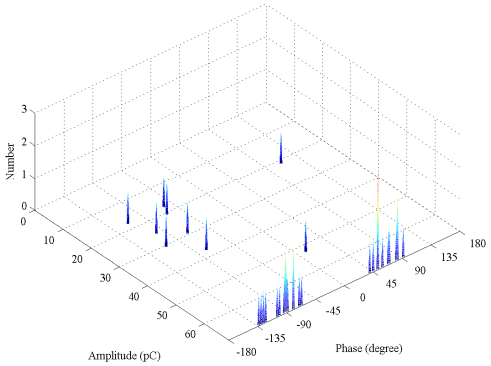

a - 30kV at 15mm distance

d - 30kV at 45mm distance

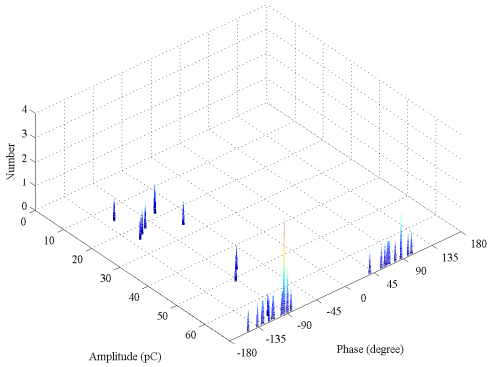

b - 30kV at 25mm distance

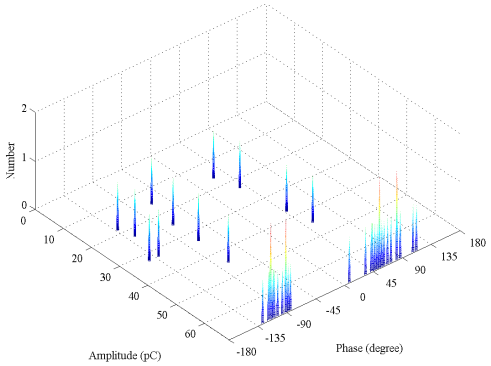

e - 30kV at 55mm distance

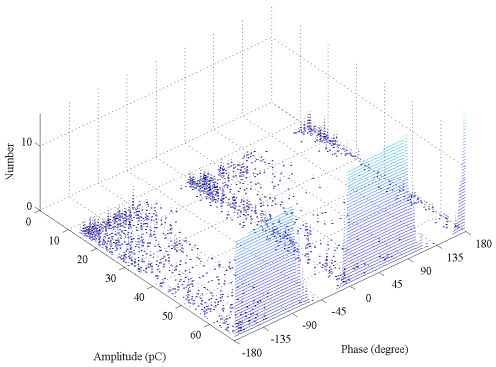

c - 30kV at 35mm distance

Figure C.14 Series of ϕ-q-n plots ~ distance for oil bath containing service aged pressboard. Robinson set to 50pC resolution

Appendix C: ϕ-q-n plots of voltage ~ distance for pressboard in oil bath

No data taken at 30kV

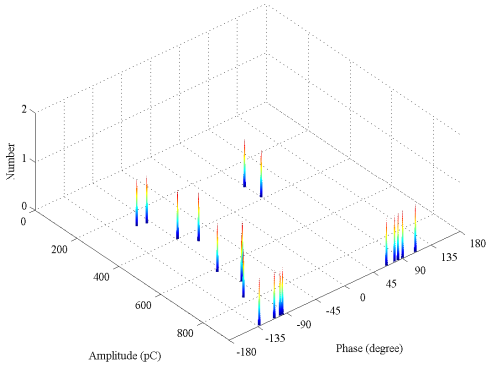

a - 30kV at 15mm distance

d - 30kV at 45mm distance

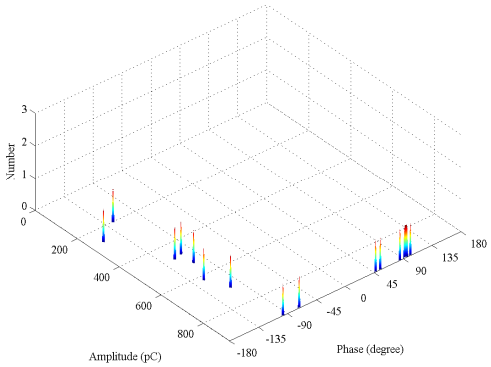

b - 30kV at 25mm distance

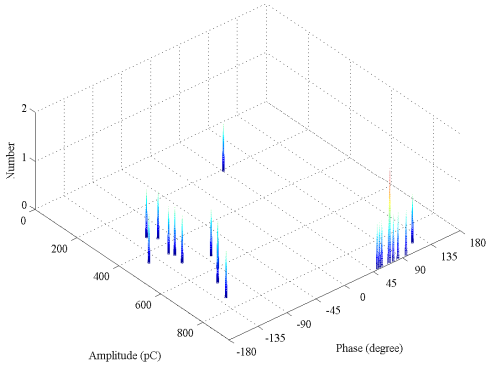

e - 30kV at 55mm distance

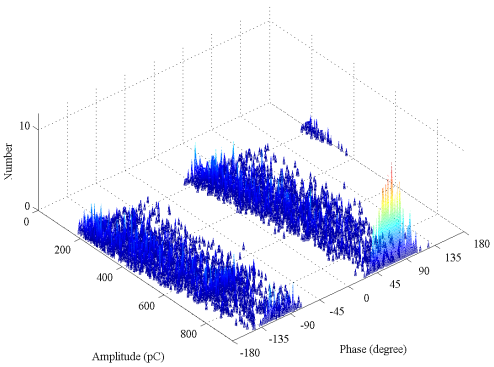

c - 30kV at 35mm distance

Figure C.15 Series of ϕ-q-n plots ~ distance for oil bath containing service aged pressboard. Robinson set to 500pC resolution

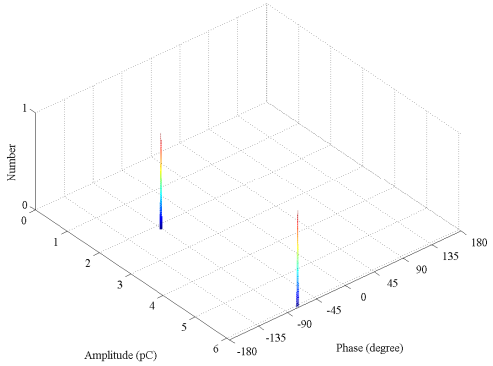

a - $V_{control}$ in phase with V_{ref}

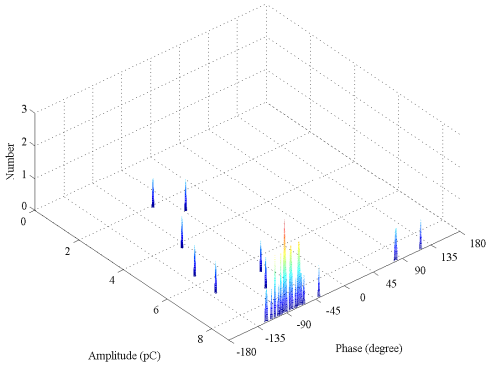

f - $V_{control}$ in anti-phase with V_{ref}

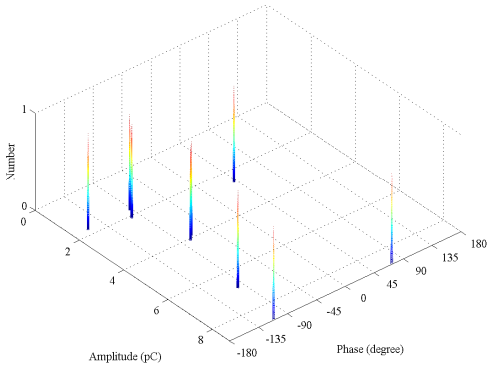

b - $V_{control}$ 60° lag with V_{ref}

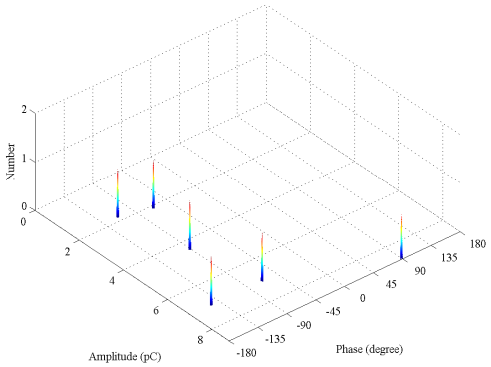

e- $V_{control}$ 60° lead with V_{ref}

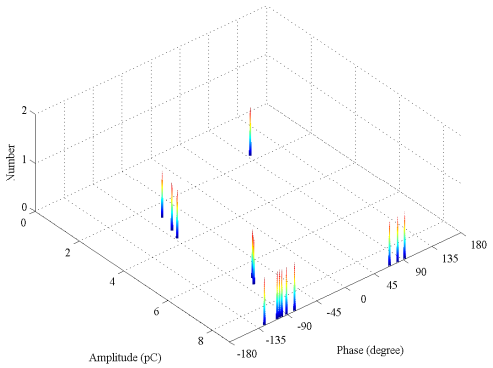

c - $V_{control}$ 120° lag with V_{ref}

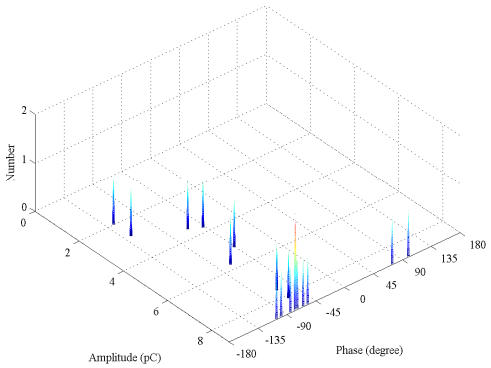

d - $V_{control}$ 120° lead with V_{ref}

Figure D.1 $V_{control}$ at 25kV for virgin pressboard conditioned to 3.6% moisture and at 30°C. Robinson set to 5pC resolution

Appendix D: ϕ-q-n plots ~ phase change for various pressboard, temperature conditions

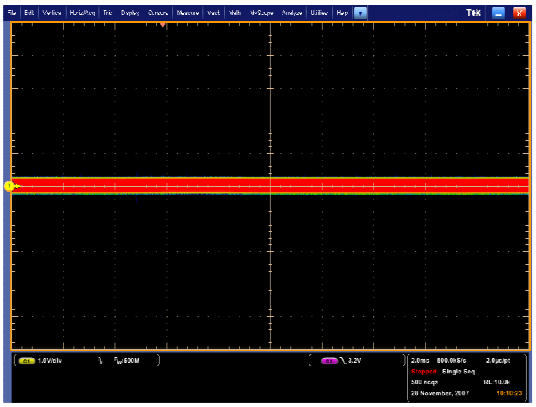

a - $V_{control}$ in phase with V_{ref}

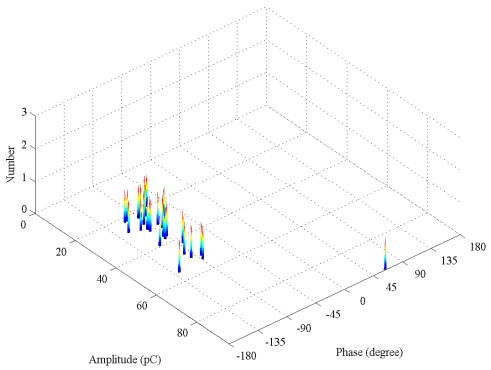

f - $V_{control}$ in anti-phase with V_{ref}

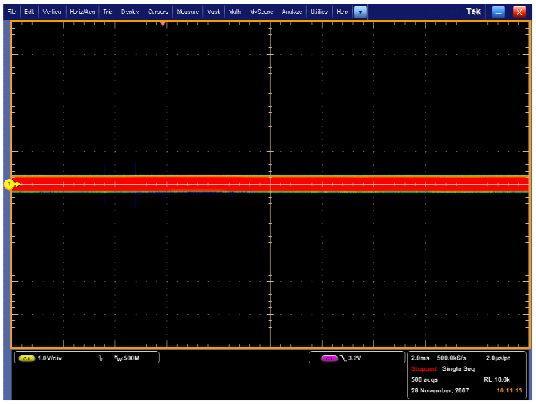

b - $V_{control}$ 60° lag with V_{ref}

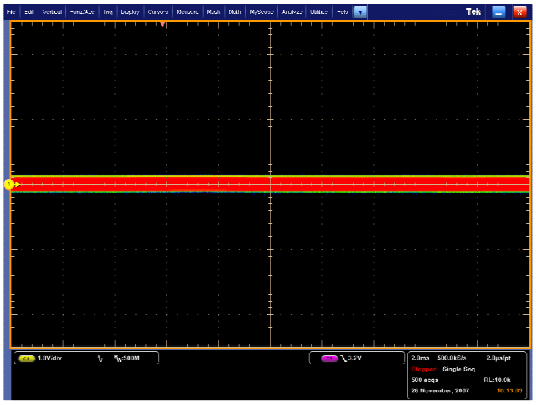

e - $V_{control}$ 60° lead with V_{ref}

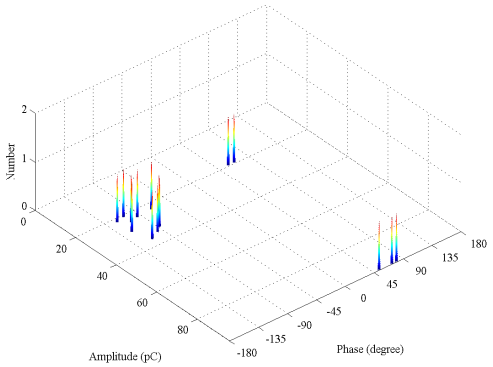

c - $V_{control}$ 120° lag with V_{ref}

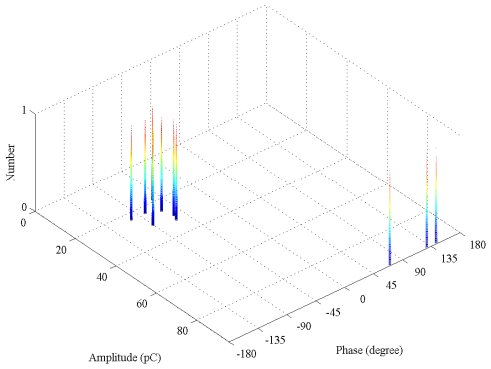

d - $V_{control}$ 120° lead with V_{ref}

Figure D.2 $V_{control}$ at 25kV for virgin pressboard conditioned to 3.6% moisture and at 30°C. Robinson set to 50pC resolution

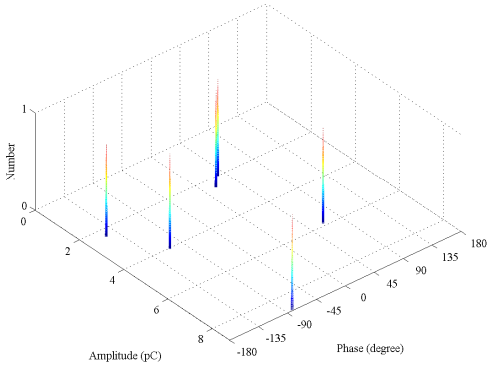

a - $V_{control}$ in phase with V_{ref}

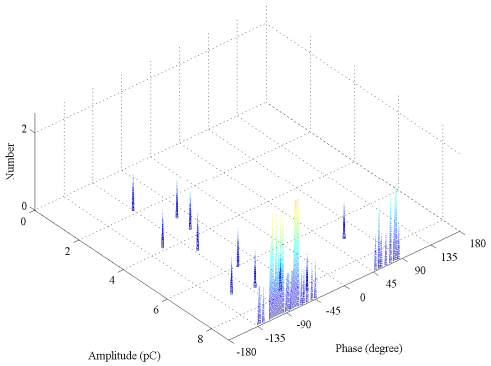

f - $V_{control}$ in anti-phase with V_{ref}

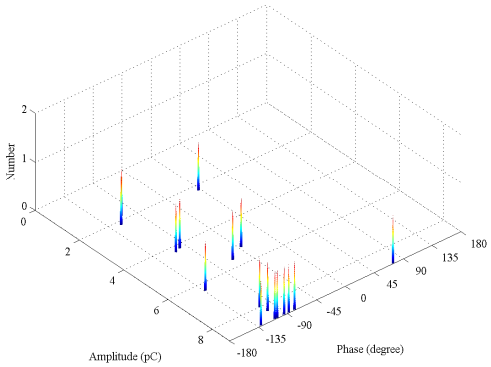

b - $V_{control}$ 60° lag with V_{ref}

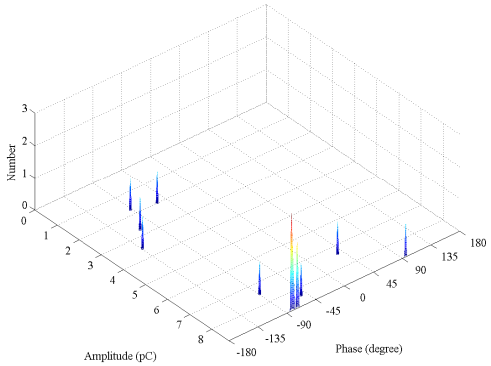

e - $V_{control}$ 60° lead with V_{ref}

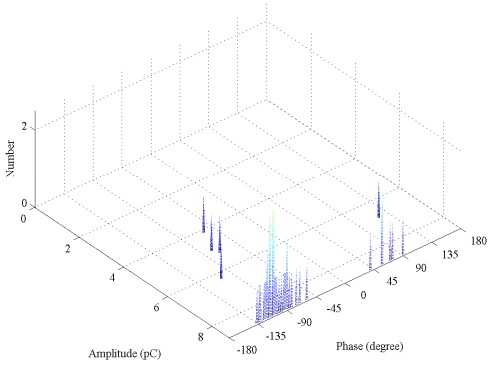

c - $V_{control}$ 120° lag with V_{ref}

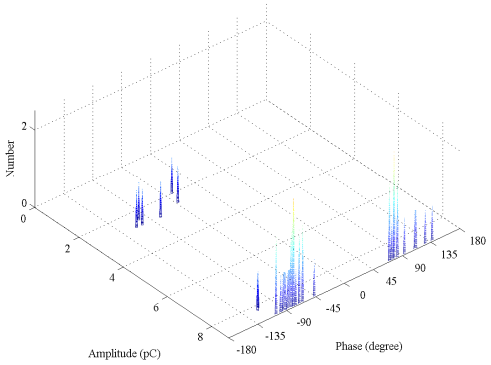

d - $V_{control}$ 120° lead with V_{ref}

Figure D.3 $V_{control}$ at 30kV for virgin pressboard conditioned to 3.6% moisture and at 30°C. Robinson set to 5pC resolution

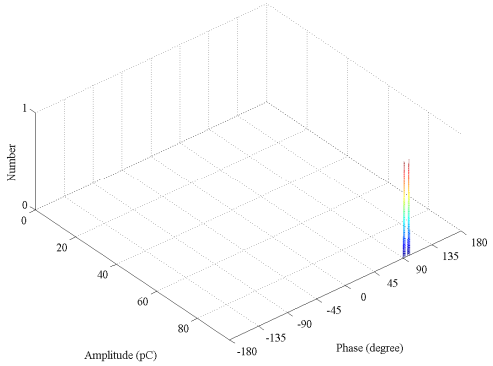

a - $V_{control}$ in phase with V_{ref}

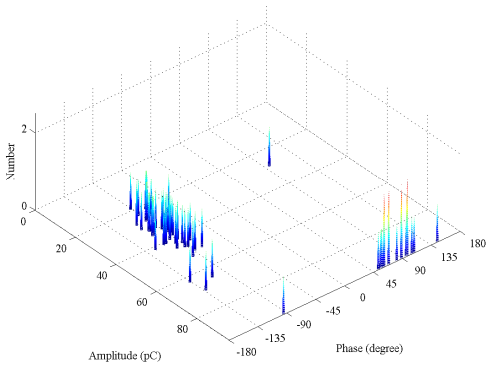

f - $V_{control}$ in anti-phase with V_{ref}

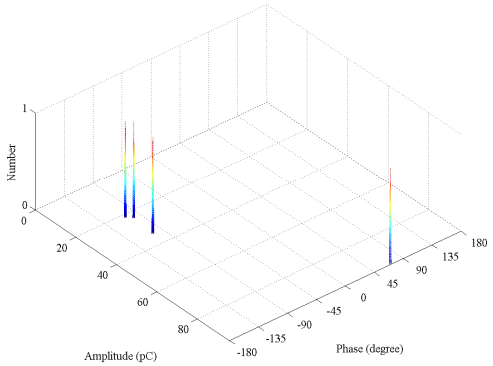

b - $V_{control}$ 60° lag with V_{ref}

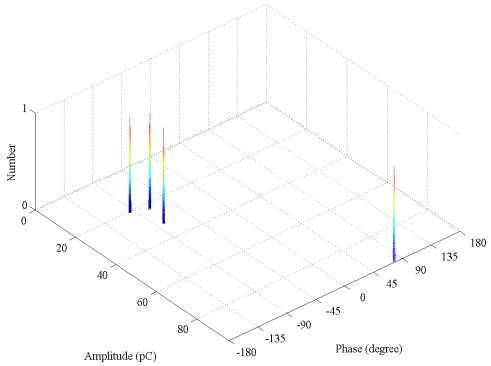

e - $V_{control}$ 60° lead with V_{ref}

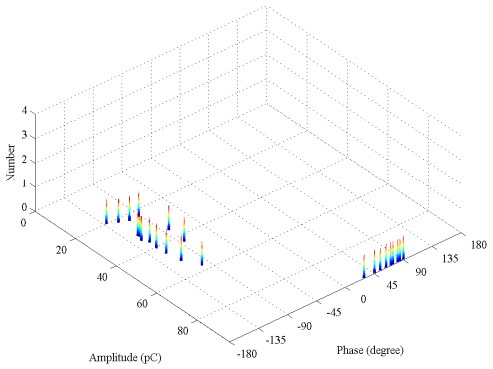

c - $V_{control}$ 120° lag with V_{ref}

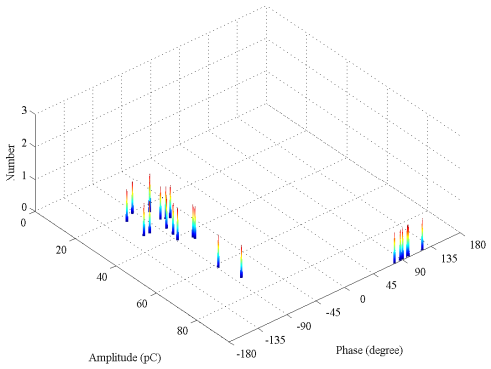

d - $V_{control}$ 120° lead with V_{ref}

Figure D.4 $V_{control}$ at 30kV for virgin pressboard conditioned to 3.6% moisture and at 30°C. Robinson set to 50pC resolution

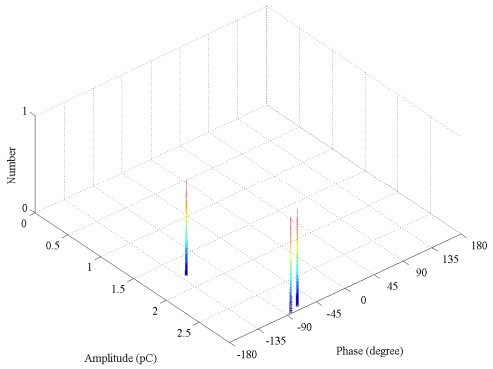

a - $V_{control}$ in phase with V_{ref}

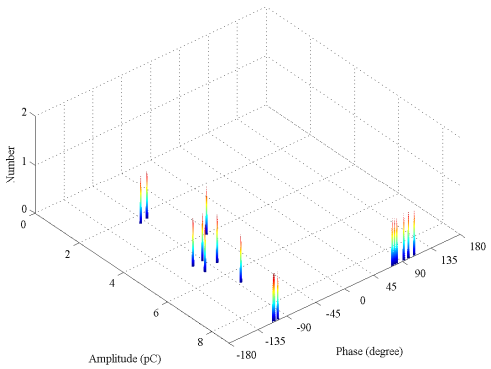

f - $V_{control}$ in anti-phase with V_{ref}

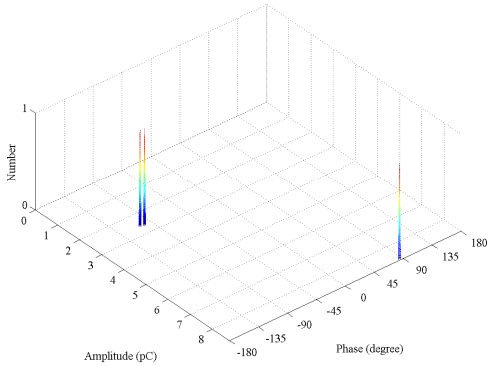

b - $V_{control}$ 60° lag with V_{ref}

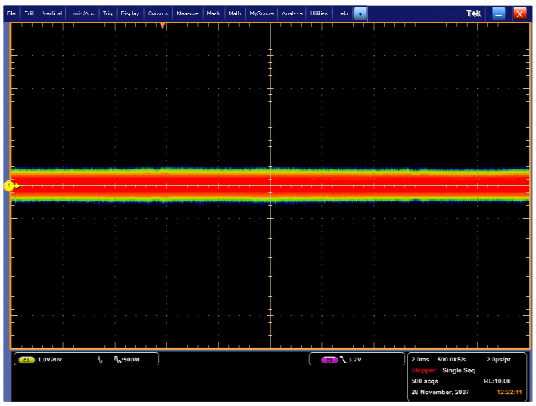

e - $V_{control}$ 60° lead with V_{ref}

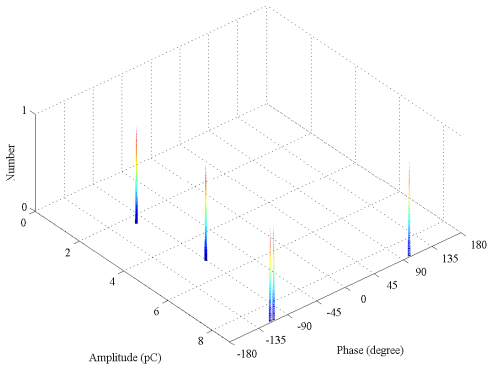

c - $V_{control}$ 120° lag with V_{ref}

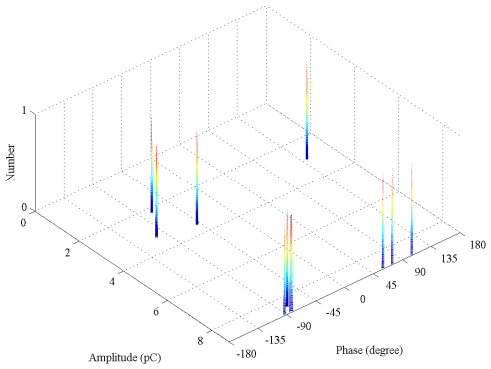

d - $V_{control}$ 120° lead with V_{ref}

Figure D.5 $V_{control}$ at 25kV for virgin pressboard conditioned to 3.6% moisture and at 40°C. Robinson set to 5pC resolution

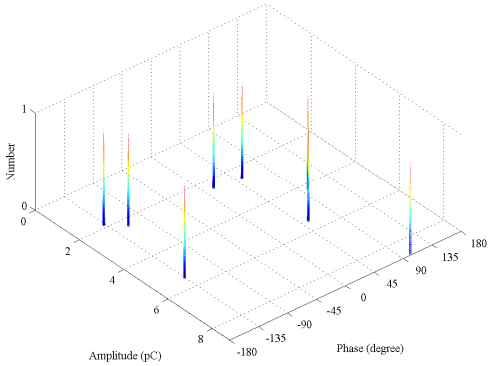

a - $V_{control}$ in phase with V_{ref}

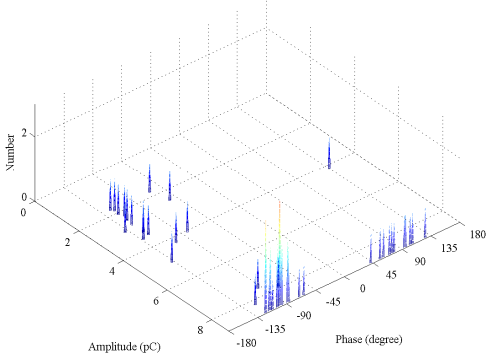

f - $V_{control}$ in anti-phase with V_{ref}

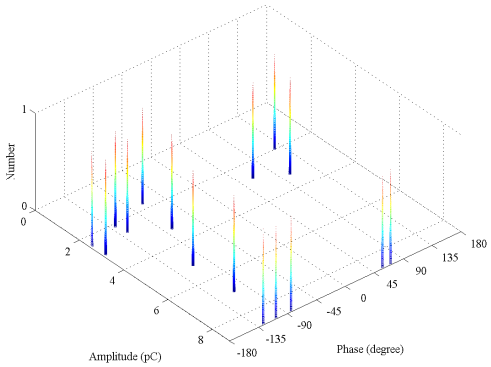

b - $V_{control}$ 60° lag with V_{ref}

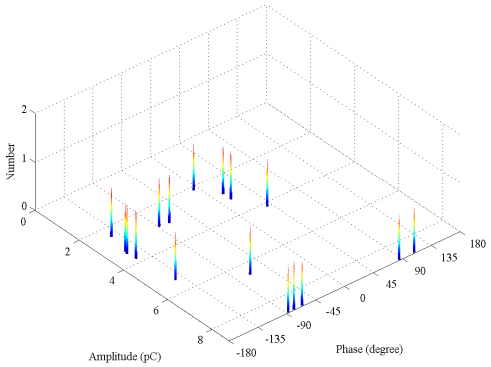

e - $V_{control}$ 60° lead with V_{ref}

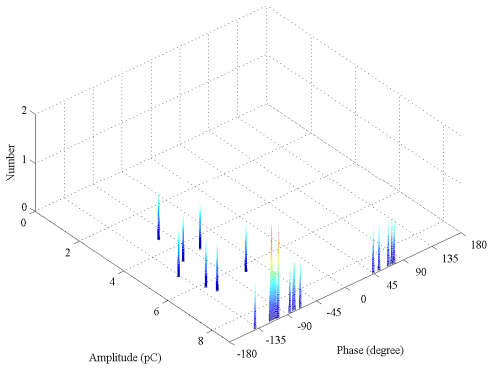

c - $V_{control}$ 120° lag with V_{ref}

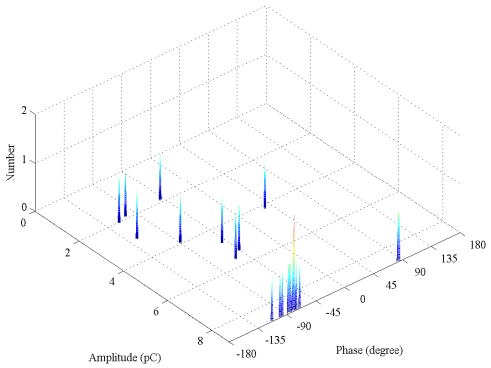

d - $V_{control}$ 120° lead with V_{ref}

Figure D.6 $V_{control}$ at 30kV for virgin pressboard conditioned to 3.6% moisture and at 40°C. Robinson set to 5pC resolution

Appendix D: ϕ-q-n plots ~ phase change for various pressboard, temperature conditions

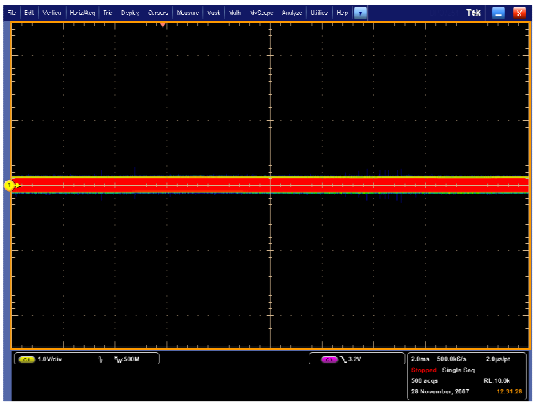

a - $V_{control}$ in phase with V_{ref}

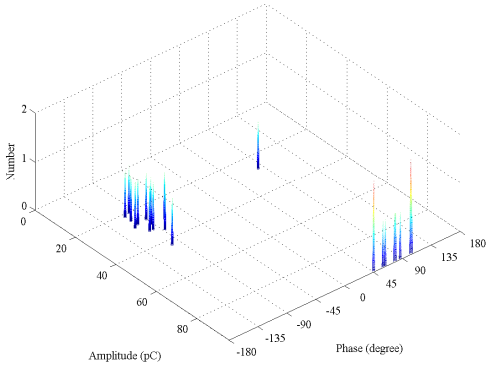

f - $V_{control}$ in anti-phase with V_{ref}

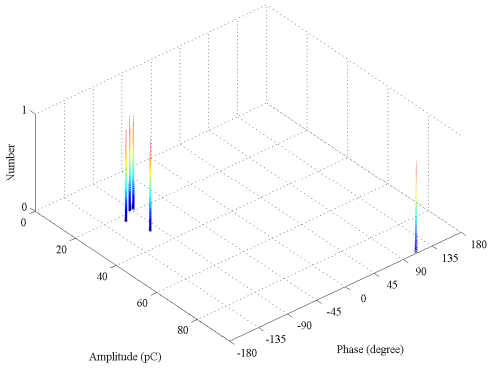

b - $V_{control}$ 60° lag with V_{ref}

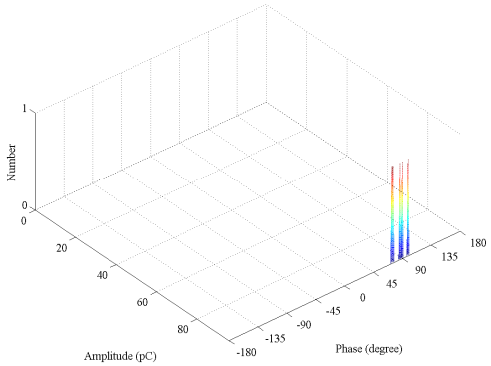

e - $V_{control}$ 60° lead with V_{ref}

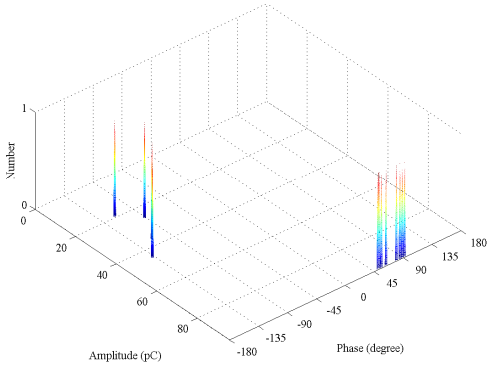

c - $V_{control}$ 120° lag with V_{ref}

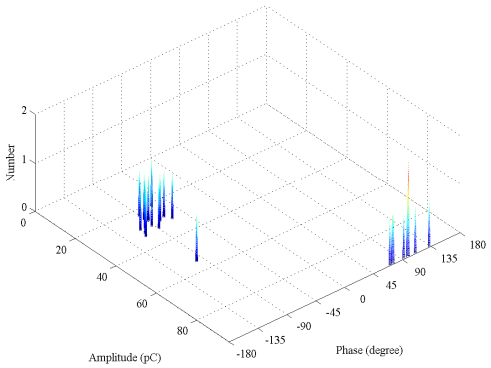

d - $V_{control}$ 120° lead with V_{ref}

Figure D.7 $V_{control}$ at 30kV for virgin pressboard conditioned to 3.6% moisture and at 40°C. Robinson set to 50pC resolution

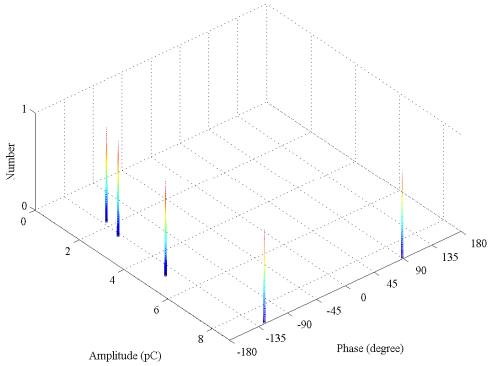

a - $V_{control}$ in phase with V_{ref}

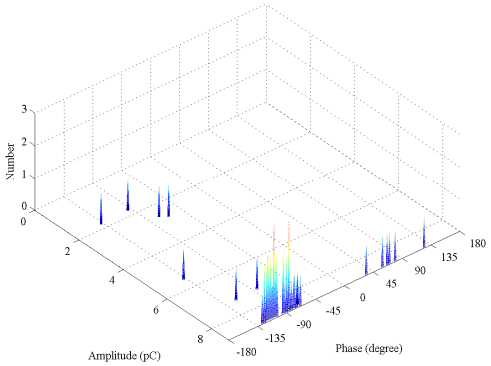

f - $V_{control}$ in anti-phase with V_{ref}

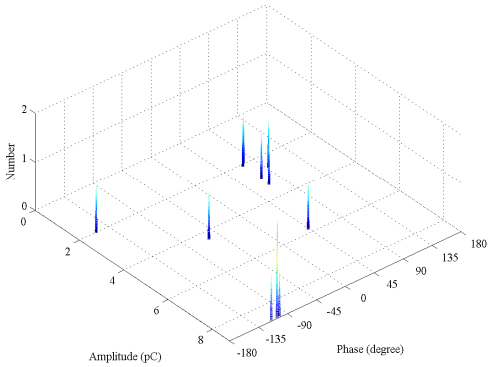

b - $V_{control}$ 60° lag with V_{ref}

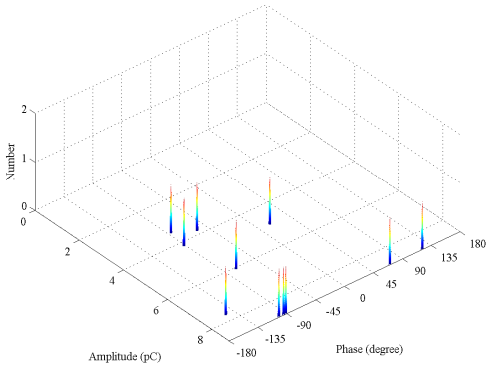

e - $V_{control}$ 60° lead with V_{ref}

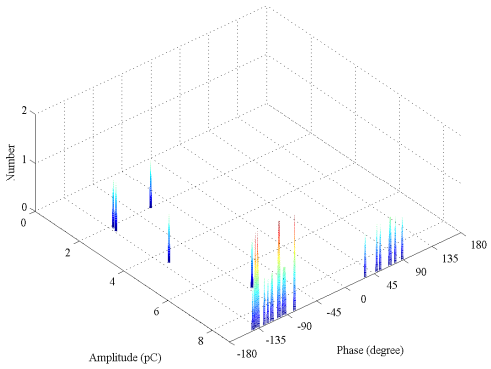

c - $V_{control}$ 120° lag with V_{ref}

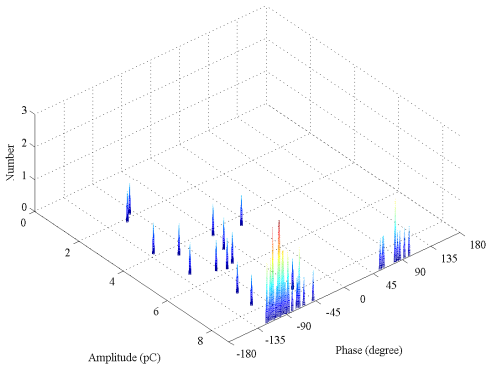

d - $V_{control}$ 120° lead with V_{ref}

Figure D.8 $V_{control}$ at 35kV for virgin pressboard conditioned to 3.6% moisture and at 40°C. Robinson set to 5pC resolution

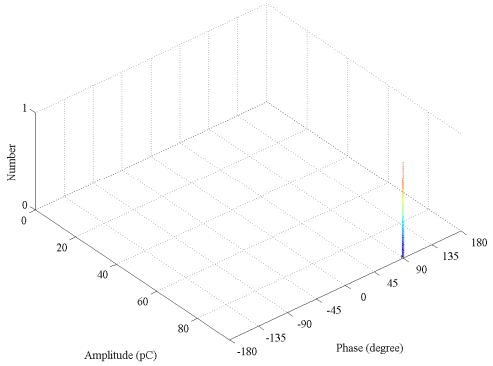

a - $V_{control}$ in phase with V_{ref}

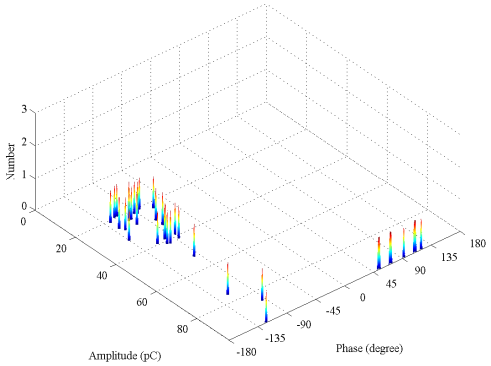

f - $V_{control}$ in anti-phase with V_{ref}

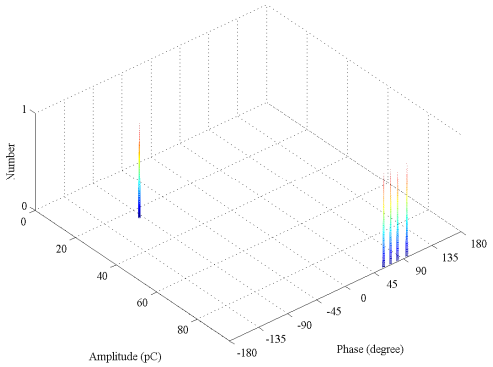

b - $V_{control}$ 60° lag with V_{ref}

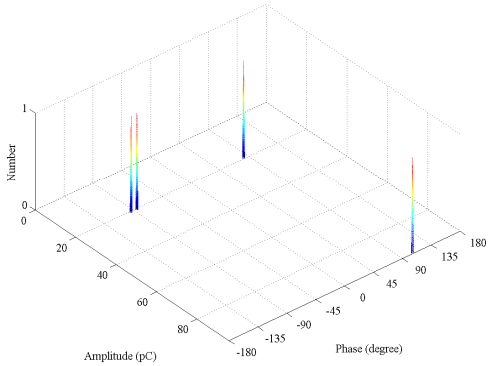

e - $V_{control}$ 60° lead with V_{ref}

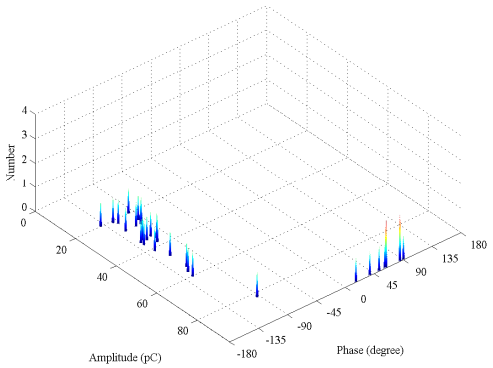

c - $V_{control}$ 120° lag with V_{ref}

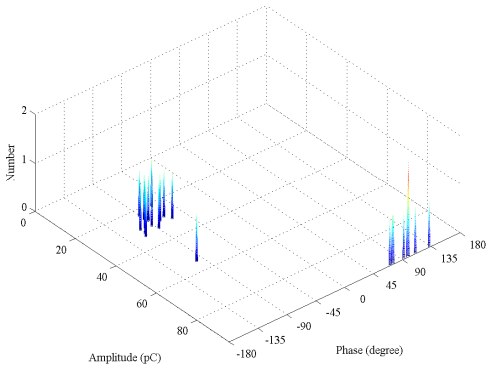

d - $V_{control}$ 120° lead with V_{ref}

Figure D.9 $V_{control}$ at 35kV for virgin pressboard conditioned to 3.6% moisture and at 40°C. Robinson set to 50pC resolution

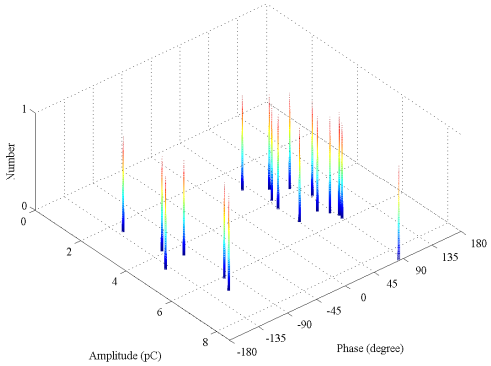

a - $V_{control}$ in phase with V_{ref}

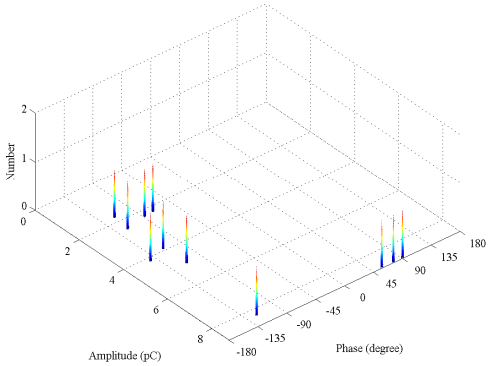

f - $V_{control}$ in anti-phase with V_{ref}

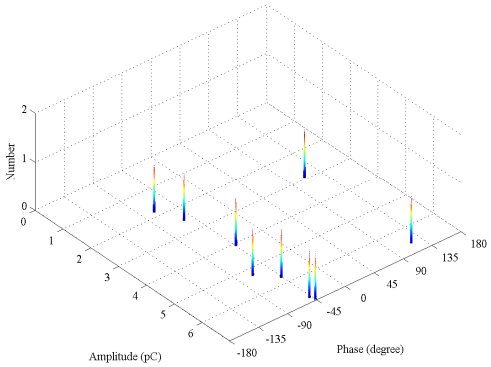

b - $V_{control}$ 60° lag with V_{ref}

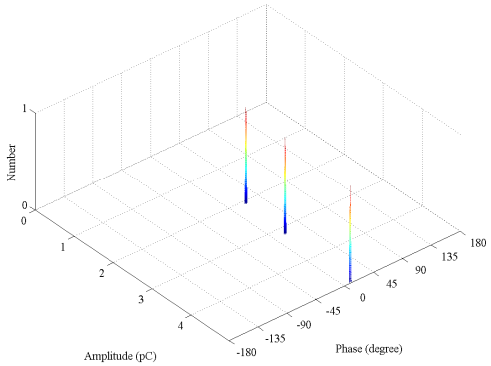

e - $V_{control}$ 60° lead with V_{ref}

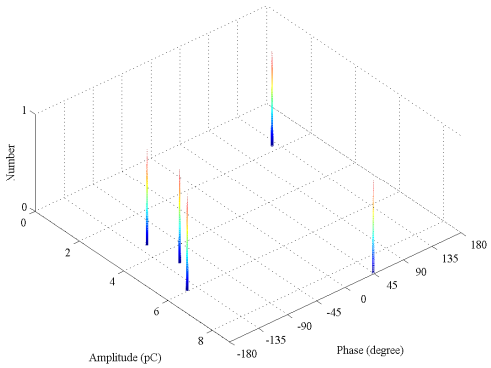

c - $V_{control}$ 120° lag with V_{ref}

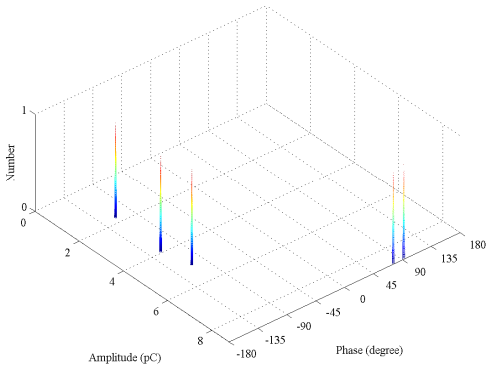

d - $V_{control}$ 120° lead with V_{ref}

Figure D.10 $V_{control}$ at 30kV for virgin pressboard conditioned to 3.6% moisture and at 50°C. Robinson set to 5pC resolution

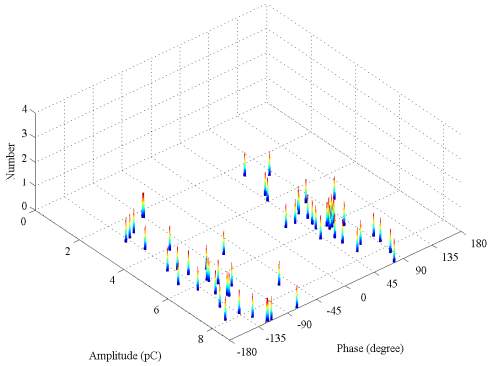

a - $V_{control}$ in phase with V_{ref}

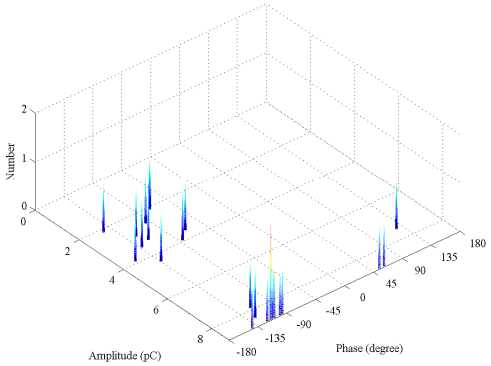

f - $V_{control}$ in anti-phase with V_{ref}

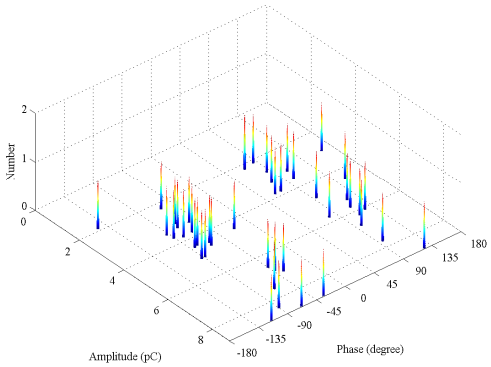

b - $V_{control}$ 60° lag with V_{ref}

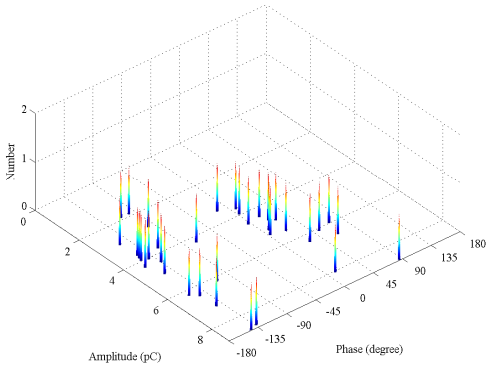

e - $V_{control}$ 60° lead with V_{ref}

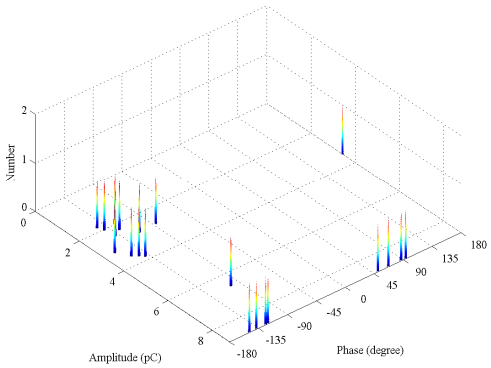

c - $V_{control}$ 120° lag with V_{ref}

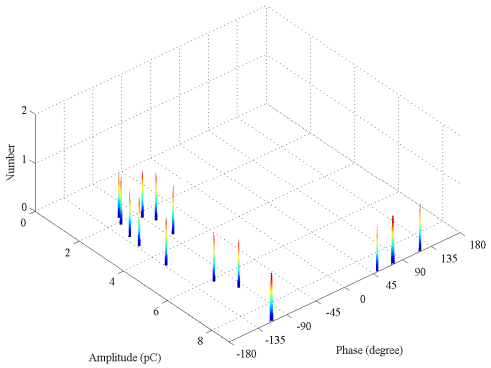

d - $V_{control}$ 120° lead with V_{ref}

Figure D.11 $V_{control}$ at 35kV for virgin pressboard conditioned to 3.6% moisture and at 50°C. Robinson set to 5pC resolution

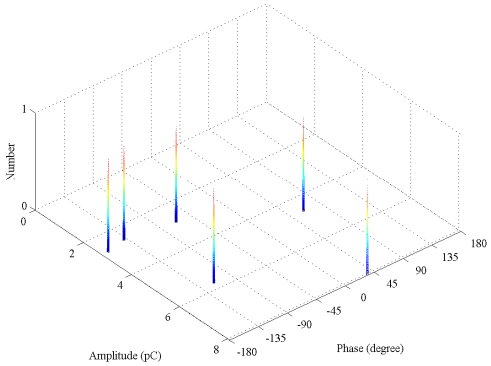

a - $V_{control}$ in phase with V_{ref}

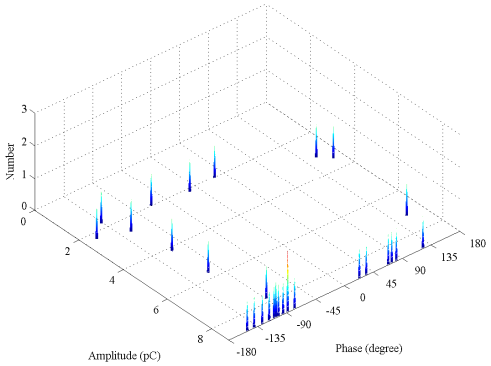

f - $V_{control}$ in anti-phase with V_{ref}

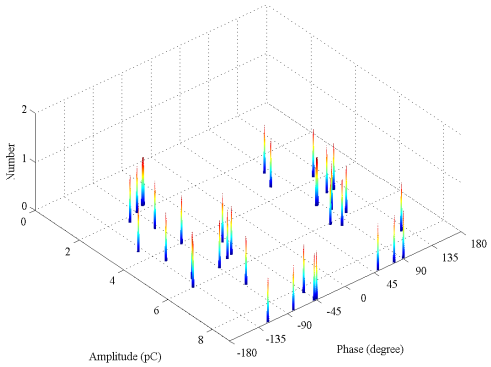

b - $V_{control}$ 60° lag with V_{ref}

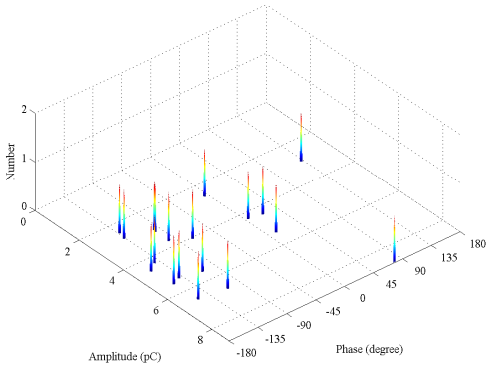

e - $V_{control}$ 60° lead with V_{ref}

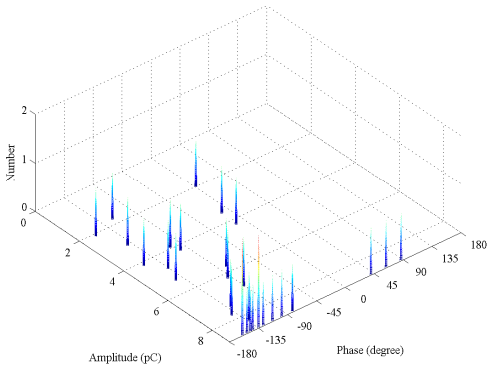

c - $V_{control}$ 120° lag with V_{ref}

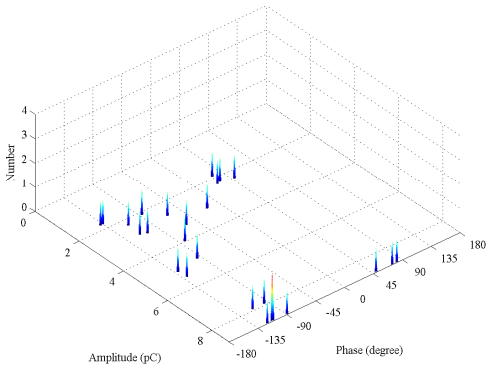

d - $V_{control}$ 120° lead with V_{ref}

Figure D.12 $V_{control}$ at 40kV for virgin pressboard conditioned to 3.6% moisture and at 50°C. Robinson set to 5pC resolution

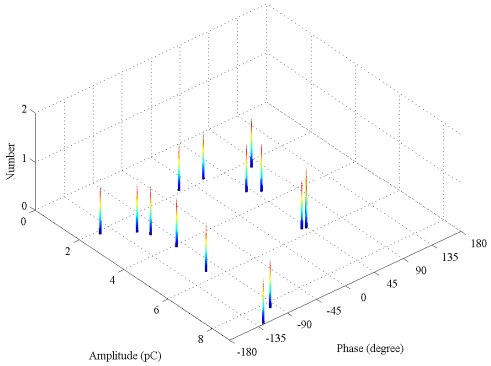

a - $V_{control}$ in phase with V_{ref}

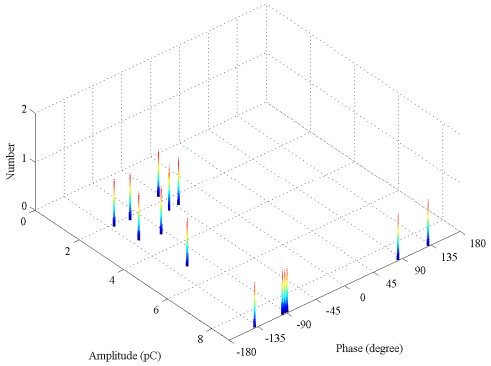

f - $V_{control}$ in anti-phase with V_{ref}

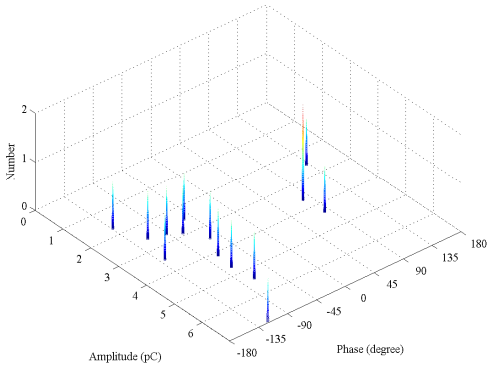

b - $V_{control}$ 60° lag with V_{ref}

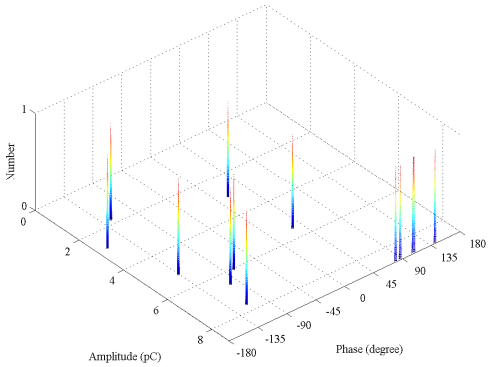

e - $V_{control}$ 60° lead with V_{ref}

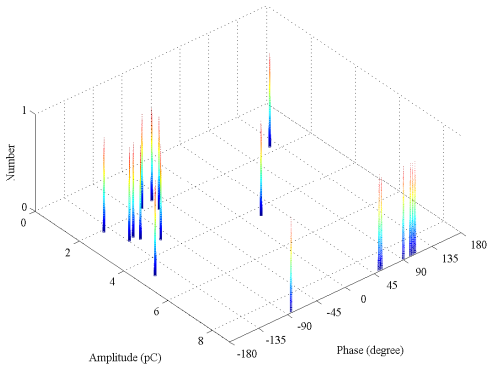

c - $V_{control}$ 120° lag with V_{ref}

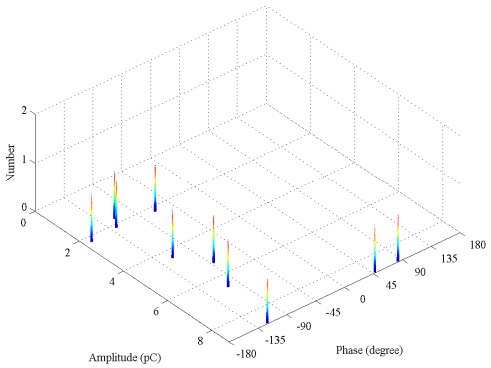

d - $V_{control}$ 120° lead with V_{ref}

Figure D.13 $V_{control}$ at 40kV for virgin pressboard conditioned to 3.6% moisture and at 60°C. Robinson set to 5pC resolution

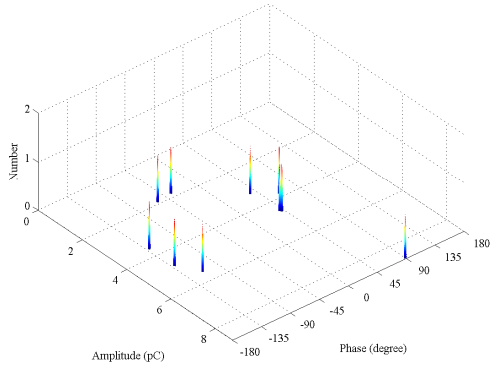

a - $V_{control}$ in phase with V_{ref}

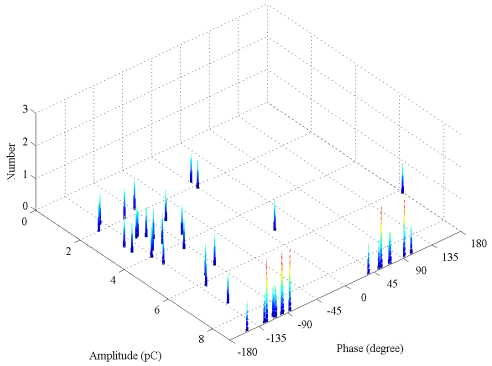

f - $V_{control}$ in anti-phase with V_{ref}

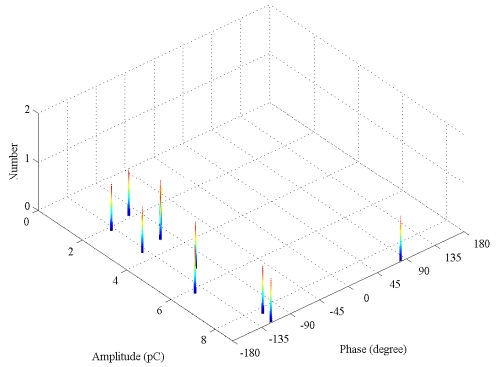

b - $V_{control}$ 60° lag with V_{ref}

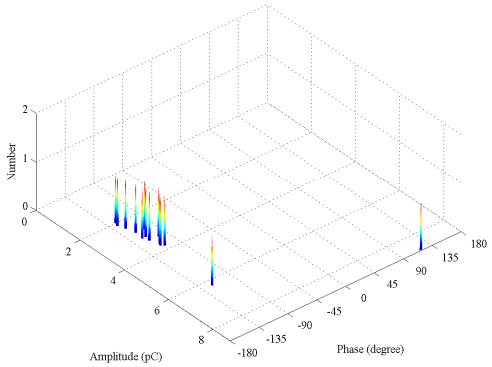

e - $V_{control}$ 60° lead with V_{ref}

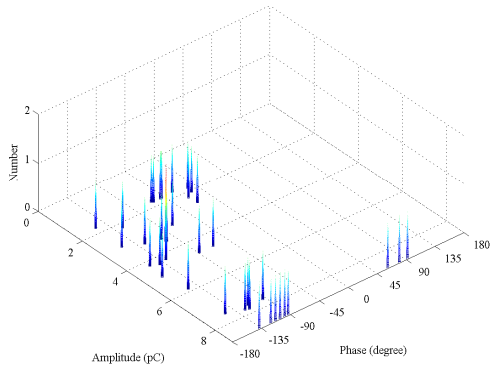

c - $V_{control}$ 120° lag with V_{ref}

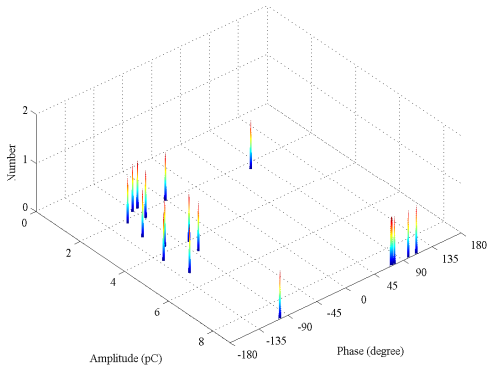

d - $V_{control}$ 120° lead with V_{ref}

Figure D.14 $V_{control}$ at 45kV for virgin pressboard conditioned to 3.6% moisture and at 60°C. Robinson set to 5pC resolution

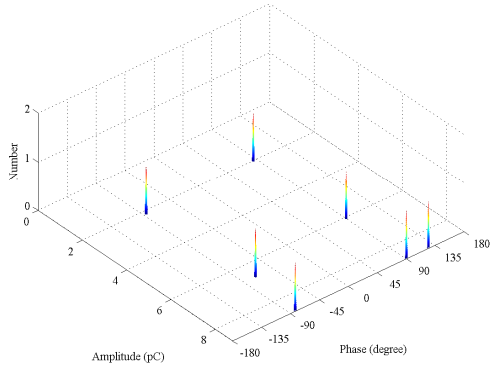

a - $V_{control}$ in phase with V_{ref}

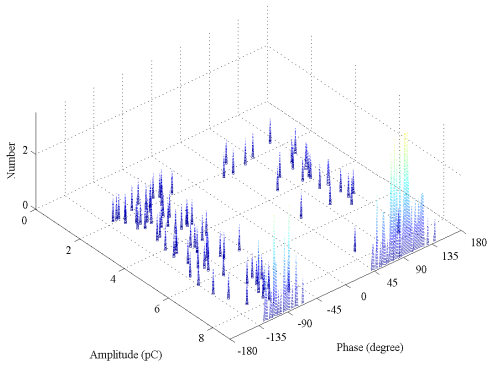

f - $V_{control}$ in anti-phase with V_{ref}

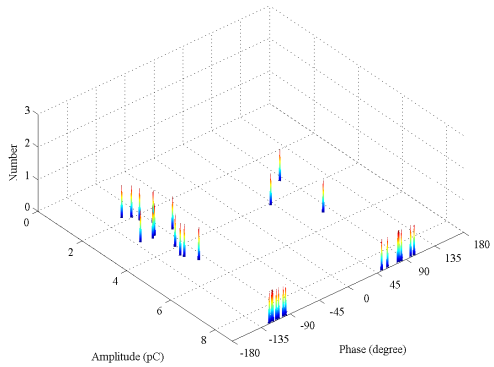

b - $V_{control}$ 60° lag with V_{ref}

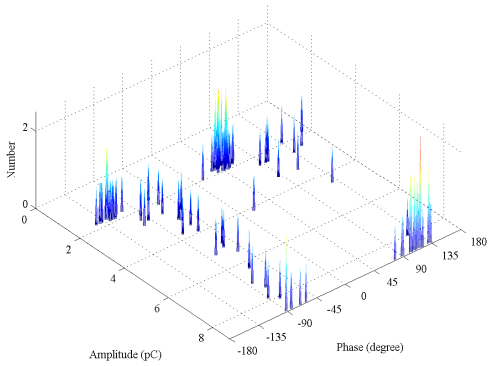

e - $V_{control}$ 60° lead with V_{ref}

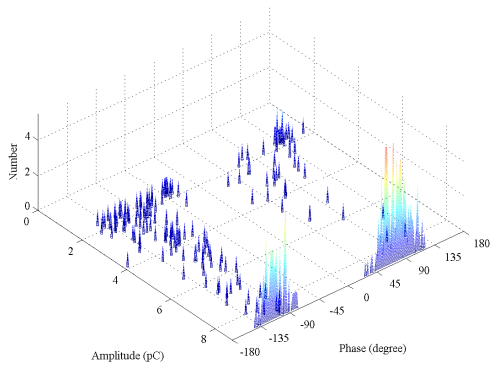

c - $V_{control}$ 120° lag with V_{ref}

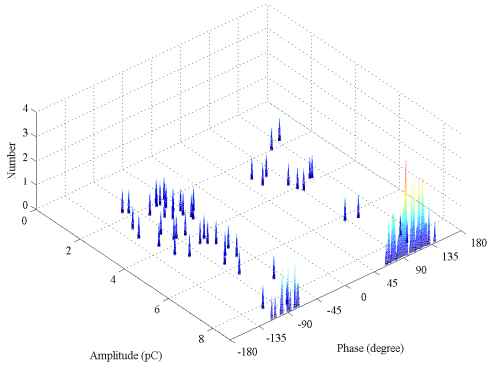

d - $V_{control}$ 120° lead with V_{ref}

Figure D.15 $V_{control}$ at 25kV for virgin pressboard conditioned to 7.2% moisture and at 20°C. Robinson set to 5pC resolution

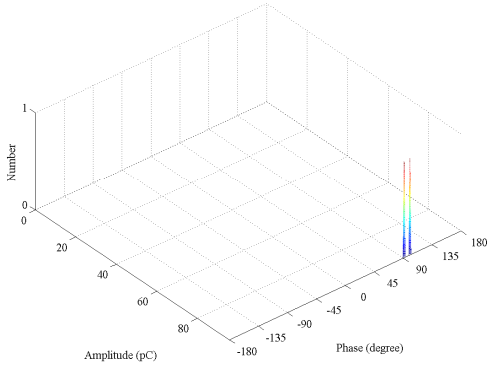

a - $V_{control}$ in phase with V_{ref}

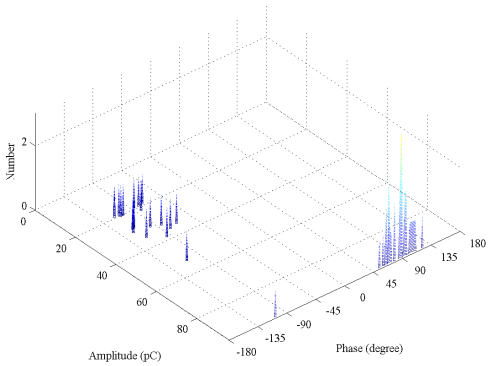

f - $V_{control}$ in anti-phase with V_{ref}

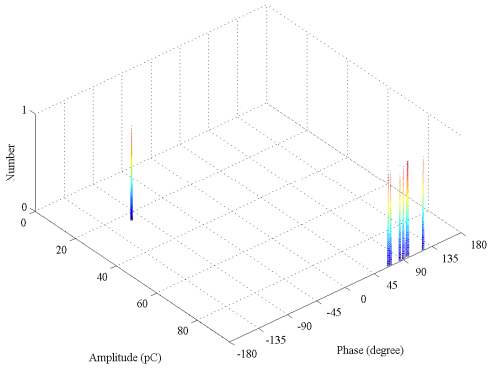

b - $V_{control}$ 60° lag with V_{ref}

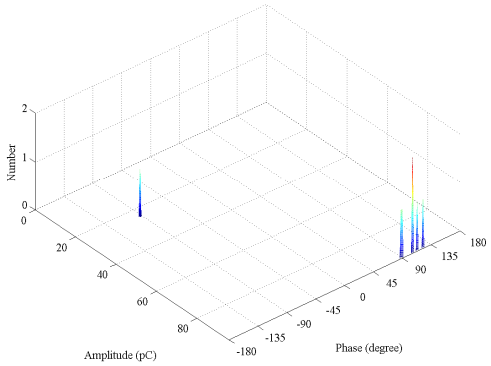

e - $V_{control}$ 60° lead with V_{ref}

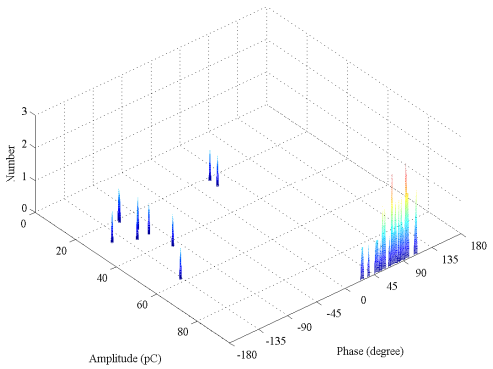

c - $V_{control}$ 120° lag with V_{ref}

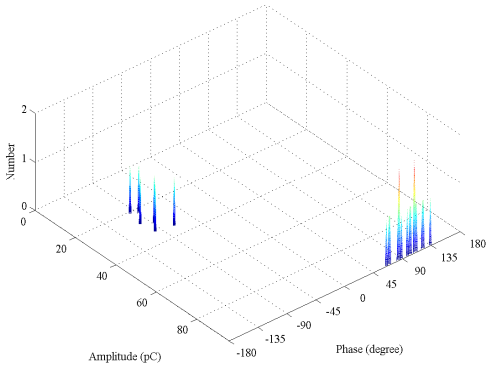

d - $V_{control}$ 120° lead with V_{ref}

Figure D.16 $V_{control}$ at 25kV for virgin pressboard conditioned to 7.2% moisture and at 20°C. Robinson set to 50pC resolution

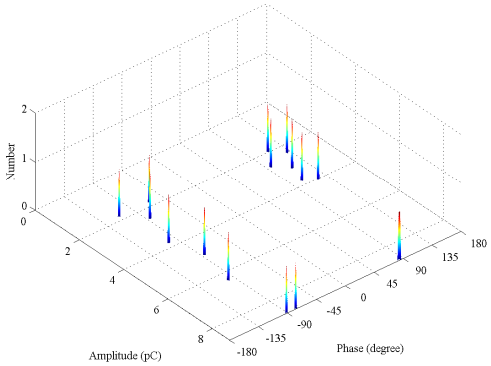

a - $V_{control}$ in phase with V_{ref}

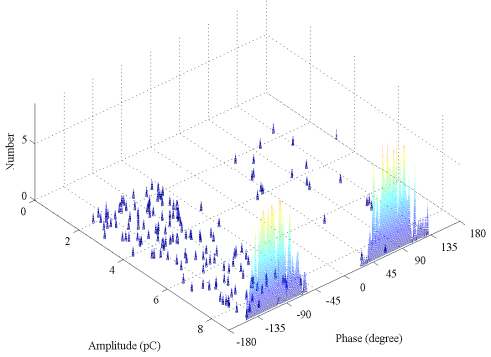

f - $V_{control}$ in anti-phase with V_{ref}

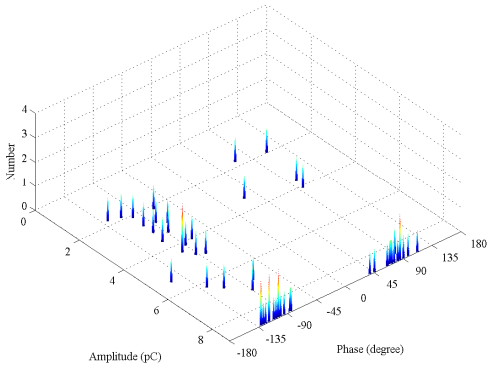

b - $V_{control}$ 60° lag with V_{ref}

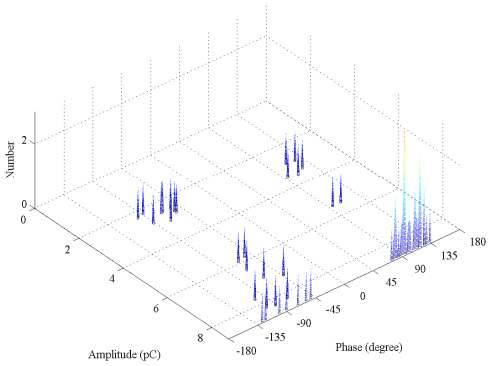

e - $V_{control}$ 60° lead with V_{ref}

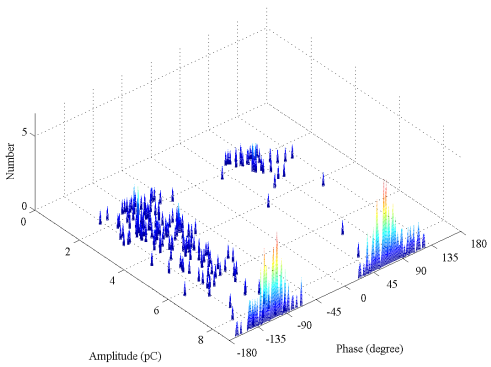

c - $V_{control}$ 120° lag with V_{ref}

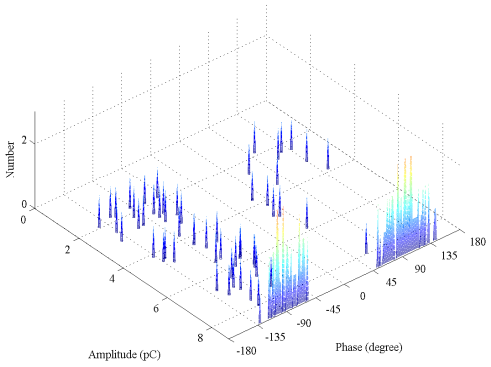

d - $V_{control}$ 120° lead with V_{ref}

Figure D.17 $V_{control}$ at 30kV for virgin pressboard conditioned to 7.2% moisture and at 20°C. Robinson set to 5pC resolution

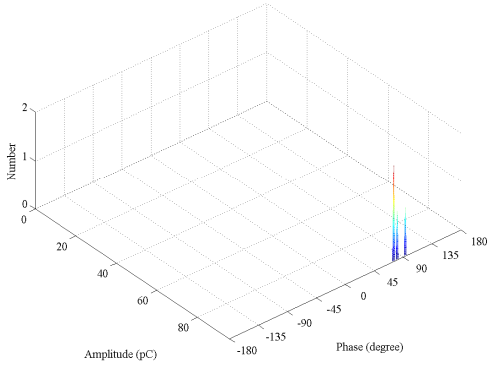

a - $V_{control}$ in phase with V_{ref}

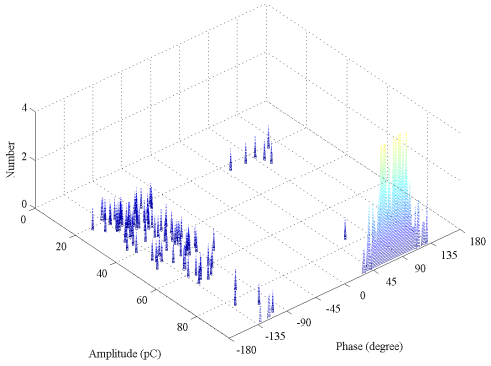

f - $V_{control}$ in anti-phase with V_{ref}

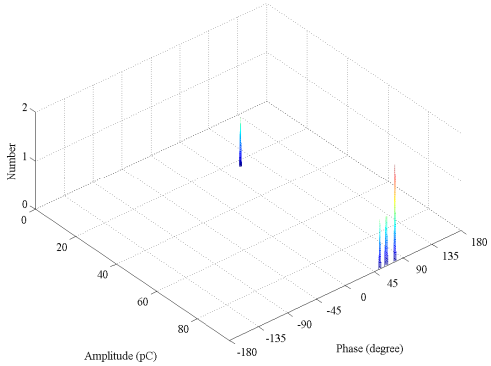

b - $V_{control}$ 60° lag with V_{ref}

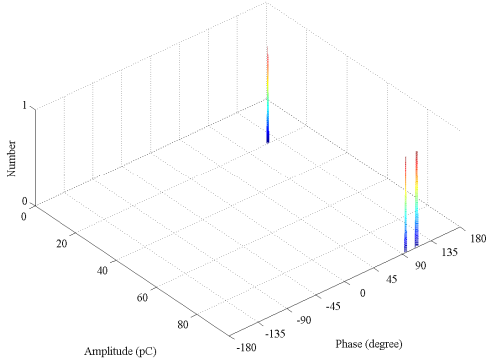

e - $V_{control}$ 60° lead with V_{ref}

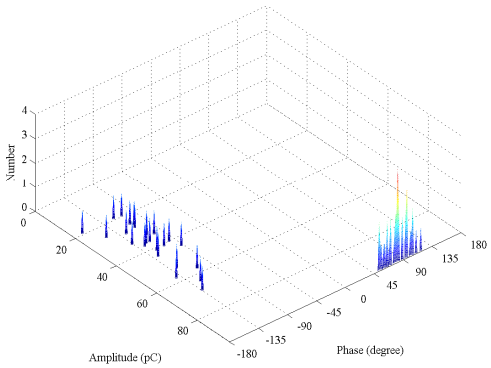

c - $V_{control}$ 120° lag with V_{ref}

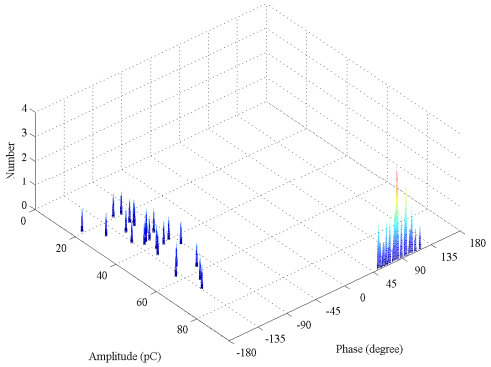

d - $V_{control}$ 120° lead with V_{ref}

Figure D.18 $V_{control}$ at 30kV for virgin pressboard conditioned to 7.2% moisture and at 20°C. Robinson set to 50pC resolution

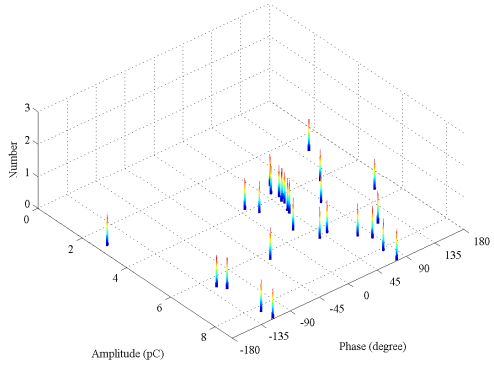

a - $V_{control}$ in phase with V_{ref}

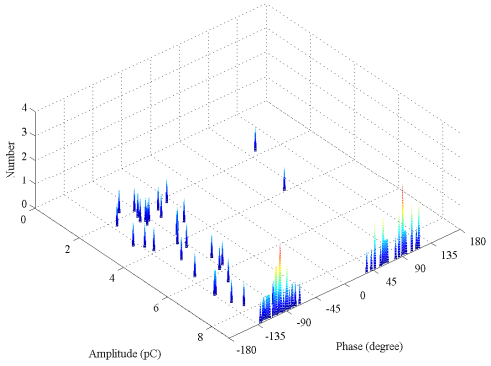

f - $V_{control}$ in anti-phase with V_{ref}

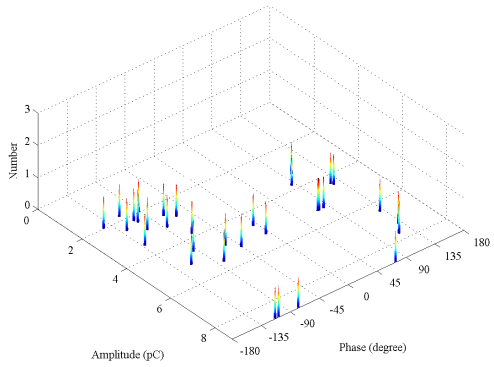

b - $V_{control}$ 60° lag with V_{ref}

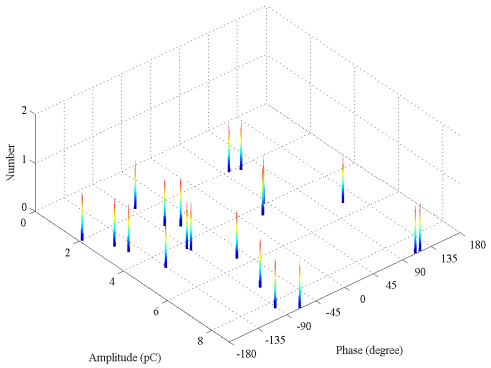

e - $V_{control}$ 60° lead with V_{ref}

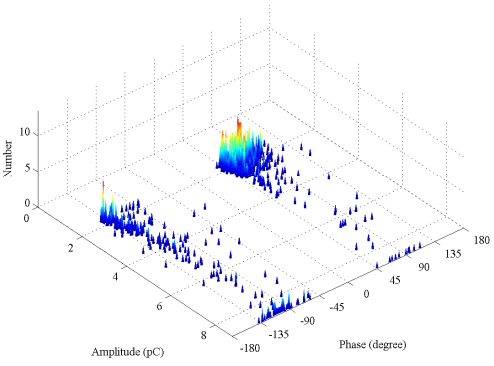

c - $V_{control}$ 120° lag with V_{ref}

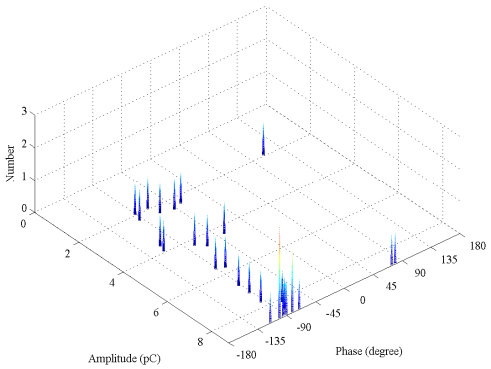

d - $V_{control}$ 120° lead with V_{ref}

Figure D.19 $V_{control}$ at 25kV for virgin pressboard conditioned to 7.2% moisture and at 30°C. Robinson set to 5pC resolution

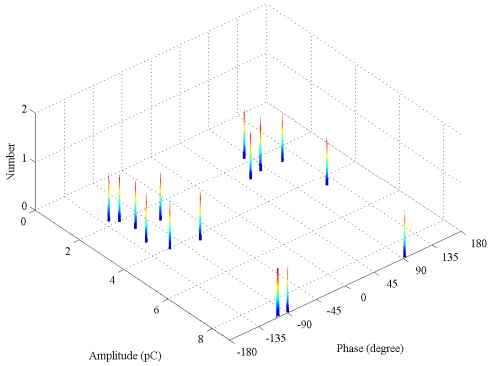

a - $V_{control}$ in phase with V_{ref}

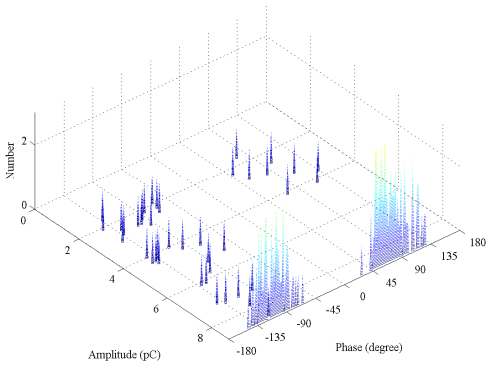

f - $V_{control}$ in anti-phase with V_{ref}

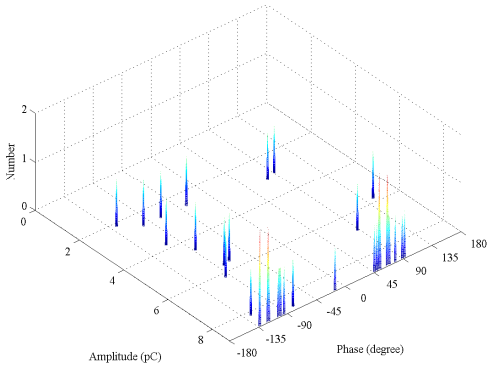

b - $V_{control}$ 60° lag with V_{ref}

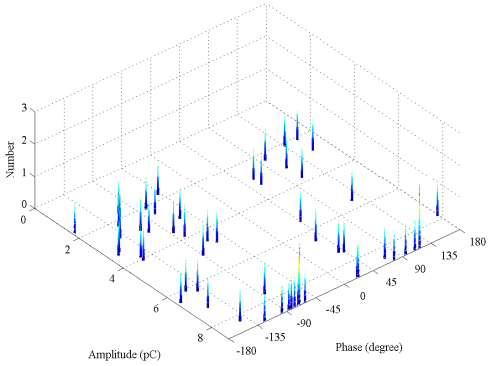

e - $V_{control}$ 60° lead with V_{ref}

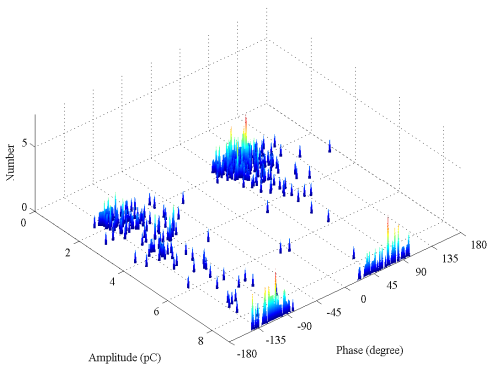

c- $V_{control}$ 120° lag with V_{ref}

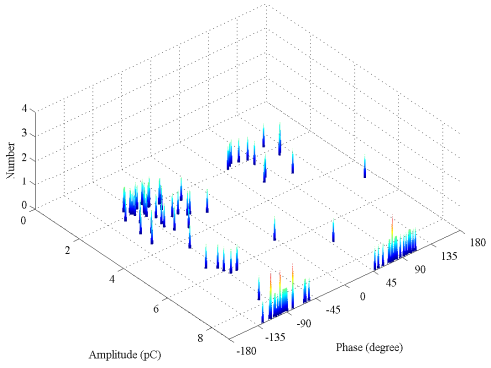

d - $V_{control}$ 120° lead with V_{ref}

Figure D.20 $V_{control}$ at 30kV for virgin pressboard conditioned to 7.2% moisture and at 30°C. Robinson set to 5pC resolution

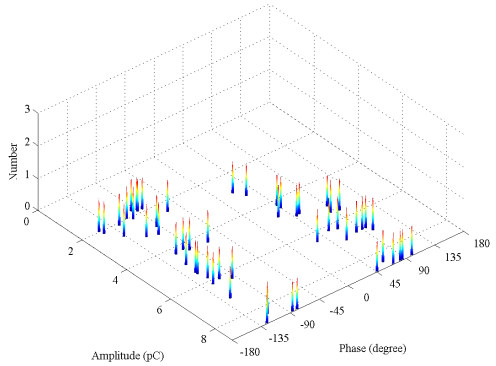

a - $V_{control}$ in phase with V_{ref}

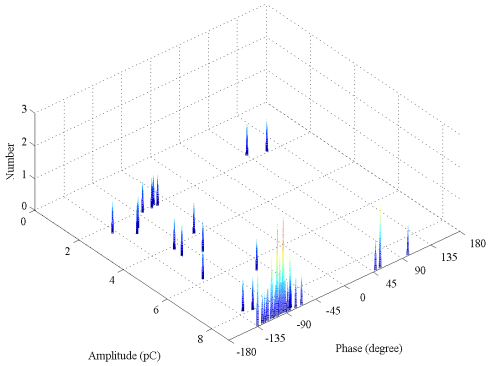

f - $V_{control}$ in anti-phase with V_{ref}

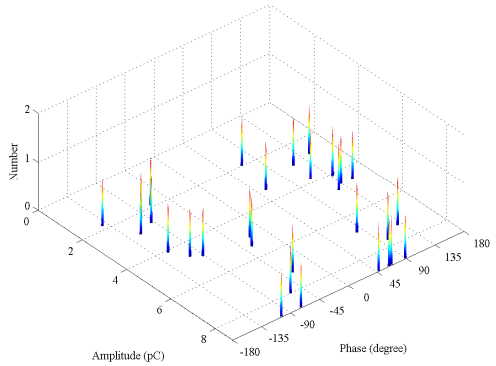

b - $V_{control}$ 60° lag with V_{ref}

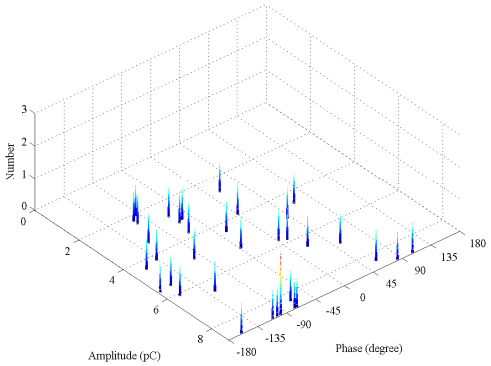

e - $V_{control}$ 60° lead with V_{ref}

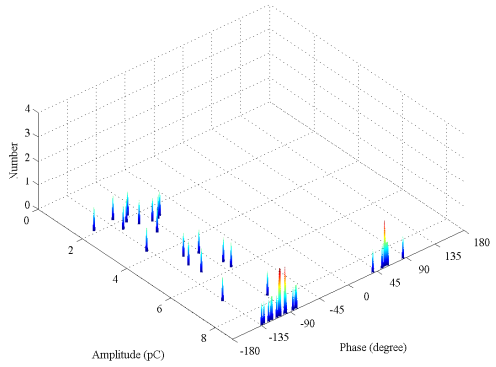

c - $V_{control}$ 120° lag with V_{ref}

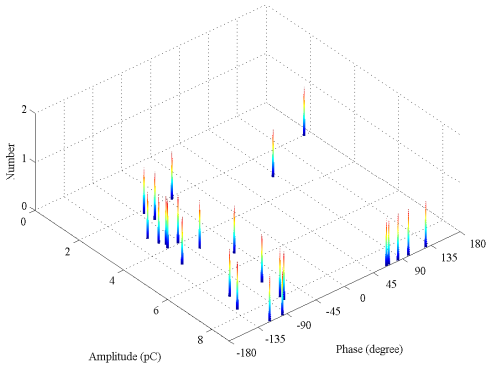

d - $V_{control}$ 120° lead with V_{ref}

Figure D.21 $V_{control}$ at 25kV for virgin pressboard conditioned to 7.2% moisture and at 40°C. Robinson set to 5pC resolution

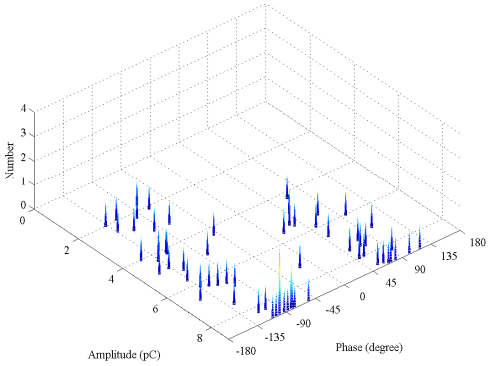

a - $V_{control}$ in phase with V_{ref}

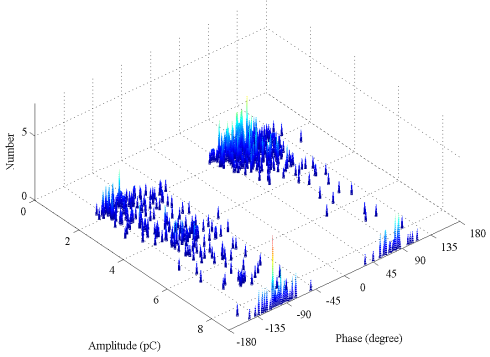

f - $V_{control}$ in anti-phase with V_{ref}

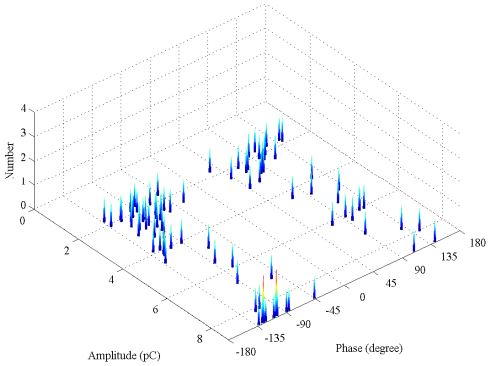

b - $V_{control}$ 60° lag with V_{ref}

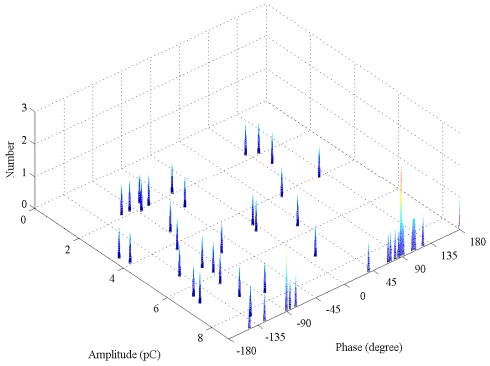

e - $V_{control}$ 60° lead with V_{ref}

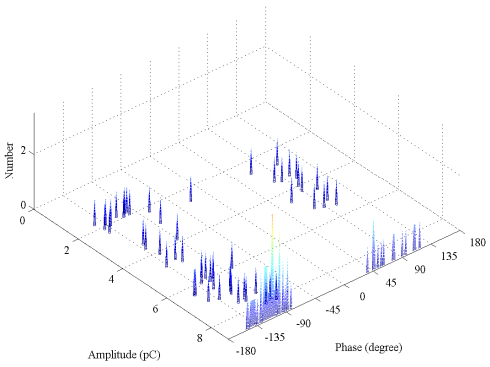

c - $V_{control}$ 120° lag with V_{ref}

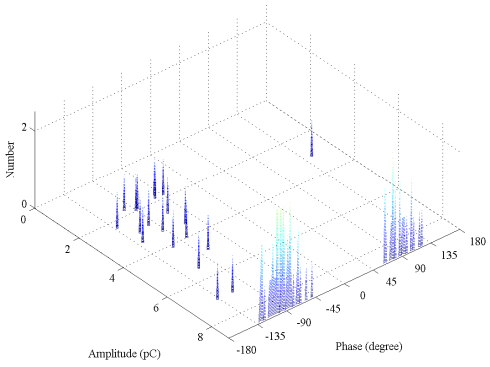

d - $V_{control}$ 120° lead with V_{ref}

Figure D.22 $V_{control}$ at 30kV for virgin pressboard conditioned to 7.2% moisture and at 40°C. Robinson set to 5pC resolution

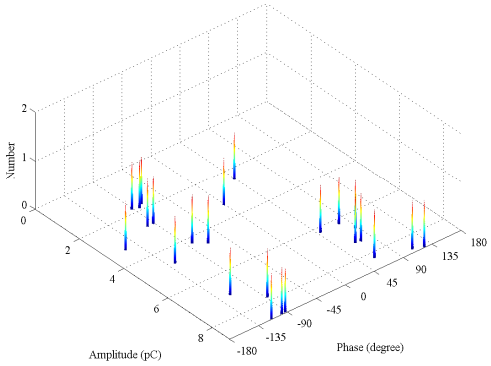

a - $V_{control}$ in phase with V_{ref}

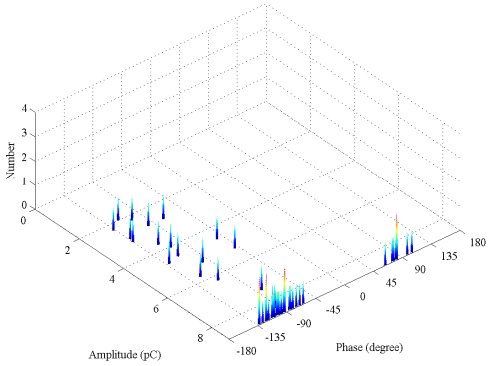

f - $V_{control}$ in anti-phase with V_{ref}

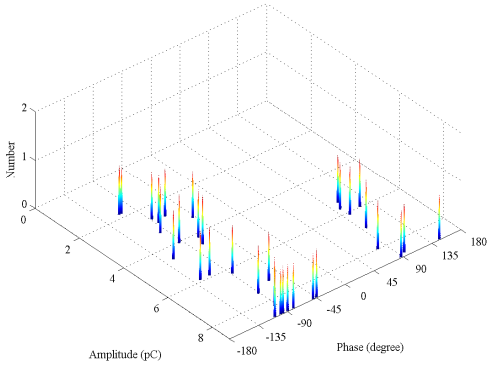

b - $V_{control}$ 60° lag with V_{ref}

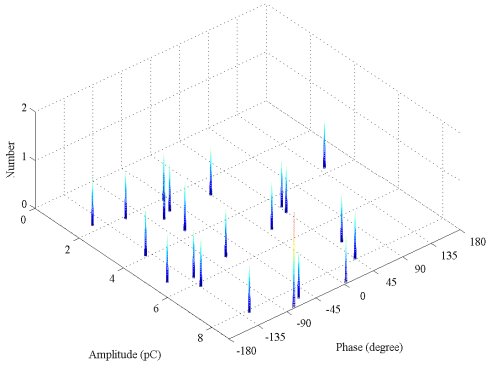

e - $V_{control}$ 60° lead with V_{ref}

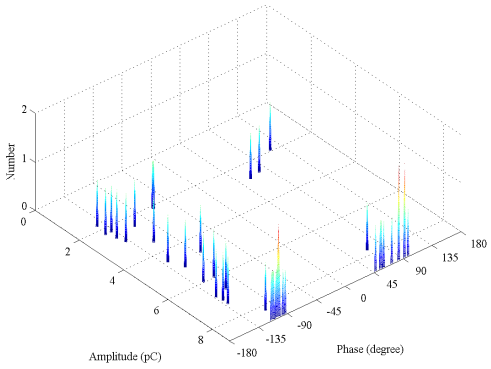

c - $V_{control}$ 120° lag with V_{ref}

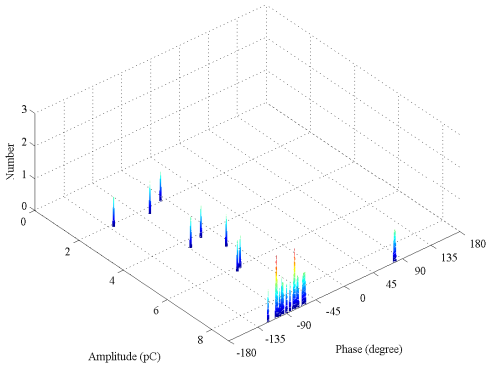

d - $V_{control}$ 120° lead with V_{ref}

Figure D.23 $V_{control}$ at 25kV for virgin pressboard conditioned to 7.2% moisture and at 50°C. Robinson set to 5pC resolution

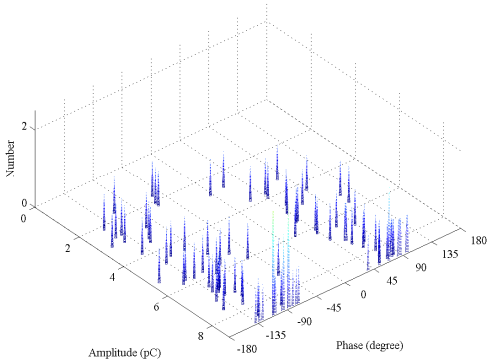

a - $V_{control}$ in phase with V_{ref}

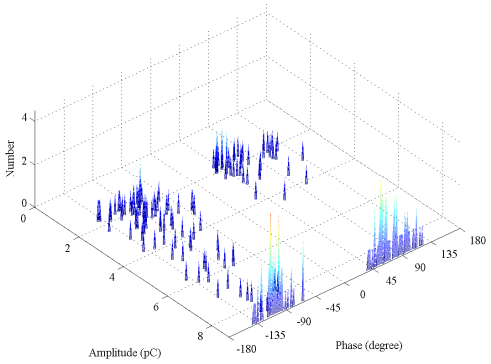

f - $V_{control}$ in anti-phase with V_{ref}

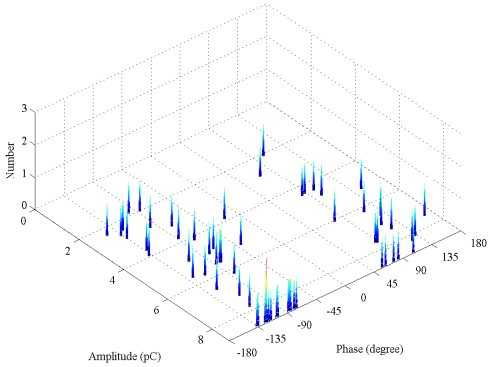

b - $V_{control}$ 60° lag with V_{ref}

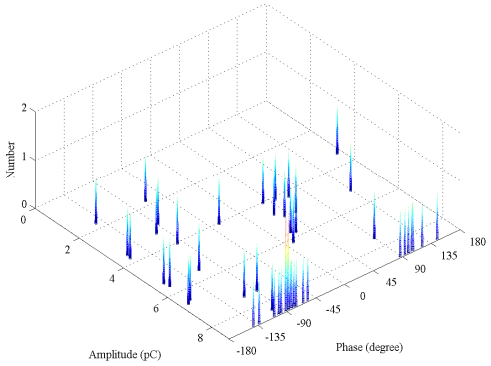

e - $V_{control}$ 60° lead with V_{ref}

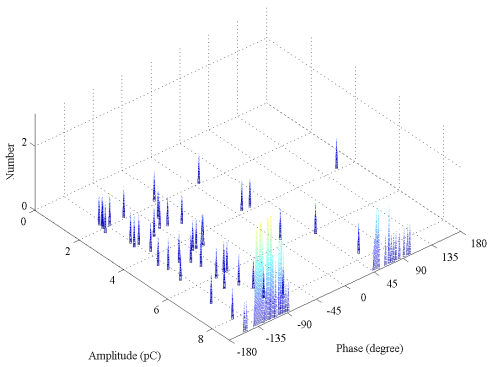

c - $V_{control}$ 120° lag with V_{ref}

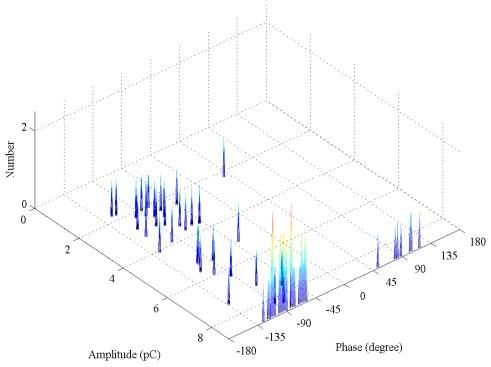

d - $V_{control}$ 120° lead with V_{ref}

Figure D.24 $V_{control}$ at 30kV for virgin pressboard conditioned to 7.2% moisture and at 50°C. Robinson set to 5pC resolution

No PD detected at 50pC resolution

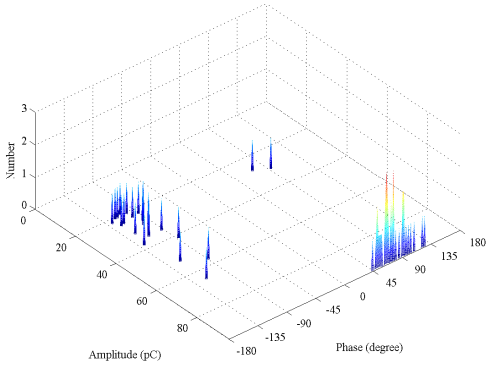

a - $V_{control}$ in phase with V_{ref}

f - $V_{control}$ in anti-phase with V_{ref}

No PD detected at 50pC resolution

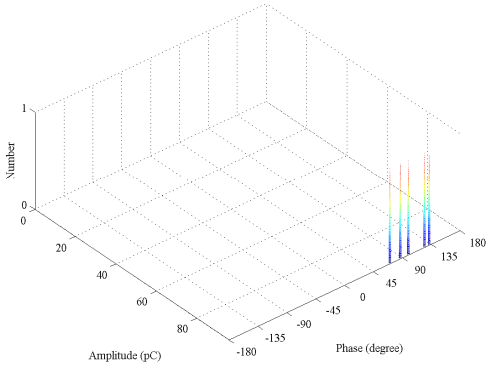

b - $V_{control}$ 60° lag with V_{ref}

e- $V_{control}$ 60° lead with V_{ref}

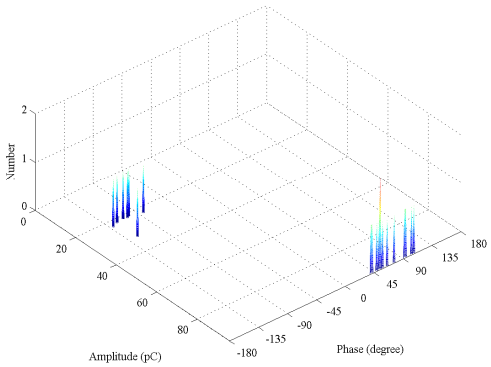

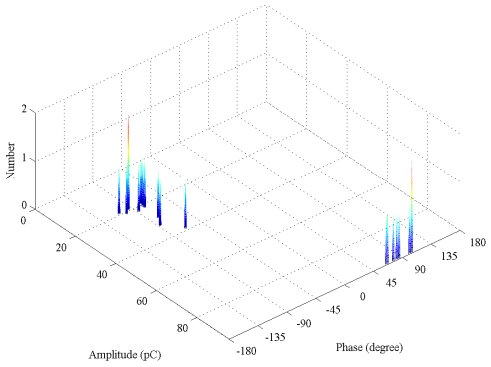

c - $V_{control}$ 120° lag with V_{ref}

d - $V_{control}$ 120° lead with V_{ref}

Figure D.25 $V_{control}$ at 30kV for virgin pressboard conditioned to 7.2% moisture and at 50°C. Robinson set to 50pC resolution

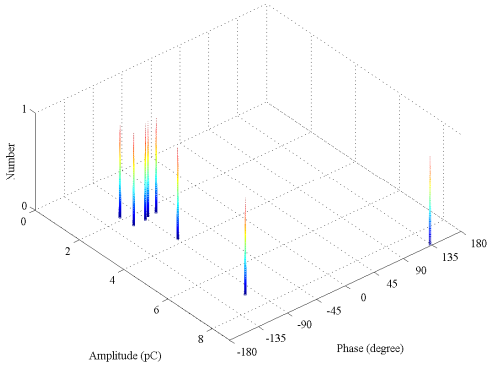

a - $V_{control}$ in phase with V_{ref}

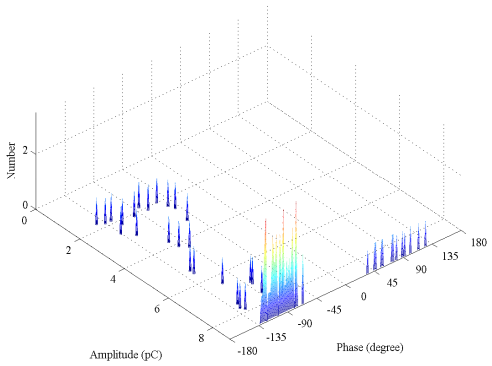

f - $V_{control}$ in anti-phase with V_{ref}

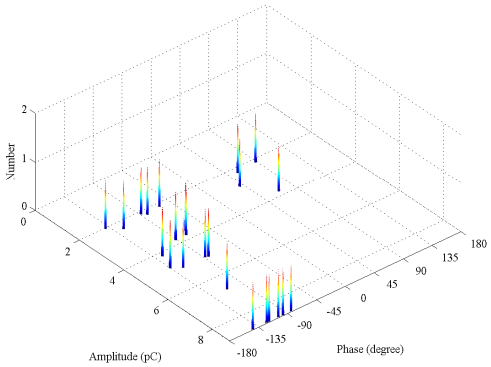

b - $V_{control}$ 60° lag with V_{ref}

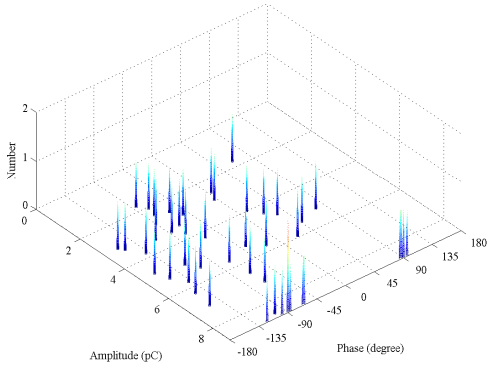

e - $V_{control}$ 60° lead with V_{ref}

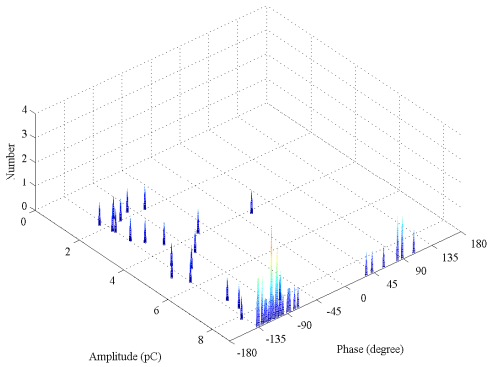

c - $V_{control}$ 120° lag with V_{ref}

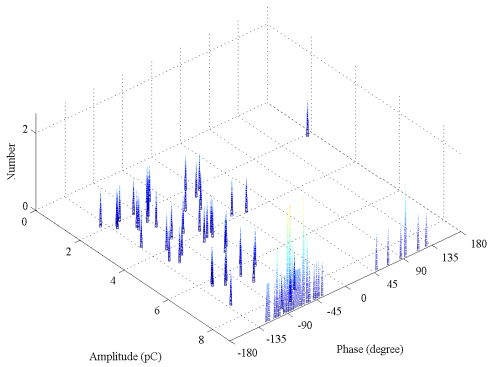

d - $V_{control}$ 120° lead with V_{ref}

Figure D.26 $V_{control}$ at 35kV for virgin pressboard conditioned to 7.2% moisture and at 60°C. Robinson set to 5pC resolution

No PD detected at 50pC resolution

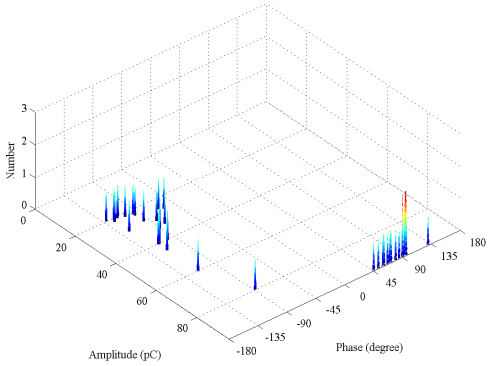

a - $V_{control}$ in phase with V_{ref}

f - $V_{control}$ in anti-phase with V_{ref}

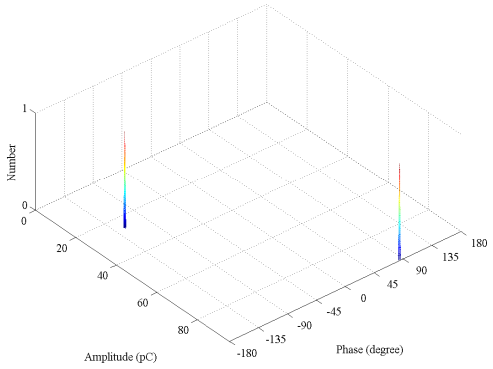

b - $V_{control}$ 60° lag with V_{ref}

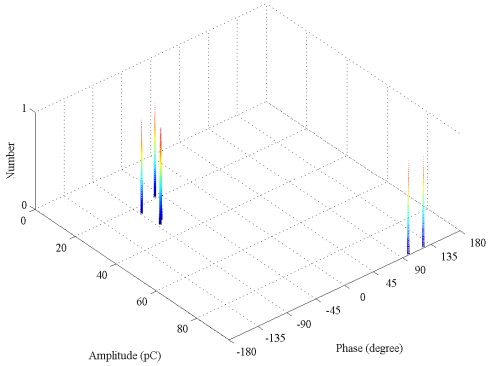

e - $V_{control}$ 60° lead with V_{ref}

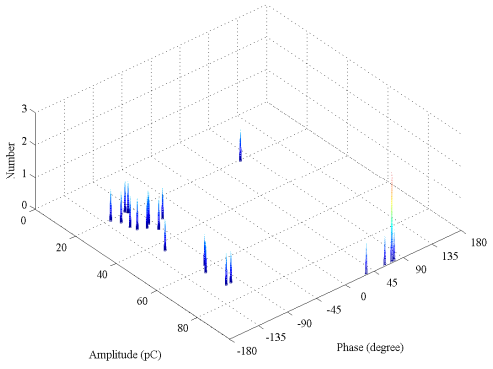

c - $V_{control}$ 120° lag with V_{ref}

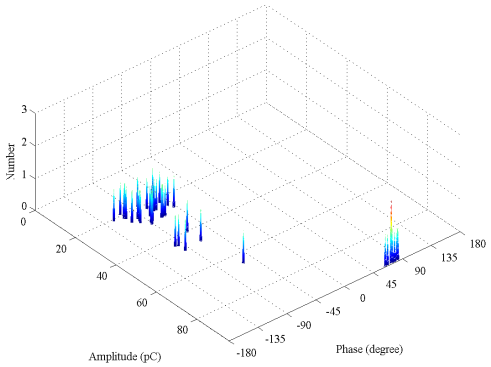

d - $V_{control}$ 120° lead with V_{ref}

Figure D.27 $V_{control}$ at 35kV for virgin pressboard conditioned to 7.2% moisture and at 60°C. Robinson set to 50pC resolution

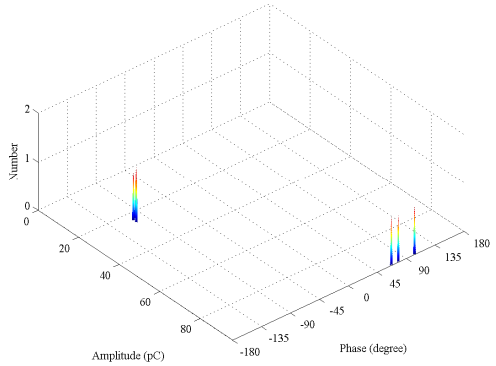

a - $V_{control}$ in phase with V_{ref}

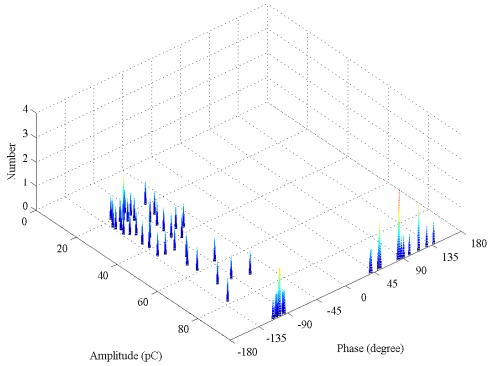

f - $V_{control}$ in anti-phase with V_{ref}

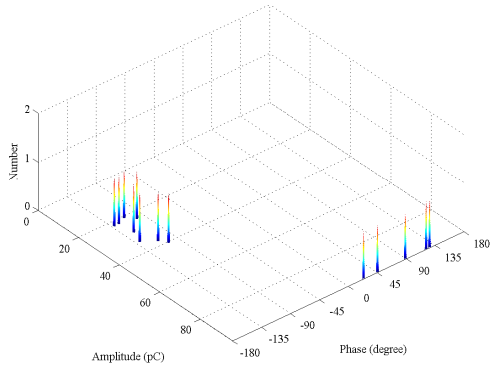

b - $V_{control}$ 60° lag with V_{ref}

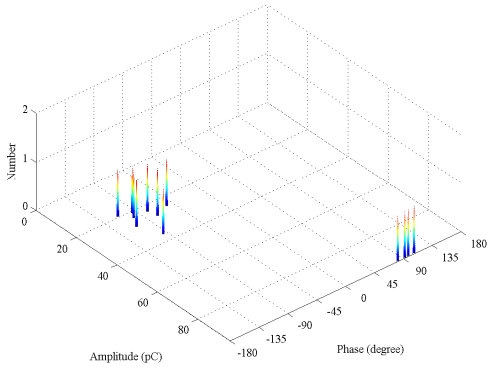

e - $V_{control}$ 60° lead with V_{ref}

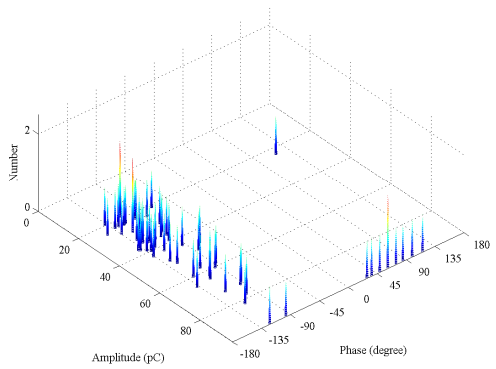

c - $V_{control}$ 120° lag with V_{ref}

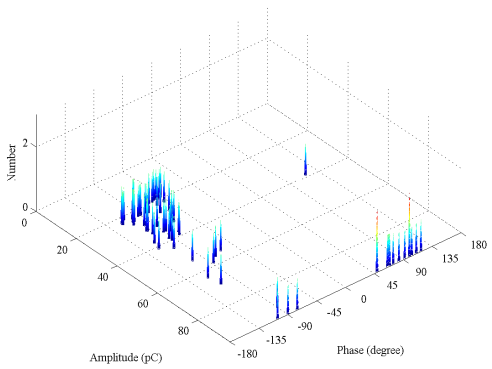

d - $V_{control}$ 120° lead with V_{ref}

Figure D.28 $V_{control}$ at 40kV for virgin pressboard conditioned to 7.2% moisture and at 60°C. Robinson set to 50pC resolution

Appendix E: Related work published as conference papers

- P. M. Mitchinson, I. L. Hosier, P. L. Lewin, A. S. Vaughan, G. Chen and P. Jarman, *"An experiment to evaluate the benefits of processing aged transformer oil"*. International Symposium on Electrical Insulation, Toronto, June 2006.

- P. M. Mitchinson, P. L. Lewin, I. L. Hosier, G. Chen and P. Jarman, *"Oil reclamation – just a question of moisture*?*"* Conference on Electrical Insulation and Dielectric Phenomena, Kansas, October 2006.

- P. M. Mitchinson, P. L. Lewin, G. Chen and P. N. Jarman, *"Creep stress failure in high voltage transformer winding insulation"* Conference on Electrical Insulation and Dielectric Phenomena, Vancouver, October 2007.

- P. M. Mitchinson, P. L. Lewin, G. Chen and P. N Jarman, *"A new approach to the study of surface discharge on the oil-pressboard interface"*, International Conference on Dielectric Liquids, Poitiers, July 2008.

References

1 "*Modern Power Station Practice*", 3rd Edition, Volume K, EHV transmission, British Electricity International, London, Pergamon Press, 1991, Chapter 1, §1.

2 2008/08 Transmission system map as at 31st December 2007 , National Grid plc. GB SYS Fig A.1.2.

3 National Grid plc. "*GB Seven Year Statement 2008*", Chapter 6, Transmission System.

4 M. R. Allison, K. G. Lewis and M. I. Winfield, "An integrated approach to reliability assessment, maintenance and life cycle costs in the National Grid Company", IEE Conference Publication: *The reliability of Transmission and Distribution Equipment Conference*, March 1995.

5 Z. Li and J. Guo, "Wisdom about age", *IEEE Power and Energy Magazine*, May/June 2006.

6 J. N. Jaegers, J. Khosa, P. J. De Klerk and C. T. Gaunt, "Transformer reliability and condition assessment in a South African utility", Paper T6-442. *15th International Symposium on High Voltage Engineering*, 2007.

7 S. White. "Life management of primary distribution transformers", *IEE Transformer Life Management Colloquium*, October 1998.

8 Richard E. Brown and Bruce G. Humphrey. "Asset management for transmission and distribution", *IEEE Power and Energy Magazine*, May/June 2005.

9 D. J. Vrey, M. E. N. du Preez and H. H. van de Merwe, "Network Asset Condition Assessment and Refurbishment planning", *Association of Municipal Electricity Undertakings South Africa Convention*, 2005.

10 Areva T and D. Commercial Brochure, "*Power transformers and reactors for power generation and Transmission networks*", Product L2- HV Transformers and Reactors 0779-EN 2004.

11 D.J. Allen and A. White, "Transformer design for high reliability", IEE Conference Publication: *The reliability of Transmission and Distribution Equipment Conference*, March 1995.

12 J.A. Lapworth, "Transformer reliability surveys", Cigré study committee report SCA2. *Electra* No. 227, August 2006.

13 V. Sokolov, Z. Berler and V. Rashkes, "Effective methods of assessment of insulation conditions in power transformers: A view based on practical experience", Proceedings, *Electrical Insulation Conference*, pp 659 - 667, 1999.

14 V. V. Sokolov, "Understanding failure modes of transformers", *EuroTechCon.*, 2005.

15 A. K. Lokhanin, G. Y. Schneider, V. V. Sokolov, V. M. Chronogotsky and T. I. Morozova, "Internal failure mechanisms of HV equipment under service conditions", *Cigré* Session 2002, Paper 15-201.

16 J.A. Lapworth, P.N. Jarman and T. Breckenridge, "Transformer internal over-voltages caused by remote energisation", *Cigré* Session 2006, Paper A2-305.

17 A. Cancino, R. Ocon, G. Enriquez and R. Malewski, "In-service failure of 230kV transformers due to steep front lightning over-voltages at Mexican west coast", *Cigré* Session 2006, Paper A2-201.

18 W. McDermid, D. H. Grant, A. Glodjo and J. C. Bromley, "Analysis of converter transformer failures and application of periodic on-line partial discharge measurements", Proceedings of the *Electrical/Electronics Insulation Conference*, 2001.

19 William H. Bartley, "Investigating transformer failures, The Hartford Steam Boiler Inspection and Insurance Company", *The International Association of Engineering Insurers Conference*, Stockholm 2003.

20 Y. Kieffel, C. Perrier, J. L. Béssède, F. Davaux, M. Saravolac and P. Long, "Improvement of the reliability of power transformer insulation", Proceedings of the 10th *INSUCON International Electrical Insulation Conference*, May 2006.

21 K. Yusuf Billah and Robert H. Scanlan, "Resonance, Tacoma Narrows bridge failure and undergraduate physics text books", *American Journal of Physics*, Vol. 59, No 2, February 1991.

22 J. S. T. Looms, "Insulators for high voltages", London, Peregrinus on behalf of the Institution of Electrical Engineers, 1987. ISBN 0863411169, pages 4 – 5.

23 Richard M. Jacobs, "Product Recall – A Vendor/vendee Nightmare", *Microelectronics and Reliability*, Vol. 36, No 1, Jan 1996.

24 ABB "*Fast Forward*", Issue 15, Autumn 2006. Corporate industrial magazine.

25 A. C. Franklin and D. P. Franklin, "*The J & P Transformer Book*", Butterworth's 11th Edition 1983, Chapters 1 -28.

26 L. F. Blum, A. Boyajian, G. Camilli, T. C. Lennox, S. Minneci and V. M. Montsinger, *"Transformer Engineering"*, John Wiley & Sons, Inc., 1961 Fifth Printing, 2nd Ed, Chapters I – XVIII.

27 Richard L. Bean, Nicholas Chackan, Harold R. Moore and Edward C. Wentz, "Transformers for the Electric Power Industry" McGraw-Hill Book Company, 1959, pp 1 – 388.

28 J. B. Birks, "*Modern Dielectric Materials*", Heywood and Company, 1960, pp 12 44 (paper), pp 45-67 (mineral oils).

29 Data Sheet Transformerboard TIV, Weidmann Electrical Technology.

30 Thomas A. Prevost and T. V. Oommen, "Cellulose insulation in oil filled power transformers: Part I: History and Development", *Electrical Insulation Magazine*, Vol. 22 No 1, Jan/Feb 2006

31 BS EN 60450: 2004. Measurement of the average viscometric degree of polymerisation of new and aged cellulosic electrically insulating materials.

32 R. W. Sillars, "*Electrical insulating materials and their application*", Peter Peregrinus Ltd. ISBN 0-901223-40-9. pp89 – 116 (test methods), pp 117 – 125 (paper) and pp 205-223 (mineral oils).

33 BS 5626-1:1979, IEC 60554-1: 1977, Cellulosic papers for Electrical Purposes. Definitions and general requirements.

34 BS EN 60641-3-1:1994, IEC 60641-3-1:1992. Specification for pressboard and presspaper for electrical purposes. Specifications for individual materials. Requirements for pressboard, types B .0.1, B.2.1, B.2.3, B.3.1, B.3.3, B.4.1, B.4.3, B.5.1, B.6.1 and B.7.1.

35 BS EN 60763-1:1996, IEC 60763-1:1983. Specification for laminated pressboard. Definitions, classification and general requirements.

36 BS EN 61628-1:1998, IEC 61628-1:1997. Corrugated pressboard and presspaper for electrical purposes. Definitions, designations and general requirements.

37 A.C.M. Wilson, "*Insulating liquids; their Uses, Manufacture and Properties*", Peter Peregrinus Ltd. ISBN 0 906048 23 0, pp 1- 82.

38 BS EN 60247: 2004. Insulating liquids – Measurement of relative permittivity, dielectric dissipation factor (tan δ) and d.c. resistivity.

39 BS 5730: 2001. Monitoring and maintenance guide for mineral insulating oils in electrical equipment.

40 BS EN 60156:1996, IEC 60156:1995. Insulating liquids. Determination of the breakdown voltage at power frequency. Test method.

41 M. Eklund, "Mineral insulating oils; functional requirements, specifications and production", Conference Record , *International Symposium on Electrical Insulation*, 2006

42 BS 148:1998. Specification for unused and reclaimed mineral insulating oils for transformers and switchgear.

43 BS EN 60296:2004. Fluids for electrotechnical applications. Unused mineral insulating oils for transformers and switchgear.

44 Y. Bertrand and L.C. Hoang, "Vegetal oils as substitute for mineral oils", Proceedings of the IEEE *International Conference on Properties and Applications of Dielectric Materials*, v 2, 2003, p 491-494.

45 I. Fofana, V. Wasserberg, H. Borsi and E. Gockenbach, "Challenge of mixed insulating liquids for use in high voltage transformer, Part 1: Investigation of mixed liquids", *IEEE Electrical Insulation Magazine*, Vol. 18, No 3, May/June 2002.

46 I. Fofana, V. Wasserberg, H. Borsi and E. Gockenbach, "Challenge of mixed insulating liquids for use in high voltage transformer, Part 2: Investigation of mixed liquid impregnated paper insulation", *IEEE Electrical Insulation Magazine*, Vol. 18, No 4, July/August 2002.

47 T. V. Oommen and Thomas A. Prevost, "Cellulose insulation in oil filled power transformers: Part II: Maintaining insulation integrity and life", *Electrical Insulation Magazine*, Vol. 22 No 2, March/April 2006.

48 T. W. Dakin, "Electrical insulation deterioration treated as a chemical rate phenomenon", *AIEE Transactions*, Vol. 67, 1948.

49 BS EN 60085: 2004. Electrical Insulation – Thermal Classification.

50 IEC EN 60216-1:2001. Electrical insulating materials - properties of thermal endurance. Part 1: Ageing procedures and evaluation of test results.

51 P. Cygan and J. R. Laghari, "Models for insulation ageing under electrical and thermal stress", *IEEE Transactions on Electrical Insulation*, Vol. 25, No 5, Oct., 1990.

52 Y. Du, M. Zahn, B. C. Lesieutre, A. V. Mamishev and S. R. Lindgren, "Moisture equilibrium in transformer paper-oil systems", *IEEE Electrical Insulation Magazine*, Vol. 15, No 1, Jan/Feb 1999.

53 B. Buerschaper, O. Kleboth-Lugova and T. Leibfried, "The electrical strength of transformer oil in a transformer-board oil system during moisture non-equilibrium", *Annual Report on Electrical Insulation and Dielectric Phenomena*, pp 269 – 272, 2003.

54 B. Garcia, J. C. Burgos, A. M. Alonso and J. Sanz, "A moisture in oil model for power transformer monitoring. Part I; Theoretical Foundation", *IEEE Transactions on Power Delivery*, Vol. 20,No 2, April 2005.

55 B. Pahlavanpour, M. Martins and Dr Eklund, "Study of moisture equilibrium in oil-paper system with temperature variation", Proceedings of the 7th *International Conference on the Properties and Applications of Dielectric Materials*", pp 1124 -1129, June 2003.

56 H. P. Gasser, Ch. Krause and T. Prevost, "Water absorption of cellulosic insulating materials used in power transformers", Proceedings of the 2007 *IEEE International Conference on Solid Dielectrics*.

57 I. Hohlein and A. J. Kachler, "Ageing of cellulose at transformer service temperatures. Part 2: Influence of moisture and temperature on degree of polymerisation of pressboard, dissolved gasses and furanic compounds in oil", *IEEE Electrical Insulation Magazine*, Vol. 21, No5, Sept./Oct. 2005.

58 L. E. Lundgaard, W. Hansen, D. Linhjell and T. J. Painter, "Aging of oil-impregnated paper in power transformers", *IEEE Transactions on Power Delivery*, Vol. 19. No. 1.

59 I. Fofana, H. Borsi and E. Gockenberg, "Results of aging of cellulose paper under selective conditions" *Conference on Electrical insulation and Dielectric Phenomena* IEEE Annual Report pp 205 – 208, 2001.

60 ASTM D1816-04 Standard Test Method for Dielectric Breakdown Voltage of Insulating Oils of Petroleum Origin Using VDE Electrodes.

61 M. G. Danikas, "Breakdown of transformer oil", *IEEE Electrical Insulation Magazine*, Vol.6, No 5, Sept/Oct 1990.

62 O. Lesaint, A. Saker, P. Gournay, R. Tobazéon, J. Aubin and M. Mailhot, "Streamer propagation and breakdown under ac voltage in very large oil gaps", *IEEE Transactions on Dielectrics and Insulation*, Vol.5, No 3, June 1998.

63 L. E. Lundgaard, W. Hansen, S. Ingebrigsten, D. Linhjell and M. Dahlund, "Ageing of Kraft paper by acid catalysed hydrolysis", 2005 *IEEE International Conference on Dielectric Liquids*, ICDL 2005.

64 BS EN 61198: 1994 IEC 1198: 1993. Mineral insulating oils – Methods for the determination of 2-fuffural and related compounds.

65 John A. Palmer et al., "Effect of ageing on the spectral response of Transformer oil", Conference record of the 2000 *IEEE International Symposium on Electrical Insulation*.

66 Barry H. Ward, "A survey of new techniques in insulation monitoring of power transformers", *IEEE Electrical Insulation Magazine*, Vol. 17 No 3, May/June 2001.

67 M. Wang, A. J. Vandermaar and K. D. Srivastava, "Review of condition assessment for power transformers in service", *IEEE Electrical Insulation Magazine*, Vol. 18 No 6, Nov/Dec 2002.

68 G. Csépes, I. Hamos, R. Brooks and V. Karius, "Practical foundations of the RVM (Recovery Voltage Method) for oil-paper insulation diagnosis", Proceedings of the 1998 67th *IEEE Annual Conference on Electrical Insulation and Dielectric Phenomena*.

69 A. Krivda and G. Russell, "Assessment of oil impregnated paper insulated transformers using recovery voltage measurements", *IEEE International Conference on Conduction and Breakdown in Solid Dielectrics* June 1998.

70 S.M. Gubanski et al., "Dielectric response methods for diagnostics of power transformers", *IEEE Electrical Insulation Magazine*, Vol. 19 No 3, May/June 2003.

71 M. Checksfield and A. Westlake, "Experiences with operating and monitoring generator transformers", *IEE Transformer Life Management Colloquium*, October 1998.

72 I. Hohlein, “Unusual cases of gassing of transformers in service”, *IEEE Electrical Insulation Magazine*, Vol. 22 No 1, Jan/Feb 2006.

73 M. Duval and J. Durkarm, “Improving the reliability of transformer gas-in-oil diagnosis”, *IEEE Electrical Insulation Magazine*, Vol. 21 No 4, July/Aug 2005

74 I. L Hosier, A. S. Vaughan and S. J. Sutton, “A novel optical diagnostic tool for condition assessment of insulating oils”, Conference record of the 2006 *IEEE International Symposium on Electrical Insulation*.

75 H. Herman, M. J. Shenton, G. C. Stevens and R. J. Heywood, “A new approach to condition assessment and lifetime prediction of paper and oil used as transformer insulation”, *IEEE International Conference on Solid Dielectrics* 2001.

76 Patrick J. Baird, H. Herman and G. C. Stevens, “Laboratory and field measurement of aged transformer insulation using optical probe spectroscopy and multivariate analysis”, Conference record of the *10th international Conference on Electrical Insulation*.

77 R. Bartnikas, “Partial Discharges, their mechanism detection and measurement”, *IEEE Transactions on Dielectrics and Electrical Insulation*, Vol. 9, No 5, October 2002.

78 G. C. Stone, “Partial discharge diagnostics and electrical equipment insulation condition assessment”, *IEEE Transactions on Dielectrics and Electrical Insulation*, Vol. 12 No 5, Oct. 2005.

79 Wang et al. “Acousto-optical PD detection for transformers”, *IEEE Transactions on Power Delivery*, Vol. 21 No 3 July 2006.

80 Martin D. Judd, Yang Li and Ian B. B. Hunter, “Partial discharge monitoring for power transformers. Using UHF sensors. Part 1: sensors and signal interpretation”, *IEEE Electrical Insulation Magazine*, Vol. 21, No 2, March /April 2005.

81 Martin D. Judd, Yang Li and Ian B. B. Hunter, “Partial discharge monitoring for power transformers. Using UHF sensors. Part 2: field experience”, *IEEE Electrical Insulation Magazine*, Vol. 21, No 3, May/June 2005.

82 H. Lamela-Rivera, C. Macia-Sanahuja and J. A. Garcia-Souta, “Detection and wavelet analysis of partial discharges using an optical fibre interferometric sensor for high power transformers”, *Journal of Optics A: Pure and Applied Optics*, December 2002.

83 I. Fofana, V. Wasserberg, H. Borsi, E. Gockenbach and M. Farzaneh, “Drying of transformer insulation using zeolite”, *IEEE Electrical Insulation Magazine*, Vol. 20, No 1, Jan/Feb 2004.

84 Transformer Service Brochure. “*Solutions for wet transformers*”, ABB Transformers commercial document. Date 10.04.04.

85 Transformer Service Brochure. "*Reclaiming of oil in power transformers*", ABB Transformers commercial document. Date 10.04.04.

86 P. M. Mitchinson, P. L. Lewin, I. L. Hosier, G. Chen and P. Jarman, "Oil reclamation – just a question of moisture?" *Conference on Electrical Insulation and Dielectric Phenomena,* Kansas, October 2006.

87 V. Wasserberg, H. Borsi, E. Gockenbach, "Effects of different drying procedures on the composition of a liquid impregnated solid insulation", Conference record of the 2002 *IEEE International Symposium on Electrical Insulation*.

88 I. Fofana, V. Wasserberg, H. Borsi and E. Gockenbach, "Retrofilling conditions of high voltage transformers", *IEEE Electrical Insulation Magazine*, Vol. 17, No 2, Mar/April 2001.

89 L. A. Dissado and J. C. Fothergill, "*Electrical Degradation and Breakdown in Polymers*", Peter Peregrinus Limited. ISBN 0-86341-196-7, Chapter 2.2 and page 63.

90 J. Millman and Christos C. Halkias, "*Integrated Electronics*", published by McGraw-Hill 1971 ISBN 07-085493-9, pp 1 – 42.

91 J. C. Anderson, *"Dielectrics"* pp 49-54, Chapman and Hall Ltd., 1964. Reprinted 1966 by Spottiswoode, Ballantyre and Co.

92 P. J. Harrop. "*Dielectrics*", pp 28 – 32, Butterworth Group, 1972. ISBN 0408703873.

93 BS 171: 1970. Specification for power transformers.

94 BS EN 60076 Series: 1997. Power transformers.

95 BS 7735: 1994 IEC 354: 1991. Guide to loading of oil- immersed power transformers.

96 BS EN 60214 -1: 2003. Tap changers: Part 1 Performance requirements and test methods.

97 BS EN 60137: 2003. Insulated bushings for alternating voltage above 1000V.

98 BS EN 60085: 2004. Electrical Insulation - thermal classification.

99 BS EN 60071-1: 2006. Insulation co-ordination. Part 1: Definitions, principles and rules.

100 BS EN 60071-2: 1997, IEC 71-2: 1996. Insulation co-ordination. Part 2: Application guide.

101 J. Keith Nelson, "Some steps towards the automation of the design of composite dielectric structures", *IEEE Transactions on Dielectrics and Electrical Insulation*, Vol. 1, No 4. August 1994.

102 Y. Kamata et al., “Development of low permittivity pressboard and its evaluation for insulation of oil-immersed EHV power transformers”, *IEEE Transactions on Electrical Insulation*, Vol. 26, No 4, August 1991.

103 K. Giese, “The effect of cellulose insulation quality on electrical intrinsic strength”, *IEEE Electrical Insulation Magazine*, Vol. 10, No. 5, Sept / Oct 1994.

104 V. Wasserberg, M. Kris, H. Borsi and E. Gockenbach, “Investigations on cavities in liquid immersed paper and pressboard insulation materials and their influence on the electrical behaviour”, Conference: *International Symposium on Electrical Insulation*, April 2000.

105 H. P. Moser, H. J. Kirch and E. Schneider, “Transformerboard insulation under HVDC”, 2nd International *Conference on the Properties and Applications of Dielectric Materials*, 1998.

106 D. W. Crofts, “The static electrification phenomena in power transformers”, *IEEE Transactions on Electrical Insulation*, Vol. 23, No 1, January 1988.

107 J. Zhang and L. J. Cao, “The study on flow electrification of oil-cellulose insulating system in large power transformer”, *Proceedings of the International Conference on Energy Management and Power Delivery*.

108 O. Moreau, G. Artana, H. Romat and G. Touchard, “A contribution to modelling and experimental studies of flow electrification in transformers. 12th International *Conference on Conduction and Breakdown in Dielectric Liquids*, Rome 1996.

109 E. Moreau, T. Paillat and G. Touchard, “Flow electrification in high power transformers: BTA effect on pressboard degraded by electrical discharges”, *IEEE Transactions on Dielectrics and Electrical Insulation*, Vol. 10, No 1, February 2003.

110 Jong U. Kim, “Electric double layer, revisit based on boundary conditions”

111 I. A. Metwally, “Influence of the solid insulating phase on streaming electrification of transformer oil”, *IEEE Transactions on Dielectrics and Electrical Insulation*, Vol. 4, No 3, June 1997.

112 P. Mas, T. Paillat, O. Moreau and G. Touchard, “Flow electrification in power transformers: temperature influence on space charge distribution and charge accumulation in pressboard”, *Journal of Electrostatics* 51-52 (2002).

113 T. Paillat et al., “Influence of pressboard ionisable groups on static electrification in power transformers”, *Conference on Electrical Insulation and Dielectric Phenomena* 2002.

114 A. Sierota and J. Rungis, “Electrostatic charging in transformer oils”, *IEEE Transactions on Dielectrics and Electrical Insulation*, Vol. 1, No 5, October 1994.

115 T. Kobayashi, K. Yajima, S. Tsukao, Y. Ebisawa and N. Hosokawa, "Major factors influencing static electrification in an aged transformer", *Conference on Electrical Insulation and Dielectric Phenomena*, 2005.

116 L. Peyraque, A. Béroual and F. Buret, "Static electrification of pressboard /oil interface and transient phenomena", *IEEE Transactions on Dielectrics and Electrical Insulation*, Vol. 5, No 3, June 1998.

117 A. Bourgeois et al., "Flow electrification in power transformers: Study of a potential remedy", *IEEE Transactions on Dielectrics and Electrical Insulation*, Vol. 13, No 3, June 2006.

118 S. J. Fitton, "Surface discharge within oil insulated apparatus", *IEE Colloquium* 1997.

119 E.O. Forster and G. J. Fitzpatrick, "Electrical breakdown in dielectric liquids", *Physics in Technology*, Vol. 16, No 6, November 1985.

120 E. Kuffel, W. S, Zaengl, J. Kuffel, "*High Voltage Engineering: Fundamentals*", 2nd Edition, Butterworth - Heinemann, 2000, pp 385- 387 and Chapter 7.

121 E. O. Forster, "Critical assessment of the electrical breakdown process in dielectric fluids", *IEEE Transactions on Electrical Insulation*, Vol. EI-20, No 5, October 1985.

122 W. G. Chadband, "The Ubiquitous Positive Streamer", *IEEE Transactions on Electrical Insulation*, Vol. 23. No 4, August 1988.

123 D. Linhjell, L. Lundgaard and G. Berg, "Streamer propagation under impulse voltage in long point-plane oil gaps", *IEEE Transactions on Dielectrics and Electrical Insulation*, Vol. 1, No3, June 1994.

124 L. Lundgaard, D. Linhjell, G. Berg and S. Sigmond, "Propagation of positive and negative streamers in oil with and without pressboard interfaces", *IEEE Transactions on Dielectrics and Electrical Insulation*, Vol. 5, No3, June 1998.

125 E. O. Forster, "The metal/liquid interface: the charge injection process", *IEEE Transactions on Electrical Insulation*, Vol. EI-19, No 6, December 1984.

126 Rongsheng Liu, Christer Tornkvist and Kenneth Johansson, "Space charge distribution in composite oil/cellulose insulation", *Conference on Electrical Insulation and Dielectric Phenomena*, 1994.

127 S. M. Mahajan and T. S. Sudarshan, "Measurement of the space charge field in transformer oil using the Kerr effect", *IEEE Transactions on Dielectrics and Electrical Insulation*, Vol.1, No 1, February 1994.

128 Werner F. Schmidt, "Electric conduction processes in dielectric liquids", *IEEE Transactions on Electrical Insulation*, Vol. EI-19, No 5, October 1984.

129 M. Kurtz, “Tracking”, *IEEE Electrical Insulation Magazine*, Vol.3, No 3, May 1987.

130 N. Yoshimura, S. Kumagai and B. Du, “Research in Japan on the Tracking Phenomenon of Electrical Insulating Materials”, *IEEE Electrical Insulation Magazine*, Vol.13, No 5, Sept/Oct 1997.

131 L. L. Alston, “*High Voltage Technology*”, Oxford University Press 1968, pp 4 – 5.

132 BS EN 60112: 2003. Method for the determination of the proof and the Comparative Tracking Indices of solid insulating material.

133 BS EN 60270:2001 IEC 60270: 2000. High voltage test techniques – Partial discharge measurements.

134 Haefely Trench Modular AC Test System Instruction Manual ACS 300-0.19.

135 “Recognitions of Discharges”, paper presented by *Cigré* Working Group Study Committee No 21.03. High Voltage Cables.

136 C. Vincent, Trinh N. Giao, R. Olivier and J. Aubin, “Behaviour of an oil-paper interface in presence of carbon particle contamination”, *International Symposium on Electrical Insulation*, 1994.

137 G. Berg and L. Lundgaard, “Discharges in combined oil/paper insulation”, Proceeding of the 13th *International Conference on Dielectric Liquids*, Japan, July 1999.

138 C. Dervos, P. D. Bourkas, E. A. Kayafas and I. A. Stathopulos. “Enhanced Partial Discharges due to Temperature Increase in the Combined System of a Solid-liquid Dielectric”. *IEEE Transactions on Electrical Insulation*. Vol. 25, No3 June, 1990.

139 Ekram Husain, Kamaluddm, Imtiaz Ashraf, Atif lqbal, “Study of breakdown of transformer oil in the presence of barrier”. Proceedings of the 4th International *Conference on Properties and Applications of Dielectric Materials*, Brisbane Australia, July 3-8, 1994.

140 Yang Jia-Xiang, Chi Xiao-Chun, Ding Li-Jian and Liu Ji, “Creeping discharge performance of oil-paper insulation with streaming electrification”. IEEE Transactions on Dielectrics and Electrical Insulation, Vol. 4, No. 6, December 1997.

141 M. Krins, H. Borsi, and E. Gockenbach. “Impact of carbon particles on the impulse flash-over behaviour of different solid/liquid interfaces in a non-uniform field”. Proceedings of 1998 *International Symposium on Electrical Insulating Materials*, in conjunction with 1998 Asian International *Conference on Dielectrics and Electrical Insulation* and the 30th *Symposium on Electrical Insulating Materials*, Toyohashi, Japan, Sept. 27-30, 1998.

142 Transformer oil type Nytro 10GBN. Nynas Naphthenics product data sheet. Date 2005-08-03.

143 R Neimanis. L. Arvidsson and P. Werelius, "Dielectric spectroscopy of aged transformer oils", *Electrical Insulation Conference and Electrical Manufacturing and Coil Winding Conference and Exhibition, 2003.*

144 L. Lundgaard, K. Herstad, M. U. Anker and J. Sletbak, "Flashover along solid surfaces parallel to the electric field in liquid insulation at 50 Hz", *Cigré* Proceedings, 1986.

145 Thomas A. Prevost, "Dielectric Properties of natural esters and their influence on transformer insulation system design and performance", *Proceedings of the IEEE Power Engineering Society Transmission and Distribution Conference,* 2006.

146 P. K. Poovamma and R. Jagadish, "Influence of surface roughness and thickness of pressboard on the charging characteristics of Transformer oil", *International Symposium on Electrical Insulation*, June 1994.

147 T. Paillat, L. Onic, O. Moreau, Y. Bertrand, G. Mortha, N. Charvet and G, Touchard, "Influence of pressboard physio-chemical composition on static electrification in power transformers". *IEEE transactions on Industry Applications*, Vol. 39, No 2 March/April 2003.

148 Report on "Viscometric measurement of Degree of Polymerisation on samples of pressboard insulation" by Doble PowerTest, Ref 3411, Issue 2.

149 T. V. Oommen and S. R. Lindgren, "Streaming electrification study of transformer insulation system using paper tube model", *IEEE Transactions on Power Delivery*, Vol. 5, No 2, April 1990.

150 C. Ekanayake, S. M. Gubanski, A. Graczkowski and K Walczak, "Frequency response of oil impregnated pressboard and paper samples for estimating moisture in transformer insulation", *IEEE Transactions on Power Delivery*, Vol. 21, No 3, July 2006.